DOE/SC-0087

Fusion Energy Sciences Advisory Committee

Review of the Inertial Fusion Energy Program

March 2004

U.S. Department of Energy
Office of Science

Table of Contents

EXECUTIVE SUMMARY

Igniting fusion fuel in the laboratory remains an alluring goal for two reasons: the desire to study matter under the extreme conditions needed for fusion burn, and the potential of harnessing the energy released as an attractive energy source for mankind.

The inertial confinement approach to fusion involves rapidly compressing a tiny spherical capsule of fuel, initially a few millimeters in radius, to densities and temperatures higher than those in the core of the sun. The ignited plasma is confined solely by its own inertia long enough for a significant fraction of the fuel to burn before the plasma expands, cools down and the fusion reactions are quenched. The potential of this confinement approach as an attractive energy source is being studied in the Inertial Fusion Energy (IFE) program, which is the subject of this report.

A complex set of interrelated requirements for IFE has motivated the study of novel potential solutions. Three types of "drivers" for fuel compression are presently studied: high-average-power lasers (HAPL), heavy-ion (HI) accelerators, and Z-Pinches. The three main approaches to IFE are based on these drivers, along with the specific type of target (which contains the fuel capsule) and chamber that appear most promising for a particular driver.

In his charge letter (Appendix A) to the chair of the Fusion Energy Sciences Advisory Committee (FESAC), Dr. Orbach, Director of the Office of Science in DOE, noted "the considerable scientific and technical progress" in IFE and asked for "an assessment of the present status of" IFE research carried out in contributing programs. These programs include the HI beam, HAPL, and Z-Pinch drivers and associated technologies, including Fast Ignition. The letter noted that these programs reside in two different parts of DOE, and that both Defense Programs in the National Nuclear Security Agency (NNSA) and the Office of Science "support this review and concur that it be carried out by FESAC."

An IFE Panel was formed to address the charge. The assessment of the quality of the technical work was assigned to those Panel members who are not participants in the IFE program. Overall, they were very impressed by the progress across the program, noting that *the three main approaches (HI accelerators, HAPL, and Z-pinch) are at different levels of maturity. The balance between the science and technology emphasis necessarily varies. The recent progress related to these approaches is substantial and the quality of the science and engineering research is excellent. All approaches are currently on track for developing the science and technology to properly evaluate their potential for IFE.* However, the planned termination of technology programs in support of the HI approach is not consistent with their importance to HI-IFE, and the Panel is concerned about the impact of this action.

The Panel also examined the potential impact that the Fast Ignition (FI) concept might have on IFE, and observed that *each of the approaches to IFE may benefit if the technique of Fast Ignition proves effective. However, since FI is at an early stage of development it would be premature for any of the IFE approaches to rely on the success of FI to achieve an attractive fusion energy system. During the next several years, there is an opportunity to assess the potential of the FI concept utilizing facilities in both Japan and the US (OMEGA, Z, and possibly NIF) through modest OFES investments.*

The primary issues currently facing the IFE program provide the framework for an appropriate set of research plans, which assume continued funding. From this list, the Panel identified the single

near-term issue that appears to be the most critical for each of the approaches (HI, HAPL, and Z-Pinch) and for the FI concept. They are:

HI -- *Physics limits to the maximum phase-space density of space-charge-dominated HI beams and the resulting implications for HEDP and fusion ignition.*

HAPL -- *Durability of KrF lasers, and efficiency and beam smoothing in DPSSLs,*[1] *that will scale to the high-energy requirements for IFE.*

Z-Pinch -- *Physics limitations on power flow in a recyclable transmission line, including the coupling to the pulsed-power driver and the integral target assembly.*

FI -- *Physics of fuel compression to a uniform-density sphere and of energy transport by relativistic electrons to that high-density fuel to achieve ignition.*

These issues, along with many other important basic and applied science issues that form the basis of IFE research plans, must be addressed to assess the potential of IFE. The critical issues related to fuel ignition and burn affect all of the approaches but were not included in the above list because they are being addressed mainly by the ICF program. The Panel acknowledges this vital role of the ICF program and notes *the tremendous leverage that allows the comparatively modest funding for IFE-specific programs to continue to yield important advances*. This is a synergistic relationship where *IFE research* also *directly benefits the NNSA mission.*

The Panel also found that IFE capabilities have the potential for significantly contributing to HEDP and other areas of science. For example, *isochoric heating of substantial volumes to uniform, elevated temperatures should be achievable using HI beams. Investigations of the Fast Ignition concept can lead to exploration of exotic HEDP regimes. Moreover, the rapid turn-around capabilities envisioned for IFE drivers could accelerate progress in HEDP science by enabling a wide community of users to conduct "shot-on-demand" experiments with data rates and volumes far exceeding those obtained on large systems that currently require long times between shots.*

In sum, the IFE Panel is of the unanimous opinion that the IFE program is technically excellent and that it contributes in ways that are noteworthy to the ongoing missions of the DOE. Moreover, the Panel agrees with the IFE community that the most efficient way to achieve the ultimate goal of fusion energy is to carry out a coordinated program with some level of research on all of the key components (targets, drivers, and chambers), always keeping the end product and its explicit requirements in mind. The Panel also notes that *the scientific and technical challenges posed by IFE, along with their many connections to HEDP,* have attracted *many outstanding researchers from academia as well as federal laboratories.* Success will depend on sustaining the commitment and involvement of such people in a broad spectrum of scientific disciplines.

[1] The HAPL program is exploring the potential of two types of lasers: the krypton-fluoride (KrF) gas laser, and the diode-pumped solid-state laser (DPSSL).

1. INTRODUCTION

1.1. Background

Ever since the discovery that thermonuclear fusion is the source of energy that powers our sun and all the stars, there has been the dream to ignite fusion fuel in the laboratory. The interest is driven by two desires: to study matter under the extreme conditions needed for fusion burn, and to explore the potential of harnessing the energy released as an attractive energy source for mankind.

The conditions required to ignite the fuel and sustain a fusion burn include temperatures of about 100,000,000 degrees or more. The fuel must also be confined and insulated well enough so that energy released from the initial fusion reactions can sustain the fusion process. Achieving those conditions in the laboratory has proved to be a daunting challenge. In stars, the enormous pressure exerted by their gravity leads to these conditions of high temperature and confinement. On earth, the two main laboratory approaches being pursued are magnetic confinement fusion and inertial confinement fusion. Depending on its type and age, a star succeeds in fusing a variety of light nuclei to form heavier nuclei. Attempts to achieve fusion burn in the laboratory will use the fuel that requires the least extreme conditions to create a burning plasma. That fuel is a mixture of deuterium and tritium, two isotopes of hydrogen.

Magnetic Confinement and Inertial Confinement. The magnetic approach uses magnetic fields to confine and insulate the hot fuel, which becomes an ionized gas (a plasma) at the temperatures required for fusion. The inertial approach involves the rapid compression of a tiny spherical capsule of fuel, initially a few millimeters in radius, to densities and temperatures higher than those in the core of the sun. The ignited plasma is confined solely by its own inertia long enough (less than a billionth of a second) for a significant fraction of the fuel to burn before the plasma expands, cools down and the fusion reactions are quenched.

The world scientific community is finally poised to create a burning plasma in the laboratory after more than 50 years of scientific and technological advances. International negotiations are underway to select the site to construct ITER, which will use the magnetic confinement approach. The National Ignition Facility (NIF) is already under construction in the US, and will use the inertial confinement approach.[2] A similar facility, Laser Mega Joule (LMJ), is under construction in France.

These facilities will allow the study of burning plasmas under very different conditions involving very different physics. For example, the fusion conditions in NIF will require densities that are about a 100 billion times greater than those in ITER. These NIF experiments will provide high-energy-density-physics (HEDP) conditions never before achievable in the laboratory. The rich scientific opportunities in HEDP are described in a recent National Research Council report [1].

[2] Inertial fusion experiments conducted at the Nevada Test Site have demonstrated excellent performance, but NIF is projected to produce the first burning plasmas in a controlled laboratory environment enabling easily repeatable, highly diagnosed studies.

1.2. Inertial Fusion Energy (IFE)

The inertial confinement approach has the potential to be an attractive path to fusion energy. That potential is being explored, and these IFE research activities are the subject of this report.

The motivation for fusion energy research includes the promise of an energy source with no greenhouse gas emissions, and with a virtually inexhaustible fuel supply that is widely available. While these and other features of IFE are attractive, an earlier FESAC report "recognized that difficult scientific and technological questions remain for fusion development." [2] A diversified basic and applied science research portfolio is required to prepare for the realization of the ultimate goal of fusion energy production and to reduce developmental risk. IFE and MFE (magnetic fusion energy) are pursued because they present major opportunities for advancing both science and fusion energy. While they share a common goal, IFE and MFE have significantly different scientific and technological challenges and opportunities. Because of this diversity, the parallel pursuit of IFE and MFE broadens the contributions to science while reducing developmental risk.

Conceptually, IFE can be harnessed to generate electricity and other useful products from a steady sequence of inertial confinement fusion (ICF) events. Each ICF event involves placing a small capsule of fuel in a chamber and then compressing and heating it to ignition by some type of "driver" that generates intense pressure on the outside of the capsule. Fusion-power system studies indicate that the energy released per event could range between hundreds of megajoules and several gigajoules. The corresponding repetition rates would range from several per second to about once every ten seconds for a 1-GW(e) power plant.

Four principal technical requirements must be achieved in a cost-competitive, environmentally attractive manner for IFE to be successful:

1) *High Energy Gain and Efficiency:* The efficiency of the driver in converting energy from the electrical power grid to the energy needed to compress the capsule, coupled with the energy "gain" of the capsule (ratio of energy released to the energy needed to compress and heat the fuel) must be sufficient to yield substantial net energy.

2) *Repetition Rate:* The driver, target (which includes the fuel capsule) fabrication, and reaction chamber must operate at a repetition rate that is sufficient to produce economically useful power. The chamber must be restored to a sufficiently quiescent state after each shot to allow insertion of the next target, and for the transmission and focusing of the next pulse of energy from the driver to that target.

3) *Energy Conversion and Tritium Breeding:* The energy released from the burning deuterium-tritium (DT) fuel is mainly in the form of energetic ions, neutrons, and x rays. This energy must be absorbed by the chamber and converted into "high-grade" thermal energy that can be efficiently used to drive electric generators. The chamber must also utilize the emitted neutrons to breed sufficient new tritium (from lithium) to sustain the fuel supply.

4) *Durability:* The components in an IFE system must carry out the above functions with sufficient durability for the high capacity factors required in an attractive energy system.

Approaches to IFE. This complex set of interrelated requirements for IFE has motivated the study of novel potential solutions. Three types of "drivers" for fuel compression are presently studied: high-average-power lasers (HAPL), heavy-ion (HI) accelerators, and Z-Pinches. The

need for efficient coupling of energy from these drivers to the capsule has motivated different conceptual designs for the "targets," which contain the capsule of fuel.

In broad terms the targets can be categorized as "direct drive" or "indirect drive" types. Both types of targets have been used in the ICF program for various physics studies. Fusion capsules for both target types are conceptually similar, and are envisaged to consist of a tiny, spherical, cryogenic solid shell of DT fuel or DT-wetted foam, coated with plastic or other materials. In the case of direct drive, the driver beams (e.g., lasers) are focused directly on the surface of this coating. For indirect drive, the driver energy is delivered to the interior of a high-Z (heavy element) enclosure (hohlraum) so that the material at or near the inside surface of the hohlraum is heated to 2 to 3 million degrees. This creates blackbody x-ray radiation that impinges on the capsule at the center of the hohlraum.

The impinging energy (directly from driver beams or from x-rays) heats up the coating on the outer surface of the capsule. The heated coating ablates radially outward, generating an inward momentum impulse very much like a standard rocket engine. Driven by this "rocket" the shell implodes, reaching high velocities, and then slows down as the pressure builds up in the fuel. As the shell slows down, its kinetic energy is converted into internal energy (i.e. pressure) of the material enclosed by the imploding shell. The rapidly converging fuel creates a "hot spot" at the center that reaches its maximum temperature and pressure when the shell stagnates. At pressures of hundreds of gigabars and a temperature[3] of about 10 keV the hot spot ignites and a fusion burn front propagates outward through the bulk of the compressed fuel.

System studies indicate that each driver type is best matched with a specific target design and to a specific reaction chamber (including energy conversion) design. Two general types of chambers are being examined to accommodate the specific needs of the different drivers and targets. Dry-wall chambers have armor to withstand the energetic radiation and debris from the targets. The thick liquid-wall chambers have the advantage of continually replacing the surface exposed to this radiation and debris but with the added complexity of managing the flowing liquid. The three main driver types (HAPL, HI, and Z-Pinch), coupled with their corresponding target and chamber types, become the three main approaches to IFE. The following paragraphs briefly describe the present concepts for these three approaches.

High-Average-Power Lasers. The HAPL approach involves research on both krypton-fluoride (KrF) gas lasers and diode-pumped solid-state lasers (DPSSL). The main-line approach for either laser is to use direct-drive targets to maximize energy coupling efficiency to the capsule. Advances in laser techniques indicate that the spherical uniformity of illumination required by these targets may be achievable. Dry-wall chambers for energy conversion appear to be most compatible with the final optics and the penetrations in the chamber wall needed for spherical illumination. Dry walls are also compatible with the relatively low x-ray output from direct-drive targets, as compared with that from indirect-drive targets.

Heavy-Ion Accelerators. The HI-accelerator approach plans on indirect-drive targets because the large ICF target physics database for indirect drive allows good definition of HI beam requirements, and because two-sided illumination is compatible with thick liquid protected chambers. The loss in efficiency compared to direct drive should be offset by the higher

[3] Plasma temperatures are frequently measured in units of electron volts (eV) or thousands of electron volts (keV). Since 1 eV = 11,600 ^{o}K, then 10 keV is slightly more than 100 million degrees.

efficiency that is expected from HI accelerators. Liquid wall techniques for absorbing the energy while protecting structural material appear usable with the HI approach due to geometrically limited wall penetrations (spherical illumination not needed) and less demanding requirements for protecting final focusing optics from chamber and target debris compared with lasers.

Z-Pinches. The Z-Pinch approach produces x-rays from an imploding cylindrical array of current-carrying wires that stagnate on a low-density-foam cylinder. One or two of these assemblies provide the x-rays inside of a hohlraum for the indirect-drive-target design. The high x-ray-generation efficiency of the pulsed-power driver and the z-pinch should compensate for the lower efficiency of this indirect-drive target design. The Z-Pinch driver, in contrast with the other two IFE approaches, is physically connected to the target by transmission lines. Lower repetition rates than HAPL or HI, and hence higher fusion yields per target, are envisioned to allow for replacing the transmission lines on each shot. Liquid walls are the baseline chamber approach, as in the HI approach, and they should be useful in dealing with the larger fusion yields.

The development of high-energy petawatt (10^{15} Watts) lasers raises the possibility of reducing the compression-driver requirements for any of the three approaches. The potential improvement relies on the extremely short pulse (~10 ps) of a petawatt laser to heat and ignite a small portion of the fuel near the edge of a compressed capsule. This "Fast Ignition" concept separates the functions of compression and ignition, and potentially relaxes the constraints on compression-driver energy and target uniformity because no central hot spot is required. This flexibility may allow higher-gain capsules, and simplification of chamber and driver specifications.

1.3. IFE and Inertial Confinement Fusion (ICF) Programs

The IFE program in the US exists in the context of both weapons and energy research. The DOE National Nuclear Security Agency (NNSA) has a major program in ICF because of its relevance to the nuclear weapons Stockpile Stewardship Program (SSP). The ICF program, funded at $504M in FY03, supports major facilities including the 1.8-MJ NIF laser ($290M) being constructed at the Lawrence Livermore National Laboratory, the 30-kJ OMEGA laser facility at the University of Rochester, the 2-MJ Z pulsed-power facility at Sandia National Laboratories, and the 3-kJ Nike laser at the Naval Research Laboratory.[4] These facilities and the program more generally devote a major fraction of their resources toward SSP research that is much broader than just achieving ignition, and includes a variety of high-energy-density physics (HEDP) topics.

Decades of experimental, theoretical, and computational R&D carried out in the ICF program have led to an understanding of the science and technology needed for single-shot ignition and burn. Much of this information is also essential to the IFE program. Relevant topics include driver-energy absorption by the capsule, driver asymmetries, capsule nonuniformities, implosion hydrodynamic stability, hot-spot ignition, and burn propagation. The ICF program has the goal of achieving ignition on NIF within the next decade. The close interactions between the ICF and IFE programs, particularly in the area of target physics, are essential to the success of the much smaller IFE program.

IFE research programs currently exist in both NNSA and the Office of Fusion Energy Sciences (OFES) within the DOE Office of Science. Congress has added significant funding to the NNSA

[4] The energies listed represent the energy that each facility can deliver to a target.

budget for IFE during the past five years, including $25M this year (FY04), to support research through the High Average Power Laser (HAPL) program. The HAPL program is focused on developing the science and technology for the laser drivers and other components needed for fusion energy production, and is closely coupled with the target physics work carried out in the ICF program. This year Congress also added $4M to explore the Z-Pinch as an IFE driver. These efforts are focused on the goals and needs of IFE that are beyond those of ICF.

The OFES component of the IFE program is focusing mainly on the scientific underpinnings of the Heavy-Ion (HI) approach. This strategy emphasizes research topics such as non-neutral plasmas and accelerator physics issues essential for the HI approach and relevant to other fields of science. Indeed, because of the potential for IFE research to contribute to the field of HEDP, OFES has adopted the following performance measure for its IFE program [3]: "High Energy Density Physics/IFE: Progress in developing the fundamental understanding and predictability of high energy density plasma physics, including potential energy producing applications." The OFES has also sponsored research in the areas of target design and fabrication, Fast Ignition, HI chambers, and system studies for HI and lasers. In FY03 the OFES budget for all IFE activities was about $17M. The FY04 appropriations provided only $15M for IFE, including only closeout funds for technology. Systems studies were eliminated. The closing out of these programs is reflected in Table 1, which summarizes the funding source for various activities important to the IFE program.

Table 1
Source of Funding for IFE-Relevant Activities

	NNSA Program	OFES Program	Report Section
HEAVY-ION BEAMS			
Driver Science		OFES-IFE	3.2.1
Final Optics (magnets)			3.2.1
Target Physics		OFES-IFE	3.1.1
Target Fabrication			3.1.4
Target Injection	HAPL		3.1.4
Chamber			3.4.1
LASERS			
Driver Science/Technology	HAPL		3.2.2, 3.2.3
Final Optics (mirrors)	HAPL		3.2.3
Target Physics	ICF (+HAPL)		3.1.2
Target Fabrication	HAPL (+ICF)		3.1.4
Target Injection	HAPL		3.1.4
Chamber	HAPL		3.4.1
Z-PINCHES			
Driver Science/Technology	Z-IFE		3.2.4
Recyclable Transmission Line	Z-IFE		3.2.4
Target Physics	ICF		3.1.1
Target Fabrication	ICF (+Z-IFE)		3.1.4
Chamber	Z-IFE		3.4.1
FAST IGNITION			
Petawatt Lasers	ICF		3.3
Target Physics		OFES-IFE	3.1, 3.3
Target Fabrication	ICF	OFES-IFE	3.1.4

Since the distinction between the IFE and ICF programs is essential for the clarity of this report, the following descriptions are provided for the reader's convenience:

IFE program -- the DOE-sponsored research in inertial fusion energy, including the OFES research in Heavy-Ion Beams and Fast Ignition, and the NNSA HAPL and Z-Pinch-IFE programs.

ICF program -- the NNSA-funded program in inertial confinement fusion, excluding the HAPL and the Z-Pinch-IFE programs.

Only a few countries have major research programs in inertial fusion. These include Japan and France, with the US program being the largest. The Japanese program is exclusively devoted to energy research. The emphasis is on Fast Ignition using the 12-beam ~10-kJ GEKKO laser and a 0.4-kJ petawatt laser. The work is carried out at the Institute for Laser Engineering at Osaka University, where the FIREX1 construction project is adding a ~10-kJ, 10-ps, 4-aperture laser to GEKKO for Fast Ignition research. The French program is mainly oriented toward weapons research and HEDP. Facilities include a 1-kJ petawatt laser capability at LULI (Ecole Polytechnique) in Paris and the 60-kJ LIL facility at CESTA near Bordeaux. As mentioned earlier, the LMJ facility is under construction and will have an energy level comparable to NIF. It also has a similar schedule for reaching ignition.

1.4. Formation and Activities of FESAC's IFE Panel

Charge to FESAC. In his charge letter (Appendix A) to the chair of the Fusion Energy Sciences Advisory Committee (FESAC), Dr. Orbach, Director of the Office of Science in DOE, noted "the considerable scientific and technical progress" in IFE and asked for "an assessment of the present status of" IFE research carried out in contributing programs. These programs include the HI-beam, HAPL, and Z-Pinch drivers and associated technologies, including Fast Ignition. The letter noted that these programs reside in two different parts of DOE, and that both Defense Programs in NNSA and the Office of Science "support this review and concur that it be carried out by FESAC."

IFE Panel Organization and Activities. FESAC's IFE Panel membership (Appendix B) includes 7 members of FESAC and 13 additional experts. Ten of the members are experts associated with IFE programs and the other ten are not, but have expertise in MFE, HEDP, and other relevant disciplines.

The IFE experts were assigned the responsibility of ensuring that all of the relevant information about the status of the programs, including recent advances, was made available to the Panel through presentations and written material. They were also responsible for explaining the major issues facing the programs and identifying possible approaches to resolving those issues. In addition, they were responsible for providing information about how IFE research has or might contribute to other scientific endeavors, including HEDP.

The members who were not participants in the IFE program were assigned the responsibility of assessing the quality of the IFE research and reviewing the key issues facing the program. They were also to comment on the appropriateness and timelines of possible research activities to resolve the issues, taking into account the availability of resources and appropriate facilities, and the value of the advances in technical understanding that might accrue. They were also assigned

the task of evaluating the potential impact of the IFE programs on HEDP and other areas of science.

The Panel began its work by creating a reading list (Appendix C), which includes recent reviews of the IFE program. The Panel met twice and held 5 formal conference calls. The agendas are provided in Appendix D. The meetings involved researchers from the IFE community in addition to Panel members. As indicated in the agendas, representatives of the US government and one IFE expert from Japan were among those who interacted with the Panel. The Panel extensively used a website and email to share information between meetings and during conference calls.

The FESAC Priorities Panel sought input from the IFE Panel on key issues that motivate MFE and IFE research, as expressed in a list of Overarching Questions and Topical Questions. The IFE Panel response was provided in a letter and a subsequent email (see Appendix E).

Outline of Report. First, the report describes a few general observations and findings that grew out of the Panel's many discussions. Second, the report provides assessments of the technical progress in IFE, and of the research quality. Third, it describes the critical scientific issues for the IFE program, and evaluates the readiness of the program to embark on activities that will lead to new advances in understanding toward the goal of fusion power. Fourth, the report considers potential contributions from IFE programs to HEDP, the ICF program, and other areas of research.

The report responds to the following four topics quoted from the charge letter:

1. The current status of the scientific basis and related technology of each of the approaches to IFE, including an assessment of the quality of work being carried out in the programs. [See Section 3]

2. Critical scientific issues identified in each of the approaches to IFE that would contribute to understanding the long-range potential of IFE. [See Sections 3 and 4]

3. The impact that fast ignition as a concept improvement may have on IFE. [See Sections 3 and 4]

4. The potential contribution of the various IFE program elements to the emerging field of High Energy Density Physics. [See Section 5]

2. SOME GENERAL OBSERVATIONS AND FINDINGS

The Panel found it challenging to attempt a coherent and effective evaluation of IFE when the activities funded through OFES and NNSA differ both in their near-term strategies and in their technical approaches to achieving fusion energy. The OFES-funded IFE activities have been asked to emphasize a subset of the science relevant to IFE, with particular emphasis on areas relevant to HEDP. The NNSA-funded HAPL and Z-Pinch IFE activities take an integrated approach to developing the key science and technologies together as a coherent system needed for fusion energy. Each program also pursues technical approaches that differ greatly in their scientific and technology issues. The set of general observations and findings in this section derive from the process of working through this assignment.

These findings are listed here to set the context for the rest of the report. More specific findings, including those that respond to the itemized topics in the charge letter, are found within the text of Sections 3 through 5.

Finding: *The Panel recognizes and respects the reasons for the differences in near-term focus of OFES and NNSA sponsored programs. Although near-term strategies differ, the ultimate goal of all IFE research is fusion energy production. The long-term potential for fusion power provides an exciting and unifying purpose for all IFE research activities.*

Each of the approaches to IFE (see Table 1) involves basic and applied scientific challenges. These challenges are described in Sections 3 and 4. The scientific topics include accelerator physics, equations of state in the HEDP regime, plasma chemistry, laser-plasma interactions, the material science underpinning optical damage at high intensities, physics limits of power flow in transmission lines, and energy absorption in materials (chamber walls) that reach HEDP intensities, to name just some.

Finding: *IFE research involves a rich set of scientific challenges. Substantial advances in a spectrum of scientific disciplines will be required to effectively assess the long-term potential of IFE. Many outstanding researchers from academia as well as federal laboratories are pursuing a range of exciting IFE science topics.*

The IFE program needs to address the scientific and technical issues associated with the complex interrelated requirements for targets, drivers, and chambers that pose the greatest uncertainty in assessing the ultimate potential of IFE. As the Panel struggled with selecting the most critical near-term issues identified in Section 4, it was guided by the ultimate goal of IFE and by the present understanding of the various elements of an energy producing system.

Finding: *Understanding the interrelated scientific and technological issues of the key components of IFE within the framework of an integrated system is an essential input for prioritizing IFE research activities, whether for the science-focused OFES program or for the NNSA program. Careful prioritization is particularly important given the limited resources available to these IFE activities.*

The prevailing view in the IFE Panel is that the most efficient way to achieve the ultimate goal of fusion energy is to carry out a coordinated program with some level of research carried out on all of the key components (targets, drivers, and chambers), keeping the requirements of the end product in mind. However, the Panel members had widely varying views on the relative levels of effort among the components and the degree of focus on science or technology that would

provide the most efficient development path, given the present state of understanding. Keeping in mind this broad description of a coordinated program, the Panel supports the following finding.

Finding: *Carrying out a coordinated IFE research program allows a more efficient approach for developing a fundamental understanding of the science that is necessary for IFE.*

An obvious challenge for IFE is the long timescale that is projected, given present funding levels, to resolve the interrelated scientific and technical issues and to demonstrate the potential of IFE. This challenge requires the continuing recruitment, training, and retention of outstanding young people.

Finding: *The scientific and technical challenges posed by IFE, along with their many connections to HEDP, and the grand ultimate purpose of fusion power highlight both the need and the opportunity to attract outstanding researchers for future success. In order to identify and exploit key opportunities and synergies with HEDP and other exciting topics, improved coordination is needed between various scientific communities. The series of workshops on laboratory astrophysics with lasers is a model that could be emulated.*

3. ASSESSMENT OF THE TECHNICAL STATUS -- RECENT PROGRESS AND CHALLENGES

Given the large number of possible combinations of drivers, targets, and chambers, it is prudent to focus most of the research resources on the combinations that appear to be most promising. As described in the Introduction, the HAPL program emphasizes direct-drive targets and dry-wall chambers. The HI accelerator and Z-Pinch efforts emphasize indirect-drive targets and thick liquid-wall protection. Fast Ignition may be compatible with both target/chamber combinations and any of the compression drivers.

This section contains an overview of the recent advances made on these three main approaches to IFE and on the Fast Ignition concept. The primary remaining issues for each topic are noted along with the general plans of the program to address them. A brief assessment of the quality and appropriateness of the work in each of these areas is also provided. In carrying out this assessment, the members of the Panel who are outside of the IFE program examined the achievements in light of the goals that were established for the various program elements in recent years [4,5,6] while taking into account the availability of funds since the goals were established. Additional factors in the assessment process included the presentations given to the panel by IFE experts, the publication record of the researchers, including the level of exposure in national and international meetings, and the identification of the remaining critical issues with defined research programs to resolve them.

3.1. Targets

Although targets being evaluated for IFE can be broadly categorized as either indirect drive or direct drive, target details can vary substantially depending on the choice of driver and chamber. Figure 1 illustrates some of this diversity.

For IFE, a key parameter in matching a target with a driver is the target gain, G. G must exceed a certain minimum that depends on the fusion system's driver efficiency. The inverse of the product of $\eta G \varepsilon$ is the fraction of the electric energy produced that is used to power the driver, where η is the driver efficiency and ε is the overall efficiency of conversion of thermonuclear energy to electricity. For example, for $\varepsilon = 50\%$ and a driver efficiency $\eta = 10\%$, a target gain of 100 would result in 20% of the electric output being used to power the driver. In general, indirect-drive targets have lower gains than direct-drive targets, and therefore require higher efficiency drivers. Indirect-drive targets are also more complex, but they impose less stringent requirements on the focusing and uniformity of driver energy delivered to the target.

The Fast Ignition (FI) concept uses one of the drivers (HI, HAPL, or Z-Pinch) to compress the target shown in Figure 1g, and then uses an extremely intense (10^{19}–10^{20}W/cm^2) laser beam to ignite a propagating thermonuclear burn wave in the compressed, but cold, target. This concept has the potential of increasing target gain and/or easing the detailed requirements on compressor-driver energy delivery to the target. The concept is at an early stage of investigation, the physics is complex, and the technology is challenging. The potential and the challenges are described in Section 3.3.

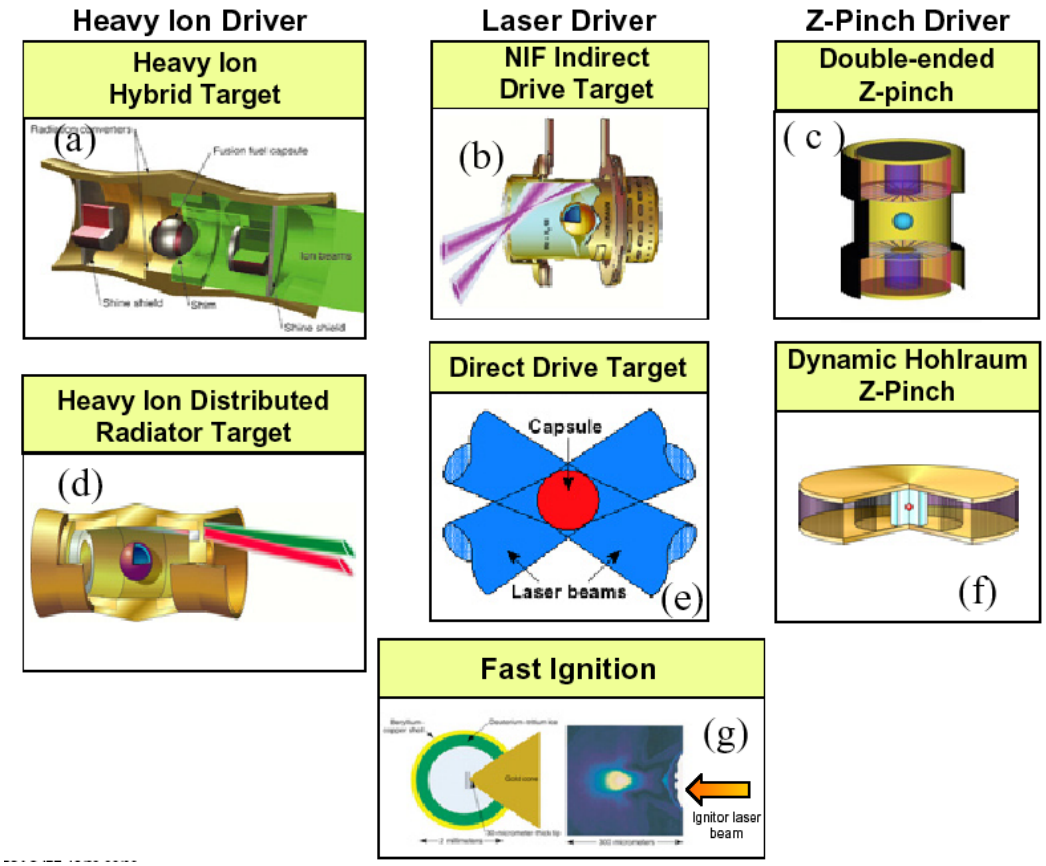

Figure 1. A wide range of targets is being examined for IFE.

3.1.1. Indirect Drive

The major differences between laser (NIF), HI, and Z-Pinch indirect drive targets are related to the physics issues of x-ray production and the detailed hohlraum geometry utilized to achieve symmetry of the radiation driving the implosion. Capsule physics is essentially independent of the source of x-rays. Also, the physics of x-ray transport within the various hohlraum concepts as well as of hohlraum energetics is common to all indirect-drive targets. Therefore, OMEGA, Z, and NIF can investigate implosion and ignition issues for all of the indirect-drive targets being considered for IFE. Similarly, IFE target innovations and insights can, and have been, incorporated into the ICF program.

Indirect Drive with Lasers (NIF)

This is the baseline approach to ignition on NIF (Figure 1b). OFES supports a small amount of IFE target design work on techniques that could simplify the laser-beam geometry relative to that utilized on NIF. Essentially all other target design work for laser indirect drive is supported by the ICF Program and is specifically aimed at improving the performance of NIF. For example, hohlraums are being designed with material mixtures that reduce x-ray losses into the wall, and with smaller laser entrance holes. These improvements are expected to enable reduced hohlraum sizes, increased coupling efficiency to the capsule, and higher gain. There are now indirect-drive

target designs for NIF with gains up to 50. These advances have positive implications for IFE. For NIF, the major challenge is to control laser-plasma interaction (LPI) effects with only a modest (10 – 20%) energy penalty.

Indirect Drive with Heavy-Ion Beams

Indirect drive is the baseline target concept for the HI-beam approach, which will benefit from the ignition target physics studies being planned for NIF. In addition, HI drivers are expected to have an efficiency of 25-40%, so relatively low target gains (25 to 50) are projected to be adequate for HI IFE.

All recent HI-driven target design work has been funded by OFES. Since beam focusing to a small spot size is a challenge for HI beams, this target research included a systematic study of the tradeoffs among drive symmetry, beam spot size, and capsule hydrodynamic stability. Two designs of interest resulted. One more efficiently utilizes driver energy but requires a more challenging (1-2 mm radius) ion beam spot on target (Figure 1d), and the other greatly relaxes the beam radius requirement (~ 5 mm radius), but ~20% more delivered beam energy is required (Figure 1a). It is noteworthy that optimization of capsule performance of HI-driven targets has had a substantial impact on the optimization of capsules for NIF targets. At present, the most critical issue for HI fusion is to better understand the physics that may limit beam brightness on the target.

Indirect Drive with Z-Pinches

Recent breakthroughs in efficiently producing intense, z-pinch-driven, thermal x-ray sources and achieving symmetric capsule implosions on the Z facility have created a new path for achieving indirect-drive ICF. This research is supported by the NNSA ICF program as part of a broad-based effort to evaluate options for targets with yields of greater than 500 MJ. The "double-ended z-pinch hohlraum" configuration (Figure 1c) and the "dynamic hohlraum" (Figure 1f) configuration have both demonstrated x-ray production with about 15% overall electrical efficiency when a cylindrical, radially imploding z-pinch plasma stagnates on a low-density foam cylinder. Since x-ray production efficiencies of up to 25% are feasible, IFE target gains in the range of 50 or more are required.

.

The DT-fuel-capsule location is quite different in the two cases. In the double-ended z-pinch target, the capsule is in a static hohlraum. A decade of experiments has demonstrated control of radiation symmetry to within a factor of two of that required for high-yield capsule implosions. Further advances are needed in the scaling of x-ray power and pulse shape as the current is increased from 20 MA to the ~60 MA required for high yields.

The dynamic-hohlraum concept embeds the spherical fusion capsule inside the low-density foam cylinder that is centered in the single high-Z wire array. This arrangement offers the potential for about twice the efficiency in delivering energy to the capsule, compared with the double-ended z-pinch target. However, the physics issues associated with achieving a highly symmetric capsule implosion are closely coupled to the physics of the z-pinch implosion itself.

While the target designs take advantage of much of the capsule physics developed in the laser ICF program, the capability to perform fully integrated 2D and 3D calculations that include the physics of the wire arrays is still being developed.

3.1.2. Direct Drive with Lasers

Direct-drive targets (Figure 1e) are conceptually simpler than indirect drive targets and they have higher overall energy-coupling efficiency to the fuel capsule. Direct-drive target design has been supported entirely through the ICF and HAPL programs of NNSA.

The efficiencies of laser drivers (KrF and DPSSL) are projected to be about 7% percent. At these values, target gains of at least 120 are needed for IFE. Recent work predicts capsule gains of 120-170 for a few-MJ driver.

The major challenge in realizing sufficient gain from a direct-drive target is suppression of hydrodynamic (Rayleigh-Taylor) instabilities, which can be seeded by the non-uniformities of either the capsule surface or the driver-beam illumination. Experiments have shown that adding a thin high-Z layer (such as Pd) on the surface of the target substantially reduces the imprint of laser non-uniformities, and hence mitigates the seeding of hydrodynamic instabilities. In addition, the energy-deposition scale length in the ablator is much shorter for direct drive than for indirect drive. For laser beams impinging directly on the ablator, the scale length is determined by electron thermal conduction; for indirect drive, the scale-length is set by the more deeply penetrating x-rays. However, by tailoring the post-shock entropy profile of the ablator, calculated instabilities in direct-drive targets can be reduced to levels comparable to those seen in indirect-drive targets, while still maintaining high gain. The major experimental challenge now is to see whether instabilities can actually be controlled to the level that is predicted to be needed for achieving ignition and burn.

Obtaining optimal gain in direct-drive targets is anticipated to require a beam-pointing accuracy that is greater than that for indirect drive. Determining the pointing accuracy requirements, and achieving them under IFE conditions where targets are rapidly injected into a chamber, is the subject of ongoing research.

Assessment Analysis: Progress toward understanding the issues that affect the gain in IFE target designs was the metric used by the Panel in assessing the target physics work. Noteworthy accomplishments are: (1) the much improved understanding of the trade-offs (among drive symmetry, beam spot size, and capsule hydrodynamic stability) in the design of high-gain, HI indirect-drive targets; and (2) the discovery that instabilities in direct-drive targets can be suppressed by thin, high-Z capsule coatings, as well as by tailoring the ablator's post-shock entropy profile, and hence its density profile.

Finding: *The combined IFE plus ICF target physics research portfolio is appropriately diverse, and the technical work is of very high quality. Excellent progress involving one or more of the key performance criteria – implosion symmetry, capsule stability, and high gain – continues to be made on central hot-spot targets being designed for the various driver schemes.*

3.1.3. Theory and Simulation

NNSA-funded efforts in ICF and IFE have developed a variety of computer codes to simulate the performance of inertial fusion targets. These include the 3D radiation hydrodynamics codes HYDRA (developed at LLNL) and FAST3D (developed at NRL), as well as a number of 1D and 2D codes. These codes have all of the physics packages needed to simulate a broad range of problems in capsule design, and in hohlraum design for indirect drive. In addition, the investments made by NNSA through its Advanced Strategic Computing Initiative (ASCI) have markedly improved many of the computational tools, as well as dramatically increased the

available computing power. Another important component of the success of simulation is a robust program of validation of the codes against experiments performed at Nike, OMEGA, Z, and NIF. As a consequence of these investments, simulation has become an important tool for target design, leading to improvements in robustness and predicted yield.

There are a number of areas in which advances in simulation capability are needed by the IFE program. Uncertainties in material properties such as opacities of high-Z materials and some equations of state impose fundamental limitations on the *a-priori* accuracy of calculations of the performance of targets designed for ignition and burn. There is an ongoing ICF research program to reduce these uncertainties and to validate material models currently in simulation codes. (As an example, the compressibility of hydrogen in the megabar range, based on several recent experiments, is uncertain to 50%. This, in turn, leads to an uncertainty in the precise pulse shape required for a low-entropy implosion.) In addition, in some areas, improvements in simulation capability are needed to obtain higher-fidelity computations. These include modeling such physical processes as laser-plasma instabilities and magnetohydrodynamic effects, as well as new computational capabilities such as adaptive meshing and more accurate numerical modeling of material interfaces. These advances will increase the range of length scales that can be represented in a single calculation. Such algorithmic improvements are particularly important for simulating the growth of interface instabilities, for which nonlinear multimode effects are important. All of the developments mentioned here will be of critical importance to the success of the Fast Ignition concept, because of the higher energy densities, the broader range of scale lengths, and the multidimensionality of the geometry.

The impact of the NNSA-funded simulation efforts on IFE research is quite substantial. The investments in code capabilities, material models, and experimental validation at ICF facilities all are applicable to support the resolution of corresponding problems in IFE. Furthermore, simulation is the bridge between IFE and HEDP science: simulation codes and models that are bench-marked using IFE experiments can then be used to investigate the corresponding phenomena in areas such as astrophysics, for which controlled experiments are not possible. However, since many of the NNSA-developed codes are not widely available to university researchers, theoretical collaboration with some IFE communities can be significantly limited.

Assessment Analysis: The Panel's metric for measuring the success of simulation in IFE target design is the extent to which simulation is an integral tool to the target design process and quantitative analysis of experiments. Such a successful use of simulation in science is difficult to achieve, and consequently represents an outstanding accomplishment. Of particular note for laser indirect drive targets, a variety of 1D, 2D, and 3D codes have been used to improve the design of all aspects of the capsule, including the effect of the shape of the laser pulse, of the composition of the ablator, and of the composition and thickness of the high-Z shell on the growth of instabilities and therefore the overall gain.

Finding: *Simulation has a substantial impact on enhancing the performance and understanding of existing and advanced target concepts. The ICF and IFE programs have developed valuable capabilities for driver-matter interactions, including an extensive validation program against experiments performed at NIKE, Z, and OMEGA. Nonetheless, new simulation capabilities are needed, particularly in the areas of material models, laser-plasma interactions, and in the range of scales that can be represented. The IFE program would also benefit from developing an open-source simulation capability in the area of capsule physics, particularly in connection with HEDP.*

3.1.4. Target Fabrication

Credibility of the IFE program depends upon a viable fabrication plan for the large quantities of targets (100,000 to 500,000 per day for a 1000-MW(e) plant, depending on the target yields being considered) that will have to be made for a fraction of a dollar per target. In recent decades, the ICF program has developed and used a wide range of techniques to generate spherical, cylindrical and planar laser and z-pinch targets in small numbers for room temperature as well as cryogenic experiments. Robust processes are being developed that are capable of producing large quantities of stringently specified, but virtually identical targets and delivering them to the center of a target chamber with high accuracy. Significant IFE advances have been made in capsules, DT-fuel filling and layering, hohlraum production, and target injection, with potential benefits also accruing back to ICF target activities (see Section 5.2).

Processes needed for supplying targets for an IFE power plant have been identified, and the critical issues are understood. Figure 2 shows a potential target fabrication sequence for direct drive (HAPL) and indirect drive (HI). Capsules are fabricated, filled with DT and cooled to near the DT triple point where a DT ice layer is formed. The layered capsules are loaded into a hohlraum or a sabot, injected into the chamber, and tracked in flight to provide data for the final beam steering. The current status and future challenges associated with these target supply steps, and extensions to Z-Pinch drivers and Fast Ignition, are briefly described in this Section.

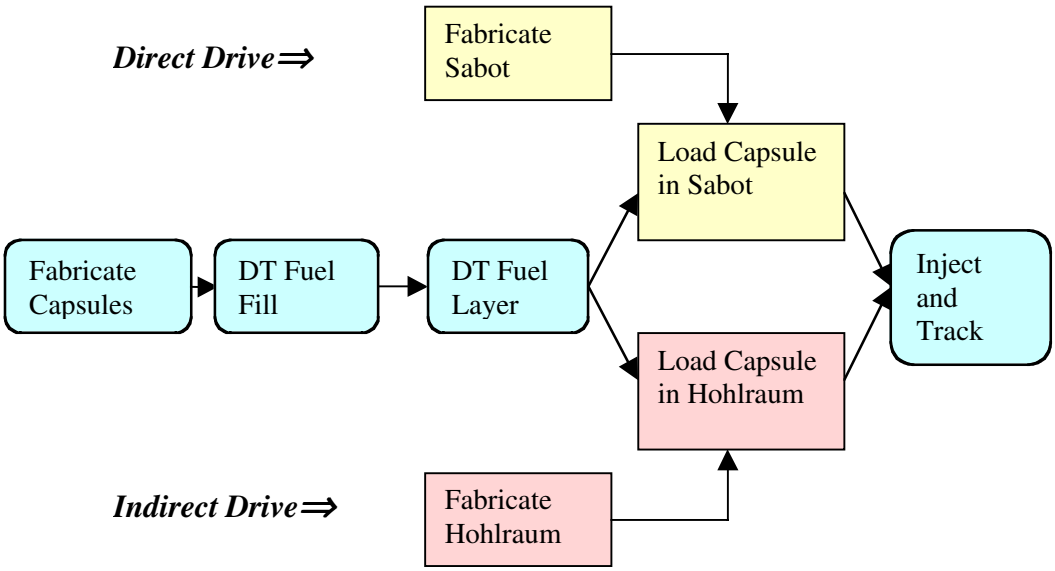

Figure 2. Likely target fabrication sequence for IFE targets.

By leveraging the ICF program technological base, IFE feasibility and proof-of-principle target development efforts have made progress in several areas. In the case of the HAPL targets (see Appendix H), the feasibility of producing foam capsules of appropriate dimensions and density on a batch production basis has been demonstrated. Further work is needed to improve capsule

quality, reproducibility and large-scale production. Methods have been demonstrated to apply the overcoat to the foams and apply a DT-permeable, IR-reflecting layer outside the target. Modeling of the DT-fuel filling process has indicated that capsule filling systems can operate with acceptably low (<1 kg) tritium inventories. Other initial steps have been taken to address the open questions concerning the feasibility of high-rep-rate fusion-target manufacture and injection into a chamber, such as DT-ice-layer formation in foams; and layering of multiple targets in a fluidized bed (using a surrogate fuel material at room temperature to simulate DT ice). In the case of HI targets, hohlraum production using advanced fabrication processes like those used for micro- and nano-electronics component fabrication has been identified, and experiments to demonstrate the use of laser chemical-vapor deposition as a means of producing low-density metal foams are underway.

Each of the individual processes needed for ignition-target fabrication has been conceptualized or demonstrated at some level, but neither direct-drive nor indirect-drive targets have yet been fabricated that meet the stringent specifications needed to achieve ignition, even for single-shot ICF. Although the integration of these processes to produce the required targets has not yet been demonstrated, there are no barriers known at this time that should prevent success.

Targets for Z-Pinches are also being investigated conceptually, and Fast-Ignition targets and target production processes are being scoped for a range of compression drivers. The HAPL program has built a target injection facility and used it to accelerate surrogate IFE direct-drive targets to the proper velocity, and to demonstrate the concept of the separable sabot. These tests have been done both single-shot and in 3-shot bursts. The facility could also be used to study injection of HI and FI targets. An upgrade for rep-rated use with cryogenic targets should be completed in the future that eventually could accelerate mass-produced targets that meet fusion power requirements. These should be injected into a high temperature test chamber to demonstrate survival and target tracking in the hostile environment during injection. The target will be shot with a low-energy pulsed laser beam in flight, all at full operating rates of about 6 Hz. A suite of target characterization and in-flight diagnostics will be used to verify the achievement of all aspects of the process.

Assessment Analysis: The metric used by the Panel to assess target fabrication efforts was the progress toward understanding how to mass-produce cost-effective high-yield IFE targets and how to deliver them, as needed, to a fusion chamber. To this end, the individual processes required for fabrication of laser- or HI-beam-driven targets have all been identified and studied individually at some level. Additionally, there are efforts to improve Z-Pinch- and FI-target-fabrication concepts, which are in the early stages of development. Very promising target injection experiments are now underway at a new, versatile facility. The Panel noted that there has been substantive progress concerning each of the key fabrication and injection issues, and moreover that no barriers to the eventual, successful integration of the relevant processes have been identified.

Finding: *Substantial progress in target fabrication has been made, by using a combination of modeling and experiments with surrogate materials, as well as by leveraging the ICF program knowledge base. The work in this area has been of high quality. Current-day targets do not meet all ignition specifications, but concepts for producing practical IFE targets have been developed and there is a plan to demonstrate these concepts. However, many difficult questions have yet to be addressed experimentally. The IFE program will benefit from continuing its emphasis on high-rep-rate target production and target placement in the chamber, including near-term fabrication of materials and targets for testing of physics codes and the development of long-term solutions*

for mass production. The planned elimination of OFES funding for target fabrication is not consistent with its importance to the HI-IFE program.

3.2. Drivers

3.2.1. Heavy-Ion (HI) Accelerator Drivers

Worldwide experience with high-energy accelerators has long supported the prospect that an HI-accelerator driver for IFE can achieve the necessary efficiency, pulse-rate, and durability. As a result, the DOE has supported HI-fusion research since the late 1970s. Recent power-plant studies and research in the US and Germany predict additional favorable HI-fusion characteristics including efficient ion-target coupling, compatibility with indirect-drive targets and thick-liquid-wall chambers, and the durability of focusing magnets.

The major near-term challenge for HI-fusion is to achieve the beam brightness on target required for ignition and high gain, as described earlier in Section 3.1.1. In the longer term, an experimental target-matter interactions program will be needed that is comparable to those presently underway for lasers and z-pinches. The near-term goal of the HI program, in the area of beam physics, is to determine the physics limits to intense HI-beam generation, acceleration, transport, pulse-length compression, and focusing that most impact the utility of HI beams to study high-energy-density physics (HEDP) and to drive IFE targets in the future.

This goal has been pursued in recent years by science campaigns (experiments, diagnostic development, theory, and simulations) primarily in the areas of:
1. High-brightness beam transport, to determine the technical requirements for preserving high brightness during transport of intense high-current ion beams,
2. Transverse focusing to millimeter spots, to develop a basic understanding of how beam-plasma interactions can be used to optimize the focusing of intense ion beams, and
3. Extensive advanced theory and particle simulations, to model the physics in the experiments, and to explore brightness degradation due to several non-ideal effects.

Research accomplishments in these areas are relevant not only to accelerators for HI fusion and HI-driven HEDP, but also to high-energy particle accelerators, non-neutral plasma physics, the physics of high-intensity particle beams, and particle-in-cell computer simulation development. (See Section 5)

Highlights of Recent Progress. (See details and references in Appendix F.) At low (mA-scale) beam currents, where beam-wall interactions are minimal, normalized beam emittance and brightness were preserved in transport through 86 accelerator elements, consistent with computer simulation predictions. Also at low current and low energy, ballistic focusing of a beam with 1/10 of the charge density of a reactor scale beam was demonstrated experimentally, and neutralizing electrons from a hot filament reduced the focal spot size by an amount consistent with computer simulations. Furthermore, the measured brightness of high-current-density beamlets from an RF-generated Argon plasma source exceeds the IFE brightness requirements.

In transport experiments with over 100-mA beams, the initial low beam emittance (0.5 π mm-mr with envelope parameters within required tolerances) exhibited negligible growth over 10 accelerator units, again as computer simulations predicted. Secondary electron production due to grazing-incidence HI impact of accelerator walls was found to be consistent with other

accelerator data in preliminary experiments. Observations of large (1-2 cm) focal spots in vacuum, due to the effect of high space charge, becoming ten times smaller (1.4 mm) with pre-formed neutralizing plasma added to the transport chamber are in quantitative agreement with computer simulations.

Primary Remaining Issues and Research Plans. Experiments over the next three years (FY04-06, assuming the FY2004 budget and no growth) will use the existing 0.4-to-2-MV beam injectors, together with computer simulations, to address HI-beam losses induced by gas desorption and secondary electrons under space-charge-dominated conditions (space charge potentials > 1 keV). The ultimate goal of this work is to develop a predictive capability for beam loss scaling with magnet-aperture fill factor, field errors, and wall conditions. This research will be of broad interest to the accelerator community. Experiments supported by simulations will also address how the parallel ion temperature increases during strong longitudinal bunch compression under both un-neutralized, and beam-plasma-neutralized conditions. The role of instabilities due to transverse-longitudinal temperature anisotropy, and beam-plasma two-stream instabilities will also be investigated.

Over the next five years (FY04-08), 0.4-to-2-MV experiments and simulations will be carried out to give a predictive capability for focal-spot-size growth due to emittance growth from residual electric fields in target chamber plasma, from longitudinal beam temperature, and due to aberrations in the final focusing magnets. Over that same time frame, beam experiments at 2 to 5 MeV, together with modeling, will evaluate the uniformity with which isochoric heating can be achieved in thin targets. These tests will use short-duration, tailored-current-profile HI pulses to optimize energy deposition for both HEDP and IFE applications. Over the next ten years, experiments intended to fully test integrated beam physics models will be needed. Ultimately, multiple-beam experiments at energies up to 200 MeV will test the characteristics (pulse shaping, focusing, target shimming, etc.) predicted to be optimum for HI-IFE by integrated computer simulations together with hohlraum experiments on Z, NIF and possibly OMEGA. Relevant experiments on these facilities are possible today or in the near future.

3.2.2. Krypton-Fluoride (KrF) Laser Drivers

The decision to pursue KrF lasers as a fusion-energy driver was based on several attributes born out by experience with the NRL Nike facility. (Nike has been routinely used for laser target experiments in support of the NNSA mission since its completion in 1996.) KrF lasers have the short wavelength and demonstrated high beam uniformity for optimum laser-target physics, the brightness to achieve the required intensity on target, the ability to readily adjust spot size to follow the imploding capsule, a modular architecture for lower development costs, and a pulsed-power-based industrial technology that scales to an IFE-power-plant-sized system.

KrF lasers for IFE applications are pumped by counter injecting two electron beams into a laser cell filled with a mixture of krypton, fluorine, and argon. The laser-gas pressure (1 to 2 atm) and the electron-beam parameters (500 – 700 keV, 100 - 500 kA, and 200 - 400 ns) are adjusted to achieve uniform energy deposition across the cell, consistent with efficient laser operation. The laser gas, at around one atmosphere, is isolated from the electron-beam diode, immersed in vacuum, by a foil, which is supported by a structure known as a “hibachi”. The laser beam propagates perpendicular to the electron beam direction. A recirculator flows the laser gas along the third axis to cool and quiet the lasing medium.

For the IFE application, the laser system must meet the fusion energy requirements for repetition rate (5 Hz), efficiency (> 7%), durability (> 3 x 10^8 shots, or two years at 5 Hz) and cost (< $400

per Joule). These numbers come from power plant studies, and assume the target gain is at least 120. (Current target designs have gains at 150 or more.) The goal of the NRL Electra Laser is to develop the science and technology required to meet these requirements. Electra was started in 1999 and is funded by NNSA as part of the Congressionally mandated HAPL program. In addition, the HAPL program is developing final optics that are robust at high laser power and can survive target radiation and debris for the long lifetimes needed for IFE.

Highlights of Recent Progress. The Electra laser produces over 650 J of laser light in short repetitive bursts and uses technologies that can scale to a full-size system (See Appendix G). The requirements for repetition rate and the cost of the pulsed power component of the laser (< $10/Joule) have been met, and overall efficiencies of about 7.4% have been projected based on experiments and modeling of the individual components. The ability to project such a favorable efficiency, which meets the requirement, is based on four advances: 1) Identification and stabilization of the "transit time instability" that previously plagued large-area electron-beam diodes. This was accomplished through experiments, theory, and 3D particle-in-cell computer simulations. 2) Development of an advanced diode/hibachi geometry that configures the electron beam to miss the hibachi ribs. These two advances increased the electron deposition efficiency into the laser gas from 35-40% to over 75%. More than 80% is predicted for a fusion scale system. 3) Operation as a KrF oscillator, which leads to a projected intrinsic efficiency for an amplifier of greater than 12%. 4) Development of an all-new, solid-state laser-triggered switch, which will be the basis for an ultra fast, efficient pulsed-power system [7]. This pulsed-power system is all solid-state, and therefore is expected to meet the IFE cost and durability requirements.

Primary Remaining Issues and Research Plans. The main outstanding challenge is to develop long-lived hibachi foils. A less challenging, but important issue is the development of long-lived amplifier windows. For the next two years the research campaign will concentrate on these two durability issues and a better understanding of the KrF physics. Foil development requires a coordinated research and development effort in materials, cathode physics, electron-beam transport, and thermal management. Preliminary experiments show the foil can be cooled by periodically deflecting the laser gas, but this needs further work. Window development requires high transmission fluorine resistant coatings that can survive the hostile environment of the cell. One promising candidate is already undergoing initial tests. KrF physics understanding is being carried out with a new KrF Physics Code called "Orestes" [8]. Orestes includes electron deposition, plasma chemistry, laser transport and amplified spontaneous emission (ASE). Deposition and laser transport are treated in 1D, whereas the ASE is modeled in 3D. The code follows over 22 species in at least 130 reactions. The code accurately predicts the behavior of several different KrF systems over a wide range of conditions, but needs further validation before it can be used to design the next generation system, which can cost $100M or more. This validation will be accomplished with experiments on the two amplifiers in Nike and Electra.

The next step, which is intended to start in 2-3 years, is to build a full-scale (50 kJ) beam line. The beam line will consist of eight identical e-beam systems, each about ten times the size of Electra. A fusion power plant is envisioned to have about 50-60 of these beam lines. The beam line will allow resolution of the science and technology issues that need a full-sized system to be properly addressed. This step is predicated on success with Electra, as well as commensurate advances in the other components needed for Laser IFE, including target physics, target fabrication, target injection, final optics, and chamber development.

3.2.3. Diode-Pumped Solid-State Laser (DPSSL) Driver

Solid-state lasers have many applications in science, national security, and manufacturing. For IFE, however, several performance demands are unique, and require a directed R&D program to achieve the goals for fusion as outlined above in the KrF section. The Mercury Laser research and development program, part of the HAPL Program funded by the NNSA, is intended to carry out proof-of-principal steps along the development path to meet these goals. Much of the science and technology foundation for the Mercury system is based on advances made in the ICF program in the early 1990's.

Highlights of Recent Progress. The Mercury laser program (see Appendix H) has activated and operated one of two amplifier heads. In operation at the fundamental wavelength of 1053 nm, Mercury has achieved 34 J in a 15 ns single-shot, and 23 J at 5 Hz for 10^4 shots. The efficiency was 4% in a 5-times diffraction-limited beam. In order to reach this point, it was necessary to develop special diode arrays, an inexpensive mass-producible silicon heatsink (which subsequently became the subject of a technology-transfer action), a new bandwidth-enhanced front-end for the laser (developed with LLE University of Rochester), and the first thermally compensated high-power Pockels cell.

The Mercury Laser DPSSL Program achievements are characterized by scientific investigation followed with technology demonstration. For example, the decision to use the Yb:S-FAP gain medium required an understanding of the $Sr_5 (PO_4)_3F$ (S-FAP) materials science issues including the chemical compositions and lattice structures that characterize transitions in the phase diagram. The compositions and structures of defects led to an appreciation of the instabilities that exist at the melt-solid interface during crystal growth. Eventually, laser medium crystals exceeding requirements were grown using an off-stoichiometry melt, reduced YbF_3 dopant, and highly conditioned power to stabilize the melt-solid interface.

The development of a scalable optical architecture of the system is another highlight of the research. Detailed models were developed by accounting for the quasi-three-level character of the Yb^{3+} laser ion, pump bleaching, and gain; by linking to ray-trace models of the diode pump light delivery via a hollow lens duct; and by coupling a nonlinear model of laser beam propagation. This work led to the development of a new laser architecture that is more robust against nonlinear ripple growth and damage than previous systems.

Another notable multidisciplinary achievement was the development of the helium gas-cooled amplifier. Aerodynamics, heat removal, and stress-optic calculations were combined to design the first high-speed (Mach ~ 0.1) gas-cooled laser slabs. This achievement eventually led to the successful demonstration of the 7-slab (34-J) amplifier.

Primary Remaining Issues and Research Plans. The goals for the Mercury Laser are 10 Hz, 100 J 3-ns pulse, and 10% efficiency. The efficiency goal is for unconverted (1053 nm) unsmoothed light. When the frequency is tripled, the beams are smoothed for IFE, and other practical matters are taken into account, the efficiency is predicted to be around 7%. Significant research and development effort will be devoted in the near-term to implementing the front-end operation with spectral – temporal – spatial tailoring; activation of the second amplifier head with 7 more laser slabs, improved damage resistance for several optics in the system (including the final optics research described below), and implementation of a faster and more extensive control system to rapidly detect optical damage and diode-tile failure. The major scientific issue that demands fundamental understanding is that of optical damage, including the field enhancements arising from surface cracks of different morphologies. It is also important to note that much of the

Mercury research is directly related to the development of high-average-power short-pulse lasers needed for the Fast Ignition concept.

After the 100-J system is functioning at the fundamental frequency, the engineering science effort will focus on designing and implementing a high-average-power frequency-conversion module to yield 351-nm light.

The successor to the Mercury Laser is envisioned as a 4-kJ aperture system. A pressing issue that must be addressed is the management of amplified spontaneous emission (ASE) and stimulated Raman scattering (SRS), which must be modeled in great detail and then experimentally verified at the appropriate scale. Furthermore, larger laser slabs (20 x 30 cm^2 compared to 4 x 6 cm^2 currently) must be fabricated. Several avenues are being investigated including "flat interface growth" to alter the convection currents in the melt, and water-glue bonding which entails identifying a chemically compatible adhesive. Cost is an issue, so a commercial source of low-cost diode arrays must be established.

Final Optics. A HAPL program on final optics for both KrF and DPSSL lasers has begun testing a design concept based on grazing incidence metal mirrors. The radiation and laser-induced threats have been characterized, and facilities for sub-scale components have been assembled to measure laser, x-ray and ion damage. The mirrors have a reflective coating (such as aluminum) bonded to a neutron-damage-resistant substrate (such as silicon carbide). The research has shown that this type of mirror has high reflectivity (>99% has been measured), and high durability (>80% above anticipated laser fluence at prototypical wavelengths and for 10^5 shots). However, the durability must be confirmed in large-scale samples, and eventually, with shot lifetimes required for IFE. The material microstructure and bonding of the reflective coating has been studied in order to improve damage resistance. The damage threat has been modeled for ions and x-rays. Initial x-ray testing has demonstrated single-shot survival and higher shot counts are now being obtained.

3.2.4. Z-Pinch Drivers

A Z-Pinch IFE program was initiated in 1999 following the successes on the Z facility at Sandia, which demonstrated outstanding overall efficiency (15% of the stored electrical energy converted into x-rays). One purpose of the program was to investigate ways to increase the repetition rate of this x-ray source for indirect-drive IFE. The concept of a recyclable transmission line (RTL) was developed to address the principal issue of physically connecting a repetitive pulsed-power driver to a fusion target. In contrast to the Z facility where a massive (8000 kg) transmission line must be removed and cleaned between experiments, in the RTL concept the transmission line is designed to be a low-mass (50 kg) structure that is destroyed along with the target on each shot. By making the RTL from the chamber coolant or from a material that is easily separable from the coolant materials, the RTL materials can be continually recycled to manufacture new RTLs. The continuous on-site manufacturing of the RTLs with the recycled materials means that only a small inventory of transmission lines would be needed. With relatively high per-pulse yields of about 3 GJ, the rep-rate per chamber can be relatively slow (about 0.1 Hz), for a 1-GW(e) power plant. Such a plant would have 8 to 10 chambers with a common RTL and target factory. The RTL concept eliminates the problems of final optics, high-speed target injection, and accurately pointing many beams at a fast moving target. Since it is a relatively new approach, the Z-Pinch IFE program is in the concept development phase of determining if it is feasible and potentially economically attractive for energy production.

The primary research activities have been the following:

1. RTL science, including initial electron flow, power flow uniformity, minimum mass, electrical conductivity, and structural properties, etc., has been investigated in order to determine the basic feasibility of the RTL concept;
2. Repetitive pulsed power concepts have been studied to determine the most appropriate repetitive pulsed-power technology for energy;
3. High-yield target studies have been carried out for yields of ~ 3 GJ; and
4. Conceptual Z-Pinch IFE power plant studies have investigated thick liquid-wall chambers, RTL/target manufacturing feasibility and cost, RTL operational cycle with vacuum and electrical connections, activation analysis, waste stream analysis, etc.

It is noteworthy that in the last two years, ICF implosion experiments using the Z machine radiation drive have coupled nearly 40 kJ of x-ray energy to a capsule and achieved the first fusion neutrons (~8 x 10^{10} D-D neutrons, an order of magnitude higher than has been produced from any other inertial fusion facility) from a z-pinch driven capsule implosion. These experiments have been well modeled, giving further impetus to the Z-Pinch IFE program.

These initial IFE studies were supported by internal (LDRD) funds at SNL. In FY04, a larger program within NNSA is being started, supported by a Congressional initiative of $4M.

Highlights of Recent Progress. (See Appendices I and J for more details and references.) Transmission-line electrical-power-flow-uniformity experiments carried out at the 10-MA level on Saturn showed that the electron flow in RTL candidate material coatings of tin, Al, and stainless steel all initiated rapidly when subjected to high electric gradients such as those that would occur in an RTL in a power plant. RTL masses of 50 kg would have very low electrical losses (~ 10%). Structural analysis shows that a full-scale RTL of mass 50 kg would survive (without buckling) in a chamber background pressure of 10-20 Torr. Manufacturing studies show a ferritic steel RTL cost of about $3.60 each (including capital costs) at the 90% confidence level (which is consistent with the allowed RTL budget assuming 3 GJ yields).

Target studies for 3-GJ yields from the two leading Z-Pinch target-driver configurations (double-ended z-pinch and dynamic hohlraum) require 30-36 MJ of x-ray drive (gains of 80-100), so that both target concepts are contenders for Z-Pinch IFE.

An initial (not optimized) power-plant study was completed for a 1-GW(e) Z-Pinch power plant. The study included a low-activation ferritic steel RTL, the complete recycle operation for these RTLs, vacuum and electrical connections, thick liquid (Flibe) walls, and automation of the RTL process.

Primary Remaining Issues and Research Plans. At this early stage in development, the key issue is still feasibility of the RTL concept. Questions of RTL shape, inductance, material (frozen coolant or easily separable material), mass, electrical characteristics, structural characteristics, manufacturing, recycling, activation, and cost must still be addressed. The primary pulsed-power science issue is the physics of power flow in a high-power-density transmission line. The power-flow limits and the optimal RTL configuration for power flow (coax, triax, convolute, etc.) must be explored. Chamber interface issues, including electrical/vacuum connections, sensitivity to post-shot electromagnetic-pulse/plasma/debris flow up the RTL, and shielding of sensitive power flow feed parts must be examined. Proof-of-principle-scale RTLs for the 1-MA level need to be designed, built and tested. Design, cost, and scheduling of an RTL demonstration on Z needs to be done. RTLs would be of benefit to Z and NNSA by reducing the time required between shots

on the facility. A baseline 60-MA RTL design will be developed to serve as a focus for the continuing development studies.

Possible approaches for the pulsed power to drive the RTLs must be assessed, including Marx generator/water line technology, magnetic switching technology, and LTD (Linear Transformer Driver) technology. A study of long-lifetime repetitive switches will also be necessary. Plans also include the design, construction, and testing of a 1-MA, 1-MV, 100-ns, 0.1-Hz repetitive driver as a proof-of-principle-scale driver.

Since a 3-GJ yield is larger than typical yields for other IFE concepts, shock mitigation with thick liquid wall coolant streams is an issue that needs to be studied. Scaled shock experiments with explosives and water (or other liquid) flows can be used to address this issue. Codes that are benchmarked against these experiments can then be used to model full-scale reactors.

Longer term issues are largely related to optimization, including the optimum high-yield target for the double-ended z-pinch and dynamic-hohlraum configurations and the necessary power-flow geometry for each, the optimum repetition rate, and the development of a practical RTL insertion process at ~ 0.1-Hz rep-rate. All of the parts must, of course, fit together in a viable power-plant configuration, including a survivable chamber, RTL/target production, robotic operation, recycling of materials, heat cycle optimization, etc. Therefore, a complete proof-of-principle system to demonstrate RTL/z-pinch insertion, vacuum/electrical connections to the primary pulsed-power system, firing of the z-pinch, and removal of the remnants, must be designed, built and tested at ~ 0.1 Hz as a precursor to design and construction of larger test facilities.

Comment on Drivers: The OFES-funded HI program concentrates on the scientific understanding needed to accelerate and focus the HI beams needed for IFE target compression. The NNSA-funded KrF and DPSSL HAPL program leverages heavily on the NNSA scientific program for laser-driven ICF, and emphasizes the technical development of efficient, durable, high-rep-rate laser drivers for IFE application. The NNSA-funded Z-Pinch-IFE program leverages off the NNSA-funded Z-Pinch ICF program and has concentrated on concept development of technology permitting a 0.1-Hz repetition rate with the recyclable transmission lines needed for IFE application.

Assessment Analysis: In assessing the quality and appropriateness of the work done on the HI and HAPL drivers, the Panel made primary use of the research goals to be achieved in 5 years, as set down by the community and endorsed by FESAC [4]. The Panel was particularly impressed with the following examples of progress. *For the HI program*: the key science objectives were (i) to carry out validating single-beam, high-current experiments at 10-times-higher line-charge density and, (ii) to perform focusing and chamber transport experiments at intermediate scale. The HI program has met these objectives, with successful experiments carried out at the 100-mA beam level and very successful demonstration of plasma neutralization assisted focusing. *For the laser drivers*: the key technical and scientific objectives were to achieve (i) an energy of several hundred joules in a laser architecture scalable to 2 MJ at a cost of ≤ $500/J; (ii) wall-plug efficiency of 6-10% at a repetition rate of 5 Hz; (iii) reliability of 10^5 to 10^8 shots between maintenance cycles; and (iv) irradiation uniformity of ≤ 0.3%. The HAPL KrF program has made very good progress in reaching most of these goals. The following have been achieved but not yet simultaneously: Energy greater than 650J/pulse at repetition rates of 1 Hz and 5Hz, beam uniformity of 0.2 – 0.3% single shot, and efficiency greater than 7% (predicted from advances in the principal individual components). Only the reliability (owing to the hibachi foil lifetime)

remains significantly below (factor of 100) the 1999 objectives level. The HAPL Mercury Laser DPSSL program has also made very good progress by achieving simultaneously 4% efficiency (at the 1053 nm fundamental) at 23 Joules and 5 Hz for 10^4 shots. Producing the necessary beam uniformity at 100 J and 7% efficiency (at 351 nm) on target have yet to be achieved.

Since the outstanding progress in z-pinch x-ray generation was just beginning to be reported in 1999, there was no comparable set of goals established by FESAC for the Z-Pinch driver. Therefore, the Panel based its assessment of quality and appropriateness of research on the achievement of x-ray power and energy levels from the Z machine to the level needed to carry out ICF compression experiments, the extensive list of recent conference and peer reviewed publications, and the substantial progress reported to us on the concept development of the recyclable transmission line necessary for IFE application of the Z-Pinch driver.

Finding: *The three main approaches (HI accelerators, HAPL, and Z-pinch) are at different levels of maturity. The balance between the science and technology emphasis necessarily varies. The recent progress related to these approaches is substantial and the quality of the science and engineering research is excellent. All approaches are currently on track for developing the science and technology to properly evaluate their potential for IFE.*

3.3. Fast Ignition

The Fast Ignition (FI) concept employs two drivers -- one for compression, which can in principle be any of the four types described in Section 3.2 (KrF and solid state lasers, HI accelerators, and Z-Pinches), and one to ignite a portion of the compressed fuel. The igniter laser must meet challenging requirements including high brightness (10^{19}- 10^{20} W/cm^2) at high energy (~10-100 kJ), a short pulse (~10-20 ps), and small spot size (~20-40 μm). Solid-state petawatt lasers that employ the Chirped Pulse Amplification (CPA) technique are today the most advanced drivers for FI but a KrF laser using transient Raman scattering is also viable.

Fast Ignition potentially offers several attractive features: higher gain, lower driver energy, and more compression-driver flexibility. Without a hot spot, more fuel can be efficiently compressed to the required areal density, ρR, where ρ is the fuel density and R is the fuel radius. Most assessments of the gains achievable with FI assume that the fuel has been compressed to a uniform-density sphere. The main requirement -- and challenge -- for FI is to deliver the ignition energy to the compressed fuel. Petawatt laser energy is nominally deposited in the coronal plasma surrounding the compressed fuel at (or below) the critical plasma density, which is ~10^{-5} of the compressed fuel density ρ. The igniter-laser-beam energy deposition results in a relativistic electron beam. Ignition depends on the successful propagation of that electron beam to the fuel and the effective heating of a small portion of that fuel.

The most developed FI scheme involves the so-called “cone focus” target shown in Figure 1g. In this concept a cone is inserted into a fuel capsule with its tip positioned near where the fuel layer will be at the end of the compression. The cone is made of dense high-Z material to minimize wall motion during the ~10 ns fuel compression. At present both indirect and direct-drive approaches utilize this cone design, although the more limited intervening plasmas associated with direct drive may allow other coronal “plasma clearing “ techniques such as laser channeling. The cone may provide additional benefits by focusing the igniter beam energy, as indicated in recent experiments in Japan (Appendix K).

Highlights of Recent Progress. Numerous experiments have shown energy-conversion efficiencies of ~40% from a petawatt-laser beam into relativistic electrons at relevant plasma conditions for FI. Transport experiments have highlighted the importance of background plasma conditions as well as identifying and exploiting high-energy ions. Fuel assembly experiments done primarily in the US with cone and hemispherical targets utilizing both indirect and direct drive have achieved core densities of ~20-30 g/cm^3 and are well modeled by hydro codes.

The most impressive FI experiments have been performed at the GEKKO facility in Japan (see Appendix K). With a 9-beam cone-focus direct-drive implosion using ~2.4 kJ of 532 nm light and a one-beam "igniter" laser with ~300 joules at 1053 nm in a ~0.5-ps pulse, the experiments showed a three-order-of-magnitude increase in neutron yield (to ~10^7) compared to the 2.4-kJ implosion alone (at ~10^4). A self-consistent increase in ion temperature from 150 eV to 800-1000 eV was also observed. These increases occurred only when the igniter pulse was timed to arrive at the time of peak compression. Although conditions achieved in these experiments are far removed from the regime in which ignition and gain would occur, their success has generated optimism for the prospects for FI.

Primary Remaining Issues and Research Plans. Efficient transport of the relativistic electrons through the plasma corona surrounding the imploded shell and into the high-density fuel is the key scientific issue of the FI concept, and it is a topic of much current research. The giga-amp energetic-electron currents must be largely neutralized by a return current that is composed of relatively cold, highly collisional electrons in order for the relativistic-electron energy to be efficiently transported through the coronal plasma and into the dense core. A wide range of plasma collective phenomena is predicted to occur that could inhibit the energy flow into the core. Experiments and theoretical analyses have shown that the background plasma conditions have a major impact on the transport properties of the high-energy electrons. FI experiments that study energy transport must therefore involve plasmas that mimic the conditions found in an imploded DT target. This represents a significant experimental challenge. There also are substantial computational challenges; these include relativistic laser-plasma coupling and self-consistent, high-energy electron transport with neutralization by cold, collisional electrons, all in three spatial dimensions. New computational methods are being developed to tackle these problems.

The relative ease of transport of energetic ions through the low-density plasma surrounding dense fuel, plus the ability to focus these ions have recently motivated FI concepts that employ ions. Limited experiments to date have shown maximum efficiencies of converting the laser energy to energetic ions of only ~10%, but laser-produced ions have already been used for isochoric heating of plasmas to temperatures of order 60-70 eV [9,10]. Much of the research in the generation and applications of petawatt laser produced ions has been funded by an OFES innovative concepts initiative. This new research topic also has attracted significant interest for its other possible applications, such as radiography, compact accelerators, and novel ion sources.

While there has been substantial progress in FI target design, there is as yet no self-consistent 2D implosion for a cone-focus target that achieves the ideal final state of a uniform density sphere. The limited number of experiments that do not use a cone have not been encouraging.

Research over the next several years will need to focus on the issues of fuel assembly and energy transport at relevant conditions. Modeling of both direct and indirect drive implosions that achieve nearly uniform density core conditions -- validated by experiments on facilities such as OMEGA, Z, NIF, and GEKKO -- is critical. For instance, hemispherical capsule implosions have already been radiographed on Z, in preparation for future FI physics experiments. Integrated

experiments that, if successful, would be "proof of principle" of the FI concept, should soon be possible. If such experiments show great promise, up to 20 beams of NIF could be configured for short pulse operation for a demonstration of Fast Ignition.

Assessment Analysis: FI is an exploratory concept that was funded (at a low level) by the IFE program subsequent to the FESAC report [4] where key 5-year goals for the IFE program were established. As noted above, the promise of FI lies in higher gain and/or lower driver energy for IFE, so quality can be assessed by noting progress in establishing the physics basis to realize that potential. Of particular note was the recent demonstration of increased neutron yield achieved with a 300 Joule FI laser pulse onto a 2.4-kJ 9-beam implosion target plasma in the GEKKO facility. In addition, experiments have shown 40% conversion of petawatt-laser energy into relativistic-electron-beam energy. Well-diagnosed cone-implosion experiments achieved 20 to 30 g/cm^3 compressed core densities.

Finding: *Each of the approaches to IFE may benefit if the technique of Fast Ignition proves effective. Recent experiments on the GEKKO laser in Japan have offered very encouraging indications that efficient igniter-beam energy transport to and heating of a compressed core are being observed. However, since FI is at an early stage of development it would be premature for any of the IFE approaches to rely on the success of FI to achieve an attractive fusion energy system. During the next several years, there is an opportunity to assess the potential of the FI concept utilizing facilities in both Japan and the US (OMEGA, Z, and possibly NIF) through modest OFES investments.*

3.4. Chambers and Integrated Concept Studies

3.4.1. Chamber Science and Engineering

IFE targets emit neutrons, ions, x-rays and gamma rays. Following each inertial fusion target explosion, particles and radiation propagate into the surrounding medium, interact with materials in various states of matter, and finally are converted into heat and, in the case of breeding blankets, fuel to supply further fusion reactions. Depending on the chamber design, the target emissions may interact with solids, liquids, gases and/or plasmas. Chamber science and engineering research in the US explores these basic interactions and attempts to solve key questions related to chamber operability and survival. This research has been carried out with funding from NNSA and OFES.

Highlights of Recent Progress. The HAPL program has adopted a reference chamber concept based on solid first walls, *e.g.,* tungsten armor on steel (see Appendix H). The choice was based on the inherent simplicity of the approach, and the fact that a solid wall is feasible with a direct-drive target whose emissions are dominated by energetic ions and neutrons, and not prompt x-rays. (Only ~2% of the target output is in the form of high-energy x-rays.) Progress has been made on the detailed characterization of post-burn target emissions, energy transport through a gas background and absorption in the surrounding armor. Materials studies have been carried out to better understand the prompt effects of pulsed ion deposition in first-wall armors, including thermomechanical effects as well as ion implantation and transport. Evolution of the chamber environment following target explosions has been simulated numerically in order to establish the ability to propagate targets and driver beams with a repetition rate consistent with economic energy production.

OFES-funded chamber research is currently focused on a chamber concept based on neutronically thick liquid jets to handle the indirect-drive target emissions. This chamber is consistent with the needs of HI fusion and has the potential to simplify the fusion chamber material development challenges. Progress has been made in a range of technical disciplines, including thermal-hydraulics of high Reynolds number jets, aerosol creation and transport, liquid response to high-energy-density x-ray bursts and isochoric neutron heating, and transport of target debris into background gases and magnetic fields. A small fraction of the program has explored laser-IFE issues such as mirror damage and laser propagation.

SNL internal funds have been used for initial studies of Z-Pinch chambers, including neutronics studies, activation analysis, and initial analysis of the RTL breakup following the capsule explosion.

Primary Remaining Issues and Research Plans. The remaining key issues and R&D needs for dry-wall and thick-liquid chambers are quite different. For dry-wall chambers, long-term survival of the chamber armor remains the most visible feasibility issue. The HAPL program has undertaken a series of experiments and modeling to understand materials responses at a microscopic level and to develop damage-resistant armors using engineered microstructures. The experiments are performed on irradiation facilities (x-ray, ion, and laser) at several national labs and universities. "Chamber clearing" (how the chamber returns to a state that allows insertion of a new target and delivery of the driver energy to the target) is an important issue for all IFE approaches. For solid-wall chambers, the HAPL program has developed a code that uses compressible Navier-Stokes equations and an adaptive-mesh grid to model the post-shot behavior in the chamber (Appendix H). Predicting these dynamic interactions requires a detailed understanding of hydrodynamics and radiation transport in the partially ionized afterglow plasma. The modeling will continue, and experiments to test this modeling will use a recently completed small rep-rated laser facility at UCSD.

For thick-liquid chambers needed for HI fusion, the dominant near-term issue is establishing the basic flow configuration while meeting the requirements for neutron shielding and HI-beam transport. Studying the formation and hydrodynamics of stationary and oscillating jets has been the focus of the OFES chamber program over the past 5 years. The results on shape control and droplet formation are encouraging, and warrant a more integrated examination of the complete flow geometry. The generation and transport of aerosols requires further study in order to demonstrate successful propagation of targets and HI beams into the liquid pockets. Rapid absorption of x-rays in liquid surfaces can lead to intense non-equilibrium responses, such as spinodal phase decomposition, with absorbed energy density as high as 10^{12} J/m^3, well into the HEDP regime. Future progress on these issues is in jeopardy due to the planned closeout of IFE chamber research funded by OFES.

Thick-liquid chambers are also under study for Z-Pinch IFE. The key near-term issue is to establish the basic flow configuration that will provide adequate shock mitigation to the structural wall, given the higher fusion yield (3 GJ) per target being planned for this approach.

Assessment Analysis: Much progress has occurred during the past five years in chamber research. A large number of refereed journal publications and presentations at international conferences have occurred during this period. This impressive list speaks clearly to the issue of depth and quality of the research being carried out in this difficult area, which is at the intersection of several traditional disciplines. The Panel notes that all of the elements of a thick liquid wall chamber have been explored both empirically and numerically. Flow geometries include stationary circular and sheet jets, oscillating sheet jets and vortex flows. The flow

formation and hydrodynamics have been demonstrated, including extensive research on flow conditioning that is needed to maintain laminar conditions and avoid hydrodynamic sources of droplet ejection. Another topic of research that has progressed significantly is the understanding of the mechanisms for aerosol production due to pulsed energy deposition. These mechanisms include isochoric heating, phase explosion, and shock-induced liquid fracture.

Finding: *The dynamic response of chambers following target explosions is a critical scientific issue in determining the repetition rate and durability and hence the ultimate attractiveness of all IFE concepts. Important chamber issues requiring further work for their resolution include thick liquid chamber dynamics and shock mitigation, aerosol generation and transport, armor survival, and chamber clearing. The closeout of chamber R&D being planned by OFES is not consistent with its importance to the HI-IFE program.*

3.4.2. Integrated Concept Studies

Integrated concept studies play an essential role in the IFE program by providing self-consistent integrated design options based on the available database as well as technical requirements needed for a viable fusion reactor. The studies foster innovations that help move the science and technology in directions that will meet the ultimate needs. Through analysis and systems integration, the output of concept studies is used to direct R&D towards the highest leverage and most critical tasks. New results from R&D programs are then fed back into concept studies in a continuous cycle of improvement. These studies are needed to identify not just the most effective experiments that need to be conducted in the near term, but also the most cost-effective routes to the evolution of the experimental, scientific and technological programs.

Design requirements are derived from the demands of the marketplace, including reliable plant operation, tritium self-sufficiency, efficient energy conversion, minimal environmental impact, and economic viability. For example, the need for high thermal conversion efficiency drives the design process for both liquid and solid chambers. Examples of how this impacts R&D include:

1. Flibe coolant was chosen for the HI and Z-Pinch liquid chamber largely because it gives reasonable energy efficiency, considering both pumping power and thermal constraints.
2. The operating temperature of dry-wall chamber armor determines damage mechanisms and influences direct-drive target survival during injection into the hot chamber.

Highlights of Recent Progress. A 3-year OFES-funded activity was recently concluded under the umbrella of the ARIES concept studies team. This research explored design windows for chambers, including key driver and target interfaces. Various combinations of target, driver and chamber were explored in order to establish design windows and to identify key research needs. This activity has been completed with no immediate plans for ongoing research.

Also within OFES, the Virtual National Laboratory for HI Fusion has recently published a "robust point design" based on a multi-beam induction LINAC driver [11]. This point design defines key technologies, nominal parameters and design requirements for a self-consistent energy source based on HI indirect-drive targets and neutronically thick liquid-wall chambers.

Initial R&D needs for the High Average Power Laser program were defined largely based on earlier studies, such as the Sombrero KrF Concept [12], ARIES [13], a DPSSL concept study [14], and new target physics results [15]. The HAPL program has spent the last four years experimentally evaluating the assumptions and parameters that went into these studies.

Primary Remaining Issues and Research Plans. New integrated concept studies become appropriate when substantial new research results become available. Both the HAPL and Z-Pinch programs are poised to embark on such studies. Based on results from the past 3 years of R&D, the multi-institutional HAPL team will soon undertake a new concept study; the initial Z-Pinch power plant study (ZP-3) [16] will be refined and improved during the coming years as a result of new physics results.

Assessment Analysis: One of the most important measures of the quality of power plant studies is the impact that they have on the base program of R&D. In the IFE program, as in the MFE program, there are many recent cases in which integrated concept studies have affected R&D programs. As a noteworthy example, requirements on cyrogenic target survival emerged from recent power plant studies. In these studies, trade-offs between the minimum gas pressure required to protect dry walls from ions and the maximum gas pressure allowed to avoid target degradation (and hence, unreliable implosion) were clearly articulated. These results significantly affected research in the areas of target physics, target design and engineering, and chamber armor.

Finding: *Integrated power plant studies play an important role in identifying critical issues and in driving innovation in science, technology, and engineering for IFE. The planned elimination of integrated studies is not consistent with their importance to the OFES HI-IFE program.*

4. KEY NEAR-TERM ISSUES

4.1. Summary of IFE Issues

The primary issues currently facing the various elements of the IFE program were identified in the previous section. Now this section of the report summarizes and organizes these issues, and then selects from them the most critical near-term feasibility issues.

Some preliminary comments are necessary to place in proper context both the scientific issues, as requested in the charge letter, and the prevailing views of the IFE community concerning overall program directions. These comments provide the motivation for the way the summary material is organized.

The IFE program is strongly guided by its ultimate goal of fusion energy. The accomplishment of this mission will require research in numerous science and engineering disciplines, as well as integrated systems analysis. The science research covers a rich variety of physical phenomena including plasma physics (neutral and non-neutral plasmas), high-energy-density physics, materials science, nuclear physics, and strongly non-linear hydrodynamics. There is a similar richness in the basic engineering science and technology research required for target fabrication, driver development, and chamber design. The prevailing view in the IFE community is that the most efficient way to achieve its ultimate energy mission is for the required R&D in science and engineering to be carried out in the context of an integrated system, always keeping the end product and its explicit requirements in mind. Consequently, although commercial fusion energy, either MFE or IFE, is still decades away, it is this long-term view that guides the choice of problems to be investigated in the near term – 10 years or less. These near-term issues are the basis of the research plans described in the previous section.

In this context, the three main approaches to IFE – HI, HAPL, and Z-Pinches -- must address issues in the same three major component areas – targets, drivers, and chambers. Below is a brief, generic description of the overall issues that must be resolved for each of these components within the context of a fusion system that is cost competitive and environmentally attractive. Following this generic description is a more detailed discussion that focuses on the most critical near-term issues, directly addressing the request in the charge letter. These issues are organized approach-by-approach, consistent with the need for a long-range integrated plan.

- **Target Issues:** The overall goal is to produce a target design that has sufficient gain for fusion energy, and that can also meet the requirements for the rates of fabrication and injection into a hostile reaction-chamber environment. The near-term issues focus on hydrodynamic instabilities, and symmetric and asymmetric implosion dynamics needed for ignition and high gain. IFE target research has been primarily focused on symmetric implosions although the relatively new and novel idea of Fast Ignition requires an asymmetric implosion. The long-range issues involve the design, characterization, and cost-effective manufacture of targets, and their injection or placement in the chamber.

- **Driver issues:** The overall goal is to develop a driver that can meet the fusion energy requirements for power focusing, efficiency, repetition rate, and durability. These requirements are, of course linked to the performance of the target. For example, the lower the target gain, the higher the required driver efficiency. Thus, the near-term research issues are driver efficiency, power focusing, pulse shaping, overall target energy gain, and energy absorption by the capsule. The long-term issues are durability and reliability at high-rep-rate,

especially of the energy-delivery or focusing components that are exposed to the chamber environment.

- **Chamber Issues:** The overall goal is to design a chamber that can meet the requirements for wall durability, while allowing highly reliable target injection/placement, and efficient driver-energy delivery to the target. The near-term issues focus on radiation transport, rapid energy deposition by neutrons, charged particles, and x-rays, on wall materials, shock stresses on the walls, and understanding the post-pulse chamber environment and, for HI and HAPL, its impact on beam focusing and propagation and on target injection. The related long-term issues involve the development of the survivability of first walls and high rep-rate capability, while allowing the accurate and rapid injection/placement of targets into the chamber. These capabilities must also be consistent with efficient energy conversion, tritium production, and environmental acceptability.

The near-term issues from the above list were examined to identify which ones appear to be the most critical. The critical issues of ignition and burn affect all of the approaches, but those challenges are being addressed mainly by the ICF program. For that reason, they are not considered here as candidates for the single most important near-term issue facing each IFE approach and the FI concept. The remainder of this section describes these issues and how progress therein can lead to substantial improvements in the long-range overall desirability of IFE.

4.2. Heavy-Ion Fusion

The key near-term challenge for HI fusion is the focusing of HI beams to a very small spot size (~2 – 5 mm radius) and compressing the pulse length to a few nanoseconds. This focusing and compression must be accomplished at progressively higher intensity levels to ultimately meet the requirements of a high-gain fusion target.

The solution to the problem requires substantial research in plasma physics. The electric space charge of a non-neutralized ion beam tends to spread the beam out. This effect can be mitigated by introducing plasma into the beam path. Smaller beam spot sizes are achieved, because the plasma neutralizes the space charge, but at the expense of some growth in the beam temperature. This temperature and any small spread in energies about the beam velocity will limit how small the spot size and pulse duration can be made.

The near-term goal is to develop a sufficient understanding to identify techniques that minimize the effects of space charge and temperature on beam spot size at the target. This requires that the beam dynamics be controlled with high precision along the entire beam trajectory through the accelerator and target chamber. A fundamental understanding of the collective processes and nonlinear dynamics of intense, high-brightness, HI beams, and accelerator systems is essential to progress.

The research plans for the next five years will make use of the existing 400-keV and 2-MeV ion-beam facilities and existing particle-in-cell codes in the HI program. The science campaigns (experiments and simulations) will address key intense beam physics issues in high-brightness beam transport, longitudinal bunch compression, and final focusing with plasma neutralization. With some enhancements, these facilities and codes will also be sufficient for achieving a successful outcome to the OFES/OMB 10-Year Measure for Inertial Fusion Energy (IFE) and High Energy Density Physics.

The most critical near-term issue facing HI fusion can thus be summarized as:

> *Physics limits to the maximum phase-space density of space-charge-dominated HI beams and the resulting implications for HEDP and fusion ignition.*

4.3. Laser Fusion

For laser fusion the critical near-term goal is to demonstrate a path to achieving an overall energy gain that is sufficient for practical fusion energy. There are two key elements for achieving this goal. One is to produce a reliable, durable laser that can meet the IFE requirements for efficiency. This is the motivation for the KrF and DPSSL research in the HAPL program. The second element involves the design of higher gain targets that are readily fabricated in large numbers. Much of this research is carried out under the auspices of the NNSA ICF program[5]. Note that these two challenges are inextricably linked, in that capsule gain can be traded for laser efficiency.

KrF lasers have very smooth beam profiles and a fundamental wavelength of 248 nm that is ideal for coupling to a direct drive target. The primary near-term challenge is to discover ways to maintain the predicted efficiency and realize durable long-lived "hibachi" foils through which electron beams are injected into the laser gas. This will require research into electron-beam generation, electron-beam physics, and the physics and chemistry of materials. Furthermore, these foils cannot be investigated in isolation but must be developed as part of a fully integrated laser system. Based on current R&D, which show KrF laser efficiencies predicted to be 7% or greater, and target gain calculations exceeding 150, projected KrF-laser IFE efficiencies are consistent with a viable power plant.

For DPSSLs the beam smoothing is not as effective as for KrF, and the fundamental wavelength is 1053 nm. As result, the frequency must be tripled for ICF/IFE applications, and beam smoothing presents an important challenge. The near-term challenge facing the DPSSL approach involves discovering ways to meet the 7% efficiency requirement at the tripled frequency and to improve beam smoothing at progressively higher energy levels. This will be done along with specific research aimed at understanding damage resistance of key semiconductor optical components.

Turning to targets, the most important near-term issue is Rayleigh-Taylor instabilities seeded by non-uniformities in the laser deposition profile or in the target. This hydrodynamic instability must be suppressed sufficiently to allow the required high gains from the direct-drive target.

Recent innovations hold promise for mitigating the impact of hydrodynamic instabilities, including using high-Z target coatings to reduce beam imprint, and tailoring the target's post-shock entropy profile. Simulations and experiments indicate that a carefully designed laser pre-pulse shapes the entropy profile and reduces the instability growth such that high gain is predicted for direct-drive targets.

[5] This ICF-funded activity is mentioned here because target gain is of particular importance to the HAPL approach. The efficiency projected for lasers is lower than for HI or Z-Pinch, and therefore higher target gains are required.

In terms of immediate research plans, adequate resources and facilities are in place to address these near-term issues. The DPPSL and KrF laser programs have complete working facilities and supporting theoretical programs, and anticipate that these issues will be resolved on these systems within the next 2-3 years, given continued support of the NNSA/HAPL program. The target issues, including fabrication challenges, will be addressed as part of the ICF program using 2D and 3D codes and experiments on Nike, OMEGA and, when it becomes available, NIF.

Since the target issues are largely being addressed in the ICF program, the most critical near-term issue facing the HAPL program is:

> *Durability of KrF lasers, and efficiency and beam smoothing in DPSSLs, that will scale to the high-energy requirements for IFE.*

4.4. Z-Pinch Fusion

For the Z-Pinch, the critical near-term issue involves the need for a direct physical connection between the pulsed-power supply and the Z-Pinch assembly "target" containing the fusion fuel capsule. This is in contrast to HI or HAPL where capsules are repetitively injected into the chamber and illuminated by multiple driver beams, but without any physical contact between driver and target. The Z-Pinch concept addresses the "direct connection" problem by means of a recyclable transmission line (RTL). On each shot the RTL will be destroyed, but the RTL materials will be collected and continually recycled. A new RTL will be inserted for each shot, with a repetition rate of about once every 10 seconds. Achieving this capability will require the resolution of both scientific and engineering issues.

The key scientific issues for Z-Pinch IFE are related to the power flow in the RTL. The Z machine uses high-power-density transmission lines that work well at the 20-MA level. However, IFE will require ~60 MA or more. Understanding the fundamental limits to power flow in the RTL is the main scientific concern as the currents are raised to IFE levels. Therefore, RTL research will be the focus in FY04 and for several years. The initial RTL experiments can be designed with existing codes (e.g. the ALEGRA MHD code, the LSP hybrid code, and the Quicksilver PIC code) and performed on the Saturn and Z facilities.

Thus, for the Z-Pinch approach to IFE the most important near-term issue is:

> *Physics limitations on power flow in a recyclable transmission line, including the coupling to the pulsed-power driver and the integral target assembly.*

4.5. Fast Ignition

The most critical near-term goal for Fast Ignition is developing an approach to assembling a compressed sphere of fuel of uniform density and then efficiently heating a small part of that sphere under conditions that scale to ignition. The method of achieving the ideal state of a uniform-density sphere has not yet been found, even without the complexity of a cone imbedded in the target. A petawatt igniter laser beam will strongly interact with the plasma surrounding the compressed fuel, and convert about 40% of its energy to a relativistic electron beam. However, the HEDP issues of the beam transport to the fuel and energy deposition in the fuel are not well understood.

In the next several years, research can be carried out on existing or planned facilities to address critical feasibility issues for Fast Ignition. Numerical codes to design targets for fuel assembly exist. Codes to design and interpret energy transport experiments for the igniter-generated beam are required although some aspects of the physics can be addressed today. Plans for FI research include using existing facilities such as OMEGA, Z, and GEKKO in Japan, and then using FIREX1, OMEGA EP, and NIF in the future. Multi-kilojoule petawatt lasers coupled to implosion facilities should be available on OMEGA, Z, and GEKKO in the next 5 years.

Thus, the most critical near-term issue facing the Fast Ignition concept is:

> *Physics of fuel compression to a uniform-density sphere and of energy transport by relativistic electrons to that high-density fuel to achieve ignition.*

5. POTENTIAL CONTRIBUTIONS TO HIGH-ENERGY-DENSITY PHYSICS AND OTHER SCIENCE

The study of physical systems in which various combinations of high temperature, density, ionic charge state, magnetic field, etc., result in pressures exceeding a megabar (equivalently, energy densities exceeding about 1 eV/ angstrom^3) is now commonly called high-energy-density physics (HEDP). As illustrated in Figure 3, high energy density situations arise in astrophysics and planetary physics, as well as in inertial fusion science. The conditions of interest to IFE range from warm dense matter, to hot very dense plasmas, to extremely hot (even relativistic) plasmas. A great variety of HEDP topics is being addressed at universities within the US and abroad. The National Research Council reports, "Frontiers in High Energy Density Physics – The X-Games of Contemporary Science" and "Connecting Quarks with the Cosmos," noted that the intellectual challenges of HEDP stem from the interplay of non-linear, non-perturbative, and in some cases relativistic, many-body phenomena. The interested reader may refer to the first of these documents for a more thorough discussion of many issues discussed below as well as other, related topics. The focus here is on the synergies of IFE/ICF research and HEDP, plus some other applications of IFE science and technology.

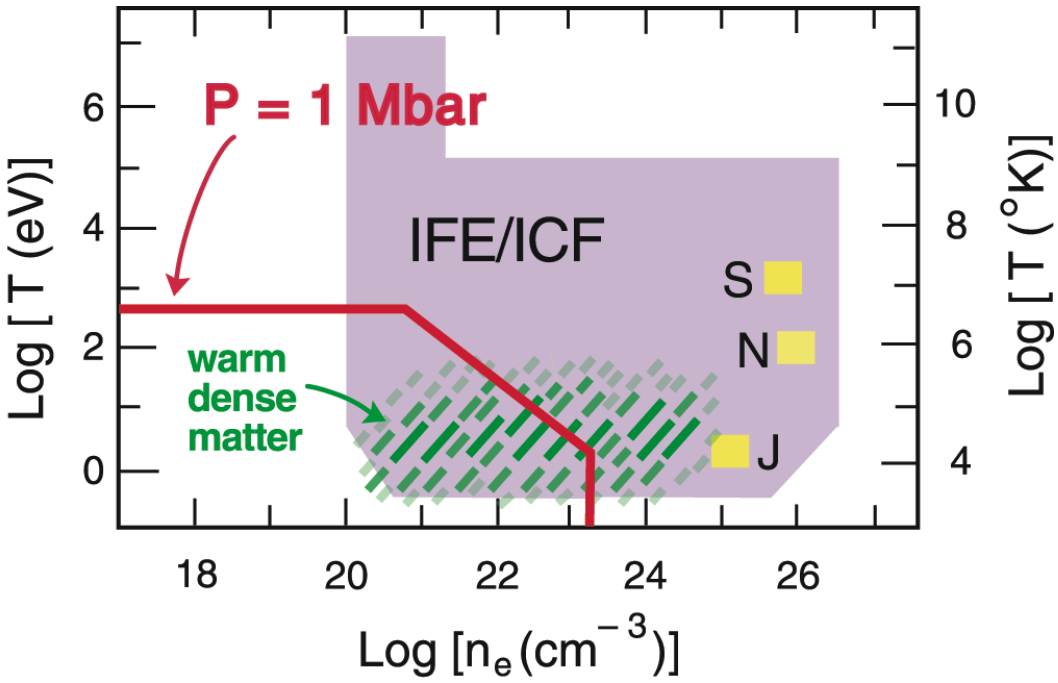

Figure 3. Some important high-energy-density regimes in the temperature-density plane. Above and to the right of the solid red line pressures exceed 1 Mbar; segments represent contributions due to radiation (P~T^4), ideal gases (P~nT), and degenerate electrons (P~n$^{5/3}$). The shaded region indicates the large range of conditions encountered or expected in some aspect of IFE/ICF research. Small squares identify astrophysical conditions characteristic of the cores of the sun (S) and Jupiter (J), and the surface of a neutron star (N). Warm dense matter lies within the hatched green area.

The ongoing development of the physics basis for fusion ignition and burn has been a driving force in a wide range of HEDP experiments. Substantial progress has been made within the NNSA-sponsored ICF program, but the need to achieve ignition, and then to achieve high gain in IFE targets, is pushing the limits of understanding of HEDP phenomena. An understanding of the physics of warm dense matter is also important for science and technology developments in the IFE and ICF programs and other aspects of the Stockpile Stewardship program, as well as planetary science and astrophysics. Thus there are natural synergies among topics in HEDP, in warm dense matter physics, and in the ICF and IFE programs.

The development of rapid-shot-rate capabilities is a requirement for IFE. As these capabilities become available they could be used to enhance the accessibility of experimental facilities used to study HEDP and warm dense matter regimes. Existing major facilities that are in high demand could be modified, or additional intermediate-sized facilities could be built that would enhance availability to a broader range of users. This "shot-on-demand" could potentially meet any rate that would be useful for research on such facilities, which would likely be less than several tens of shots per day compared with the many per minute required for IFE. This potential benefit to HEDP and other areas of science is described further in the sections that follow.

5.1. IFE Synergies with High-Energy-Density Physics and Astrophysics

There are numerous examples of HEDP phenomena being studied in the laboratory that also occur on cosmic scales [17]. Hydrodynamic instabilities similar to those observed in ICF afflict supernovae and have been modeled by similar numerical methods. The study of radiation transport in ICF-relevant regimes has resulted in improved understanding of radiative jets and related astrophysical phenomena. The need for better opacity data led to opacity experiments with iron that have improved models of Cepheid variables. The need for better equation-of-state (EOS) data for hydrogen is leading to a wide body of research important for understanding the interiors of large gaseous planets and objects outside of our solar system [18].

High-energy petawatt lasers can potentially facilitate laboratory astrophysics experiments that probe matter in the presence of intense, quasi-static magnetic fields (B) such as found in certain white dwarf stars (B~10^8 Gauss), and in the crusts of some neutron stars (B~10^9 Gauss). Spectroscopic and EOS data for this regime are needed to validate astrophysical models that will be used to interpret data from present and future space observatories.

There are other astrophysical applications. Fast Ignition calls for laser fluxes of order 10^{20} W/cm^2, hence energy densities exceeding 10^4 eV/Angstrom^3 and relativistic electron quiver velocities, to create a multi-MeV electron beam that ignites the fuel. Such laser fluxes would open up new regimes of laser-plasma interaction that should have astrophysical relevance. For instance, it has been suggested [19] that the Weibel instability of such beams is also responsible for the magnetic fields of relativistic collisionless shocks in gamma-ray bursters. This astrophysical instability has been studied with codes that were developed for laser-driven plasmas [20].

The dynamic response of warm dense matter to several Mbar pressures, temperatures of several hundred eV, *and* with controlled megagauss-magnetic-field conditions can be investigated using the Z machine. As an example, recent studies have used lasers and the Z machine for accessing warm dense matter regions of the phase diagram of hydrogen and its isotopes that are inaccessible

with other facilities [21,22]. This type of research could be conducted in a more timely way if the IFE-funded development of RTL technology for the Z machine and the HAPL technology are successful in providing shot-on-demand capabilities.

HI beams have a potential role in HEDP EOS studies since calculations suggest that properly tailored HI energy profiles produced in short pulses can heat solid targets with better than a few percent uniformity. If target thickness is short compared to the ion range, it is thought that short HI pulses could deposit energy in solid targets at energies near the Bragg peak, heating them at constant volume (isochoric heating). These experiments would thus be valuable for determining EOS properties of important materials along trajectories in pressure-temperature-density space corresponding to warm dense matter. This information is presently a critical need of the scientific community and would have a broad impact across several scientific disciplines and programmatic activities.

5.2. IFE Synergies with the NNSA-funded ICF Program

DPSSL and KrF lasers could be used to perform dense plasma experiments in support of ICF applications. Data are needed from EOS experiments for optimizing shock timing in ICF implosions, from studies of laser-plasma interactions, and from studies of plasma opacities, all of which provide a foundation for validating advanced ASCI material models. The improved statistics that arise from a large number of experiments should prove valuable. Such "shot-on-demand" capabilities may also be extended to studies needing short-pulse, high-energy pulses using either specially configured DPSSL or KrF lasers. Examples of HEDP topics for these capabilities include EOS [23], intense ion-beam generation and use [9,10], filamentation and nonlinear Brillouin scattering [24,25] saturation mechanisms for parametric instabilities [26,27] and many-body collisional effects in dense plasmas [28].

Near-term improvements in Electra potentially allow substantial advances in the energy and pulse shaping capabilities of Nike, which could benefit the NNSA ICF program. Because of the shot-on-demand capability, HAPL can also contribute to the development and testing of higher photon energy x-ray backlighting techniques that would be useful in ICF applications. An attractive feature of Mercury is that beam-plasma or ion-surface interaction experiments can be performed with infrared, green or blue, as well as ultraviolet light, which would be useful to fundamental studies of optical damage thresholds, testing of large area optical elements, and calibration of experimental diagnostics.

IFE target fabrication research can benefit the NNSA ICF program. Examples include: foam capsules envisioned for IFE high-yield targets that are now beginning to be used at OMEGA; IFE studies of DT material and thermal transport properties that are synergistic to an overall understanding of DT-ice behavior (and tritium handling in target systems) important for ICF targets; and IFE layering research with foam capsules that potentially has substantial impact on NIF indirect drive cryogenic capsule development. In the area of high-precision target placement, IFE injection techniques could potentially be utilized on NIF to reduce the amount of debris-producing material near the implosion. Progress toward the central objective of IFE target research – namely, producing low-cost targets with high-yield – may in the future lead to still more developments useful to the ICF program, as well as in HEDP research.

Development of armor for solid wall IFE chambers could provide a means of protecting high value components inside an ICF chamber of a high-yield facility such as NIF. Innovative energy-absorbing materials tested in the HAPL program already have been evaluated for use on NIF as

beam dumps or localized debris traps. Methods of debris mitigation, such as magnetic deflection, could be applied to diagnostics or other sensitive in-chamber components.

From a complementary perspective, there also are a variety of ways that the ICF scientific program can continue to make major contribution to IFE efforts. The baseline approach to ignition on NIF is indirect drive. Since the capsule physics, as well as the physics of x-ray transport and energy balance within hohlraums, is largely independent of the source of x-rays, the process of reaching ignition on NIF would yield much of the critical target physics base for HI and Z-Pinch targets. NIF can also address the critical ignition physics for direct-drive targets essential for current laser IFE concepts when enhanced beam smoothing techniques are implemented. Valuable early results for direct-drive targets could be obtained with planar targets using a subset of NIF beams and possibly by carrying out polar direct-drive experiments on NIF. Following initial demonstration of ignition, there will be important experiments which can be done on NIF to test such issues as the performance of targets that could be mass manufactured for IFE applications. Several workshops [29-34] have identified a variety of IFE related experiments that could be carried out on NIF. In addition to potential experiments on NIF, other NNSA facilities also can be used to address important IFE target physics issues. For example, symmetry control techniques that are common between Z-Pinch targets and HI targets are now being studied on Z.

The high-energy petawatt capabilities being implemented on Z, OMEGA, and NIF will be essential for developing the physics of Fast Ignition. If warranted NIF could be modified for a Fast Ignition demonstration.

5.3. Potential IFE Contributions to Other Scientific Disciplines

A wide variety of experimental studies of condensed matter under rapid loading is required for developing *ab initio* theories of material response. A major issue in condensed-matter physics concerns development of complete equations of state to accurately describe material response. This requires accurate information in high-pressure, high-temperatures regions, as well as high-pressure, low-temperature regions. Since many applications involve the transition of a solid from one crystalline form to another in nanosecond or shorter times, it is also important to understand the fundamental scientific issues involving the thermodynamic conditions and kinetics of how these polymorphic transitions occur.

The development of Recyclable Transmission Lines (RTL) on the Z machine would allow increased access that could potentially accelerate its use for condensed-matter physics studies, including the recently developed technique on Z for producing isentropic compression experiments that are unique in the high-pressure scientific community. This capability produces relatively cold states of matter to multi-Megabar pressures that far exceed the capabilities of any other existing technique, such as diamond anvil cells and gas guns. It has also proved useful in high-pressure isentropic EOS studies [35], studies of radiation defects on dynamic material response [36], and transformation kinetic studies of polymorphic phase transitions [35].

The development of more efficient pulsed-power sources through the IFE program (both Z-Pinch and HAPL) is also allowing development of compact generators for a variety of applications. Such systems have considerable commercial potential and a spin-off system from the Z machine for materials studies is already being marketed.

The HI-beam accelerators being studied for IFE applications are proving useful for exploring gas-electron cloud effects caused by HI-beam losses in quadrupole transport channels in accelerators. These effects are important in accelerators used for a variety of nuclear physics studies, such as the structure of heavy nuclei and properties of rare isotopes produced when beam ions collide with ions in dense plasmas [37]. HI research also provides opportunities to investigate fundamental beam physics issues. These include determination of: (1) technical requirements for preserving high beam brightness during beam transport, (2) a basic understanding of beam-plasma interactions for focusing beams, and (3) conditions for achieving longitudinal beam compression.

The very high beam uniformity of KrF lasers should be attractive for a broad range of scientific investigations including material science studies of large-scale thin-film optics coatings, and evaluation of optically induced laser damage mechanisms over large surfaces. Higher test rates and less expensive targets, both of which should evolve through the HAPL program, will allow fundamental discovery experiments for understanding basic physics and materials issues. Many aspects of the science and technology involved in the HAPL program are also applicable to the emerging field of extreme UV lithography for next-generation semiconductors. These aspects include: efficient high average power pulsed lasers, low-cost mass-produced targets, precise high-throughput target alignment, optimized laser-target coupling for efficient radiation production, and mitigation of debris from expanding laser plasmas.

Finding. *IFE capabilities have the potential for significantly contributing to HEDP and other areas of science. Isochoric heating of substantial volumes to uniform, elevated temperatures should be achievable using HI beams. Investigations of the Fast Ignition concept can lead to exploration of exotic HEDP regimes. Moreover, the rapid turn-around capabilities envisioned for IFE drivers could accelerate progress in HEDP science by enabling a wide community of users to conduct "shot-on-demand" experiments with data rates and volumes far exceeding those obtained on large systems that currently require long times between shots.*

Finding: *The NNSA-funded ICF program has the vital role of achieving ignition, and its research on target physics offers tremendous leverage that allows the comparatively modest funding for IFE-specific programs to continue to yield important advances. Carrying out a coordinated IFE research program now will guide future experiments on OMEGA, Nike, Z, and soon NIF, to develop the advanced target designs that not only meet the IFE physics requirements of high gain, but also the IFE requirements for fabrication, injection, and recycling.*

Finding: *IFE research directly benefits the NNSA mission. A vigorous IFE research program will continue to foster innovation that may lead to improved NNSA capabilities in targets (design, fabrication, and characterization), driver performance, and chamber/optics components.*

6. REFERENCES

1. R. C. Davidson, chair, "Frontiers in High Energy Density Physics – The X-Games of Contemporary Science," National Research Council Report (2003).

2. R. Goldston, chair, "A Plan for the Development of Fusion Energy," Final Report to FESAC, March 5, 2003, page 18.

3. N. A. Davies, Presentation given to FESAC, November 17, 2003.

4. C. Baker, chair, "Report of the FESAC Panel on Priorities and Balance -- Meeting in Knoxville, TN, August 18-21, 1999," September 13, 1999.

5. C. Baker, chair, "Report of the Panel on Criteria, Goals and Metrics," Final Report to FESAC, October 8, 1999.

6. R. Bangerter, G. Navratil, and N. Sautoff, co-chairs, "2002 Fusion Summer Study Report – Next Major Steps in Fusion," Snowmass, CO, June 2003.

7. D. Weidenheimer, *et al*., "Advanced Pulsed Power Concept and Component Development for KrF Laser IFE," International Power Modulator Conference, Hollywood, CA, June 30-July 3, 2002.

8. R. H. Lehmberg and J. L. Giuliani, "Simulation of Amplified Spontaneous Emission in High Gain KrF Laser Amplifiers," *Journal of Applied Physics*, **94**, 31 (2002).

9. R. A. Snavely, *et al*., "Proton Beam Focusing and Heating in Petawatt Laser-Solid Interactions," Proceedings of IFSA 2003.

10. P. Patel, *et al*., "Isochoric Heating of Solid Density Matter with an Ultrafast Proton Beam," *Phys. Rev. Lett.* **91**, 125004 (2003).

11. S. S. Yu, *et al*., "An Updated Point Design for Heavy Ion Fusion," *Fusion Sci. Tech.* **44** Sept. 2003, 266-273.

12. W. R. Meier *et al*., "Osiris and Sombrero Inertial Fusion Power Plant Designs," WJSA-92-01, DOE/ER/54100-1, March 1992 (http://aries.ucsd.edu/LIB/REPORT/OTHER/OSIRISOMBRERO/).

13. F. Najmabadi, *et al*., "Assessment of Chamber Concepts for Inertial Fusion Energy Power Plants - The ARIES-IFE study," Inertial Fusion Science and Applications 2001, Kyoto Japan, Sept. 2001, 701-705.

14. C.D. Orth, S.A. Payne, and W.F. Krupke, "A diode pumped solid state laser driver for inertial fusion energy," *Nuclear Fusion* **36**, Number 1, January 1996.

15. S. E. Bodner , *et al*., "High-Gain Direct-Drive Target Design for Laser Fusion," *Physics of Plasmas* **7(6),** June 2000, pp. 2298-2301.

16. G. E. Rochau, *et al*., "ZP-3, A Power Plant Utilizing Z-Pinch Fusion Technology," Inertial Fusion Sciences and Applications 2001, Elsevier (Editors: K. A. Tanaka, D. D. Meyerhofer, J. Meyer-ter-Vehn), 706 (2002).

17. D.D. Ryutov and B.A. Remington, "Scaling astrophysical phenomena to high-energy-density laboratory experiments", *Plasma Physics and Controlled Fusion* **44**, B407 (2002).

18. T. Guillot, "Interiors of Giant Planets Inside and Outside the Solar System." *Science* **286**, 72 (1999).

19. M.V. Medvedev and A. Loeb, "Generation of magnetic fields in the relativistic shock of gamma ray burst sources", *Astrophysical J.* **526**, 697 (1999).

20. L.O. Silva, *et al*., "Interpenetrating Plasma Shells: Near-equipartition Magnetic Field Generation and Nonthermal Particle Acceleration." *Astrophys. J. Lett.* **596**, L121 (2003).

21. G.W. Collins, *et al*., "Measurement of the equation of state of deuterium at the fluid insulator transition," *Science* **281**, 1178 (1998).

22. M.D. Knudson, *et al*., "Equation of state of liquid deuterium to 70 GPa", *Phys. Rev. Lett.* **87**, 225501-1 (2003).

23. Widmann, *et al*., "Interferometric investigation of femptosecond laser-heated expanded states," *Physics of Plasmas* **8**, 3869 (2001).

24. D. Pesme, *et al*., "Resonant Instability of Laser Filaments in a Plasma," *Phys Rev. Lett.* **84**, 278 (2000).

25. D.E. Hinkel, *et al*., "National Ignition Facility targets driven at high radiation temperature: ignition, hydrodynamic instability, and laser-plasma interactions," *Phys. Plasmas* **11**, 1128 (2002).

26. E.A. Williams, *et al*., "Effects of ion trapping on crossed-laser-beam stimulated Brillouin scattering," *Phys. Plasmas* **11**, 231 (2004).

27. H.X. Vu, *et al*., "Kinetic inflation of stimulated Raman backscatter in regimes of high linear Landau damping," *Phys. Plasmas* **9**, 1745 (2002).

28. M.S. Murillo and J.C. Weisheit, "Dense Plasmas, Screened Interactions, and Atomic Ionization," *Physics Reports* **302**, 1 (1998).

29. Tobin, *et al*., "The role of the National Ignition Facility (NIF) in developing Inertial Fusion Energy, Lawrence Livermore National Laboratory, UCRL0JC-114042-ABS, 1993.

30. B.G. Logan and M.T. Tobin "The Role of NIF in Developing Inertial Fusion Energy," Energy and Technology Review, Lawrence Livermore National Laboratory, Livermore, California, UCRL-52000-94-12, 33-42, (December 1994).

31. B.G. Logan, *et al*., "Utility of the U.S. National Ignition Facility for Development of Inertial Fusion Energy," Lawrence Livermore National Laboratory, Livermore, California, UCRL-JC-117018, IAEA-CN-60/B-P-15, (1994).

32. Tobin, *et al*., "Use of the National Ignition Facility for the Development of Inertial Fusion Energy," Lawrence Livermore National Laboratory, Livermore, California, UCRL-JC-117395, (1994).

33. Tobin, *et al*., "Contributions of the National Ignition Facility to the Development of Inertial Fusion Energy," Lawrence Livermore National Laboratory, Livermore, California, UCRL-JC-117698 Rev. 1, (1994).

34. M.T. Tobin, *et al*., "Utility of the National Ignition Facility for Inertial Fusion Energy and Radiation Sciences Experiments," Proc. 12th Topical Mtg. Technology of Fusion Energy (Reno, Nevada), June 16-20, 1996.

35. C.A. Hall, *et al*., "Experimental configuration for isentropic compression of solids using pulsed magnetic loading", *Rev. Sci. Instr.* **72**, 3587 (2001).

36. D.B. Reisman, *et al*., "Isentropic compression of irradiated stainless steel on the Z Accelerator," *J. Appl. Phys.* **93**, 8952 (2003).

37. OFES – German Government official agreement, "Implementing Agreement between the Department of Energy of the United States of America and the Federal Ministry of Education and Research of the Federal Republic of Germany", The Department of Energy of the United States of America and the Federal Ministry of Education and Research of the Federal Republic of Germany.

7. APPENDICES

Appendix A
Charge Letter

July 17, 2003

Professor Richard Hazeltine, Chair
Fusion Energy Sciences Advisory Committee
Institute for Fusion Studies
University of Texas at Austin
Austin, TX 78712

Dear Professor Hazeltine:

In response to the considerable scientific and technical progress in the Inertial Fusion Energy (IFE) program during the past few years, I am requesting that FESAC carry out a review of DOE's IFE program to provide an assessment of the present status of the program. Due in part to Congressional action, IFE relevant programs reside in both the Office of Science and in the Office of Defense Programs(DP) within NNSA, therefore, this charge is somewhat broader than those normally submitted to FESAC. Both SC and DP support this review and concur that it be carried out by FESAC.

The inertial path to fusion energy has been pursued by the Office of Fusion Energy Sciences (OFES) over the past 12 years. OFES has mostly funded the heavy ion beam driver and associated technologies component. DP as part of its Inertial Confinement Fusion (ICF) program, has funded high energy density physics facilities (including the National Ignition Facility) and the "target physics" relevant to ICF. The success of DP's ICF ignition program has always been viewed as a necessary precursor to the demonstration of IFE. Over the past four years, because of the strong DP laser program and DP's ICF efforts, Congress has added significant resources to the DP budget to develop the high average power laser (HAPL) driver. The DP program for the HAPL driver and related technology will have a long-term impact on the future development of IFE, and needs to be evaluated in the overall context of the Office of Science's IFE mission and program.

The specific topics to be addressed in this review are:

1. The current status of the scientific basis and related technology of each of the approaches to IFE, including an assessment of the quality of work being carried out in the programs.
2. Critical scientific issues identified in each of the approaches to IFE that would contribute to understanding the long-range potential of IFE.
3. The impact that fast ignition as a concept improvement may have on IFE.
4. The potential contribution of the various IFE program elements to the emerging field of High Energy Density Physics.

The IFE approaches to be considered in this review are those involving heavy ion beam drivers, laser drivers and the "Z" approach. Because of the breadth of the requested review, please use additional expertise outside of FESAC membership as required.

The Department is cognizant of the intense effort that FESAC has put forth during the last year and appreciates the time and energy expended by the individual members of both FESAC and its subcommittees. I will look forward to the Committee's report.

I would like to receive a final report by early 2004.

Sincerely,

/s/

Raymond L. Orbach
Director

Appendix B
FESAC Panel on the Inertial Fusion Energy Program

Professor James Asay, *Washington State University*
Professor Riccardo Betti (Vice Chair), *University of Rochester*
Mr. Michael Campbell, *General Atomics*
Dr. Phillip Colella, *Lawrence Berkeley National Laboratory*
Dr. Jill Dahlburg (Vice Chair), *Naval Research Laboratory*
Professor Jeffrey Freidberg, *Massachusetts Institute of Technology*
Professor Jeremy Goodman, *Princeton University*
Professor David Hammer, *Cornell University*
Dr. Joseph Hoagland, *Tennessee Valley Authority*
Dr. Steve Jardin, *Princeton Plasma Physics Laboratory*
Dr. John Lindl, *Lawrence Livermore National Laboratory*
Dr. Rulon Linford (Chair), *University of California (Retired)*
Dr. Grant Logan, *Lawrence Berkeley National Laboratory*
Dr. Keith Matzen, *Sandia National Laboratory*
Professor Gerald Navratil, *Columbia University*
Dr. Arthur Nobile, *Los Alamos National Laboratory*
Dr. John Sethian, *Naval Research Laboratory*
Dr. John Sheffield, *University of Tennessee, Knoxville*
Dr. Mark Tillack, *University of California, San Diego*
Dr. Jon Weisheit, *Los Alamos National Laboratory*

Appendix C
Reading List

1. 2002 Snowmass Summer Study report:
http://www.pppl.gov/snowmass_2002/snowmass02_report.html, or start here:
http://fusion.gat.com/snowmass/

2. JASON April 2003 HIGH POWER LASERS report

3. Davidson's NRC X-Games report [2003, not yet posted]
http://www7.nationalacademies.org/bpa

4. Goldston's 35-year development path report [2003]
http://www.ofes.fusion.doe.gov/More_HTML/FESAC/Dev.Report.pdf or start here:
http://www.ofes.fusion.doe.gov/More_HTML/FESAC_Charges_Reports.html

5. Baker's MFE IFE Priorities and Balance report (the 'Knoxville Summit' Report) [1999]. http://fire.pppl.gov/FESAC_Priorities_Final99.pdf

6. Last FESAC report on IFE, chaired by John Sheffield (DOE/ER-0690 July 22, 1996 Report on Inertial Fusion Energy):
http://www.ofes.fusion.doe.gov/More_HTML/FESAC_Charges_Reports.html

7. Laser IFE paper and Laser IFE issues extracted from the paper.

8. Heavy ion fusion plan (from Snowmass).

Appendix D
Panel Schedule and Agendas for Meetings and Conference Calls

Schedule

July 17, 2003 – Charge letter to Professor Hazeltine from Dr. Orbach

September 2 – First email to the IFE Panel members

October 28-29 – Meeting in Albuquerque, NM

December 3 – Conference call

December 10 – Conference call

December 16 – Conference call

January 20 – Conference call

January 27 – Conference call

February 12-13 – Meeting in La Jolla, CA

March 19 – Draft Report sent to FESAC

March 29 – Report presentation to FESAC

Agenda
IFE Panel Meeting
Hyatt Hotel
October 28-29, 2003

Tuesday, October 28

1:45	Executive Session (Introductions, Charge, Agenda)	
2:15	Need for IFE Report	
	OFES	Anne Davies
	NNSA	David Crandall
	Discussion	
3:15	Break	
3:30	Indirect Drive Target Physics NIF, HIF, & related HEDP	John Lindl
4:15	Heavy Ion Fusion (HIF)	Grant Logan
5:00	Z-Pinch	Keith Matzen
5:45	Dinner Break	
7:00	Laser Direct Drive	John Sethian
7:45	Target Fabrication and Injection	Art Nobile
8:30	Target Chambers and Reactors	Mark Tillack
9:15	Break	
9:30	Fast Ignitor	Mike Campbell
10:15	JASON Report on Petawatt Lasers	David Hammer
11:00	Adjourn	

Wednesday, October 29

9:00 NRC Report HEDP: The X Games Ron Davidson

9:45 Follow-up discussion with Davies and Crandall

10:00 Executive Session
- Strawman findings and issues
  - Targets
  - Drivers
  - Chambers and Reactors
  - Fast Ignitor

11:00 Discussion of key technical issues

11:30 Strawman findings for HEDP

12:00 Need for additional information?
Writing assignments and Report Outline
Schedule (next meeting, action items)

12:30 Adjourn

Draft Agenda
Telephone Conference
Wednesday, December 3, 2003
10:00 to 2:00 PST (1:00 to 5:00 EST)

10:00 Role call and review of agenda	Linford
10:15 Discussion of draft outline of report	Linford
10:30 Discussion of Compelling Science Questions	Linford
11:00 Break	
Presentations and discussion of first few Issues	
11:15 Equations of state in high density regimes, spherically symmetric, isobaric ignition hydro, and effects of low-mode number beam imbalance	
11:15 Presentation	Lindl
11:45 Discussion moderator	Weisheit
12:10 High-mode-number hydrodynamic instabilities (RT)	
12:10 Presentation	Betti
12:30 Discussion moderator	Colella
12:50 Break	
1:00 Discussion of Issues Section	Freidberg
1:30 Wrap up discussion	Linford
1:45 Planning for next two telecoms – draft agendas and face-to-face meeting in January or February	Linford
2:00 Adjourn	

Agenda
Telephone Conference
Wednesday, December 10, 2003
8:00 to 12:00 PST (11:00 to 3:00 EST)

8:00 Role call and review of agenda	Linford
8:10 Writing assignments and other issues	Linford
8:20 Heavy Ion Drivers	
8:20 Presentation	Davidson
8:55 Discussion moderator	Navratil
9:20 Break	
9:30 Diode-Pumped Solid State Lasers	
9:30 Presentation	Payne
9:55 Discussion moderator	Asay
10:15 KrF Lasers	
10:15 Presentation	Sethian
10:40 Discussion moderator	Asay
11:00 Discussion of draft Introduction	Betti
11:25 Discussion of Issues Section	Freidberg
11:50 Wrap up discussion	Linford
12:00 Adjourn	

Agenda
Telephone Conference
Tuesday, December 16, 2003
6:45 to 10:45 PST (10:45 to 2:45 EST)

6:45 Role call	Linford
7:00 Fast Ignition	
7:00 Presentation	Tanaka
7:30 Discussion moderator	Navratil
7:55 Break	
8:10 Z-pinches	
8:10 Presentation	Matzen
8:35 Discussion moderator	Asay
9:00 Discussion of input to Priorities Panel	Dahlburg
9:50 Potential contributions of NIF, etc., to IFE	Linford/Lindl
10:20 Writing assignments, call scheduling	Linford
10:35 Wrap up discussion	Linford
10:45 Adjourn	

Agenda
Telephone Conference
Tuesday, January 20, 2004
11:00 to 1:00 PST (2:00 to 4:00 EST)

11:00 Role call	Linford
11:05 Issues Section General content and flow of document Selected key issues for each approach (HI, HAPL, and Z) Selected key research activities / campaigns for each approach (Fast Ignition issues and research need to be included)	Freidberg
12:30 Draft response letter to Baker re Priorities Panel Questions	Linford
1:00 Adjourn	

Agenda
Telephone Conference
Tuesday, January 27, 2004
12:00 to 2:00 PST (3:00 to 5:00 EST)

12:00 Role call	Linford
12:05 Section V Contributions to HEDP and other science General content and organization Findings Recommendation	Asay
12:50 New version of Issues Section Edits and additions Findings	Freidberg
1:20 Draft letter to Baker and explanatory text	Linford
1:40 Finishing Section IV and findings	Linford
1:50 Preparation for Feb 12-13 meeting: action items	Linford
1:00 Adjourn	

Agenda
IFE Panel Meeting
General Atomics
La Jolla, CA
February 12 –13, 20004

Thursday, February 12
(Building 7, Room 120)

Please check in at GA's Visitor Reception Desk. They will give you a badge and direct you to the meeting room, which is under the cafeteria in the central circular Building 7.

8:00	Informal interactions, coffee	
8:30	Welcome and discussion of agenda	Linford
8:40	Discussion of general layout of report (Identify major items needing attention.)	Linford
9:00	Describe process for editing report	Linford
9:05	Introduction	Linford/Betti
9:20	Some General Observations and Findings	Linford/Betti
9:45	Targets (findings and recommendations)	Weisheit/Linford
10:30	Break	
10:45	Targets (body of section)	Weisheit/Linford
11:15	Drivers (findings and recommendations)	Navratil/Linford
12:00	Working lunch (summary of morning action items)	
1:00	Drivers (body of section)	Navratil/Linford
1:45	Fast Ignition (findings and recommendations)	Navratil/Linford
2:15	Fast Ignition (body of section)	Navratil/Linford
2:30	Chambers and studies (findings and recommendations)	Sheffield/Linford
2:45	Chambers and studies (body of section)	Sheffield/Linford
3:00	Key remaining issues (entire section)	Linford

3:45	Break	
4:00	HEDP (findings and recommendations)	Asay/Linford
4:45	HEDP (body of section)	Asay/Linford
5:15	Action items review	Betti/Linford
5:30	Adjourn	
6:30	No-host dinner at (restaurant yet to be picked)	

Friday, February 13
(Building 15, Room 018)

8:00	Video conference presentation and discussion	Patrick Looney
8:50	Walk to Building 7, Room 120	
9:00	Discussion of Priorities Panel interactions	Charles Baker
9:45	Executive Summary	Linford
10:30	Break	
10:45	Action items working sessions	Assigned groups
12:00	Working lunch (discussion of major items)	
1:00	Action items discussions with full panel	Linford/Assignees
3:00	Break	
3:15	Final review of Executive Summary	Linford
4:00	Final review of body of report	Linford
5:00	Adjourn	

Appendix E
Letter and Email to FESAC Priorities Panel Regarding Key Issues

Letter to Baker -- January 29, 2004

Attachments to Baker Letter:

Draft questions and explanatory text provided to the IFE Panel on January 5.
Recommended IFE-Specific Topical Questions and Explanatory Text

Email to Baker – February 27, 2004

Attachment to Email:

IFE Edits of Questions

Dr. Charles C. Baker
Virtual Laboratory for Technology
University of California, San Diego
9500 Gilman Drive, MC 0420
La Jolla, CA 92093-0420

Dear Dr. Baker:

This letter is in response to your request, as Chair of FESAC's Priorities Panel, for input from FESAC's IFE Panel. During our several conversations we discussed a list of questions being developed by the Priorities Panel that would convey the key issues being addressed by fusion energy research. On January 5, 2004, you sent me an email with the attached draft list of questions and explanatory text, and expressed interest in receiving feedback from the IFE Panel some time this month. We agreed that I would send you a letter conveying the IFE Panel comments on the draft questions.

The IFE Panel concurs with the following:

Overarching Questions

The Overarching Questions should be worded broadly enough to include both MFE and IFE.

Each question should also clearly pose a science challenge that has not been achieved, and one that is also central to fusion energy. The following wording is recommended.

O1. What are the properties of matter under conditions required for thermonuclear fusion burn?

O2. Can fusion burn be achieved and studied in the laboratory? (Or alternatively -- Can we light a star on earth and study it in the laboratory?)

O3. Can fusion power be made practical?

Science or Topical Questions

The Science or Topical Questions should fall into three groups: 1) Those that are common to MFE and IFE, 2) those that are MFE specific, and 3) those that are IFE specific. The draft list of science questions you sent contain some that are clearly in one of the first two groups, and some that appear to be oriented toward MFE but might be broadened to include IFE.

Our panel members found ways to broaden all the Topical Questions sufficiently to cover IFE and MFE, with the exception of T10. However, we felt that the real value of the Topical Questions is to convey some of the more specific scientific issues. For that reason we have only included questions in Group 1 where there was apparent scientific synergy between the MFE and IFE research.

T1, T4, T7, T8, and T11 should be in Group 1. The IFE Panel noted that T1 and T4 are somewhat generic, like the Overarching Questions, and do not convey specific scientific issues not already covered in the Overarching Questions or by other more specific Topical Questions. For that reason we recommend that the Priorities Panel consider dropping these two questions, particularly if there is a desire to minimize the number of Topical Questions.

Some of the draft topical questions use the phrase "fusion plasmas" to describe a state that has not yet been achieved. Since tens of megawatts of fusion power have been produced for short times, it might be better to use a phrase such as "burning plasmas" or "fusion burn" to describe the state that we are trying to achieve and study in the laboratory.

The following wording is recommended for the questions in Group 1.

T1. Can laboratory plasmas be confined sufficiently to achieve fusion burn?

T4. Can temperatures and energy densities sufficient for fusion burn be reached in laboratory plasmas?

T7. How do waves and photons interact nonlinearly with plasmas?

T8. How do high-energy particles from fusion reactions or externally driven beams interact with plasmas?

T11. How do fusion neutrons, photons, and particle fluxes affect fusion system materials?

T2, T3, T5, T6, T9, and T10 should be in Group 2, MFE specific. The Priorities Panel may want to consider making the wording clearer that these questions are focused on magnetic confinement.

The following IFE-specific questions (Group 3) should be added to the list.

T12. Can heavy-ion beams be compressed to high intensities sufficient for fusion ignition and high gain and for other HEDP studies?

T13. Can we resolve the scientific and technological issues such that a durable, efficient, repetitively pulsed, high-energy laser can meet the requirements for fusion energy?

T14. Can a recyclable transmission-line assembly, including an IFE target, be developed that can be connected to a high-efficiency pulsed-power driver at rates required for fusion energy?

T15. Can the physics of uniform-density fuel assembly and energy transport by relativistic electrons to high-density fuel be understood well enough to assess the potential of fast ignition?

T16. Can hydrodynamic instabilities and symmetry be controlled and thermonuclear fuel assembled in inertial fusion implosions to achieve ignition and high gain?

T17. How do target emissions interact with surrounding chamber media, and what are the key responses that limit the pulse rate and durability of inertial fusion chambers?

Explanatory paragraphs for the questions in Group 3 (IFE specific) are attached. As you and I have discussed, the Priorities Panel prefers to insert "How" in front of questions such as T12 through T16. However, the IFE panel prefers the form used in this letter. For the convenience of the Priorities Panel, we have inserted the "How" in the attachment.

I hope that these comments and recommendations will be helpful to you and the Priorities Panel in developing the next iteration of the list of questions and explanatory text.

Please let me know if the IFE Panel can be of additional help to the Priorities Panel.

Best wishes,

/s/

Rulon K. Linford
Chair, Inertial Fusion Energy Panel of FESAC

Attachments:

Draft questions and explanatory text provided to the IFE Panel on January 5.
Recommended IFE-Specific Topical Questions and Explanatory Text

cc: R. Hazeltine, Chair of FESAC

Summary

Overarching Questions:

O1. What are the properties of matter in the high-temperature plasma state?

O2. How can we create a self-heated, steadily burning starfire on earth?
or
Can fusion power be made practical?

O3. How can we make fusion power practical?
or
Can we light a "star on Earth" to create an energy-producing plasma?

Science Questions:

T1. How can we sufficiently confine fusion plasmas?

T2. What are the basic physics mechanisms by which heat and particles escape from plasmas?

T3. How are mass flows created and dissipated in plasmas?

Or combine T2 and T3 into

How are particles, energy, and momentum transported within a plasma?

T4. How can temperatures and energy densities sufficient for fusion be reached?

T5. How is plasma pressure limited?

T6. How do magnetic fields spontaneously rearrange?

T7. How do waves and photons interact with plasmas?

T8. How do high energy particles produced by fusion reactions and energetic particle beams interact with plasmas?

T9. How can we interface a stellar grade plasma to our material surroundings on earth?

T10. How much external control versus self-organization will a fusion plasma require?

T11. How do fusion neutrons and high heat and particle fluxes affect fusion system materials?

Overarching questions:

O1. What are the properties of matter in the high-temperature plasma state?

The plasma state of matter demands new physics understanding because its properties are emergent: they are not readily derivable from understanding the properties of single particles but arise as a collective action of billions of particles. Yet, it is remarkable that much of the complex, nonlinear phenomena of plasmas can be reduced to simple physics principles. Discovery and advancement of these principles is of great importance since hot plasmas constitute the core of fusion plasmas and much of the visible universe. These principles apply from spatial scale of microns in fusion plasmas to millions of light years in extra-galactic structures, and from time scales of a billionth of a second in inertially confined laboratory fusion plasmas to billions of years in galaxies.

O2. How can we create a self-heated, steadily burning starfire on earth?

A burning plasma is energy-producing and largely self-sustaining. Unlike all previous hot plasmas studied in the laboratory, the temperature of a burning plasma is not maintained dominantly by heat applied by experimenters. In a burning plasma, the very high temperature required for fusion power will be largely sustained by the energy released from the fusion reactions. The production of a burning plasma that can be sustained sufficiently steadily for fusion energy will be an enormous physics accomplishment, and it will demonstrate the scientific and technological feasibility of controlled fusion power. The creation of a burning plasma will permit numerous scientific and technical investigations of plasma self-heating and of fusion energy production.

or

Can fusion power be made practical?

It is a grand scientific and technical challenge to configure an energy-producing fusion system to provide practical fusion energy. The behavior of a magnetically confined plasma depends strongly on the structure and shape of the confining magnetic field. The behavior of an inertially confined plasma depends on the design of the target pellet and the incident laser or beam energy. Both approaches depend on the properties of the material structure and fusion components surrounding the hot plasma. It is a huge challenge to both physics and engineering science to configure and control these physical elements to provide practical fusion energy.

O3. How can we make fusion power practical?

It is a grand scientific and technical challenge to configure an energy-producing fusion system to provide practical fusion energy. Sufficient energy gain must be achieved to allow the necessary energy inputs to control the fusion system. Both physics and technical approaches are needed for steady-state or at least quasi-steady-state operation. Stellar grade plasmas with large heat and energetic particle fluxes must be interfaced to terrestrial materials. How the fusion neutrons affect the materials of the fusion system must be understood. The fusion cycle must be self-sufficient in fusion fuel. It is a huge challenge to both physics and engineering science to configure and control these physical elements to provide practical fusion energy.

or

Can we light a"star on Earth" to create an energy-producing plasma?

A burning plasma is energy-producing and largely self-sustaining. Unlike all previous hot plasmas studied in the laboratory, the temperature of a burning plasma is not maintained dominantly by heat applied by experimenters. In a burning plasma, the very high temperature required for fusion power will be largely sustained by the energy released from the fusion reactions. The production of a burning plasma will be an enormous physics accomplishment, and it will demonstrate the scientific and technological feasibility of controlled fusion power. The creation of a burning plasma will permit numerous scientific and technical investigations of plasma self-heating and of fusion energy production.

Topical Questions

T1. How can we sufficiently confine fusion plasmas?

Plasmas hot enough for fusion must be confined long enough to allow the fusion reactions to take place. Plasmas can be confined by, gravity, magnetic field, and inertia. Gravity is how the sun confines its fusion plasma. For terrestrial confinement using magnetic fields, the properties of a plasma confined by a magnetic field depends sensitively on the structure of the fields - curvature, twist, spatial symmetries, strength, and topology. These features of the fields determine the plasma stability (its tendency to grow large scale structures from noise) and turbulent transport. Understanding the influence of the many spatial features of the fields provides the basis to design configurations most favorable to fusion energy. Field structure is critical for understanding plasma confined in solar magnetic arcades, in jets emanating from plasma surrounding black holes, and in extra-galactic plasma confined in radio lobes. In inertial confinement fusion, photons or heavy ions are used to to directly compress the fusion fuel or indirectly by creating an intense x-ray radiation field into a sufficiently small, high energy density volume for fusion reactions to occur and the inertia of the fusion fuel allows it to nearly completely burn up before the fuel dissassembles

T2. What are the basic physics mechanisms by which heat and particles escape from plasmas?

The plasma medium can support a dazzling variety of electrostatic and electromagnetic waves not possible in other states of matter. The waves and turbulence can cause a plasma to lose its heat and particles. This transport can thwart the goal of assembling a laboratory fusion plasma that is hot and dense. An exciting recent development has been the realization of massive computer codes capable of exhibiting some of what are felt to be the basic physics mechanisms of transport from turbulence. Understanding the fundamental processes of turbulent transport can lead to techniques to control it. Another exciting development in recent years has been the realization and experimental demonstration that plasma flows can stabilize turbulence and decrease the heat and particle leakage. Turbulent transport can also determine how a rotating plasma falls onto a black hole, how cosmic rays diffuse through galaxies, and how clusters of galaxies form from halos.

T3. How are mass flows created and dissipated in plasmas?

Magnetic and inertially confined plasmas, stellar plasmas, and interstellar plasmas exhibit large scale coherent mass flows. Zonal flows occur in the planetary atmosphere of Jupiter and also play an important role in regulating plasma turbulence in magnetically confined plasmas. Important elements of the physics of plasma rotation and the dissipation of that rotation remain to be understood. It is important to understand the physics of plasma rotation because it plays an important role in plasma stability. Complex mass flow patterns play a crucial role in interfacing terrestrial fusion plasmas to their

material surroundings.. The eruption of CMEs and flares, the heating of the corona to temperatures several hundred times that of the sun's visible surface, the acceleration of the solar wind—all of these processes, whose detailed workings are still poorly understood, are driven or mediated by energy provided by magnetic fields generated within the upper third of the Sun's interior, in the so-called convection zone. In this region, the rotational and turbulent convective motions of the electrically conducting plasma drive a magnetic dynamo that generates and maintains the Sun's global magnetic field as well as smaller-scale local fields. The magnetic fields thus generated emerge through the photosphere, forming sunspots and other active regions and creating complex and dynamic coronal structures. The physics of mass flows can also determine how a rotating plasma falls onto a black hole, how cosmic rays diffuse through galaxies, and how clusters of galaxies form from halos.

Or combine T2 and T3 into

How are particles, energy, and momentum transported within a plasma?

Plasma waves and turbulence arise spontaneously in nearly all plasmas. The waves and turbulence can cause a plasma to lose its particles, momentum, and energy. This transport can thwart the goal of assembling a laboratory fusion plasma that is hot and dense. Understanding the fundamental processes of turbulent transport can lead to techniques to control it. An exciting development in recent years has been the realization and experimental demonstration that plasma rotation can stabilize turbulence and increase the plasma pressure. Turbulent transport can also determine how a rotating plasma falls onto a black hole, how cosmic rays diffuse through galaxies, and how clusters of galaxies form from halos.

[The eruption of CME's can be discussed in the section on magnetic reconnection.]

T4. How can temperatures and energy densities sufficient for fusion be reached?

Magnetically confined plasmas can be heated to fusion temperatures by injection of energetic neutral atoms or electromagnetic waves. While the basic physics of these processes are well understood, important issue remain on the applicability of these methods in burning plasmas. Of course, the principal objective of a burning plasma experiment is to use the energetic alpha particles produced in a fusion reaction to self-heat the plasma. Terrestrial temperatures well in excess of those found on the sun and required for fusion power have been produced.

In inertial fusion, photon or heavy ion drivers are used to compress and heat the fusion fuel to high energy densities. Ignition of a fusion pellet will first be done with a large visible laser. High repetition rate lasers or heavy ion drivers are necessary to achieve quasi-steady fusion burning. An exciting recent development that may reduce the driver energy requirements is fast ignition in which an ultra-short high energy density laser pulse is used to flash ignite a compressed capsule.

Very high ion beam intensities (high directed kinetic energy and particle density) are required for heavy ion drivers. These ion beams are non-neutral plasmas. In addition to acceleration, high intensity is accomplished by compressing the beam along the direction of motion and focusing the beam particles to a small spot size. A basic understanding of the collective processes and nonlinear dynamics of intense, high-brightness, heavy ion beams, and a determination of how best to create, accelerate, transport, compress and focus these beams to a small spot size are critical to achieving the scientific objectives of heavy ion fusion and ion-beam-driven studies of warm dense matter.

T5. How is plasma pressure limited?

For every plasma configuration there is an upper limit to the pressure. Beyond this limit, the plasma cannot be confined - it will disassemble, expand, or lose it energy. The physical manifestation of the loss of confinement depends on the nonlinear evolution of the pressure-driven instability. Effects range from enhancing the plasma transport to abrupt loss of the configuration. Substantial progress has been made on understanding the pressure limits in magnetically confined plasmas. An exciting recent discovery has been that plasma rotation can stabilize the instability of most impact, greatly increasing the stable pressure limit. Fusion energy output increases with the plasma pressure; hence, an understanding of the cause and behavior of pressure limits is needed to develop practical confinement configurations for fusion.

T6. How do magnetic fields spontaneously rearrange?

Magnetic fields in laboratory and astrophysical plasmas tend to spontaneously rearrange – the field lines can tear and reconnect, thereby self-organizing the magnetic topology. This process of "magnetic reconnection" can lead to the sudden, sometimes drastic, loss of energy in some laboratory plasmas, and to continuous turbulent loss in others. Magnetic reconnection is believed to be ubiquitous in the universe - driving solar flares, regulating star formation, accelerating particles to high energy. A fundamental theory for magnetic reconnection, applicable to the wide variety of venues, is not yet in hand.

In the outer one-third of the sun, the rotational and turbulent convective motions of the electrically conducting plasma drive a magnetic dynamo that generates and maintains the Sun's global magnetic field as well as smaller-scale local fields. The magnetic fields thus generated emerge through the photosphere, forming sunspots and other active regions and creating complex and dynamic coronal structures.

T7. How do waves and photons interact with plasmas?

The plasma medium can support a dazzling variety of electrostatic and electromagnetic waves not possible in other states of matter. Such plasma waves can interact with particles in the plasma, often through a myriad of wave-particle resonances not present in

other fluids. Waves can arise spontaneously or can be driven by experimenters in the laboratory. They can accelerate particles, thereby altering the plasma temperature and electrical current. Steady-state operation requires that currents be sustained indefinitely and that electrical currents be controlled. Plasmas can self-generate their own currents from the pressure gradients in the plasma, the so-called bootstrap currents. This subject is closely coupled to plasma stability since having high self-driven currents requires high plasma pressure gradients. Photons are used in the inertial fusion approach to compress fusion fuel. The photon pressure can drive a number of plasma instabities. Understanding the propagation of waves and photons and their interaction with plasmas can lead to techniques to control plasma behavior, and can be key to understanding effects of spontaneously occurring waves.

T8. How do high energy particles produced by fusion reactions and energetic particle beams interact with plasmas?

The fusion of deuterium and tritium nuclei gives birth to an electrically charged alpha particle with an energy much greater than that of the background plasma. The interaction of the population of these alpha particles with the plasma is complex and critical to fusion energy. The alpha particle energy is needed to sustain the hot burning plasma. Yet the energy of the alpha particles can also influence the plasma in numerous other ways. It can drive unstable waves, or even turbulence, in the plasma. The excited waves can in turn lead to the loss of the alpha particles. The alpha particle heating can alter the temperature in the plasma, which in turn can alter the turbulence and the confinement of the bulk plasma as well as the alpha particles. Some aspects of this physics can be studied by the use of energetic particle beams. Energetic particle beams can also drive electrical currents in plasmas. Heavy ion beams in inertial fusion can be used to compress targets. The interaction of these beams with the targets is complex; instabilities can be driven. The final state of the plasma is determined by these strongly coupled processes.

T9. How can we interface a stellar grade plasma to our material surroundings on earth?

Near the edge of a magnetically confined plasma exists a complex region in which the hot plasma interacts with material surfaces and is fuelled by ionization. Strong and complex flow patterns in the plasma boundary interface the stellar grade plasma to the material wall. The boundary plasma must provide exhaust of power, fuel, and impurity ions. Material surfaces must absorb high heat fluxes and eroded material transports in the boundary plasma and is redeposited. Under the right conditions, turbulent transport can be suppressed by sheared flows. A key recent result of plasma experiments, theory and modelling has been that the plasma near the edge sets boundary conditions which strongly influence transport in the hot core. Understanding and predicting these conditions, which are set by a complex interaction of turbulence, magnetohydrodynamic limits and plasma-surface effects, is a remaining but crucial challenge.

T10. How much external control versus self-organization will a fusion plasma require?

A burning, magnetically confined plasma will exhibit a complex set of feedback loops among the various physical phenomena discussed above. The alpha particle heating will be the principal means of sustaining a high plasma pressure. The pressure limit will be determined by the distributions of pressure and current in the plasma. It is desirable that the current be mainly self-generated, in which case the distribution of the current depends on the distribution of the pressure. Auxiliary sources will supply both heat and current drive. The distributions of pressure and current will create mass flows, which affect the transport from turbulence and, with the distribution of the alpha and auxiliary heating, determine the pressure distribution. These complex linkages of physical phenomena can be studied in existing experiments, but the crucial role the dominant alpha heating and alpha driven instabilities will play will first be studied in a burning plasma experiment. These complex linkages represent substantial self-organization of the plasma. Various magnetic configurations have varying degrees of self-organization versus external control.

T11. How do fusion neutrons and high heat and particle fluxes affect fusion system materials?

The material wall surrounding a hot fusion plasma must survive fluxes of millions of Watts of energy per square meter and particle fluxes that erode the materials. The structure must be robust, must not inject material back into the plasma, and must minimize production of radioactivity. In inertial fusion, the chamber wall will receive the pulsed heat loads from each target explosion. Chamber clearing between targets is an important issue. Many new scientific phenomena occur in this system of materials, particularly at the interfaces among coolants, breeders, neutron multipliers, structural materials, conducting shells, insulators, and tritium permeation barriers.

Fusion neutrons can cause activation of system structures and degradation of material properties, leading to lifetime limitations. Fusion neutrons must also be slowed down and their heat captured as the principal method of heat extraction in a fusion system. Fusion neutrons also interact with lithium-containing liquids or ceramics in a chamber material system surrounding the plasma to regenerate the tritium fuel component. Basic material studies are needed to understand the impact of fusion neutrons on structural materials. Studies of the impact of fusion neutrons on various methods of fabrications, such as welds, need to be done on significant sized components. Materials that limit activation must be developed. Various methods of extracting heat from the neutrons need to be explored.

T12: How can heavy-ion beams be compressed to high intensities sufficient for fusion ignition and high gain and for other HEDP studies?

Supporting Narrative: Charged particle beams are one-component nonneutral plasmas that have been accelerated to high kinetic energy. Most of this kinetic energy is in the directed motion of the beam particles, but a small fraction is in random kinetic energy, characterized by the effective temperature of the beam particles. To create the conditions for warm dense matter and propagating fusion burn, very high beam intensities (high directed kinetic energy and particle density) are required. In addition to acceleration, high intensity is accomplished by compressing the beam along the direction of motion and focusing the beam particles to a small spot size. The beam temperature is a key property that limits the smallest achievable spot size and pulse duration. To minimize the beam temperature, and thereby maximize the energy deposition in the target, the beam dynamics must be controlled with high precision throughout its entire trajectory, using accurately positioned and tuned confining magnets, accelerating fields with precise timing and voltage regulation, and final charge neutralization techniques that do not degrade the beam quality. A basic understanding of the collective processes and nonlinear dynamics of intense, high-brightness, heavy ion beams, and a determination of how best to create, accelerate, transport, compress and focus these beams to a small spot size are critical to achieving the scientific objectives of heavy ion fusion and ion-beam-driven studies of warm dense matter. There are also key synergistic relationships of the research on intense heavy ion beams to understanding the nonlinear dynamics of charged particle beams for high energy and nuclear physics applications, including minimization of the deleterious effects of collective processes such as the two-stream (electron cloud) instability, and the use of a charge-neutralizing background plasma to assist in focusing intense beams to a small focal spot size (plasma lens effect).

T13. How can we resolve the science and technology issues such that a durable, efficient, repetitively pulsed, high-energy laser can meet the requirements for fusion energy?

The laser must meet three top-level scientific requirements. It must be durable enough to provide sufficient availability, it must be efficient enough to realize net energy, and it must operate at a sufficient repetition rate to produce meaningful fusion power. Realizing these goals will require advanced science and technology development in laser physics, optics, materials, and pulsed power. Two types of lasers are under development, the KrF Laser and the Diode Pumped Solid State Laser. KrF Lasers are gas lasers pumped with electron beams. The electron beams are formed in a vacuum diode, and are injected through a thin “hibachi” foil into the laser gas. The main outstanding challenges are to demonstrate the efficiency in an integrated system and develop high durability long lived hibachi foils. The latter requires a coordinated R&D effort in materials, cathode physics, electron-beam transport, and thermal management. In Diode Pumped Solid State Lasers

light from an array of diodes is used to pump a laser crystal, typically Yb:S-FAP. As all the components are solid state, the DPPSL is expected to meet the durability requirements. The near term challenge is meeting the efficiency requirements (10% is the goal) at the required wavelength and beam smoothing. The major scientific issue is that of optical damage, including the field enhancements arising from surface cracks of different morphologies.

T14. How can a recyclable transmission-line assembly, including an IFE target, be developed that can be connected to a high-efficiency pulsed-power driver at rates required for fusion energy?

In the heavy-ion and laser-driven IFE concepts, fusion targets are repetitively accelerated to a high velocity and fired into the reactor chamber, after which many heavy-ion or laser beams are directed at the target. The repetition rate for this process is several times per second. For the Z-pinch IFE concept, a recyclable transmission line (RTL) connects a high-efficiency pulsed-power driver to the fusion target (the Z-pinch assembly containing a fuel capsule). The RTL is destroyed on each shot, but the RTL materials are continually recycled and a new RTL-target assembly unit is inserted into the reactor chamber for each pulse. By utilizing higher yield fusion capsules, the repetition rate is decreased to the relatively slow rate of once every 10 seconds. The key scientific questions for the RTL involve 1.) the limits of power flow through a mass-produced, low-mass vacuum-transmission-line assembly, and 2.) power flow at the very large current densities that occur near the Z-pinch load. For example, understanding the physics of plasma formation and motion within the high fields of the magnetically insulated transmission lines is critical to the successful design and operation of the RTLs. The anode-cathode gap at the Z-pinch load location must be optimized to maximize the current delivered to the Z pinch while minimizing the radiation losses from the capsule hohlraum.

T15. How can the physics of uniform-density fuel assembly and energy transport by relativistic electrons to high-density fuel be understood well enough to assess the potential of fast ignition?

“Fast Ignition” is the concept of using an extreme intensity (~10^19 w/cm2) laser beam to ignite a propagating thermonuclear burn wave in compressed fuel that is relatively cold and uniform in density compared to the standard hot-spot ignition approach. It is the fusion energy application of the ultra high energy density physics driven by short-pulse lasers that has been receiving significant national interest. Fast ignition has the potential to achieve a higher target gain with lower total (compression plus ignition) energy input than standard hot spot ignition. It thus offers inertial fusion the potential of an improved product (significantly higher gain) with an easier development pathway (significantly smaller experimental facilities). Fast ignition may also relax the requirements for target and compression uniformity and thus impact driver uniformity requirements and chamber design. However, the physics of fast ignition is extremely complex. Energy from the

ignitor beam must be transported without dispersion to the compressed target and deposited efficiently in the core. This transport may be achieved by creation of a relativistic electron beam from interaction of the intense laser beam with matter or by the intense ion beam that can be created by this laser-plasma interaction. These complex physics issues must be studied – and understood – for the potential of fast ignition to be assessed. This effort will require improved numerical models and well-diagnosed experiments on compressed targets coupled to petawatt-scale lasers to understand the science of fast ignition inertial fusion.

T16. How can hydrodynamic instabilities and symmetry be controlled and thermonuclear fuel assembled in inertial fusion implosions to achieve ignition and high gain?

To achieve ignition and high gain, the fuel in ICF targets must be compressed to densities of several hundred to over a thousand g/cm^3, a density substantially higher than the density of about 100 g/cm^3 found at the center of the sun. To achieve these densities, the fuel must remain nearly Fermi Degenerate as the pressure generated by the fusion driver varies from about 1 Mbar to 100 Mbar during an implosion of a fuel capsule. To achieve this level of control the physics of the absorption and pressure generation of the driver must be understood precisely. The physics of these processes is complex for all IFE drivers, including such diverse topics as intense laser plasma interaction and high-energy electron transport in regions with very sharp gradients, the physics of intense ion beam stopping in warm dense matter, and the production of x-rays during the magnetically pinched implosion of a magnetohydrodynamically unstable array of wires. In all cases, the pressure generated requires precise knowledge of the equation of state and opacity of materials used in these targets. All approaches to inertial fusion use a number of driver beams, which could range from two to over a hundred. To achieve the densities required for ignition and high gain, the radius of the capsules containing the fuel typically change by a factor of 30 during compression. The final implosion must remain nearly spherical which implies that the pressure must be uniform to about 1%. Hohlraums seek to achieve uniformity by precisely controlling the position of the absorbing beams and the resultant x-ray production, and then relying on radiation transport to provide the desired uniformity. Radiation production and transport depends on the equations of state of complex high-z material, frequently in a NLTE state, in a medium that has regions that are thick and diffusive as well as thin and free streaming. In direct drive with lasers, the beams are focused directly on the target, The uniformity of the pressure is determined by a complex interplay of refraction, laser-plasma interaction, and electron conduction at very high intensity. As a capsule implodes, perturbations from fabrication as well as from the driver beams grow as a result of hydrodynamic instability. The successful implosion of a capsule to high density requires that the growth rate of these instabilities be substantially reduced below their classical value. This stabilization relies on complex phenomena that occur as a result of the ablation of a shell during an implosion.

T17. How do target emissions interact with surrounding chamber media, and what are the key responses that limit the pulse rate and durability of inertial fusion chambers?

Scientific issues of target interaction with inertial fusion chambers span a wide range of time scales and material states, ranging from the 10-nanosecond time scale for shocks and radiation transport in high temperature target plasma emission to milliseconds for gas/liquid/solid wall materials response to those target emissions. A variety of gas-dynamic and materials science issues need to be understood better to determine how rapidly inertial fusion chambers can be pulsed, and how long they can last against target neutrons, x-rays, and plasma emissions. For dry wall chambers, long-term survival of the chamber armor is the major challenge. Materials responses at a microscopic level are needed to develop damage-resistant armors using engineered microstructures. For thick liquid-walled chambers, the dominant issue is predictably controlling flow configurations while meeting requirements for shielding and for target and beam propagation at high repetition rates. Research topics include hydrodynamics and radiation transport in the partially ionized afterglow plasma, and gas and liquid hydrodynamics for recovery rates of chamber pressure and liquid flows configurations.

Appendix E (Continued)

2/17/04 9:35 AM –800, Edits to questions for Priorities Panel

To: charlie.baker
From: Rulon Linford <rulon.linford@ucop.edu>
Subject: Edits to questions for Priorities Panel
Cc: IFE Panel
Bcc:
X-Attachments: :Macintosh HD:131750:IFE Edits of Questions:

Charlie,

Thank you for participating in the IFE Panel discussion last Friday regarding the list of questions being developed by the Priorities Panel. We continue to appreciate the opportunity of providing input to that process.

The attached list is the outcome of that discussion, with some additional input from subsequent emails.

The changes result in the elimination of two IFE questions, and the modification of the language of others to align them more with the science focus of the list. This leaves just 4 IFE-specific questions. In addition, slight changes to the wording of some questions allow them to be joint between MFE and IFE. The list of joint topical questions now includes 6, 8, 9, 11, 12, 14, and 17.

If further reduction in numbers of questions is desired, we note that 9 and 11 could be combined, without any loss of specificity, by adding the words "charged particles" to 9.

Please let me know if I can be of help.

Rulon
====

IFE Edits of Questions

Introduction:

O1. What are the dynamics of matter and fields in the high-temperature plasma state?

O2. How can we create a controlled, self-heated, burning starfire on earth?

O3. How can we make fusion power practical?

Topical Questions

T1. How does magnetic field structure impact fusion plasma confinement?

T2. How do hydrodynamic instabilities impact the thermonuclear fuel assembly, ignition, burn propagation, and gain of inertial fusion implosions?

T3. How does turbulence cause heat, particles, and momentum to escape from plasmas?

T4. How are large-scale electric and magnetic fields, currents, and mass flows generated in plasmas?

T5. How do magnetic fields rearrange and dissipate their energy?

T6. Can the temperatures and energy densities required for fusion be achieved in laboratory plasmas?

T7. What limits the maximum intensity of heavy-ion beams?

T8. What limits the maximum pressure that can be achieved in laboratory plasmas?

T9. How do electromagnetic waves and photons interact with plasma?

T10. How can the optimal fuel assembly be achieved in inertial fusion implosions?

T11. How do high energy charged particles interact with plasma?

T12. How can we interface a burning plasma to its material surroundings?

T13. How much external control versus self-organization will a fusion plasma require?

T14. How does the multiple-field environment of fusion neutrons, heat and particle fluxes, photons, and magnetic field affect the plasma chamber media and systems?

T15. How can auxiliary systems be engineered to provide the required, fueling, and heating, and confinement needed for steady-state or repetitively-pulsed burningplasmas?

T16. How can we resolve the science and technology issues such that a durable, efficient, repetitively pulsed driver can meet the requirements for inertial fusion energy and high-energy-density matter generation?

Appendix F
Heavy-Ion Beam Physics Program Summary

B. G. Logan, C. M. Celata, J. W. Kwan, E. P. Lee, P.A Seidl, S. S. Yu
Lawrence Berkeley National Laboratory, Berkeley, CA 94720, USA

J. J. Barnard, A. Friedman, W. R. Meier, Lawrence Livermore National Laboratory
Livermore, CA, USA

R. C. Davidson, Princeton Plasma Physics Laboratory, Princeton, NJ 08543, USA

R. A. Kishek, P. G. O Shea, I. Haber, University of Maryland, College Park, MD, USA

This appendix to section 3.2.1 describes more detail on the science and technology status of the heavy-ion beam physics program for IFE and HEDP.

I. Introduction

The physics program of the HIF VNL is pursued for several long-term goals:

1. Realizing a vast new energy source through **inertial fusion energy**
2. Adding significantly to **intense space-charge-dominated ion beams science**
3. Application of intense heavy ion beams to **high energy density physics**.

A coordinated beam physics program by LBNL, LLNL, and PPPL (the Heavy-Ion Fusion Virtual National Laboratory) supports these long term goals through experiments, analytical theory, and simulations (science campaigns). Section II describes past progress, and section III describes selected experiments and supporting theory and simulation in the current HIF-VNL program. Relationships of HIF-VNL research with other fields of science are described in section IV. The present program investigates the high-current regime of intense ion beams through science campaigns in transport, longitudinal compression and focusing where the effects of secondary electrons, gas and plasma interactions are important. These ten-year science campaigns aim for a successful outcome to the OFES/OMB Ten-Year Measure for Inertial Fusion Energy and High Energy Density Physics: *"With the help of experimentally validated theoretical and computer models, determine the physics limits that constrain the use of IFE drivers in future key integrated experiments needed to resolve the scientific issues for inertial fusion energy and high energy density physics*". These science campaigns address the scientific issues that impact the design optimization of future heavy-ion accelerators such as the Integrated Beam Experiment (IBX). A successful outcome to the 10-year science campaigns described above should lead to a validated, predictive capability of the behavior of intense heavy ion beams relevant to IFE and HEDP. This capability is essential to driving targets for both IFE and HEDP, ultimately to beam intensities $>10^{14}$ W/cm^2, at beam energies >1 MJ, and at affordable costs.

Inertial fusion energy (IFE)

For IFE, the motivations for using heavy ion accelerators are:

1. Worldwide experience with high-energy accelerators supports the prospect that a heavy ion driver for inertial fusion energy can achieve the necessary efficiency, pulse-rate, and durability.
2. Focusing magnets are expected to survive target radiation and debris better than laser mirrors.
3. Ion-target coupling is expected to be very efficient and predictable.
4. HIF with indirect drive is compatible with long-lasting, low-activation chambers protected by thick liquid layers.

For IFE the beams must be focused to a radius of a few millimeters from a distance of several meters. The focusing system must survive at this several-meter distance from the fusion environment, where neutrons and debris from the target can be significant. The pulses must be properly shaped in time, and the beam must be accurately aimed. The driver must be efficient, reliable, durable, and environmentally attractive. A great deal of experience with accelerators for high-energy and nuclear physics shows that accelerators similar to those proposed here are reliable, durable, and energy—efficient. Moreover, particle accelerators have certain advantages over other ways of achieving fusion, in that important components can be protected from the products of the fusion blast. Electrostatic or magnetic fields focus the beams; the conductors that produce these fields are not in direct line-of-sight of the target, and therefore can be shielded from neutrons, gamma rays, and target debris. Liquid metal jets in the target chamber can be used to shield the chamber walls. Thus heavy-ion accelerators provide a plausible solution to the problem of developing focal elements and a fusion chamber that can survive in the fusion environment.

Beam Science of Intense Space-Charge-Dominated Ion Beams

Space-charge-dominated beam dynamics. An ion beam suitable for driving an IFE or HEDP target acts similarly to a non-neutral plasma, since the applied external fields act like a neutralizing background charge to the repulsive force of beam. This is also descriptive of high-power H^- beams intended to heat magnetic fusion plasmas, and of a variety of beams in high-average-power linacs and (pulsed) electron induction linacs. Such beams support internal plasma modes and are susceptible to collective instabilities through their interactions with the confining transport and accelerating system. An interesting and complicating feature is the continual pumping of the beam's phase space distribution by the application of periodic focusing (confining) elements. This pumping produces resonance and stop band features, and is capable of generating beam halos (an outlying population of ions) and internal heating of the ion distribution. In addition, the presence of even a small neutralizing electron component as a result of halo impinging upon the accelerator structure may drastically alter the ion dynamics when it is present over many beam plasma oscillations, as discussed below. The heavy-ion dynamical experiments (such as the high current experiment HCX described below) and related computer simulations are intended to elucidate this emerging field of basic and applied many-particle collective dynamics, which is also a critical part of the accelerator science of intense ion beams needed for IFE and HEDP.

Gas and electron cloud effects. As the beam (non-neutral plasma) travels through and leaves the accelerator, it passes through an environment which may contain electrons, gas, or plasma.

Beams with sufficient line charge density (> 0.1 μC/m) generate beam space-charge potentials of the order of a kilovolt or more. Theory and simulations of the new, high current experiments such as HCX, and also of high-energy ion storage rings with similar line charge densities, suggest that electrons from the vacuum walls may be attracted into the ion beam channel, modifying the beam space charge, ion transport dynamics, and halo generation, and potentially causing ion-electron instabilities. These effects must be studied in order to set limits on the amount of electrons generated, which in turn will provide limits for the vacuum pipe aperture and background pressure. Similar effects appear to be significant in proton storage rings and have been studied via simulation, although the understanding is incomplete at present. Study of these electron effects in transport, longitudinal compression and chamber focus are a new and major thrust of the HIF program as well as of theory and experiments in the high energy physics accelerator community.

Focusing beams onto targets in neutralized state. Fusion targets require beam powers of 100—1000 TW, which implies total beam currents of 10 kA—1 MA on target. HEDP targets for studies of the Equation of State of dense, strongly coupled plasmas can be driven with heavy ion beam intensities several orders of magnitude smaller than those required for IFE. Use of multiple (~100) beams and pulse compression (10x or more) after acceleration implies a power of ~0.1-1 TW/beam out of the accelerator; at ~3 GeV this is 30-300A. For comparison, the ISR at CERN had a beam power of 1 TW at a much higher ion kinetic energy of 30 GeV. Comparable HIF beam power at lower kinetic energy implies much stronger beam space charge potentials. Focusing onto the target is conventionally envisioned as being effected by magnetic lens systems, employing corrections for chromatic and geometric aberrations. A significant effort has been made by the VNL on neutralizing a beam after this magnetic focus using pre-formed plasma in the chamber, termed neutralized-ballistic focusing. In this mode, the beams are non-neutral in the final optical system but then are neutralized as they enter the fusion chamber, nearly eliminating the effect of space-charge in the final beam transport to the target. Both experimental and theoretical results at this time look extremely promising. Z-pinch discharges for neutralized ballistic focusing, called plasma lenses, and longer z-discharges for channeling the ion beam, called Assisted Pinch channels, have also been studied experimentally and theoretically, and offer the promise of stronger focusing with greater chromatic acceptance, thus reducing demands on beam quality from the driver. The beam and background plasma dynamics of these neutralization and neutralized transport processes include: multibeam effects; return current formation and dynamics (streaming and filamentation instabilities); imperfect neutralization; beam stripping; emittance growth; and photoionization of the beam ions and background gas by x-rays from the target. Multiple-beam interactions near the target will be one important focus of future research efforts; collective instabilities, such as resistive hose, filamentation and two-stream modes, will be another. These areas of physics could potentially lead to substantial improvements to the heavy ion fusion concept.

High Energy Density Physics Applications

This important and broad area includes studies of the equation of state of plasmas at megabar to terabar pressures, radiation transport and opacity at many-times solid density, ultra-high Mach number shocks, 2-D and 3-D hydrodynamic instabilities and turbulent mixing well into the nonlinear regime, coherent light sources up to x-ray energies (as a diagnostic to probe HEDP

target properties), and relativistically hot plasmas with T_e much greater than $m_e c^2$. Lasers have provided the initial entry into this field; however, heavy ions offer a new and complementary tool for high energy density science, because of the unique energy deposition property of ion beams, namely, that in very dense plasmas compared to the beam ion density, ions slow down in straight trajectories due to classical dE/dx processes. At high energies, the ion range can be large compared to the optical mean-free-paths in solid-density plasmas, allowing ion energy deposition at the Bragg peak to be well inside targets that would be opaque to laser light or soft-x-ray radiation. In contrast, lasers deposit their energy at plasma critical densities that are much smaller than solid densities, where $\omega_{laser} > \omega_p$. The deep penetration of high-energy ion beam heating allows more flexibility in some types of targets that can be used for dense plasma science, as well as allowing for the possibility of heating a larger volume of matter, making diagnostic measurements somewhat easier.

II. Past Progress

During the past several years the U.S. HIF Program has completed a set of scaled experiments that confirmed theoretical calculations of limits for space-charge-dominated beam transport and focusing [1, 2, 3]. These experiments were designed so that important dimensionless physics parameters had the same values that they would have in a full-scale fusion power plant, thus enabling the fundamental physics of transport and stability to be addressed. Examples of such dimensionless parameters include the dimensionless beam perveance (this proportional to the ratio of space-charge potential energy to the kinetic energy) and the ratios among space-charge forces, focusing forces and forces arising from beam temperature. Line charge density and current are the most important parameters describing the scale of the experiments. These parameters have typically been one to five orders of magnitude smaller than the corresponding values in a full-scale fusion driver. As the line charge density increases, the space charge potential of the beam allows significant interaction with stray electrons, the increase in the total current increases image and inter-beam forces, and in general, physics can be tested that could not be approached with low current beams. The main scientific challenges now are to study these high-current phenomena in transport, compression and final focusing to determine whether the promising low-current results can be scaled to the power levels required for IFE targets and for high-energy-density plasma science.

III. Current research

The High Current Experiment (HCX)

The High Current Experiment (HCX), located at Lawrence Berkeley National Laboratory and carried out by the HIF-VNL, is designed to explore the physics of intense beams with line-charge density of about 0.2 μC/m and pulse duration $4<\tau<10$ μs, close to the values of interest for a fusion driver [4]. Experiments are performed near driver injection energy (1-1.8 MeV). HCX beam transport is at present based mainly on electrostatic quadrupole focusing, which provides the most efficient option at low energy and provides clearing fields to remove unwanted electrons. However, magnetic transport experiments will also be performed to explore limitations associated with magnetic focusing, in particular, the onset of transport-limiting effects due to electrons trapped in the space-charge potential of the ion beam. The principal initial effort on the HCX (see FIG.1. below) has been experiments carried out with a matched and well-aligned K^+

ion beam transported through 10 electrostatic quadrupoles. The main scientific results to date are:

- There is no emittance growth ($\varepsilon_n = 0.6(\pm 20\%) mm - mrad$) within diagnostic sensitivity, and little beam loss (< 2% in the middle of the beam pulse), as expected from initial particle simulations. See FIG. 2 below showing the beam envelope (x and y vs z) through the 10 quad transport region between QD1 and the end diagnostic station (D-end) in FIG. 1 below. The beam centroid is aligned to < 0.5 mm and 2 mr of the central axis of the channel, with envelope mismatch amplitude $\approx \pm 1.0$mm.
- A long-life, alumino-silicate source of improved surface uniformity has replaced a contact-ionization source, eliminating depletion-induced experimental uncertainties.
- Significant differences between the experimental data and early theoretical calculations of the beam envelope propagating through the electrostatic quadrupoles were encountered. More detailed envelope models and simulations have resolved most of the discrepancy, and achievable limits on envelope predictability and control are being probed.
- The experimental current density distribution, J(x,y), and phase-space data are being used to initialize high-resolution simulations to enable realistic modeling and detailed comparisons with experiment. New methods have been derived for projecting the full 4-D phase space from experimental measurements, and the resulting distributions are being used in high-resolution PIC simulations of the experiment.
- Considerable progress has been made in the development of new time-resolved phase-space diagnostics, which will speed up data acquisition in this and other upcoming beam experiments in the HIF-VNL.
- A new Gas and Electron Source Diagnostic (GESD) has made preliminary measurements of the secondary electron coefficient. The secondary emission yield varies as $\cos^{-1}(\theta)$, as predicted theoretically (see FIG. 3. below). Data from the GESD will be relevant to upcoming experiments on gas, particle loss and electron effects in a magnetic quadrupole lattice.

A beam line of four pulsed magnetic quadrupoles, instrumented with diagnostics to measure the production and energy of trapped electrons, secondary atoms and ions is being installed downstream of the 10 electrostatic quads [5].

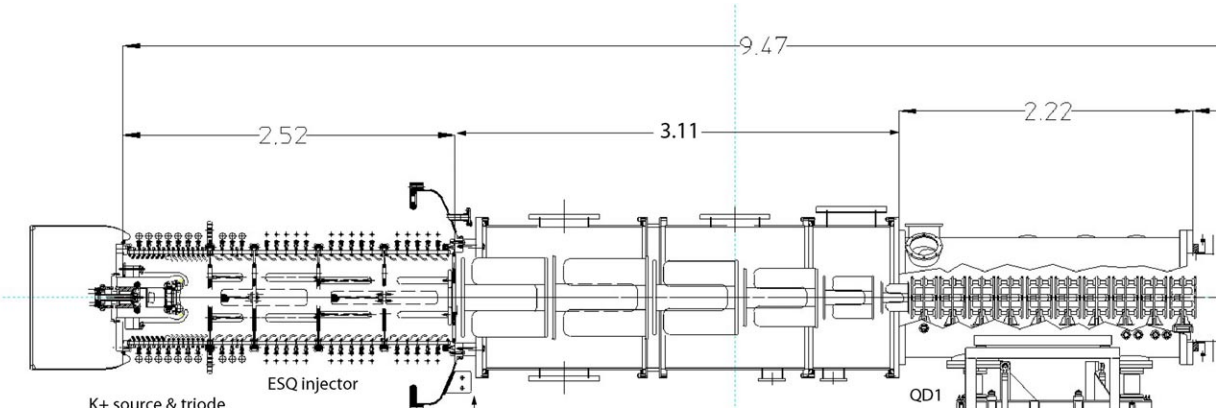

FIG. 1. Initial experimental configuration of HCX. A secondary electron, ion and gas diagnostic was installed downstream of the end station (D-end) diagnostic.

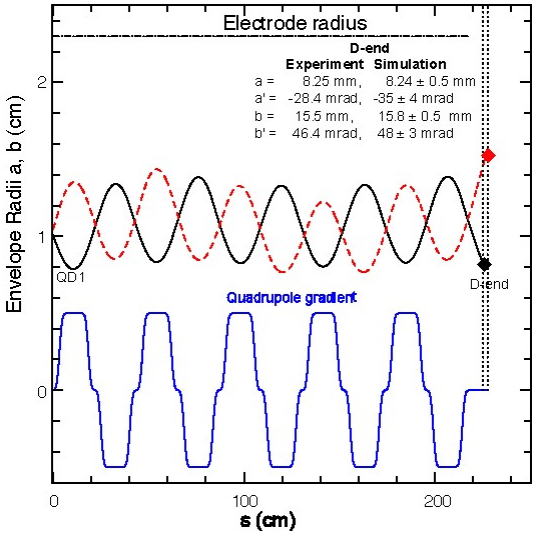

FIG. 2. Predicted HCX beam envelopes (red and black curves) are initialized with I, ε, a′ a, b, b′ measured at QD1, and projected to the diagnostic station at D-end. The tabulated envelope uncertainty at D-end is 1σ of a Monte Carlo set, from uniformly distributed (±0.5mm, ±1.0mrad) measurement uncertainty at QD1.

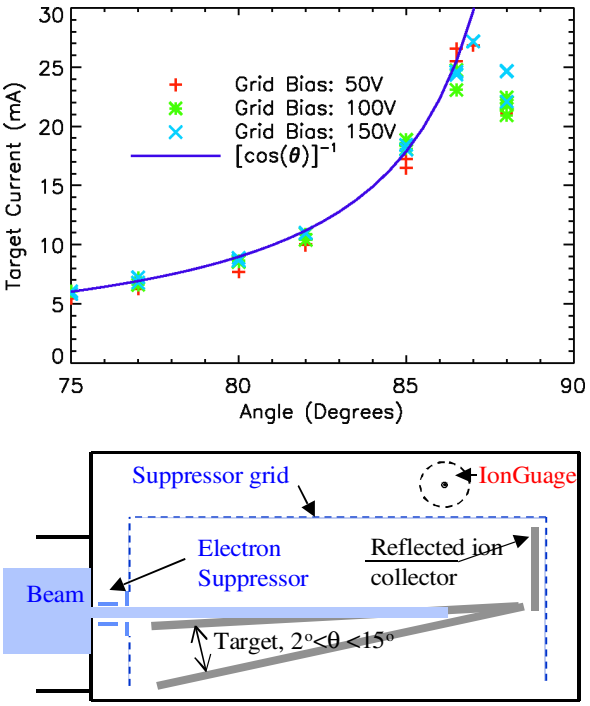

FIG. 3. Gas and Electron Source Diagnostic and initial data on secondary yield versus angle.

The Neutralized Transport Experiment (NTX)

NTX [6] is an experiment (see FIG. 8.) to test the physics of final focusing in a heavy ion fusion driver. The key components are a neutralized drift section and the preceding magnetic final focus lattice. The objective is to quantitatively study magnetic nonlinearities and emittance growth due to incomplete charge neutralization. NTX has produced and focused a beam with a variable perveance (a key dimensionless parameter for emittance growth) up to 2 x 10^{-3}, and with a sufficiently low emittance (<0.2 π mm-mr) so that variations in the focal spot radius are dominated by magnetic nonlinearities and plasma effects in final focus (Fig 4).

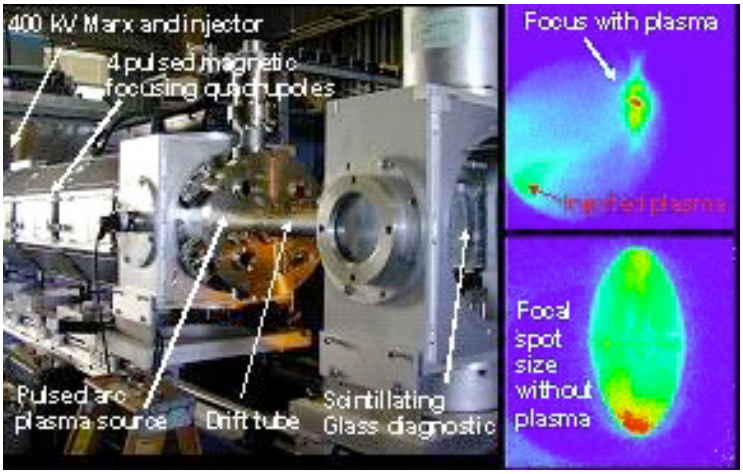

FIG. 4. The Neutralized Transport Experiment (left side of the picture) began operation in September 2002. The lower right picture shows a large focal spot size due to space-charge blow-up of a high perveance ($5x10^{-4}$) beam of 300 kV, 25 mA K^{+1} ions. The upper right picture shows a dramatically smaller focal spot when a pulsed plug of plasma is injected between the focusing magnets and the focal plane diagnostic. Theory and particle-in cell simulations (in progress for this experiment) have also shown much reduced focal spots with plasma neutralization of beams, and without deleterious beam-plasma instabilities.

Initial operation yielded the predicted 80 mA at 400 keV of K^{+} ions, and the voltage-current dependence followed the Child-Langmuir relation. The peak current density was 16 mA/cm^2. Initial measurement of the emittance at 80 mA gave 0.1 π mm-mr.

A beam aperturing experiment was performed on NTX to improve the emittance and to vary the beam perveance. A 2-cm diameter aperture was placed downstream of the exit cathode. This aperture intercepted one half (predicted and measured) of the beam current. Secondary electrons produced at the aperture were successfully confined by means of two adjacent cylinders with negatively biased potentials. FIG. 5. below shows that electrons neutralized the central portion of the ion beam, leading to enhancements of the density on axis and significant distortions of the phase space. The measured profiles and phase space were qualitatively consistent with calculations from LSP, a particle-in-cell simulation code (see next section on theory and simulation), and also with a version of EGUN adapted to include electron effects. Beam size and the divergence angle agreed with EGUN predictions. When the electron trap was turned on, a uniform profile and phase space were measured, and the emittance was then 0.05 π mm-mr (see FIG. 6 below).

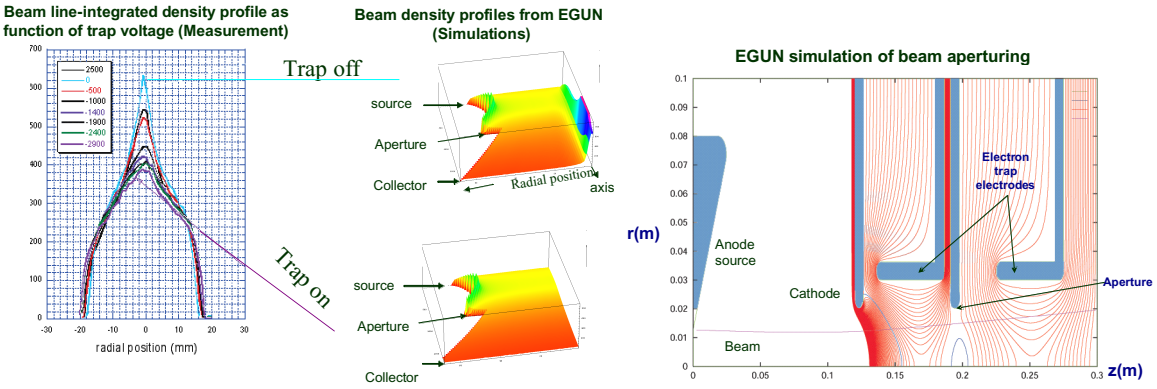

FIG. 5: The NTX beam is apertured both to control the beam current and perveance, and to improve the downstream beam quality for focusing experiments. This figure shows that effects of secondary electron clouds from the beam aperture can be mitigated with proper bias on the trapping electrodes.

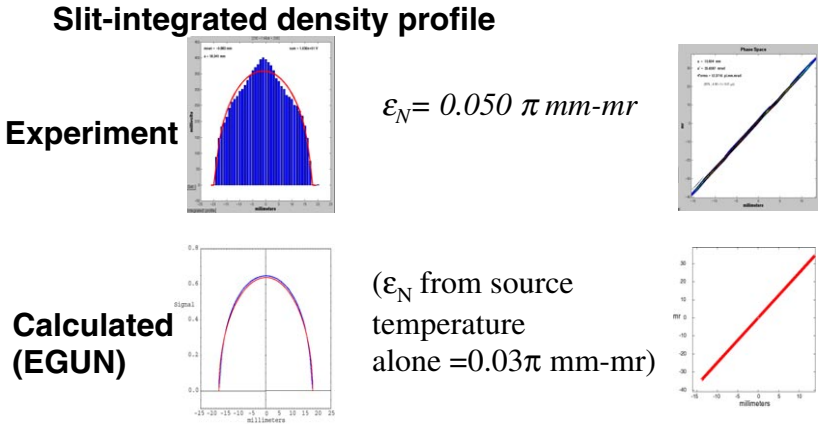

FIG.6. Line density profiles (left) and measured emittance (right) of the high brightness apertured NTX beam compared to that expected from the source temperature alone.

Theory and simulations in the Virtual National Laboratory

Analytical and simulation studies are addressing the injection, acceleration, transport and compression of the intense ion beams in the driver, and their transport and focusing in the target chamber. A large part of this effort supports the HCX, advanced injector, and NTX experimental programs described above. Other research is providing an understanding of fundamental nonlinear and collective beam dynamics, and is developing physics understanding and design concepts for the next-step Integrated Beam Experiment (IBX), an Integrated Research Experiment (IRE), and a fusion driver. Three dimensional (3D) particle-in-cell (PIC) simulations of the HCX clarified the influence of an overly-long injector voltage pulse rise time and motivated an injector triode retrofit for reduced aberrations; transverse-plane 2D PIC simulations are guiding the experimental determination of limits on the beam-pipe fill-factor (a significant determinant of driver cost). Tomographic syntheses of the 4D transverse particle distribution function from a small number of 2D phase-space measurements have been developed and are being used to initialize HCX simulations [7]. Analyses and simulations of the final drift compression process have also been carried out. Initial studies of the generation and trapping of stray electrons in the ion beam self-fields have been performed. Nonlinear perturbative

simulations in 3D have clarified the detailed behavior of collective instabilities driven by beam temperature anisotropy [8] and by interactions with unwanted background electrons [9]. Analyses and simulations [10, 11, 12] are clarifying the influence of charge and current neutralization on beam focusing in NTX and in a fusion chamber. This work is providing the basis for a benchmarked source-to-target modeling capability that will greatly aid the planning of future experiments. Here, we present three selected topics: simulation studies of the HCX injector and matching section, of the two-steam collective instability, and of beam propagation in fusion-chamber plasmas.

Simulation of beams through the HCX injector and matching section Extensive 3D and 2D WARP PIC simulations of the injector and matching section have helped explain the observed phase space structure of the beam. Simulations and theory have shown that the relaxation of collective modes launched by phase space distortions arising from an imperfect injector leads to only modest emittance growth [13]. Continuing 2D and 3D simulations support the experimental program by determining the expected beam properties, aiding in machine tuning and diagnostic interpretation, suggesting additional diagnostics, offering guidance on required diagnostic resolution, and guiding further improvements in the machine. Here, we present an example of an integrated" calculation that gives a comprehensive view of the beam. The calculation begins by using WARP in its 3D time-dependent mode on a 64×64×640 grid, computing space-charge limited emission from the source as the injector voltages ramp up. FIG. 7(a). below shows a frame from a movie of this calculation. The beam head is mismatched transversely (leading to less than 0.1% particle loss) because its line charge density differs from the nominal, a result of the overly-slow 800 ns rise time of the injector gate voltage. Simulations using a 400-ns rise time show no loss (the actual rise time in HCX is slightly less than 800 ns). The particle data at the injector exit plane is saved over the flat-top of the pulse. It is then used to initiate a WARPxy slice" calculation (in a steady-flow 2D approximation on a finer 512 ×512 grid) of the mid-pulse behavior through the matching section and ten electrostatic quadrupole lenses of the transport line. A view of this later stage is shown in FIG. 7(b). below. Detailed agreement of such end-to-end simulations with HCX results, complicated by incomplete characterization of machine imperfections, remains a goal; simulations initialized tomographically from experimental data, which complement fully integrated runs, have been initiated. Integrated simulations (with ensembles of random machine errors within projected tolerances) will be important to the planning of the IBX and other future experiments.

Two-steam collective instabilities In the absence of background electrons, the Beam Equilibrium Stability and Transport (BEST) code has demonstrated quiescent (stable) beam propagation over thousands of equivalent lattice periods [14]. In the presence of a large population of background electrons, however, a strong two-stream instability is observed. FIG. 8 below shows that this instability leads to a dipole (m = 1) transverse displacement of the beam ions and background electrons. Detailed properties of the mode have been determined as functions of beam intensity and axial momentum spread [15, 16]. The code has also been used to model an observed instability in the Proton Storage Ring (PSR) at Los Alamos.

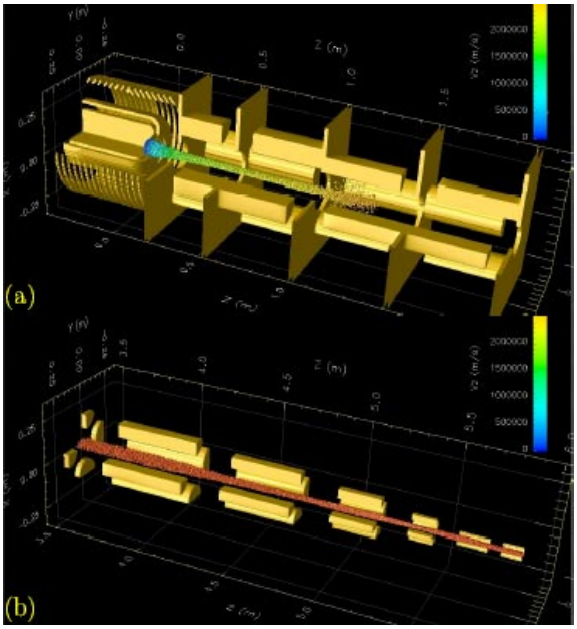

FIG. 7. WARP simulation of HCX: (a) beam head in injector; (b) mid-pulse in matching section and transport line.

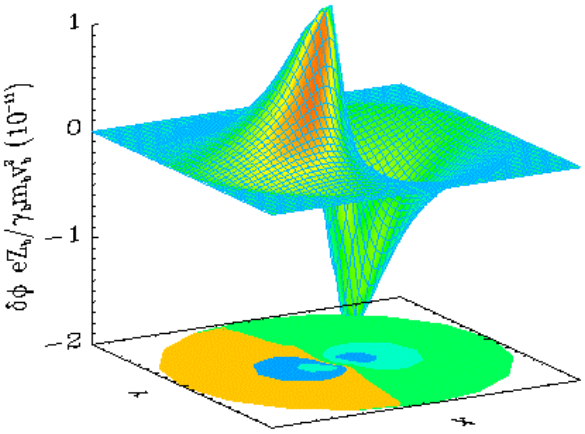

FIG. 8. BEST simulation of two-steam instability with electron density 10% that of the beam, showing perturbed potential.

Studies of beam propagation in fusion-chamber plasmas In a heavy ion driver the energy is delivered to the target in a time-shaped pulse consisting of lower energy "foot pulse" beams that arrive first, followed by the main pulse beams. The 3D PIC code LSP [12], which offers an implicit particle/fluid hybrid model, has been used to make realistic simulations of driver-like foot and main pulses in a target chamber. In these calculations, the beam enters the chamber through a conical three-meter beam port with layers of hydrogen plasma near each end to pre-neutralize the beam, then drifts three more meters through low-density BeF_2 vapor to a 5-mm radius target. In these simulations the main pulses have 2.8 kA of 2.5 GeV Xe^{+1} ions, and the foot pulses have 947 A of 1.9 GeV ions. These runs allow Child-Langmuir electron emission from conducting walls, and several also include time-dependent photo-stripping of the beam and photoionization of the background gas by X-rays from the heated target. Although these processes have major effects on the beam charge state and on the density of free electrons near the target, their overall effect in the cases examined to date is a modest reduction in the beam spot size [17]. Results from a typical main-pulse simulation are shown in FIG. 9 below, where the beam density and electron densities from several sources are shown after 80 ns of transport. At this time, electrons from the plasma layers and from the beam-pipe walls provide the largest share of beam neutralization, although neutralization by photoionization electrons becomes dominant when the beam pulse is within 50 cm of the target. An important finding of this and similar simulations is that the beam waist for either type of pulse is close to values required by current distributed-radiator targets [18].

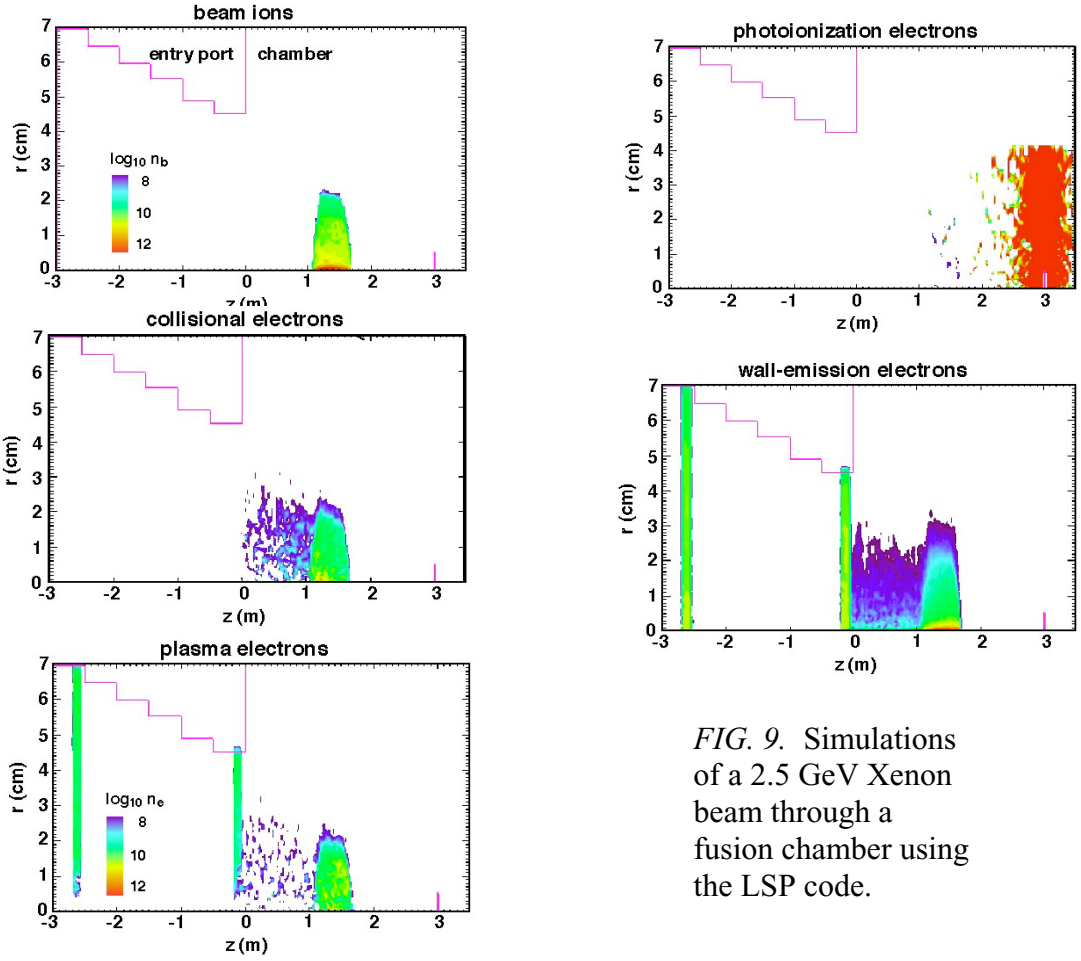

FIG. 9. Simulations of a 2.5 GeV Xenon beam through a fusion chamber using the LSP code.

IV. Opportunities for collaboration with and benefits to other areas of science:

-With the high energy physics accelerator community now:
High-energy accelerators currently operated or planned for applications requiring intense ion beams with beam potentials of order a kilovolt are discovering that electrons are being drawn into the beam and causing ion beam losses. Consequently, these larger programs are making efforts to determine causes, effects, and ways to mitigate the effects of electrons. There are some very interesting simulation and diagnostic developments looking for, and modeling, electron emission from beam pipe walls, and subsequent interactions with the ion beam. An example is efforts to observe and understand the ion-electron two-stream modes in proton storage ring/synchrotron facilities like SNS at ORNL and PSR at LANL [19,20]. The HCX and IBX experiments will also look for changes in ion dynamics due to electrons. It is the electron response to similar high beam line charge densities that creates the common interest, even though the ion energy and pulse formats are quite different. The bigger accelerator programs actually have no more advanced (in some ways less advanced) modeling efforts than those in

HIF. The VNL is sharing its experience in the computation of electron effects with researchers from LBNL who are studying these effects in the LHC at CERN.

-With the ICF and HEDP plasma physics communities in the future: The defense ICF program has developed great understanding of inertial fusion targets and a remarkable set of simulation tools to design these targets. Most of the physics of radiation-driven targets is common to all drivers, so the understanding obtained by the defense ICF program has enabled the heavy ion fusion program to develop a strong argument for the success of heavy ion targets without doing ion target implosion experiments. Nevertheless, there are important ion-specific IFE target issues, including design features to control time-dependent symmetry, ion range shortening, and ion fast ignition that cannot be fully studied using lasers. Accelerator-driven targets may ultimately have important advantages compared to other ICF and IFE approaches in terms of the efficiency x gain product, beam illumination geometry compatible with protected-wall chambers, and robustness to injection into hot gas-filled chambers. For high-energy-density plasma science, the ability to deposit beam energy inside hohlraums without holes opens up the possibility of target configurations inaccessible to lasers. Initially these experiments can be done in collaboration with the dense plasma physics program at GSI with long range, 300 MeV/u ions. Development of higher current, shorter-range (5-10 MeV/u) ion accelerators such as the IRE could extend ion-driven HED plasma experiments to higher temperatures more relevant to HIF targets.

References

[1] M.G. Tiefenback, 1986 *PhD Thesis* LBL-22465 Lawrence Berkeley Laboratory, University of California, Berkeley, CA: Technical Information Department
[2] W. M. Fawley, *et al.* 1997 *Phys. Plasmas* **4**, 880
[3] S. A. MacLaren, S. A. *et al.* 2002 *Phys. Plasmas* **9**, 1712
[4] P.A. Seidl, et al., Overview of the scientific objectives of the high current experiment for heavy-ion fusion , Proc. 2001 Part. Accel. Conf. pp. 2932-2934, IEEE #01CH37268C. LBNL-49319. See also P.A. Seidl; D. Baca; F.M. Bieniosek; C.M. Celata; A. Faltens; L.R. Prost; G. Sabbi; W.L. Waldron, The High Current Transport Experiment for Heavy Ion Inertial Fusion, Particle Accelerator Conference PAC 03 (2003) HIFAN 1245, LBNL-53014.
[5] A.W. Molvik, et al., Electron effects in intense, ion beam linacs theory and experimental planning for HCX , to be published in *Laser and Particle Beam* 20 (4), 2002. LBNL-51009.
[6] E. Henestroza; S. Eylon; P.K. Roy; S.S. Yu; A. Anders; F.M. Bieniosek; W.G. Greenway; B.G. Logan; R.A. MacGill; D.B. Shuman; D.L. Vanecek; W.L. Waldron; W.M. Sharp; T.L. Houck; R.C. Davidson; P.C. Efthimion; E.P. Gilson; A.B. Sefkow A.B.; D.R. Welch; D.V. Rose; C.L. Olson, Design and Characterization of a Neutralized-Transport Experiment for Heavy-Ion Fusion, Submitted to *Physical Review Special Topics - Accelerators and Beams* , HIFAN 1276, LBNL-53928, (2003). See also P. K. Roy; S. S. Yu; S. Eylon; E. Henestroza; A. Anders; F. M. Bieniosek; W. G. Greenway; B. G. Logan; W. L. Waldron; D. L. Vanecek; D.R. Welch; D. V. Rose; R. C. Davidson; P. C. Efthimion; E. P. Gilson; A.B. Sefkow; W. M. Sharp, Results on intense beam focusing and neutralization from the neutralized beam experiment, *Physics of Plasmas Special Issue* (in press), (2004), LBNL-553974N, HIFAN 1281.

[7] A. Friedman., et al., Use of projectional phase space data to infer a 4d particle distribution , to be published in *Laser and Particle Beams*, *Beam* 20 (4), 2002. LBNL-51211, UCRL-JC-148436.
[8] E.A. Startsev, et al., Nonlinear δf simulation studies of intense charged particle beams with large temperature anisotropy , to be published in *Laser and Particle Beams* , *Beam* 20 (4), 2002. HIFAC 1027.
[9] H. Qin, et al., Nonlinear δf simulation studies of the electron ion two-stream instabilities in high intensity beams , to be published in *Laser and Particle Beams* , *Beam* 20 (4), 2002. HIFAC 1025.
[10] I. Kaganovich, et al. (2001), Phys. Plasmas 8, 4180.
[11] T. P. Hughes, et al., (1999), Phys. Rev. ST-AB 2, 110401.
[12] D. R. Welch, et al, Simulations of intense heavy ion beams propagating through a gaseous fusion target chamber , (2002), Phys. Plasmas 9, 2344.
[13] C. M. Celata, et al., Particle-in-cell simulation on heavy ion inertial fusion , submitted for publication to *Laser and Particle Beams* 20 (4), 2002.
[14] R. C. Davidson, et al., (2001), Physics of intense charged particle beams in high energy accelerators (World Scientific, Singapore).
[15] H. Qin, et al., (2001), Proceedings of the 2001 Particle Accelerator Conference, pp. 696-701.
[16] H. Qin, et al., (2000), Physical Review Special Topics on Accelerators and Beams 3, 084401; 109901.
[17] W. M. Sharp, et al., Effects of photoionization on heavy-ion-fusion chamber transport , to be published in *Laser and Particle Beam* 20 (4), 2002.
[18] D. A. Callahan-Miller, et al., Target design activities for inertial fusion energy at Lawrence Livermore National Laboratory , *Nucl. Fusion* 39, 1999, 883.
[19] H. Qin, E. A. Startsev and R. C. Davidson, "Nonlinear Perturbative Particle Simulation Studies of the Electron-Proton Two-Stream Instability in High-Intensity Proton Beams", Physical Review Special Topics on Accelerators and Beams 6, 014401 (2003).
[20] T.-S. Wang, P. J. Channell, R. J. Macek and R. C. Davidson, "Centroid Theory of Transverse Electron-Proton Two-Stream Instability in a Long Proton Bunch" Physical Review Special Topics on Accelerators and Beams 6, 014204 (2003).

Appendix G
IEEE Paper on KrF Lasers for Fusion Energy

Electron Beam Pumped Krypton Fluoride Lasers for Fusion Energy

J. D. Sethian, M. Myers, J. L. Giuliani, Jr., R. H. Lehmberg, P. Kepple, S. P. Obenschain,
Plasma Physics Division, Naval Research Laboratory, Washington DC

F. Hegeler and M. Friedman,
Commonwealth Technology, Inc. Alexandria, VA

M. F. Wolford and R. Smilgys
Science Applications International Corporation, McLean, VA

S. B. Swanekamp
Jaycor, McLean, VA 22102

D. Weidenheimer
Titan-Pulse Sciences Division, San Leandro, CA

D. Giorgi
Optiswitch Technology, Inc

D. R. Welch and D. V. Rose
Mission Research Corporation, Albuquerque, NM

S. Searles
Research Scientific Instruments, Inc Lanham MD

I. Introduction

There is a large US program underway to develop a practical fusion power source based on lasers, direct drive targets, and solid wall chambers. In this approach an array of high-energy laser beams symmetrically and directly illuminates a cryogenic target that has been injected into a chamber. The target is a spherical shell of deuterium and tritium, 4 mm in diameter and 0.4 mm thick. The lasers ablate (or boil off) the outer layer of the shell, driving the remaining shell inward by the rocket effect. The shell is compressed to such high densities (40 x solid) that a localized hot spot in the center undergoes thermonuclear ignition. The resulting thermonuclear burn wave propagates outward releasing energy, which is converted to generate electricity. Because the target is confined by its own inertia, this is in a class of fusion concepts known as Inertial Fusion Energy (IFE). The attractiveness of the approach discussed here lies in its inherent simplicity, its separable architecture, and the modular nature of the laser driver. This lowers development costs and allows multiple options for the lasers, targets, and chambers. This paper presents the issues and progress in developing KrF lasers as a driver for a fusion power plant. The issues and progress in the development of the other components needed for Laser Fusion Energy (e.g. targets, final optics, and chambers) can be found in the references.[1]

Electron beam pumped krypton fluoride (KrF) lasers are an attractive approach for a fusion driver. They have very high beam spatial uniformity, which reduces the seed for hydrodynamic instabilities; they have a short wavelength (248 nm) that increases the rocket efficiency and raises the threshold for deleterious laser-plasma instabilities; they have the capability for "zooming", (decreasing the spot size to follow an imploding pellet and thereby increasing the coupling efficiency); and they have a modular architecture, which reduces development costs. Target designs, based on numerical simulations in both 1D [2,3] and more recently, 2D[4] have shown that a target driven by a KrF laser can have a gain above 150, which is ample for a fusion system. In addition to these laser-target advantages, the Sombrero Power Plant study showed a KrF based system could lead to an economically attractive power plant.[5] Development of KrF lasers has been pursued in Japan, [8,9] China, [10] Russia [11] the United Kingdom,[12] and Los Alamos National Laboratory in the United States.[13] Current research in the United States is centered on two lasers at the Naval Research Laboratory: The Electra laser[14] is a 400-700 J repetitively pulsed system that is being used to develop the technologies that meet the fusion requirements for rep-rate, durability, efficiency and cost. A photo of the Electra laser main amplifier is shown in Figure 1. The Nike laser[15] is a 3-5 kJ single shot device that is used to study issues with a full-scale (i.e. power plant-sized) electron beam diode. Nike is also used to investigate laser target interactions and benchmark the codes that underlie the target designs. Nike generates a laser with the proper temporal (pulse) shape required for fusion, and ablatively accelerates planar targets with the same composition (low density foam wicked with cryogenically cooled liquid D_2) and close to the same areal mass as those required for a high gain system.

Although this paper concentrates on the fusion application, the electron beam/ gas laser technology described here is appropriate for other applications as well. KrF lasers can be used in both industrial and directed energy applications. Other wavelengths can be accessed by changing the laser gas. Lasing in electron beam pumped systems has been demonstrated in Argon-Xenon at 1.733 μm,[6] XeF at 351 nm, and others.[7]

II. KrF Laser Basics

KrF is an excimer (Excited Dimer) laser based on a molecular electronic transition to a ground state which immediately dissociates. The process is as follows:

$$\text{Energy} + (Kr + F_2) \Rightarrow KrF^* + F \Rightarrow Kr + 2F + h\nu \ (\lambda = 248 \text{ nm})$$

where 248 nm is the fundamental wavelength. The transition from the bound upper level to the strongly repulsive ground state results in a very large bandwidth, typically on the order of 1-3 THz. The laser gas is driven to the excited state ("pumped") with electrons. In small systems (< 1 Joule, pulses of 10 nsec or less) the gas is pumped with discharges. This size laser is routinely used for semiconductor manufacturing. In larger systems, such as the size required for a fusion driver (10 J to 10's of kJ, pulses of 20-1000 nsec), the gas is pumped with electron beams. The concept is shown schematically in Figure 2. The electron beams are created by using a pulsed power system to rapidly apply voltage across a cathode-anode gap. The electrons are emitted by the cathode and driven across

the gap through a thin foil, which serves as the anode, and into the laser gas. The foil physically separates the diode region, which is at vacuum, from the laser cell, which is at atmospheric pressure or above. The structure that supports the foil is known as a hibachi. Typically two electron beams are injected into the laser cell from opposite sides. The laser axis is perpendicular to the electron beam propagation. The beam voltage and laser gas pressure are adjusted to give a flat deposition profile across the laser cell, in order to produce a spatially uniform laser profile. In most systems, the laser beam is amplified as it propagates through the cell, is reflected from a rear mirror, and is amplified again as it propagates back through the cell out through the entrance. (This "double pass" laser path is not shown in Figure 1 for the purposes of clarity). In a repetitively pulsed system a recirculator is needed to cool and quiet the laser gas between shots. An external magnetic field prevents the electron beam from pinching as it propagates into the laser cell. Large, single shot amplifiers have also been built without a magnetic field.[8,9,12] In those systems many smaller diodes are arranged cylindrically about the laser cell. However the magnetically guided systems have proven to be more efficient and are more compatible with the gas recirculator needed for repetitive operation.

II.A Pulsed Power Considerations

The electron beam parameters are chosen to optimize the electron beam energy deposited into the laser gas, whose composition and pressure have been adjusted for maximum laser output to maximize the laser output energy. The electron beam energy should be at least 500 keV, in order to minimize losses in the hibachi foil. The laser gas pressure should be around an atmosphere with as little Kr as possible, in order to minimize quenching of the excited state (KrF^*) that becomes more prevalent at higher pressures. The electron beam power deposited in the gas (known as the pump power) needs to be in the range 400 kW/cc -800 WW/cc in order to achieve reasonable laser gain without "burning up" the fluorine or overdriving the system to produce excessive Amplified Spontaneous Emission (ASE). ASE is a loss mechanism that compromises the system efficiency. The practical size of available output windows leads to laser cell dimensions along the electron beam of 30-100 cm. The requirement to stop the electron beam in these distances at optimal gas pressures sets the voltage between 500 and 800 keV. The pump power requirements then fix the current to between 100-200 kA. The pulse length is determined by the total energy desired from the system, but there is a practical limit of around 500- 600 nsec due that arises from balancing the conditions for an efficient laser with the requirement to have the total laser output energy below the laser fluence damage threshold on the output window. In addition to the above constraints, it is important that the voltage should rise and fall as rapidly as possible. There are two reasons for this: 1) Because the voltage is lower during the rise and fall, the energy deposition is skewed towards the foils, leading to a non-uniform laser beam profile. Thus the laser light produced during these times cannot be efficiently used for uniformly illuminating the target; and 2) the hibachi foil stops more electrons at lower voltages, hence compromising the system efficiency. All of these constraints suggest that the best way to produce the electron beam is with a pulsed power system that produces a fast rise, a fast fall, and a flat top power pulse.

II.B Beam smoothing

The large bandwidth of KrF enables one to use spatial and temporal incoherence to produce very uniform illumination of the target: The instantaneous target illumination profile of a KrF beam has the speckle pattern characteristic of all spatially multimode lasers. However, the large bandwidth causes this speckle to change on a time scale that is short compared to the response time of the target. Figure 3 shows the concept of ISI, or "induced spatial incoherence." [16, 17] An aperture is illuminated with broadband incoherent laser light which propagates through the laser system and is imaged onto the target. As long as there are minimal aberrations in the optical system, the time-averaged aperture profile is faithfully imaged onto the target. The Nike laser at NRL has demonstrated this technique and produces a very uniform focal profile. As shown in Figure 4, the RMS speckle uniformity in each laser beam is on the order of 1.0-1.3%.[15] This very high uniformity reduces the imprinting of modulations on a fusion target, and hence reduces the seeding of hydrodynamic instabilities.

II.C Time scale mismatches

Electron beams require pulse durations of several hundred nsec to produce significant energy. Yet the relaxation time of the excited KrF is less than 7 nsec: the relaxation time of KrF is 2 ns in the laser medium and the fluorescence lifetime is 7ns. This "mismatch" is resolved by continually extracting the laser light during the electron beam pulse. Another mismatch occurs because the target physics requires an 8-16 nsec drive pulse. This is solved by "angular multiplexing" the laser beams.[18] A single laser pulse (~ 10 nsec) is repeatedly divided into a series of pulses. These pulses are delayed and steered so that they are injected into the amplifier sequentially, but with each at a different angle. Thus, even though the pulses are on independent paths, the amplifier "sees" one continuous ~100 nsec pulse. After amplification the delays are removed and all the beams are steered to allow the 10 nsec beams to simultaneously illuminate the target.

II.D Pulse Shaping and Zooming

For a fusion target, the laser pulse must be "shaped" with a low intensity foot followed by a high intensity main pulse. The foot raises the isentrope of the ablator, which lowers its susceptibility to hydrodynamic instabilities.[2] In a KrF laser this is accomplished by adding a Pockels cell to modulate the light at the low power front end of the laser train. It is also beneficial to temporally decrease the laser focal spot to match the compressing target. This can boost the laser absorption by as much as 30% [2]. "Zooming" is straightforward with a KrF laser. Parallel tracks are added to the optical layout shown in Figure 2, with each track having its own unique sized aperture and a Pockels cell. By sequentially running the laser beam through smaller and smaller apertures, the laser spot size is decreased. One candidate target design [2] has three zooming steps.

III. Progress in Electron Beam Pumped KrF Laser Development

In a fusion energy system the laser would consist of a series of identical beam lines. Thus it would be only necessary to develop one beam line in order to know how to build the entire laser system. For example, in one topology under consideration there would be 40 beam lines with each beam line producing an energy of 60 kJ to produce a 2.4 MJ laser. We believe that the technology for electron beam pumped gas lasers is sufficiently mature that it would require relatively modest development to build a system of this size that could fire on a single shot basis. The main research challenge is to build one that is repetitively pulsed and can meet the fusion energy requirements for durability, efficiency and cost. These requirements, derived from both the target designs[2,3,4] and power plant studies[5], are given in the Table I (note that the first two are already met by a KrF laser):

TABLE I: Requirements for an IFE Laser Driver

Parameter	Requirement
Beam quality (high mode)	0.2%
Optical bandwidth	3 THz
Beam power balance	2%
System efficiency	6-7%
Cost of entire laser	$360/J
Cost of pulsed power	$5-10/J(e-beam)
Rep-Rate	5-10 Hz
Durability (shots)[1]	3×10^8
Lifetime (shots)	10^{10}

1 Defined as shots between major maintenance (2 years at 5 Hz)

This section describes our research and development to meet these specifications. It is organized along the key components shown in Figure 2.

III.A Pulsed Power

Generally the two electron beams are powered by their own independent pulsed power system. This eliminates the need for complicated and convoluted power feeds. This section discusses the three types of pulsed power systems used for KrF lasers, single shot, a repetitively pulsed platform for component R&D, and an advanced system for practical applications.

III.A.1. Single Shot Pulsed Power Systems

The pulsed power design for a single shot system is fairly straightforward. An example is shown in Figure 5, which shows the overall schematic of the Nike Laser 60 cm amplifier.[19] (The name is derived from the 60 cm x 60 cm optical aperture.) This is the final amplifier in the Nike system. The pulsed power consists of a gas switched Marx generator (168 kJ stored energy) that pulse charges four water insulated coaxial water

pulse forming lines to 1.4 MV in about 3.5 μsec. The pulse forming lines (PFLs) are in two sections: a 145 nsec long, 5 Ω main section, followed by a 20 nsec long, 4 Ω peaker section. The peaker gives a higher voltage to the leading edge of the pulse and thus reduces the power rise time. The PFLs are discharged through laser output switches into the electron beam diode. The output switches are SF_6-insulated and all eight (four per side) are triggered by a quadrupled ND-YAG (266 nm) laser. Reliable, low jitter triggering (< 2 nsec each switch, < 6 nsec first to last among all eight switches) is achieved when the laser intensities are greater than 9 GW/cm^2. The power from each switch is fed through its own SF_6 - insulated feed section to a common cathode shell. The emitter (cathode) is a velvet cloth that is stretched and glued over an aluminum mandrel, which in turn is pressed into the cathode shell. The overall emitter dimensions are 200 cm × 60 cm. Each side produces a 650 kV, 580 kA, 250 nsec flattop electron beam.

III.A.2 Repetitively Pulsed System for component R&D.

An example of a repetitive pulsed power system is the one used in the Electra Laser Facility[20]. This system produces two 500 kV, 100 kA, 100 nsec electron beams at a repetition rate of 5 Hz. The pulsed power can run continuously for 100,000 shots, with electron beam runs of 10,000 shots or more commonplace. This "First Generation System" is more than adequate to start the development of the other laser components (cathode, hibachi, KrF physics, etc) for IFE, and may be sufficient as is for other applications. A schematic of the First Generation System is shown in Figure 6. (There are two such systems, one for each electron beam.) A capacitor bank is charged to 86 kV and is discharged through the primary side of a 12:1 step-up auto-transformer. The secondary side resonantly charges two parallel water-insulated pulse forming lines (PFL) to 1.07 MV in 3.94 μsec. The single-pass transit time of each PFL is 59.5 nsec, but following Nike practice each line is composed of two sections: a 49.5 nsec long, 8.5 Ω line, and a 10 nsec long, 6 Ω "risetime peaker" section. Also, as in Nike, the power flows from each PFL, through its own laser-triggered gas switch and "inside-out" vacuum insulator, to a common cathode. This arrangement can be seen on the right side of Figure 6. The system can accommodate a wide variety of emitter materials. The duration of the continuous runs are limited by erosion of the Elkonite output switch electrodes. Replacing these electrodes takes less than two hours.

III.A.3 Advanced Repetitively Pulsed System

While the Electra system is sufficient to develop the laser technologies, a more advanced pulsed power system is required to meet the fusion energy requirements for durability, efficiency and cost. Durability can be realized by using all solid state switching components, whereas efficiency and cost can be met by minimizing the number of pulsed power compression stages. The latter requires that the switch in the primary energy storage stage be as fast as possible. We have developed a design for an all solid state, single stage pulse compression generator that is projected to have a wall-plug to e-beam flat-top efficiency of 87%, and a cost of $8.45/Joule. The prime store is an ultra fast (~1.6 μsec) Marx generator, which, as shown in Figure 7, will pulse charge a water

insulated PFL. At peak charge, the energy in the PFL is be transferred by a magnetic switch into transit time isolator (TTI) and then into the electron beam load. The TTI is a pulse line of the same length, geometry and construction as the PFL, and serves to sharpen the output pulse to minimize the voltage rise time. The principal behind the magnetic switch is well established.[21] An inductor is placed between the center conductors of the PFL and TTI, and is adjusted so that it blocks the current until the PFL is charged to peak voltage. At that point the core saturates, its permeability (and hence inductance) rapidly drops, and charge is quickly transferred through the inductor on a time that is much faster than the charge time. Our application follows the topology pioneered at LLNL[22] and more recently in the Sandia RHEPP modulator.[23] In practice this circuit can achieve about a factor of three to four in pulse compression. As the output voltage pulse is in the range of 400-600 nsec, the requirement to have just one magnetic compression stage requires that the PFL be charged in about 1.6 μsec or less.

We are developing a new type of switch to meet these ultra fast switching requirements. This Laser Gated and Pumped Thyristor (LGPT),[24] is shown schematically in Figure 8. The device consists of a four-layer, solid-state switch that is optically triggered by two on-board diode laser arrays. The lasers flood the entire switch volume with photons to yield switching times of less than 100 nsec. A thyristor was chosen because its internal feedback produces current gain as well as voltage gain, and because the primary energy transfer requires closing commutation only. Laser gating of such a device has been shown to dramatically reduce closing time and commutation losses.[25]

The fast Marx application described above requires a fast closing switch that can operate at 16.4 kV, and can carry approximately 2500 Amps/cm^2 with a peak rate of rise of current of di/dt ≥ 10 kA/μsec/cm^2. This working voltage calls for a bulk breakdown design of 23-25 kV, which in an asymmetric design leads to a device that is nominally 2-2.5 mm thick. The optimum laser wavelength for gating and pumping is chosen through an iterative trade-off between absorption length, interface characteristics, electrical design (thickness and doping of bases and emitters) and quantum efficiency. For this purpose we have constructed models that predict the optical and electrical characteristics using a 2D semiconductor device design code.[26] The dI/dt is determined by the rate-of-rise of optical fluence provided by the drive laser. The nominal conversion ratio (for these wave-lengths in silicon) is 1 J/Cb or 1 W/Amp. As the current laser diode bars and drive circuitry can produce rates of rise approaching 100 kW/ μsec/cm^2, the expected current rate of rise is 100 kA/μsec/cm^2.

The LGPT will be configured in a rail gap geometry to facilitate the extremely low inductance needed for the fast Marx. The device is shown Figure 9, and has a 14 cm^2 active asymmetric thyristor and a 2 cm^2 inverse parallel diode arranged as two 1 cm x 8 cm strips in a common envelope. Gating and pumping laser arrays, along with their drive electronics, are an integral part of the package.

In our first tests of this concept we modified an off-the-shelf Thyristor to accommodate a single diode laser array and its optical coupling. The switch operated at 3.2 kV for 10^5 shots at 5 Hz. The current density was 2.7 kA/cm^2 (121% of the IFE system requirement)

and the current rate of rise was 1.4 x 10^{10} A/sec/cm^2 (140% of the IFE requirement). We have built a second-generation switch that uses advanced, purpose-built construction techniques, including both anode and cathode gating arrays. This switch is designed to operate at the full IFE-required operating voltage of 16.4 kV, and our tests are nearing that goal as this is written. Further details on this device can be found in the references.[24]

III.B Cathode development

The electron beam is emitted from the cathode, and its specifications are set laser requirements. The electron beam current must rise and fall quickly and be spatially uniform. The former is to limits energy deposition in the foil, as discussed in Section II.A, the latter ensures uniform deposition in the laser gas across the electron beam. The electron beam must also have a near constant voltage throughout the pulse, to ensure a uniform the energy deposition across the laser cell (in the direction of the electron beam). This is facilitated by choosing cathodes that minimizes the velocity of the plasmas produced by the anode or cathode. The cathode current density, j, obeys the relativistic formulation of Child's Law[27], $j = 2.7[(V/0.51+1)^{1/2} - .0.85]^2/d^2$, where j is in Amps/cm^2, d is the A-K gap in cm, and V is the diode voltage in MV. Thus this plasma motion shortens the A-K gap, raises the current, and because the available amount of energy in the diode is fixed, lowers the voltage. We have set the requirements for the cathode as: rise time (< 40 nsec), uniformity (< 5%), closure velocity (< 1 cm/μsec), pulse length (100-600 nsec), and durability (> 3 x 10^8 shots). On a more practical note, it is also important that the cathode design limit the amount of gas evolved to minimize the size of the vacuum pumps needed to maintain the diode vacuum during extended repetitively pulsed runs.

We are evaluating a number of cathodes that can meet these requirements. Our work has concentrated on cold (field emission) cathodes. This is based on their simplicity, low cost, practically zero power consumption, ability to operate at ambient temperatures, and relatively modest vacuum requirements (10^{-4} Torr). Several emitter materials are under evaluation. Ultra fine double velvet cloth meets the first three performance requirements, but tends to degrade after 10,000 shots on Electra, and is not expected to meet the durability needs. Cathodes based on carbon fibers woven into an aluminum base plate appear to have longer lifetimes, but have uniformity issues. Also promising are emitters formed from carbon fibers bonded to a carbon substrate. To date we have evaluated seventeen different cathodes. Details of these cathode studies can be found in the references.[28]

One of the more promising technologies we have developed is to place a ceramic honeycomb structure in front of the emitter surface.[29] The ceramic improves the uniformity, decreases the rise and fall times, reduces the post shot evolved gas, and extends the lifetime of every cathode we evaluated. The ceramic is made of cordierite, is 5 cm thick, and composed of close packed square capillaries, with a pore density of 300 ppi. The ceramic is situated such that one surface is 2 mm from the emitter surface, and the other defines the A-K gap. There are three underlying mechanism for the improvements: 1) The close proximity of the relatively high dielectric constant ceramic (ε

= 6.3) reduces the localized reduction in electric field caused when one part of the emitter produces electrons. The electron beam is composed of a large number of beamlets. Theory and simulations show that the space charge produced by each beamlet reduces the electric field in adjacent areas, which delays those areas from emitting. The ceramic screens this localized field, allowing the field to remain uniform and hence all of the potential emission sites to emit. 2) The capillaries provide a plentiful source of secondary electrons. Multiplication factors of 10^6 or more are anticipated from our modeling. These secondaries quickly (less than 1 nsec) generate a plasma that electrically connects the emitter/ceramic gap. Thus the primary source of beam electrons comes from the inside of the capillary wall, and not explosive emission from the cathode material itself. This should significantly reduce erosion from the cathode with a concomitant increase in lifetime. 3) The large surface area of the capillaries absorbs gasses produced by the cathode and hence limits the amount of material that is released. Coating the inside of the ceramic with gamma alumina, which acts like a reactive sponge to absorb residual gases, showed even further decreases in the post shot diode pressure rise.

Results from the first tests with the honeycomb ceramic cathode arrangement are shown in Figure 10. Note the ceramic decreases the power rise time (in these shots the observed rise was actually diagnostic limited), decreases the power fall time, and produces a flatter power pulse. In addition, the diode pressure after the shot was reduced about five fold. In the case of the carbon fiber cathode, the RMS non-uniformity of the electron beam dropped from 14.8% to 4.6%. Further details can be found in the references.[29]

III.C. Electron Beam Diode Physics

Planar, space charge limited electron beam diodes are subject to the "Transit Time Instability". The diode acts like a parallel plate microwave cavity that allows RF waves to propagate back and forth. The instability imparts an axial velocity spread to the electron beam, which both lowers the electron beam energy that is deposited into the gas, and increases the amount of energy deposited into the hibachi foils. The growth rate of the instability depends on the diode size and geometry. The instability has been observed with experiments on both Electra and the Nike 60 cm amplifier, and has been successfully modeled with a particle-in-cell (PIC) code.[30] The PIC modeling also showed the instability could be mitigated by precisely slotting the electron beam emitter (cathode) and loading the slots with microwave absorbing material. The slots and absorbers turn the diode into a slow wave structure that attenuates the RF waves from propagating at the fundamental transit time frequency. Figure 11 shows the results of experiments on the Nike 60 cm amplifier[31]. The upper half shows the initial configuration with a monolithic cathode. The plot shows the measured fast Fourier transform of the rate of change of current (dI/dt). The dominate peak at 2.5 GHz is in agreement with modeling. The lower half shows the slotted cathode (with microwave absorbers inserted into the vertical slots) and the corresponding Fourier transform of dI/dt. Note the amplitude of the instability is reduced by a factor of 40,000, i.e. effectively quenched. Our measurements with a stacked foil energy spectrum analyzer confirm that the resulting electron beam is close to mono-energetic.

III.D. Hibachi Development

The hibachi holds the pressure foil that isolates the laser gas from the vacuum region of the electron beam diode. Typically the hibachi consists of a series of parallel ribs that support the foil. The hibachi must be as transparent as possible to the electron beam, in order to maximize the electron deposition into the gas. It must also be able to withstand the static pressure from the laser gas and the cyclic hydrodynamic shocks induced by the electron beam as it deposits its energy into the gas. The foil itself must be resistant to damage from electrons, x-rays, uv light, and fluorine, and have a low reflectivity in the uv to prevent unwanted ASE transverse to the main optical axis. Fluorine compatibility, low uv reflectivity and high electron beam transmission generally limits the choice of foil materials to titanium or stainless steel. High transmission requires not only that the foil be as transparent as possible to electrons, but also that the laser gas composition and pressure be adjusted to minimize back scattered electrons.

An example of a standard hibachi designs is shown in the upper half of Figure 12. The rib structure supports the pressure foil on one side, and an anode foil on the other side, i.e facing the electron beam. The electron beam is emitted from a monolithic cathode. The electron energy deposition efficiency was only about 35-40% with this arrangement.[19] This efficiency is defined as the ratio of the energy deposited in the laser gas divided by the electrical energy in the diode. For these purposes we only consider the energy deposition during the 100 nsec flat top portion of the electron beam pulse.

We have developed a hibachi concept that demonstrates energy deposition transmission efficiency of > 73% on Electra. Efficiencies of > 77 % are expected in a 800 keV system. The concept is shown in the lower half of Figure 12. The high transmission efficiency was achieved with two innovations: 1) Eliminating the anode foil that is customarily placed on the diode side of the hibachi structure, and 2) Patterning the electron emitter into strips so the beam "misses" the hibachi ribs. While conceptually simple these are difficult in practice: The individual beam strips spread while passing through the hibachi due to the highly non-uniform electric fields caused by eliminating the anode foil, and they rotate and shear due to the beam's interaction with the applied magnetic field. We compensate for these by narrowing the emitters and "counter-rotating" them so the beam strips propagate parallel to the ribs when they get to the hibachi. Note that slotting the cathode into strips also eliminates the "transit time" instability as described above.

While the topology of the strips can be determined empirically on Electra, this does not give us the predictive capability needed to design larger systems. This is a rather complex phenomenon to model and requires a full 3-D PIC simulation of the exact experimental geometry, including the rib structure, laser gas, and magnetic field. This was achieved with the Large Scale Plasma (LSP) code developed by MRC, Albuquerque. The simulations accurately predict both the cathode counter rotation angle and the energy deposition efficiency.[32] The electron beam depicted in the lower half of Figure 12 is an LSP simulation of a beam "strip". The field shapers shown in the figure are used to

reduce the current density enhancement that would normally occur at the edge of an electron beam.[33] Further details on the hibachi results can be found in the references.[34]

III.E KrF Physics/Laser Operation

Electron beam pumped KrF lasers have been in operation for quite awhile, under a wide range of operating conditions, and with outputs ranging from a few tens of Joules to several kJ.[8,9,10,11, 12, 13, 15, 35, 36 ,37] All of these have been single shot devices. In the interest of brevity and painting a coherent picture, only the results from the Electra repetitively pulsed laser will be presented here. A very comprehensive discussion of KrF laser physics can be found in the references.[38]

Electra has been operated as an oscillator. The laser cell is 30 cm wide (between pressure foils) by 30 cm high, by 100 cm long (along the laser axis). The laser resonator was created by adding a flat 98.5% reflecting rear mirror and an 8% reflecting output coupler. The required output coupler reflectivity was determined using the well established Rigrod formula.[39] The laser gas pressure was varied between 1.0 and 2.0 atm, at various concentrations of fluorine, krypton, and argon. The results are shown in Figure 13. At lower absolute pressures, the laser output decreases because the electron beam deposition decreases. At higher absolute pressures, the maximum laser output occurs at a pressure below that needed to fully stop the electron beam in the laser cell. This occurs or two reasons. First, deleterious three-body dissociation of KrF, namely the reactions $KrF+Ar+M \Rightarrow ArKrF+M$ and $KrF+Kr+M \Rightarrow Kr2F+M$, increases with pressure. (Here M is either Kr or Ar). Note the laser output also drops at higher krypton concentrations for a given pressure. This is because the three body rate constant with Kr is four times that of argon, and excess Kr leads to Kr2F which absorbs the 248 nm laser light. Second non-uniform e-beam deposition at higher pressures, particularly in the case of pure Kr, reduces the extraction efficiency.

The maximum laser output was found to be 510 Joules. In this case the electron beam pump was 700 kW/cc, the laser gas pressure was 20 psi, and the gas composition was 39.75% Kr, 60.0% Ar and 0.25% fluorine. The maximum laser energy was observed at fluorine concentrations of 0.25%. At lower concentrations there is insufficient fluorine to allow maximum lasing throughout the pulse (the so-called “fluorine burn up”), whereas at higher concentrations the excess fluorine absorbs the laser light. Complete details of our first laser operation can be found in the references.[40]

Of particular importance to an IFE system is the intrinsic efficiency of a KrF system. Figure 14 shows the laser output pulse superimposed on the electron beam deposition pulse. The deposited electron beam power is determined by measuring the pressure rise in the gas after the electron beam deposits its energy, and allowing another 10% for radiation. At the peak of the laser pulse the observed intrinsic power efficiency is ~8.4%. This observed efficiency is, after accounting for the actual window transmission in the Electra experiments of 70%-80%, consistent with previous investigations: In one case 12% efficiency was achieved with 10% Kr and a pump rate of 1800 kW/cm^2 for a relatively short (50 nsec) pulse.[41] In another case the same efficiency was achieved with

a 99.6% Kr mixture pumped at a relatively low rate (150 kW/cc) for a much longer pulse (200 nsec).[35]

The intrinsic efficiency of Electra as an amplifier is expected to be around 12% because it will be run without an output coupler and the windows will have higher transmittance. In addition, an amplifier is intrinsically more efficient because it is not amplifying a very low input in the early times as in an oscillator. In other words energy is not wasted to build up the gain. For comparison, other experiments have reported intrinsic KrF amplifier power efficiencies in the range of 12-14%.[35]

We are developing a first principals KrF kinetics code, called "Orestes" to understand the laser behavior and to develop a design tool for future systems. Orestes includes the electron deposition, plasma chemistry, laser transport and amplified spontaneous emission (ASE). The deposition and laser transport is currently treated in 1D, whereas the ASE is modeled in 3D. The code follows over 22 species in at least 130 reactions. In Orestes the e-beam ionization and excitation is determined from a Boltzmann analysis of the electron energy distribution function.[42, 43] The code includes spatial resolution along the laser axis to account for the change in gain from mirror to front window, and carries out detailed energy conservation (better than 1%) to account for the e-beam input, laser input, plasma thermal and internal energies, the Amplified Spontaneous Emission (ASE), and the laser output. Besides the gas phase kinetics, Orestes includes the two excited electronic states of KrF* with vibrational levels up to $v=53$, and includes transitions between these states and levels. The time dependence is fine enough to allow modeling of short pulses (shorter than the transit time between the amplifier sides). ASE gain narrowing is included by performing a multi-frequency transport of the incoherent light around 248 nm. Further details on Orestes can be found in references.[44]

Orestes has accurately predicted the laser output of several different KrF amplifier systems over a wide range of conditions. Figure 15 compares the results from the Nike 60cm amplifier[19], as well as two experiments performed at Keio University.[35] Orestes has been used to model the Electra oscillator as well. It predicts the observed trends, in particular the drop in output at the higher pressures and higher Kr concentrations due to three body interactions. However there is not as good a quantitative agreement as in the amplifier results in Figure 15. It also predicts the shape of the fluorine dependence curve, but predicts the peak at a slightly higher concentration. This has been observed before[45] and may require the code to include a recycling mechanism for the fluorine negative ion to counteract the burn up at low concentrations. The issue is important, because as pointed out above, fluorine is an absorber of 248 nm light, and some designs for a fusion scale laser beam line call for segmented electron beams with unpumped regions of the laser gas. Thus one would like to operate at as low a fluorine concentration as possible.

III.F Overall KrF Laser System Efficiency

Based on our current research, we project that the overall wall plug efficiency for an IFE sized KrF system will be greater than 7.0%. The breakdown is shown in Table II:

Table II, Projected Efficiency Accounting for a large system

Component	Basis	Efficiency
Pulsed Power	Advanced Switch	87%
Hibachi	No Anode, Pattern Beam	77%
KrF intrinsic	Electra Experiments	12%
Optics to target	Estimate	95%
Ancillaries	Pumps, recirculator	95%
	Total	7.2%

This table should be considered provisional, and future research will be directed towards refining these projections. Among the factors yet to be investigated are: losses due to angular multiplexing of the laser beams (each beam does not fully fill the laser cell) and pulse shaping (faithfully amplifying high contrast pulse shapes); and gains due to physics optimization and possible recirculating of the laser gas waste heat.[5]

III.G Repetition Rate Issues

We have operated Electra as an oscillator in 10 shot bursts at 1 Hz. The results are shown in Figure 16. The energy was 504 +/- 17J per pulse, which is effectively the same as the single shot result. There was no systematic degradation in energy throughout the burst. These shots were taken without any cooling so the laser gas temperature rose by about 74 C over the ten shot run. The constancy of the laser output suggests that the kinetics are not dependent on the laser gas temperature, at least in this range of pressure and temperature. The duration of these first tests were limited by a lack of cooling.

II.G.1 The Gas Recirculator

The laser gas will be cooled with a recirculator. The recirculator will also quiet the gas before each shot to ensure that the KrF laser beam is very uniform. This uniformity is essential for achieving high quality laser focal profiles. Of particular importance is the elimination of short scale-length, ordered temperature variations perpendicular to the aperture. The EMRLD laser program successfully addressed this problem: The gas in the laser cell was circulated through a series of mixing plates, diffusers, and heat exchangers. This enabled the EMRLD laser to faithfully amplify a 1.3 x diffraction limited laser beam.[46] The shot rate was 100 Hz, and the (supply- limited) duration was 1.0 second. We have designed and built a gas recirculator for Electra based on the same principles as EMRLD but with a different technology. The recirculator can be seen as the vertical ductwork in the photo of Figure 16. The gas is circulated at nominally 4 m/sec, and our modeling has shown that the recirculator should be able to quiet the laser gas density variations to better than $\Delta\rho/\rho = 10^{-4}$.

III.G.2 Hibachi Foil Cooling

Our measurements and calculations show that the foils absorbs 1 to 1.5 W/cm^2 on Electra. We expect similar numbers in a full size system. This heat can be removed with the

recirculating laser gas. Obviously a quiescent gas flow is not conducive to removing heat, but that can be overcome by periodically tripping the gas into turbulence. This is accomplished by installing a set of moveable airfoils, or louvers, just upstream of the laser cell. Before the electron beams fire, the louvers are parallel to the gas flow to ensure the laser gas is uniform and quiescent. Immediately after the electron beam pulse the louvers are rotated sideways to block all but a few cm of the 30 cm wide gas flow channel. This trips the gas into turbulence and removes heat from the foils. After 100 msec, the louvers are fully opened, which gives ample time for the gas to return to a quiescent state for the next shot. The first tests of this have demonstrated that we can cool the foils with this technique. Figure 17 shows the foil temperature (as measured with a thermocouple) for three different conditions with the system operated at 1 Hz. The working gas was argon and thus there was no laser in these tests. With no cooling at all, the foil temperature reached 360 C, whereas with the gas flowing and the louvers actuating, the foils temperature lowered to 140 C. We have taken 1250 shots continuous at 1 Hz, with no degradation in the foil. Runs at 5 Hz show a considerably higher temperature, but these were not performed at the full laser gas velocity or pressure. For further details, see the references.[34]

The maximum repetition rate with this approach is practically limited to around 10 Hz. While these rep-rates are sufficient for fusion energy, other applications may require a higher repletion rate. For those cases we are developing a second technique that continually sprays an aerosol mist of helium or air and water onto the hibachi foil. The water changes phase as it impacts the hot foil and hence absorbs significant amounts of heat, which is then carried off as steam in the stream. Preliminary bench top experiments, backed with computational modeling, have shown this method will be more than adequate to remove the expected system heat loads[47] and is adaptable to rep-rates up to 250 Hz. While this approach requires the use of an anode foil, with its attendant efficiency issues as discussed in Section III.D, the penalty is estimated to be in the range of 5% at the approximately 800 keV electron beam voltages expected for a full scale beam line. A test module for evaluation on Electra is under development.

III.H. Amplifier Window Development

The amplifier windows operate in a hostile environment--intense laser light, fluorine, uv, x-rays, electrons, and, if water is present, HF. CaF_2, MgF_2, and sapphire have proven to have good resistance to fluorine and to a lesser extent HF. In a clean system with no water, quartz can be quite resistant as well. Quartz is usually the best choice for large aperture (> 20 cm) systems, due to the availability of materials. Studies by Zvorykin have shown that induced residual in absorption in the bulk material from electrons and x-rays are significant in MgF_2, but far less (OD ~ 0.1) in quartz or CaF_2.[48] No matter which of these materials are chosen, all will require an index matching dielectric coating to minimize transmission losses. While the development of the coatings is ongoing, good fluorine laser resistance, high laser damage threshold resistance, and high transmission at 248 nm (nearly 95.5% on one surface coated, which should yield better than 99% for both surfaces) has been obtained with a Alumina/MgF dielectric stack applied on a silica substrate. The transmission was measured after laser damage testing.

IV. Next Generation System

As discussed in the beginning of Section III, a full scale beam line for a fusion power plant would produce about 50-100 kJ of laser light. It is preferable to have a parallel array of pulsed power systems driving the electron beams, rather than a single one. This is to minimize thermal issues, allow for manageable systems, and to minimize damage from fault modes. Accordingly, we are presently evaluating a large amplifier that uses segmented cathodes. The concept is shown in Figure 18, and follows a design first proposed by McGeoch.[49] The laser gas would be pumped by an array of electron beams, with each beam powered by its own pulsed power system of the designs shown in Figure 7. Each cathode would be in the range of 50 cm wide by 100 cm high, and thus be smaller than the one used in Nike. The characteristic dimension of the optical aperture would be on the order of 100 cm or less, which is again comparable to existing facilities. One issue with this segmented approach is the "unpumped regions" between the cathodes that are not pumped by the electron beams. As discussed at the end of Section III.E, fluorine is an absorber, and having these unpumped regions may compromise the efficiency. This issue is being evaluated in detail. If it turns out to be serious, there are techniques, such as shaping the cathode and hibachi foil, to minimize, if not eliminate these regions.

V. Summary/Acknowledgements

We are developing KrF laser technologies to meet the IFE requirements for rep-rate, efficiency and durability. Advances in pulsed power, electron beam propagation, hibachi design and KrF kinetics lead to a predicted overall efficiency which should be sufficient for IFE. We have operated an electron beam pumped KrF oscillator in a repetitively pulsed burst mode, and found the output to be constant at 500 J over the range of the run. A method to cool the pressure foil by deflecting the laser gas appears to be feasible, based on preliminary experiments.

The authors wish to thank T. Albert, J. Dubinger, R. Jones, A. Mangassarian, F. Mora, and W. Webster for their technical and engineering support. This work is sponsored by the US Department of Energy, NNSA/DP.

VI. Figure Captions

1. The Electra Laser Facility. Note the ladders for scale.

2. Key components of an electron beam pumped KrF laser

3. Optical train of a KrF laser. The focal profile is rapidly smoothed on the time scales of interest. The spatial profile at the aperture is imaged onto the target. A Pockels cell is used to control the laser temporal pulse shape.

4. The measured focal profile of one of the Nike Laser beams.

5. Layout of the Nike 60 cm amplifier. This is the largest and final amplifier in the system. The PFL's are bent through 90 degrees because of space considerations

6. Layout of the pulsed power for the Electra Laser system. Only one of two sides is shown.

7. Schematic of the advanced pulsed power system, using an ultra fast Marx and a magnetic switch.

8. Concept of the Laser Triggered and Pumped Thryristor (LGPT).

9. Conceptual design of an LGPT for use in the ultra fast Marx Shown in Figure 7.

10. Comparison of power and voltage waveforms without (upper) and with (lower) the ceramic honeycomb placed in front of the emitter.

11. Cathode configurations (left) and Fast Fourier transform of dI/dt (right). Upper shows results from monolithic cathode. The FFT shows instability at 2.5 GHz. Lower shows results that slotted cathode completely suppresses the instability.

12. Upper: Conventional hibachi configuration. Lower: High energy deposition hibachi configuration. The electron beam is shown as an LSP simulation.

13. Laser output as a function of laser gas pressure and composition.

14. Laser and e-beam deposition powers.

15. Predictions of Orestes KrF Physics code for two different experiments.

16. Laser oscillator output for a ten shot, 1 Hz burst. The continuously rising curve is the cumulative laser energy measured with a full aperture (33 cm x 33 cm) calorimeter. Note the calorimeter cools slightly between shots. The individual spikes are the calculated laser energy for each shot, obtained by compensating for the measured calorimeter cooling rate. The average laser energy is 500 J per shot.

17. Foil temperature under various conditions

18. Conceptual arrangement of a full scale laser beam line following Ref 49. All dimensions are approximate, and given to show scale only.

19. VII. References

[1] J.D. Sethian, M. Friedman, R.H. Lehmberg, et al "Fusion energy with lasers, direct drive targets, and dry wall chambers," to be published in Nuclear Fusion, **43,** (2003).

[2] S E Bodner, D. G. Colombant, A. J. Schmitt, and M. Klapisch, "High gain direct drive target design for laser fusion," Physics of Plasmas **7**, 2298 (2000).

[3] D. Colombant, S. E. Bodner, A. J. Schmitt, *et al,* "Effect of radiation on direct drive laser fusion targets," Physics of Plasmas **7**, 2046 (2000).

[4] A.J. Schmitt, D. Colombant, S. Velikovich, S. Zalesak, J. Bates, J. Gardner, D. Fyfe, L. Phillips, N. Metzler, "Direct drive pellet designs and performance: High resolution simulation and theory," Presented at the Third International Fusion Science and Applications Conference, Monterey CA, Sep 8-12, 2003. Paper TuO4.1. To be published in Fusion Science and Technology.

[5] I. V. Sviatoslavsky, M. E. Sawan, R. R. Peterson, G. L. Kulcinski, J. J. MacFarlane, L. J. Wittenberg, H. Y. Khater, E. A. Mogahed, and S. C. Rutledge, "A KrF laser driven inertial confinement fusion reactor 'SOMBRERO'," Fusion Technology **21**, 1470 (1992).

[6] N. G. Basov, V. V. Baronov, A. Y. Chugunov, et al, "60 J quasistationary electroionization laser on Xe atomic metastables", IEEE Journal of Quantum Electronics, Vol. QE-21, pp. 1756-1760 (1985).

[7] V. N Smiley, "Review of high power excimer lasers" SPIE Volume on High Power Gas Lasers, **1225**, 2, (1990).

[8] I. Okuda, E. Takahashi, I. Matsushima, Y. Matsumoto, H. Yashiro, E. Miura, T. Tomie, and Y. Owandano, Fusion Engineering and Design 44, 377 (1999).

[9] I. Okuda, J. Ma, E. Takahashi, I. Matsushima, Y. Matsumoto, S. Kato, and Y. Owandano, Applied Physics B-Lasers and Optics 75, 623 (2001).

[10] N. Wang, Y. Shan, and W. Ma, et al, Lasers and Particle Beams 20, 119 (2002).

[11] V. D. Zvorykin, S. V. Arlantsev, V. G. Bakaev, O. V. Rantsev, P. B. Sergeev, G. V. Sychugov, and A. Yu. Tserkovnikov, Lasers and Particle Beams 19, 609 (2001).

[12] E. Divall, C. Edwards, and G. Hirst, et al, Journal of Modern Optics 43, 1025 (1996).

[13] L. Rosocha, F. Riepe, J. Hanlon, J. McLeod, M. Kang, B. Kortegaard, M. Burrows, and P. Bowling, "Aurora multikioljoule KrF laser system prototype for inertial confinement fusion," Fusion Technology 11, 497 (1987).

[14] J. D. Sethian, M. Friedman, J L. Giuliani, Jr., R. H. Lehmberg, M. Myers, S. Obenschain, F. Hegeler, and S. B. Swanekamp, in *Inertial Fusion Sciences and Applications*, edited by K. A. Tanaka, D.D. Meyerhoffer, and J. Meyer-ter-Vehn (Elsevier, New York, 2002), Vol. **1**, p.495.

[15] S. P. Obenschain, S. E. Bodner, D. Colombant, *et al*, "The Nike KrF laser facility: Performance and intitial target experiments," Physics of Plasmas **3**, 2098 (1996).

[16] R. H. Lehmberg and J. Goldhar, "Profile control by incoherence," Fusion Technology **11**, 532 (1987).

[17] R. H. Lehmberg, A. J. Schmitt, and S. E. Bodner, "Theory of induced spatial incoherence," Journal of Applied Physics **68**, 2680 (1987).

[18] J. A. Hanlon and J. McLeod, "The Aurora laser optical system," Fusion Technology **11**, 634 (1987).

[19] J.D. Sethian, S.P. Obenschain, K.A. Gerber, C.J. Pawley, et al, "Large area electron beam pumped krypton fluoride laser amplifier," Rev Sci Instrum, **68,** 2357 (1997).

[20] J. D. Sethian, M. Myers, I. D. Smith, *et* al, "Pulsed power for a rep rate electron beam pumped KrF laser", IEEE Transactions on Plasma Science **28**, 1333 (2000).

[21] W.S. Melville, "The Use of Saturable Reactors as Discharge Devices for Pulse Generators," Proc. IEE, (London) Vol.98, Part 3 (Radio and Communication), No. 53, 1951, p.185.

[22] D.L. Birx, et al, "Experiments in magnetic switching," Proc. Third IEEE Pulsed Power Conference, p 226 (1981).

[23] L.X Schneider, et al, "Repetitive high energy pulsed power technology development," Proc, 14th Int Conf on Accelerators in Industry & Research, Denton TX, Nov 6-9 (1996).

[24] D. Weidenheimer,V. Carboni, D. Morton, *et al*, "Advanced pulsed power concept and component development for KrF laser IFE" to be published in the Proceedings of the IEEE Power Modulator Conference, Hollywood, CA, June 31-July 2, 2002 (IEEE Piscataway, NJ).

[25] L.R. Lowry, “Optically Activated Switch,” Westinghouse R&D Center, Pittsburgh, PA, April 1978, Technical Report AFAPL-TR-78-17.

[26] Medici™, Version 2001.4, Avant! Corporation, 2002.

[27] C.D. Child, “Discharges from a hot cao,” *Phys. Rev.* **32** 492(1911)

[28] M.C. Myers, F. Hegeler, M. Friedman, and J. D. Sethian, “Development of a durable, large area cathode for repetitive, uniform electron beam generation,” Digest of Technical Papers, IEEE Pulsed Power Conference, Las Vegas, Nevada, June 17-22, 2001. IEEE, NY p 710 (2001).

[29] M. Friedman, M. Myers, F. Hegeler, S.B. Swanekamp, J. D. Sethian, L. Ludeking, “Emission of an intense electron beam from a ceramic cathode honeycomb”, Appl Phys Lett, **82,** 179 (2003).

[30] M. Friedman, S. B. Swanekamp, S. Obenschain, Y. Chan, L. Ludeking, and D. Smithe, “Stability of large area electron beam diodes,” Applied Physics Letters **77**, 1053 (2000).

[31] M. Friedman, Y. Chan, S. Obenschain, J.D. Sethian, and S.B. Swanekamp, “Eliminating the Transit-Time Instability in Large-Area Electron-Beam Diodes,” App Physics Letters, 83, 1539 (2003).

[32] D. V. Rose, D. R. Welch, F. Hegeler, S. B. Swanekamp, M. C. Myers, and J. D. Sethian, “Numerical modeling of large-area electron-beam diodes for KrF lasers,” Journal Appl Phys, **94,** 5343 (2003).

[33] F. Hegeler, M. Friedman, M.C. Myers, J.D. Sethian, and S.B. Swanekamp, "Reduction of Edge Emission in Electron Beam Diodes,” *Physics of Plasmas*, **9**, 4309 (2002).

[34] F. Hegeler, M.C. Myers, J.D. Sethian, D.V. Rose, M. Friedman, M.F. Wolford, J.L. Giuliani, S.B. Swanekamp, and A. Banka, “Efficient electron beam pumping of repetitively pulsed, high energy krypton fluoride lasers”, Presented at the Third International Fusion Science and Applications Conference, Monterey CA, Sep 8-12, 2003. Paper TuPo1.31. To be published in Fusion Science and Technology.

[35] A. Suda, H. Kumagai. and M. Obara, "Characteristics of an electron beam pumped KrF laser amplifier with an atmospheric-pressure Kr-rich mixture in a strongly saturated region," Appl. Phys. Lett., vol.51, issue 4, pp.218-220 (1987).

[36] A.E. Mandl, D.E. Klimek and E. Salesky, “KrF laser studies at high krypton density”, Fusion Technology 11, 542 (1987).

[37] Y. Owandano, I. Okuda, M. Tanimoto, Y. Matsumoto, T. Kaeshi and M. Yano, "Development of a 1 kJ KrF laser system for laser fusion research," Fusion Technology 11, 486 (1987).

[38] F. Kanari, M. Obara, and T. Fujikoa, "An advanced kinetic model of electron beam excited KrF lasers including the vibrational relaxation in KrF(B) and collisional mixing of KrF(B,C),: J. Appl. Phys. 4322 (1985).

[39] W. W. Rigrod, "Saturation effects in high-gain lasers," Journal of Applied Physics, 36, 2487 (1965).

[40] M. F. Wolford, F. Hegeler, M. C. Myers, J. Giuliani, P. Kepple, and J. D. Sethian, "Electra as an oscillator: A repetitively pulsed, 500 J, 100 ns, KrF laser," Presented at the Third International Fusion Science and Applications Conference, Monterey CA, Sep 8-12, 2003. Paper Wpo4.36. To be published in Fusion Science and Technology.

[41] J.K. Rice, G.C. Tisone, E.L. Patterson, "Oscillator performance and energy extraction from a KrF laser pumped by a high-intensity relativistic electron beam," IEEE J. Quantum Electronics, **QE-16,** 1315 (1980).

[42] G. M. Petrov, J. L. Giuliani, and A. Dasgupta, "Electron energy deposition in an electron-beam pumped KrF amplifier: Impact of beam power and energy," Journal of Applied Physics, **91**, 2662 (2002).

[43] J. L. Giuliani, Jr., G. M. Petrov, and A. Dasgupta, "Electron energy deposition in an electron-beam pumped KrF amplifier: Impact of the gas composition," Journal of Applied Physics, **92**, 1200 (2002).

[44] J.L. Giuliani, P. Kepple, R.H. Lehmberg, M.C. Myers, J.D. Sethian, M.F. Wolford, F. Hegeler, G. Petrov, "Orestes: A kinetics model for electron beam pumped KrF lasers," Presented at the Third International Fusion Science and Applications Conference, Monterey CA, Sep 8-12, 2003. Paper Wpo4.31. To be published in Fusion Science and Technology.

[45] P.J.M. Peters, H.M.J. Basraens, W.J. Witterman, and T. Gerber, "A study of electron quenching of excimers in a KrF laser excited by a coaxial electron beam", Appl. Phys. B., **43**, 253 (1987).

[46] J. Moran, Textron Defense Systems, Everett MA, private communication.

[47] V. Novak,D. Sadowski, S. Shin, K. Schoonover, and S. Abdel-Khalik, "Experimental and numerical study of mist cooling for the Electra hibachi," Presented at the seventh High Average Power Laser workshop, Madison WI, (2003). Accessible at http://michelle.ucsd.edu/HAPL/

[48] V. Zvorykin, et al, Presented at the Third International Fusion Science and Applications Conference, Monterey CA, Sep 8-12, 2003. Paper Wpo4.31. To be published in Fusion Science and Technology.

[49] M.W. McGeoch , P.A. Corcoran, R.G. Altes, I.D. Smith, S.E. Bodner, R.H. Lehmberg, S.P. Obenschain, and J.D. Sethian. “Conceptual design of a 2 MJ KrF laser facility”. Fusion Technology, 32, 610 (1997).

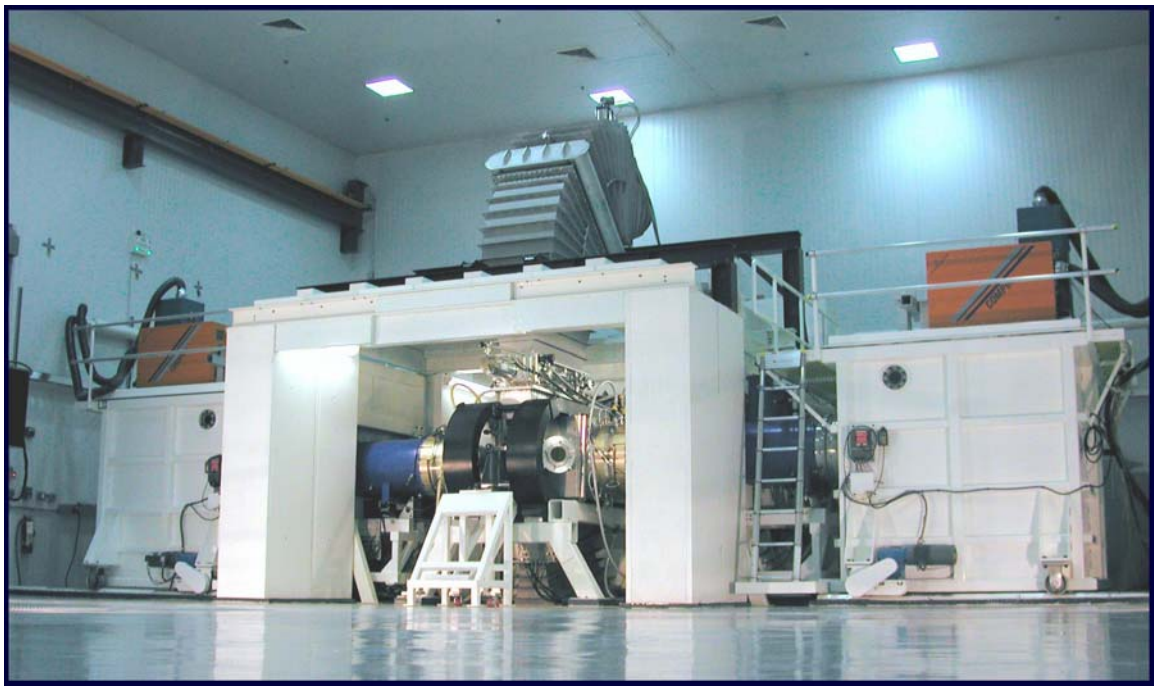

1. The Electra Laser Facility. Note the ladders for scale.

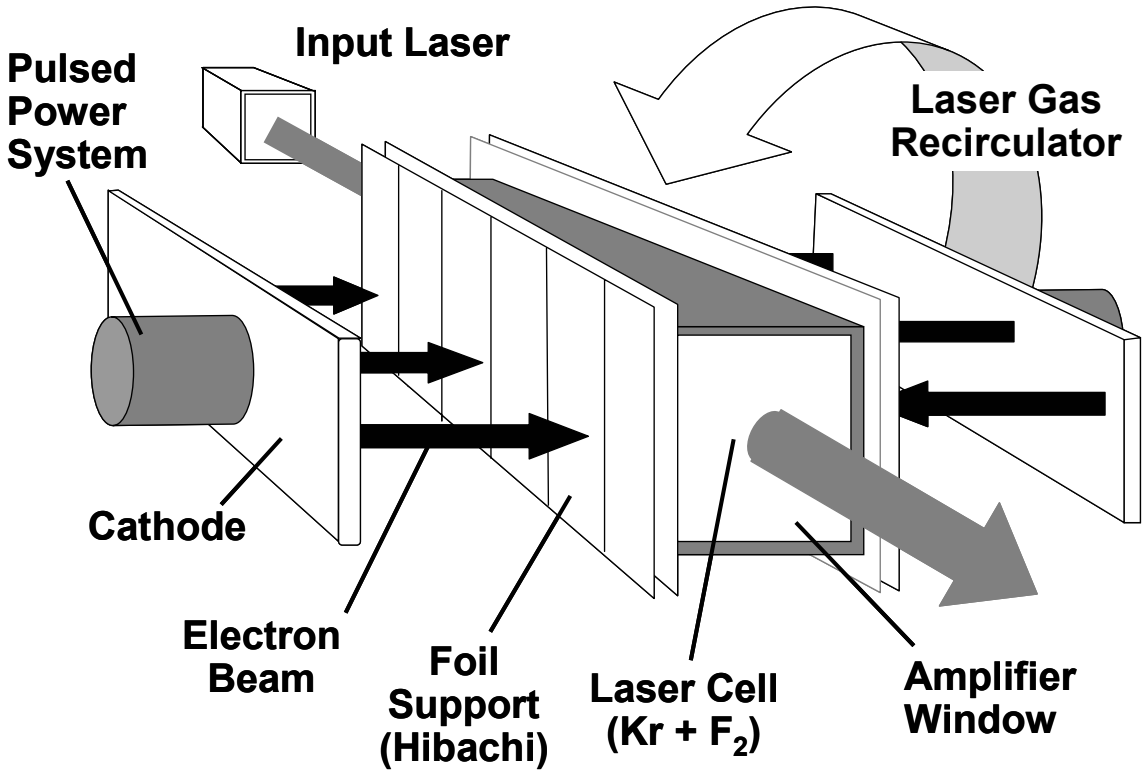

2. Key components of an electron beam pumped KrF laser

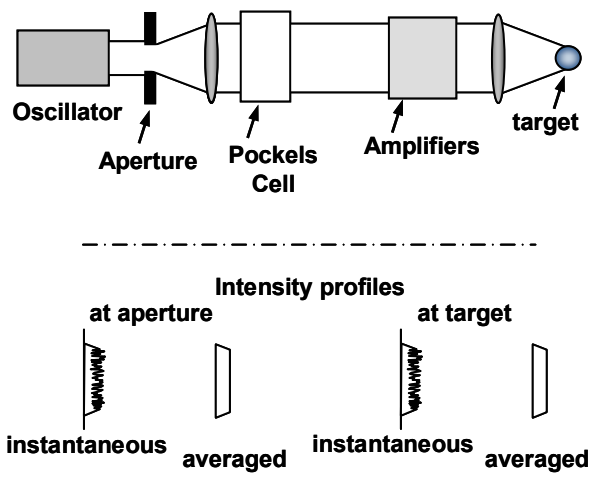

3. Optical train of a KrF laser. The focal profile is rapidly smoothed on the time scales of interest. The spatial profile at the aperture is imaged onto the target. A Pockels cell is used to control the laser temporal pulse shape.

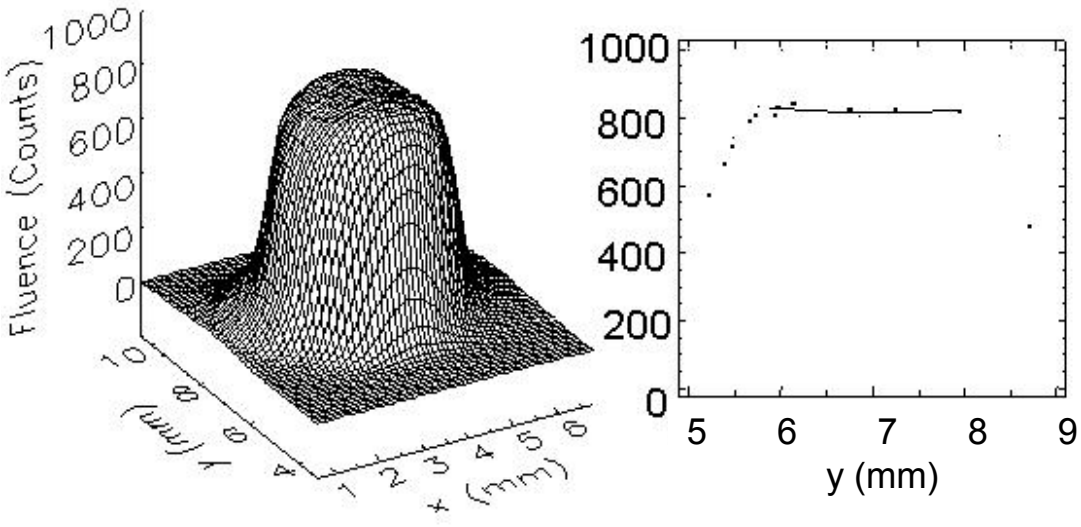

4. The measured focal profile of one of the Nike Laser beams.

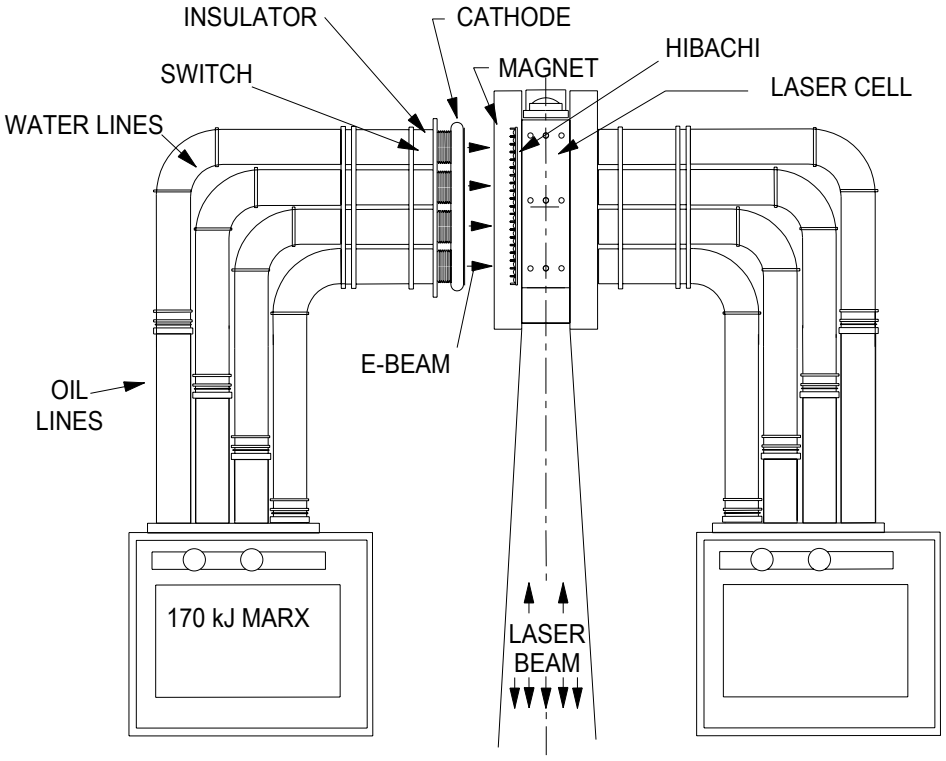

5. Layout of the Nike 60 cm amplifier. This is the largest and final amplifier in the system. The PFL's are bent through 90 degrees because of space considerations

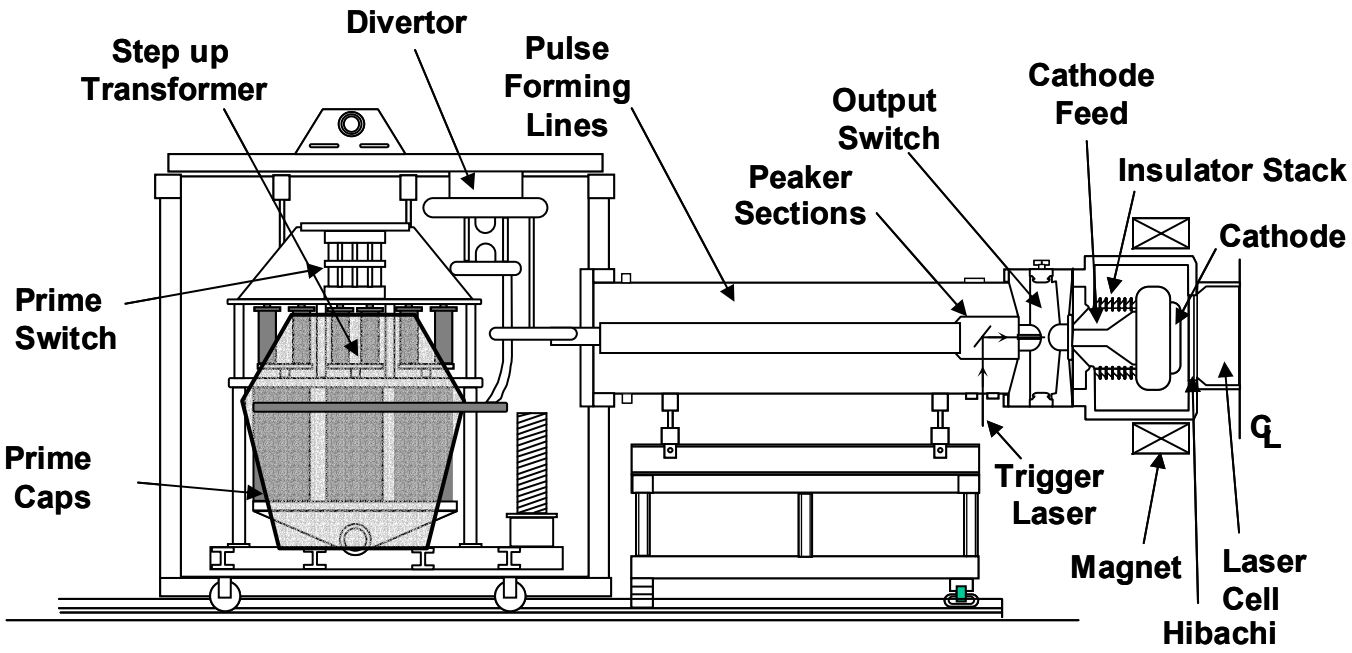

6. Layout of the pulsed power for the Electra Laser system. Only one of two sides is shown.

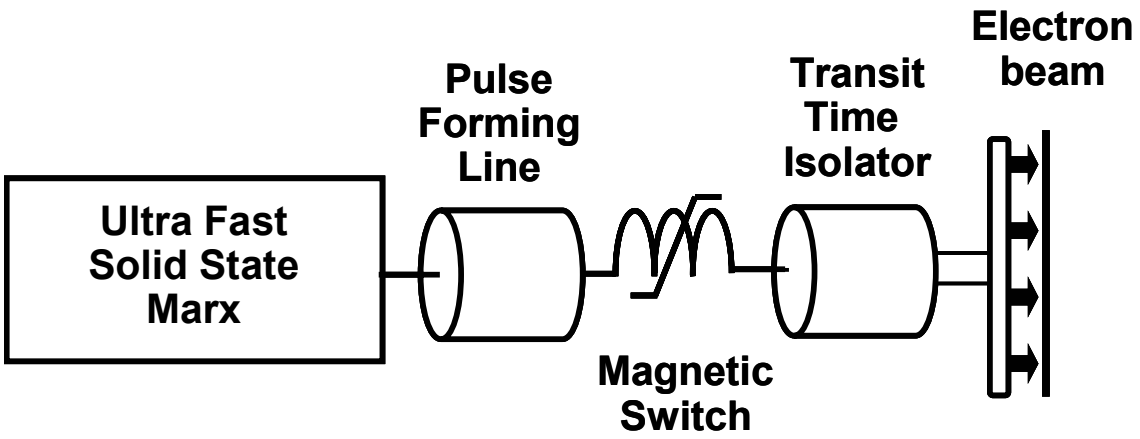

7. Schematic of the advanced pulsed power system, using an ultra fast Marx and a magnetic switch.

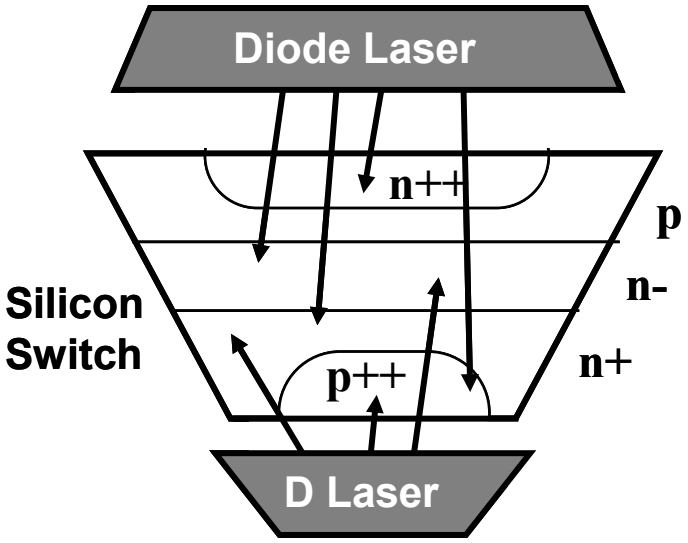

8. Concept of the Laser Triggered and Pumped Thryristor (LGPT).

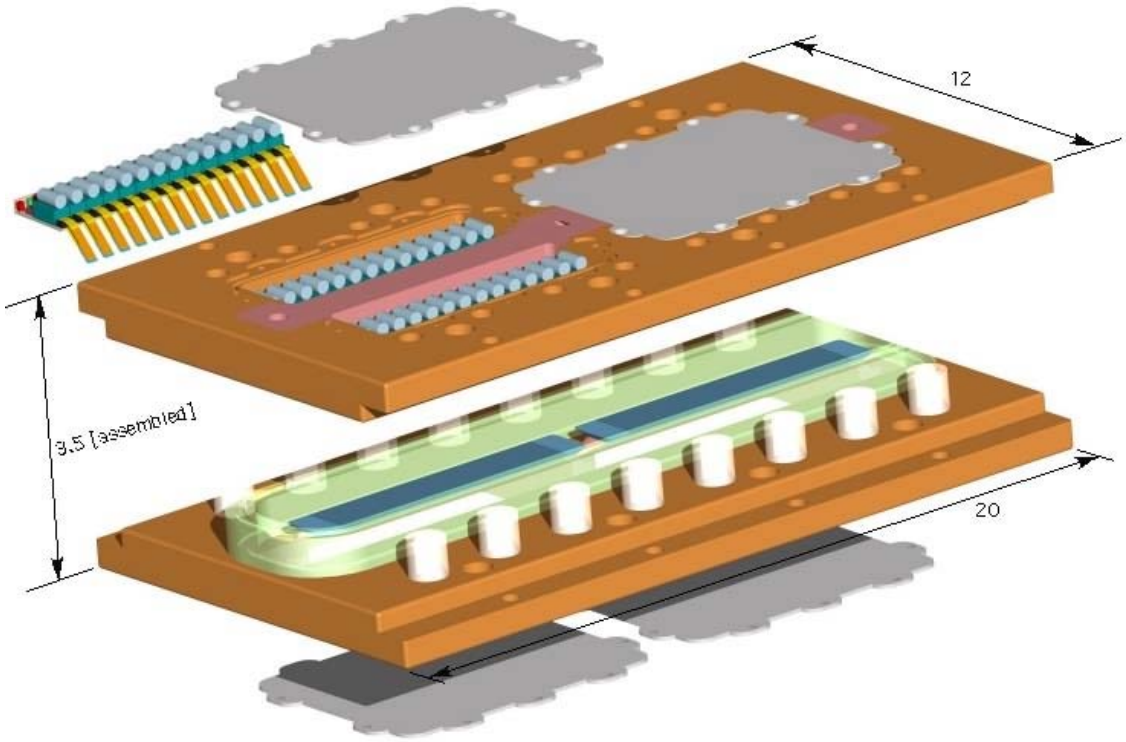

9. Conceptual design of an LGPT for use in the ultra fast Marx Shown in Figure 7.

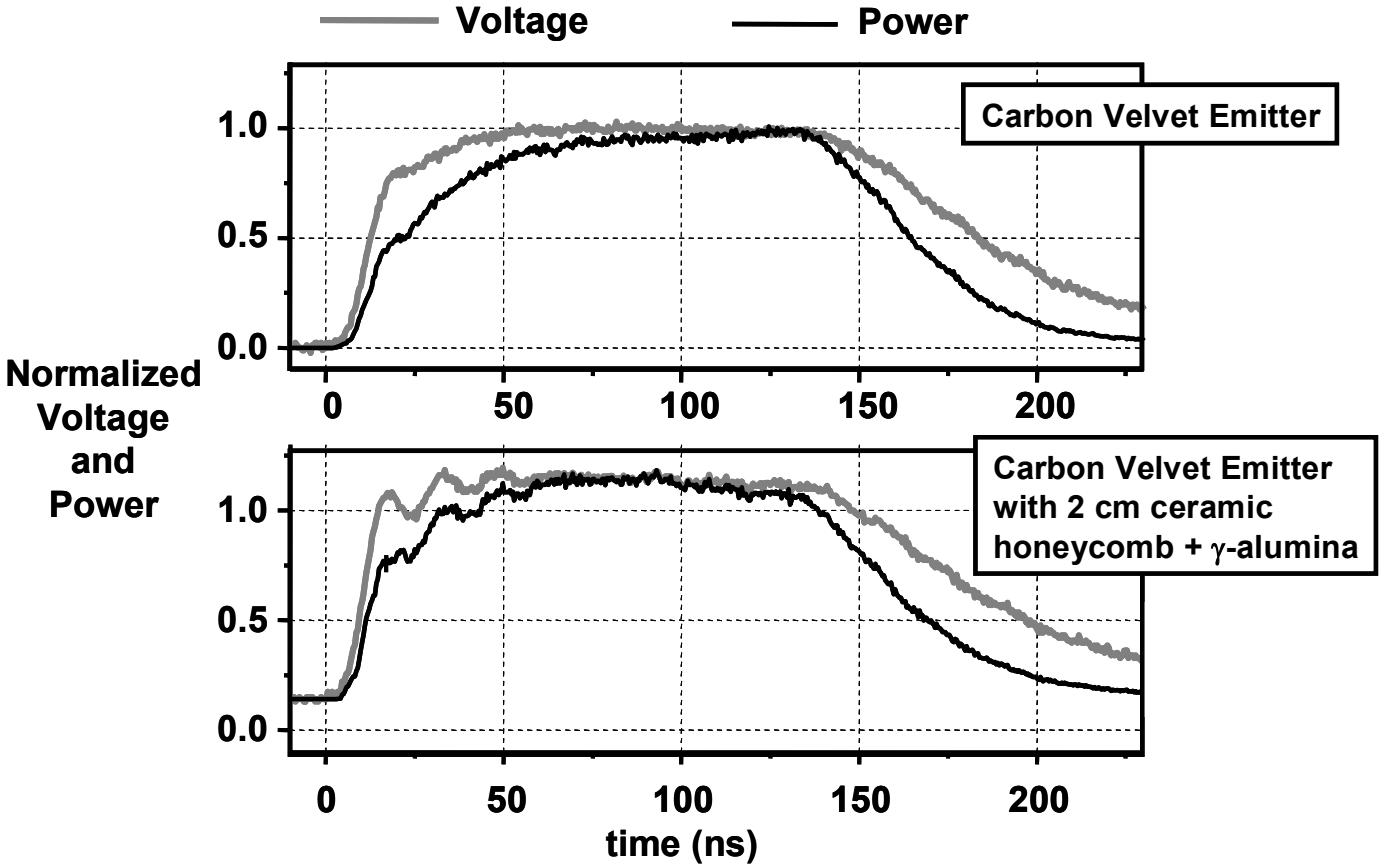

10. Comparison of power and voltage waveforms without (upper) and with (lower) the ceramic honeycomb placed in front of the emitter.

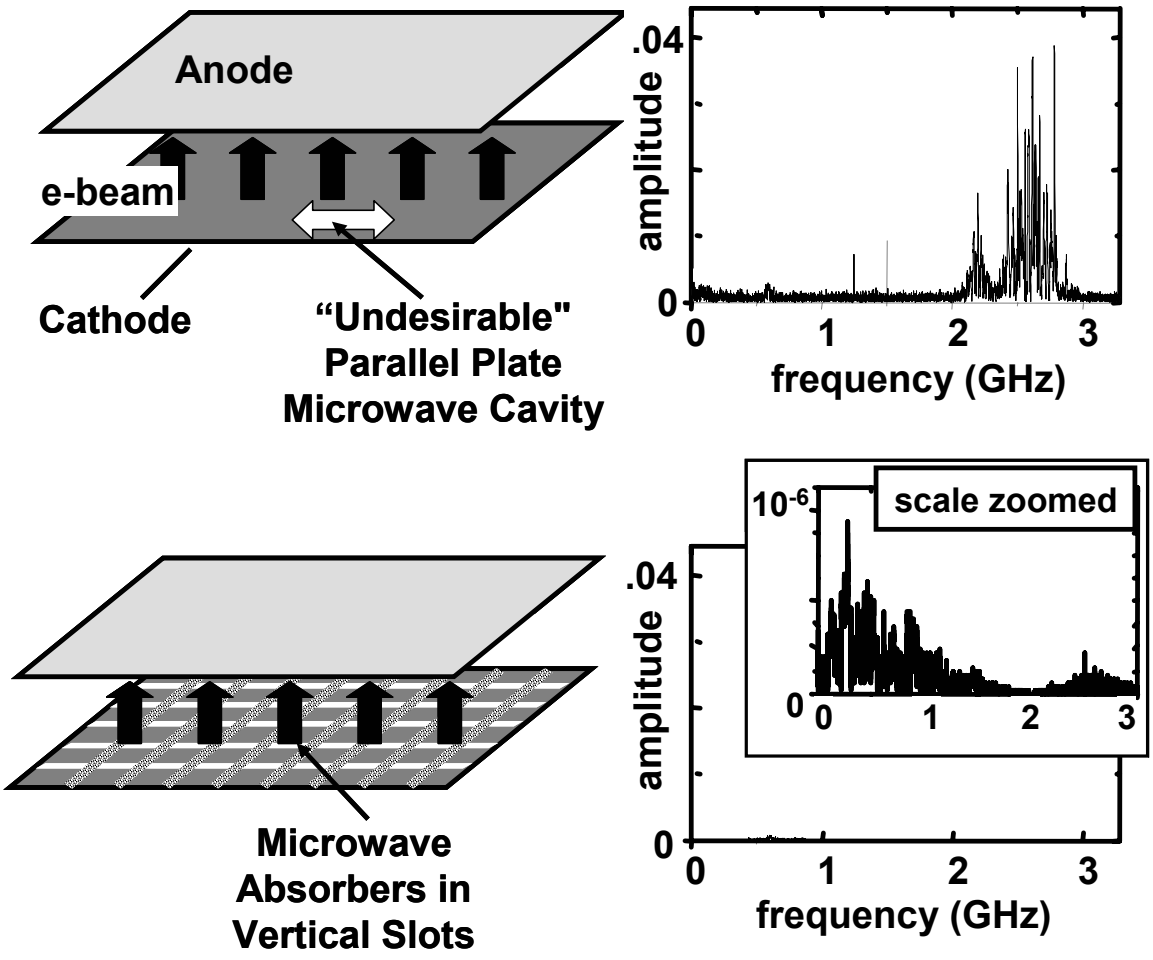

11. Cathode configurations (left) and Fast Fourier transform of dI/dt (right). Upper shows results from monolithic cathode. The FFT shows instability at 2.5 GHz. Lower shows results from the slotted cathode that completely suppresses the instability.

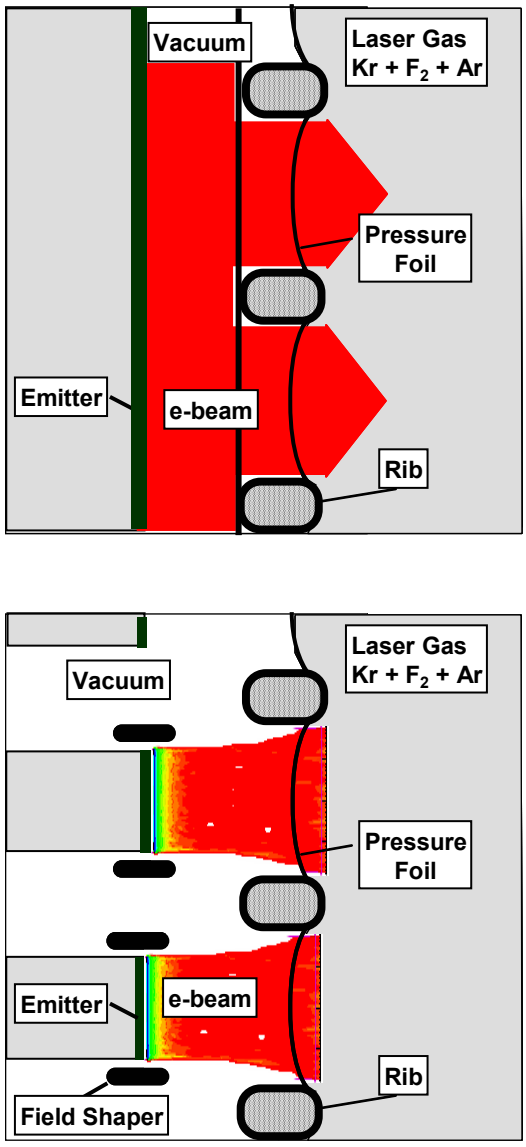

12. Upper: Conventional hibachi configuration. Lower: High energy deposition hibachi configuration. The electron beam is shown as an LSP simulation.

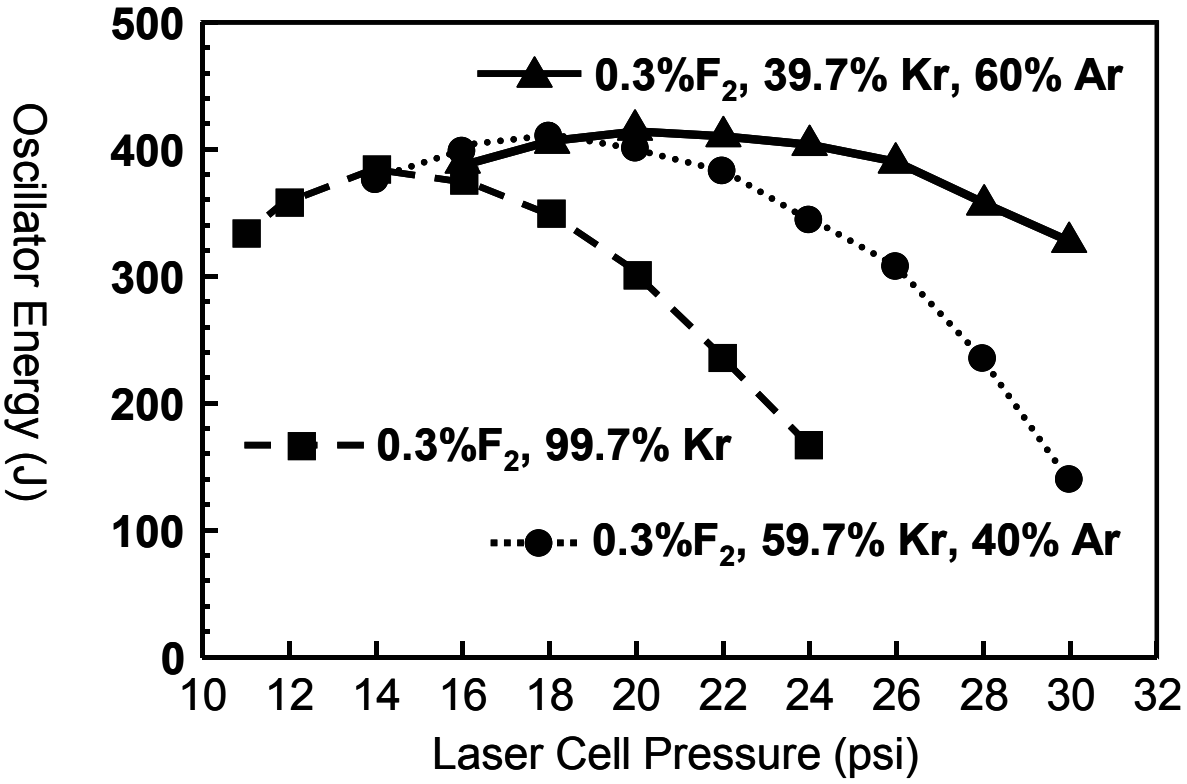

13. Laser output as a function of laser gas pressure and composition.

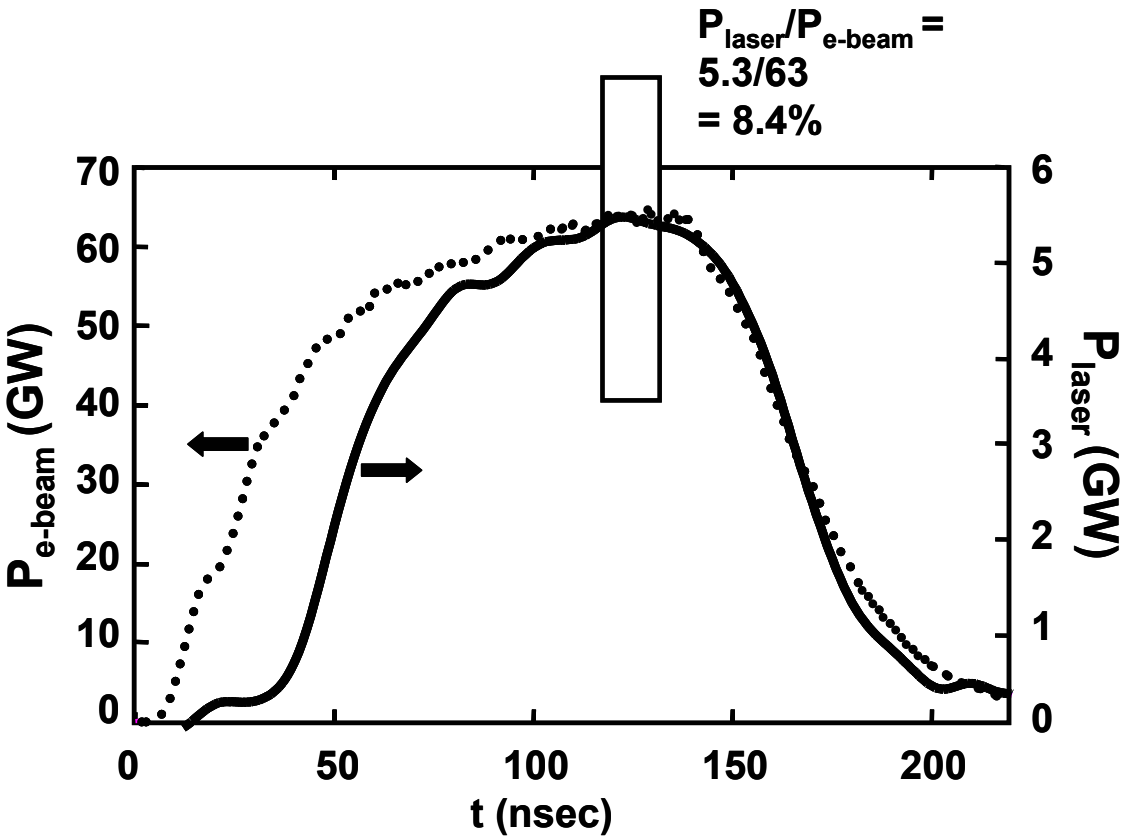

14. Laser and e-beam deposition powers.

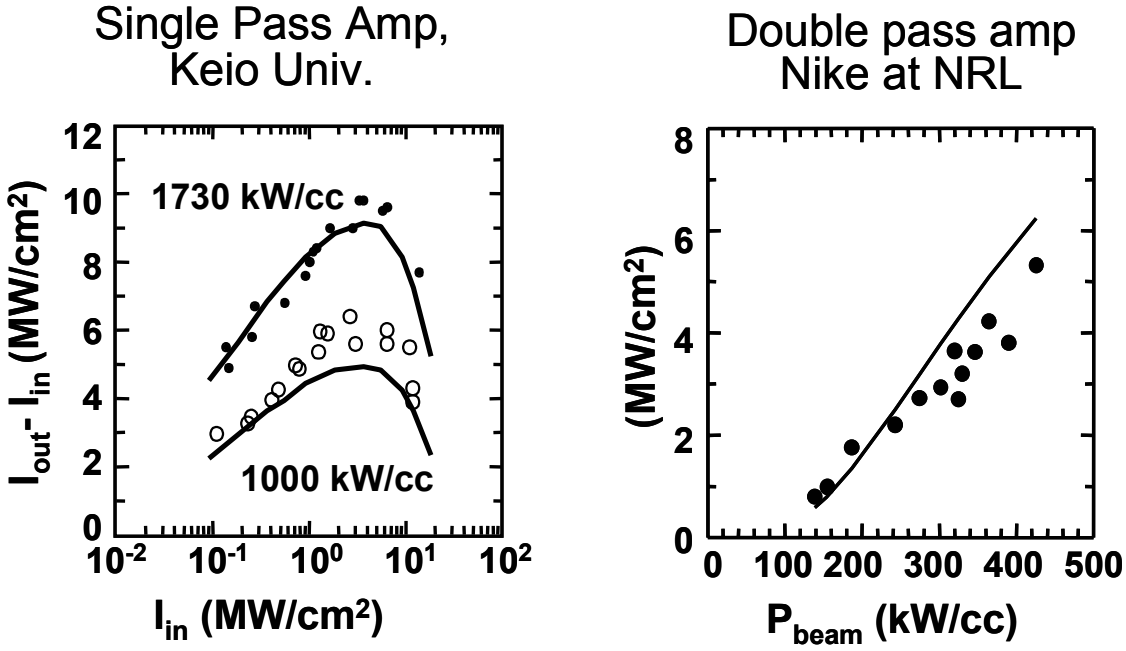

15. Predictions of Orestes KrF Physics code for two different experiments.

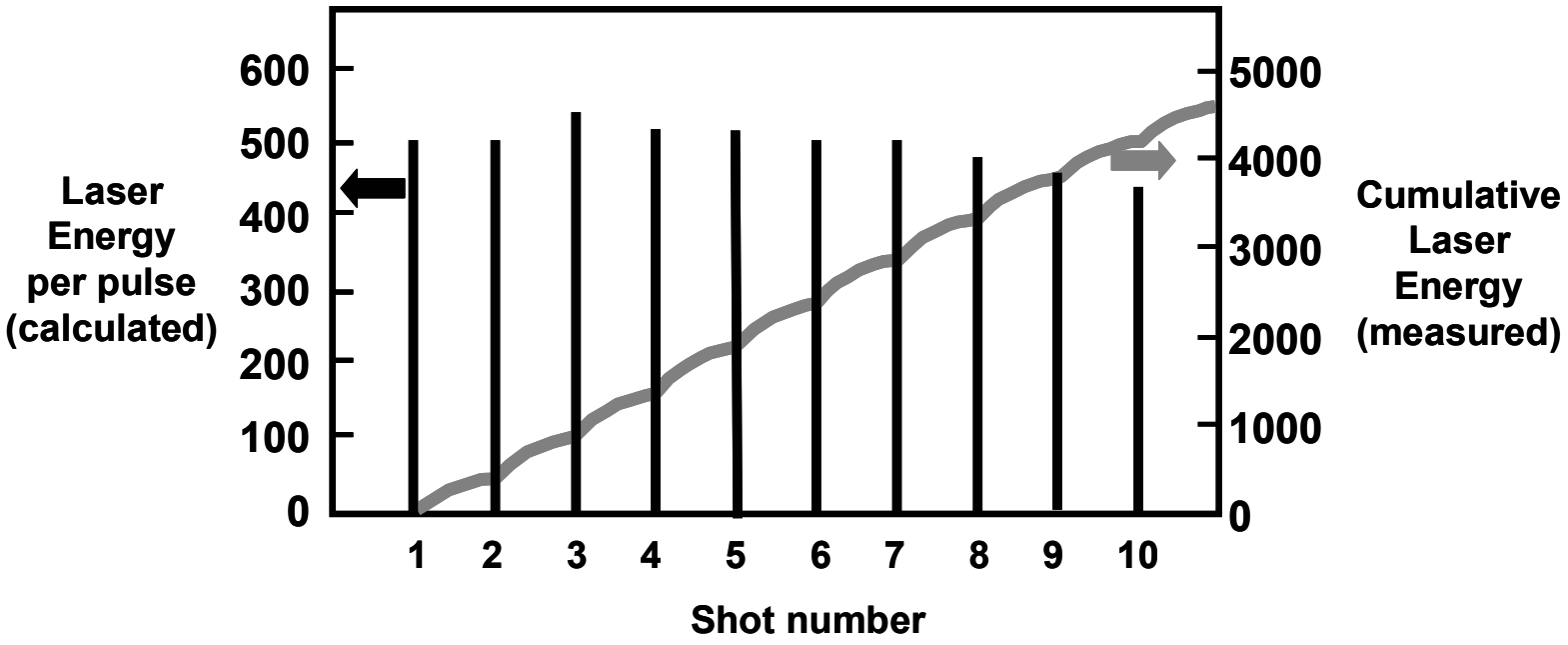

16. Laser oscillator output for a ten shot, 1 Hz burst. The continuously rising curve is the cumulative laser energy measured with a full aperture (33 cm x 33 cm) calorimeter. Note the calorimeter cools slightly between shots. The individual spikes are the calculated laser energy for each shot, obtained by compensating for the measured calorimeter cooling rate. The average laser energy is 500 J per shot.

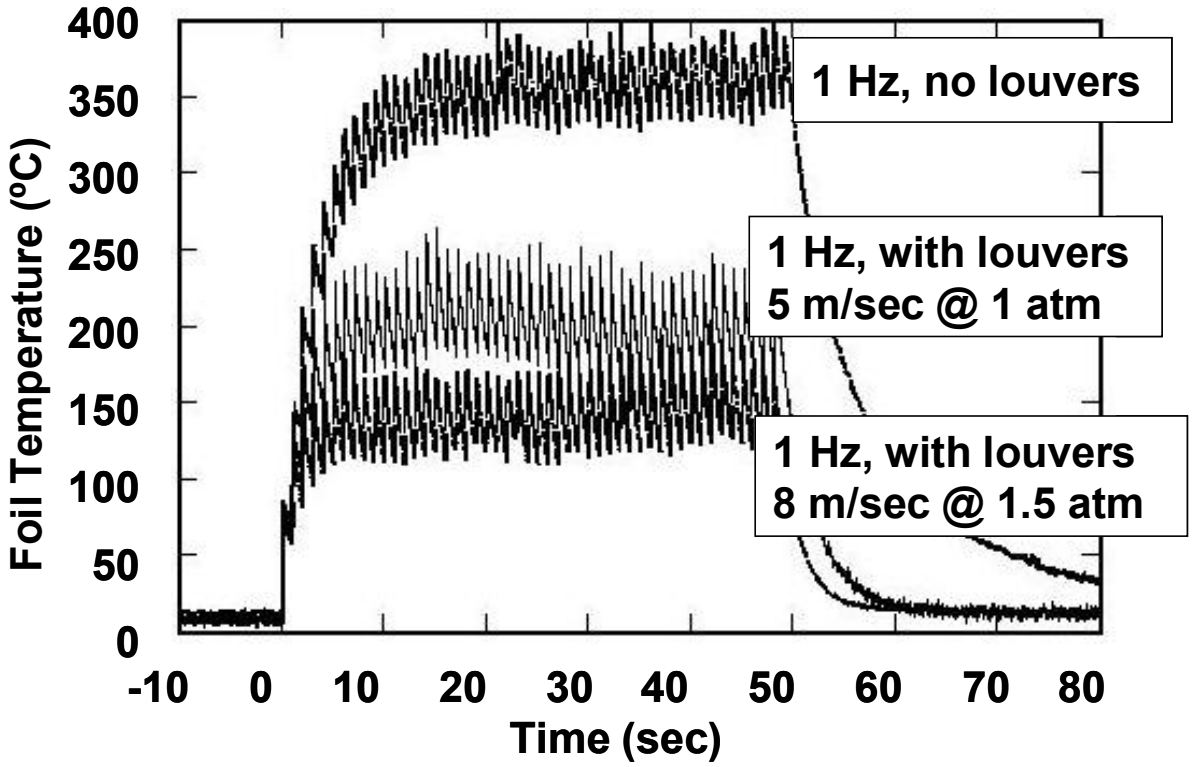

17. Foil temperature under various conditions

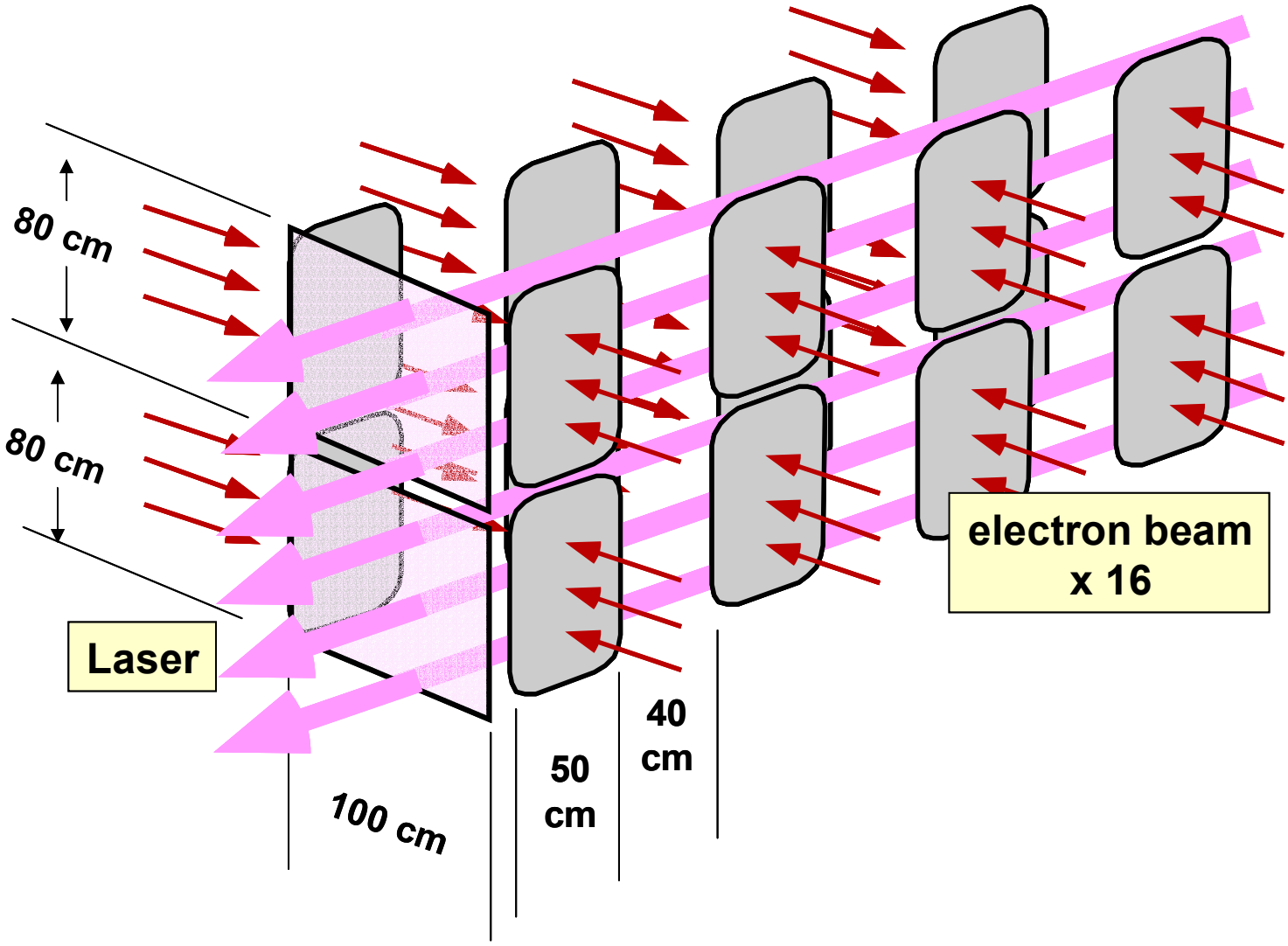

18. Conceptual arrangement of a full scale laser beam line following Ref 49. All dimensions are approximate, and given to show scale only.

Appendix H
***Nuclear Fusion* Paper on IFE with Lasers, Direct-Drive Targets, and Dry-Wall Chambers**

INSTITUTE OF PHYSICS PUBLISHING and INTERNATIONAL ATOMIC ENERGY AGENCY NUCLEAR FUSION

Nucl. Fusion **43** (2003) 1693–1709 PII: S0029-5515(03)67272-8

Fusion energy with lasers, direct drive targets, and dry wall chambers

J.D. Sethian[1], M. Friedman[1], R.H. Lehmberg[1], M. Myers[1], S.P. Obenschain[1], J. Giuliani[1], P. Kepple[1], A.J. Schmitt[1], D. Colombant[1], J. Gardner[1], F. Hegeler[2], M. Wolford[3], S.B. Swanekamp[4], D. Weidenheimer[5], D. Welch[6], D. Rose[6], S. Payne[7], C. Bibeau[7], A. Baraymian[7], R. Beach[7], K. Schaffers[7], B. Freitas[7], K. Skulina[7], W. Meier[7], J. Latkowski[7], L.J. Perkins[7], D. Goodin[8], R. Petzoldt[8], E. Stephens[8], F. Najmabadi[9], M. Tillack[9], R. Raffray[9], Z. Dragojlovic[9], D. Haynes[10], R. Peterson[10], G. Kulcinski[10], J. Hoffer[11], D. Geller[11], D. Schroen[12], J. Streit[12], C. Olson[13], T. Tanaka[13], T. Renk[13], G. Rochau[13], L. Snead[14], N. Ghoneim[15] and G. Lucas[16]

[1] Plasma Physics Division, Naval Research Laboratory, Washington, DC, USA
[2] Commonwealth Technology, Inc. Alexandria, VA, USA
[3] SAIC, McLean, VA, USA
[4] JAYCOR, Alexandria, VA, USA
[5] Titan Pulse Sciences Division, San Leandro, CA, USA
[6] Mission Research Corporation, Albuquerque, NM, USA
[7] Lawrence Livermore National Laboratory, Livermore, CA, USA
[8] General Atomics, San Diego, CA, USA
[9] University of California, San Diego, CA, USA
[10] University of Wisconsin, Madison, WI, USA
[11] Los Alamos National Laboratory, Los Alamos, NM, USA
[12] Schafer Corp., Albuquerque, NM, USA
[13] Sandia National Laboratories, Albuquerque, NM, USA
[14] Oak Ridge National Laboratory, Oak Ridge, TN, USA
[15] University of California Los Angeles, Los Angeles, CA, USA
[16] University of Santa Barbara, Santa Barbara, CA, USA

E-mail: sethian@this.nrl.navy.mil

Received 14 October 2002, accepted for publication 22 July 2003
Published 1 December 2003
Online at stacks.iop.org/NF/43/1693

Abstract
A coordinated, focused effort is underway to develop Laser Inertial Fusion Energy. The key components are developed in concert with one another and the science and engineering issues are addressed concurrently. Recent advances include: target designs have been evaluated that show it could be possible to achieve the high gains (>100) needed for a practical fusion system.These designs feature a low-density CH foam that is wicked with solid DT and over-coated with a thin high-Z layer. These results have been verified with three independent one-dimensional codes, and are now being evaluated with two- and three-dimensional codes. Two types of lasers are under development: Krypton Fluoride (KrF) gas lasers and Diode Pumped Solid State Lasers (DPSSL). Both have recently achieved repetitive 'first light', and both have made progress in meeting the fusion energy requirements for durability, efficiency, and cost. This paper also presents the advances in development of chamber operating windows (target survival plus no wall erosion), final optics (aluminium at grazing incidence has high reflectivity and exceeds the required laser damage threshold), target fabrication (demonstration of smooth DT ice layers grown over foams, batch production of foam shells, and appropriate high-Z overcoats), and target injection (new facility for target injection and tracking studies).

PACS numbers: 52.57.-z, 42.55.Xi, 42.55.Lt, 52.57.Bc, 83.60.-a, 52.57.Fg, 52.59.Mv

1. Introduction

We are carrying out a coordinated, focused research programme to develop Laser Inertial Fusion Energy (Laser IFE). The approach is based on lasers, direct drive targets, and dry wall chambers. The key components are developed in concert with one another and the science and technology are addressed at the same time. This integrated approach ensures Laser Fusion Energy will be developed as a coherent system.

The attractiveness of this approach lies in its inherent simplicity, its separable architecture, and the modular nature of the laser driver. The targets are spherical shells, which can be fabricated in droplet generators, and thus naturally lend themselves to mass production. None of the target components (except tritium) need to be recycled. The first wall is a passive structure that does not have to hold vacuum. This allows the wall to be made in individual sectors that can be replaced during the plant lifetime. It also allows more choices for the first wall material, such as advanced composites that may have radiological advantages. The separable nature of the power plant allows the principal components to be developed separately before being integrated into the system. Just as importantly, it allows economical upgrades as new technologies are developed. The laser is modular, and would consist of many (about 60) identical beam lines. Hence, it is only necessary to develop one of these lines to prove the technology. All of these factors should lead to a faster, lower risk, lower cost path to fusion energy.

Recent advances have been made in all areas of laser fusion energy. Target designs, based on codes that are being benchmarked with experiments, have been developed which have gains of 120–180. Gains >100 are considered sufficient for a fusion power plant. These are one-dimensional calculations [1]. More recent integrated two-dimensional designs show the same performance. Two types of lasers are being developed: Krypton Fluoride (KrF) gas lasers and Diode Pumped Solid State Lasers (DPPSL). Both have achieved repetitively pulsed first light and both are making progress towards meeting the fusion energy requirements for efficiency, durability, and cost. In chamber designs, an operating window has been established for target yield, chamber radius, and chamber gas pressure that will avoid first wall vaporization, allow target injection without compromising the frozen deuterium–tritium (DT) fuel, and operate at reasonable efficiency. However, long-term material behaviour is an open issue. This is being addressed both with experiments that include exposing candidate first wall materials to ions and x-rays at fusion relevant parameters, and in developing new first wall materials. A new chamber dynamics model will allow us to determine how the chamber conditions evolve between shots. In the area of final optics, experiments have shown that a grazing incidence aluminium mirror is both highly reflective ($>98\%$) and can exceed the required laser damage threshold of $5\,\mathrm{J\,cm^{-2}}$. In target fabrication, methods have been developed to apply an Au–Pd alloy coating outside the target that will meet the requirements for the target physics, DT permeation times, and the high IR reflectivity needed to help the target survive as it traverses the hot chamber. Divinyl benzene foam shells of proper dimensions and density have been produced on a batch basis that lends itself to mass production. These shells can meet the requirements for low oxygen content, mechanical strength, and straightforward over-coating. The cost of fabricating and injecting these targets on a mass production basis has been estimated to be \$0.16 each. This analysis was based on a chemical engineering analysis of all the process steps and assuming a commercial process plant environment. Recently, it has been demonstrated that ultra-smooth DT ice layers can be grown over a foam underlay, and that these ice layers remain sufficiently smooth at low temperatures. This aids target survival during injection into the chamber. A facility to accelerate, inject, and track targets is nearing completion.

The work cited in this paper leverages off the wide body of target physics research and target fabrication development carried out in the US Inertial Confinement Fusion (ICF) programme. In particular, studies at the Naval Research Laboratory [2, 3] and the University of Rochester [4–6] have been dedicated at investigating the physics and technology of direct drive targets. Results of that research have directly benefited the work discussed here.

2. High gain target design

A typical high gain target direct drive design is shown in figure 1.

The current designs share several common features:

1. The laser pulse has a low intensity 'foot' followed by a rise to maximum intensity. In some cases a single intense 'picket' pulse precedes the foot.
2. The ablator is composed of a low-density foam with DT wicked into it. The foam can significantly increase the laser absorption.
3. The design preheats the ablator by some means (shocks, x-rays, or a combination). This raises the isentrope of the ablator, and hence lowers the growth rate of the Rayleigh–Taylor instability. In some designs the ablator is preferentially heated, while the fuel remains on a lower isentrope. This increases the stability without substantially reducing gain.
4. The laser is 'zoomed': the spot size is decreased in radius to match the compressing target. This reduces the amount of light lost to refraction and/or absorbed far away from the ablation surface, and thus increases the absorption and coupling efficiency of the design.
5. The designs include a thin high-Z layer (such as Pd) outside the target. This has been shown experimentally to substantially reduce the imprint of laser non-uniformities, and hence mitigates the seeding of hydrodynamic instabilities [7]. This is shown in figure 2.

The first high gain targets [1] used radiation preheating, an incident laser energy of 1.3 MJ, and had energy gains well above 100. In these targets, α, the average isentrope within the fuel region, was slightly greater than 1. (α is the ratio of the total DT pressure to the Fermi-degenerate pressure.) A one-dimensional analysis showed that the Rayleigh–Taylor instability grew less than 6 e-folds (net growth) when averaged over the initial surface roughness spectrum. This corresponds to less than 400 times the initial perturbation amplitude. The high-Z coating was applied to the outside of the ablator to ensure that

it would be blown off before the laser pulse reached high intensities. When it was realized that it was difficult to provide enough preheat with x-rays, the design evolved to rely more on shocks to establish the higher ablator isentrope. The high-Z material was kept for imprint reduction as described above. It was originally chosen to be gold, but was later changed to palladium because the latter's permeability to hydrogen (DT) is important for target fabrication. Based on a number of calculations, any mixture of Au and Pd would allow similar target performance; the only difference being the required thickness of the coating. The predicted one-dimensional gain of these targets, as a function of the Pd layer thickness, is shown in figure 3. The figure shows results from the first generation, 154 MJ target, and a second generation, 400 MJ target.

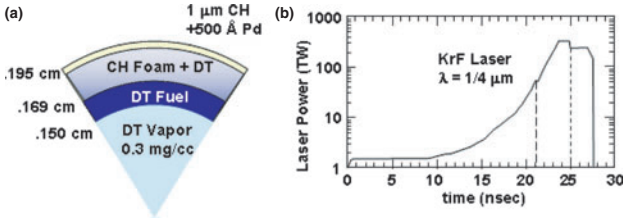

Figure 1. (*a*) Typical NRL high-gain target design. (*b*) Laser pulse shape. Dashed lines are zoom points.

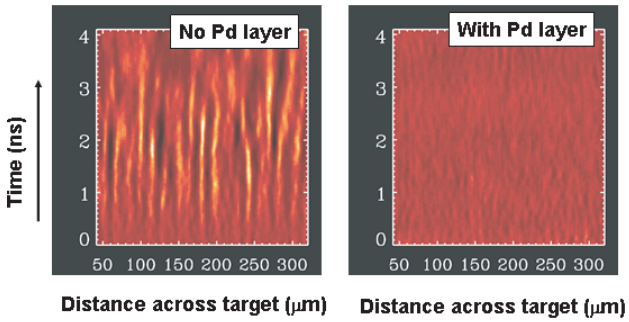

Figure 2. X-ray streak radiographs of ablatively accelerated planar targets show no measurable instability growth with 1200 Å Pd layer on target front surface.

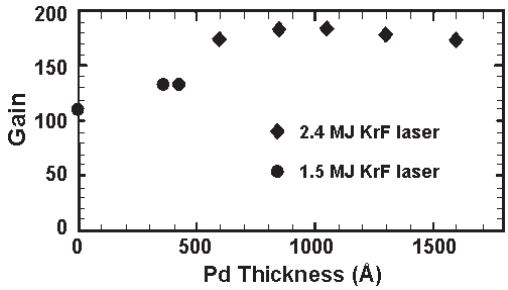

Figure 3. Target gain as a function of Pd thickness.

In a later design, the high-Z material was uniformly mixed with the ablator. The intensity of the foot pulse was the same as required for the $\alpha = 1$ design. In this case, the high-Z material can increase the isentrope of both the ablator and the fuel. Thus, to minimize the fuel preheating, only small amounts of high-Z material were added. With an incident energy of 2.5 MJ (KrF light) and zooming, the gain of the target was predicted to be 163. One-dimensional dispersion relations for this target predict that the single fastest growing mode (near $l = 150$) grew 6.8 e-folds.

Recent one-dimensional calculations show the gain is not affected if the amount of DT vapour inside the target is lower than that shown in figure 1(*a*). In fact, there is no need for any vapour at all. This allows operation at lower target temperatures, which, as discussed in section 8, benefits target injection.

Currently, the NRL FAST series of codes is being used to evaluate these targets with high-resolution two-dimensional fully integrated simulations. These resolve all the wavelengths relevant to the hydrodynamic instability. All known sources of non-uniformity are accounted for: inner and outer surface roughnesses (based on NIF pellet specifications), laser imprint from modelling of the optical smoothing, either by ISI—Induced Spatial Incoherence, or SSD—Smoothing by Spectral Dispersion, and low-mode laser pointing and power imbalances (based on modelling from the NIF laser system). Simulations are ongoing for the NIF baseline target design, and are beginning for the NRL-designed high-gain KrF-driven targets. An example calculation is shown in figure 4. More recent results show the two-dimensional gains for an IFE target driven by a 2.5 MJ laser to be the same as the one-dimensional gains described above. In those calculations the power balance around the target (irradiation non-uniformity) is assumed to be perfect, the outer surface of the target is assumed to have a roughness of 0.125 μm RMS, the inner surface has a roughness of 1.0 μm RMS, the laser has a bandwidth of 1 THz with ISI smoothing, and a picket is applied.

Two-dimensional single mode calculations for a 400 MJ target design have also been carried out with LASNEX. This target is slightly larger than that shown in figure 1, and has a 6 μm thick pure CH outer layer. The calculations show that the stability is enhanced by adding a single high-intensity spike, or 'picket' early in the foot of the laser pulse. The prepulse shock heats the ablator to a higher

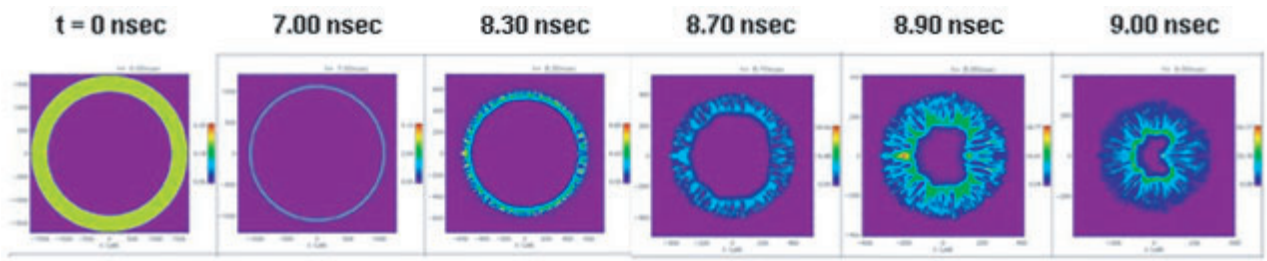

Figure 4. Two-dimensional simulations showing density during an NIF pellet implosion.

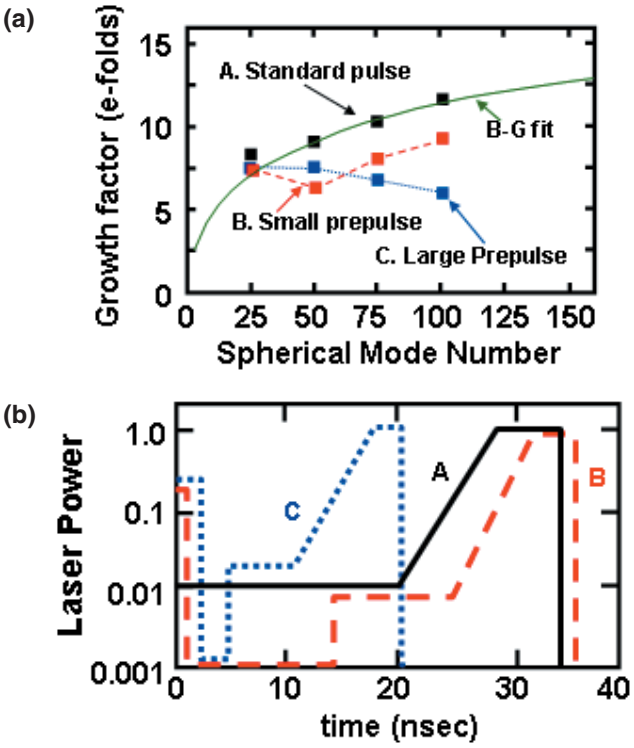

Figure 5. (*a*) Single mode e-folds versus spherical mode number for the (*b*) pulse shapes shown at right.

isentrope (with a concurrent reduction in Rayleigh–Taylor growth) but decays before reaching the fuel. This idea, including experiments, has been explored independently by the University of Rochester [8].

In these LASNEX calculations particular attention was paid to reduce the numerical noise inherent in laser energy deposition when modelling two-dimensional growth rates. It is now possible to perform full, time-dependent implosions to ignition with two-dimensional laser ray-trace in operation from time zero. Numerical noise growth amplitudes at the fuel/ablator interface at ignition have been reduced to $\sim 10^{-11}$–10^{-10} cm, which is comparable to indirect-drive targets driven by a uniform x-ray source.

Figure 5 shows plots of the single mode growth factors (e-folds) versus spherical mode number, $l = \pi r(t)/\lambda(t)$, for three different pulse shapes. Pulse shape A is the 'conventional' pulse: foot plus main drive, Pulse shapes B and C have a small and large prepulse, respectively. At spherical mode numbers around $l \sim 75$–100, growth factors have been reduced from ~10.5 (standard pulse shape) to ~6.5 e-folds (large prepulse). These are comparable to the growth factors seen for indirect drive heavy-ion targets. As shown in figure 5, the two-dimensional growth factors are in good agreement with the semi-analytic Betti–Goncharov one-dimensional model [9] plus Bell–Plesset convergence.

The impact of these growth factors on late-time shell breakup has been assessed by application of the non-linear multimode saturation model of Haan [10]. For comparison with earlier work an initial roughness spectrum based on NIF specifications was used. The results are summarized in table 1. The late-time shell breakup (the peak-to-valley bubble amplitude divided by the shell thickness) has been reduced from ~80% to an acceptable 21% with virtually no penalty in gain. This is consistent with the two-dimensional FAST modelling described above. Note that the breakup can be reduced to a negligible 2%, with a gain that is still high enough for fusion energy. However, the small prepulse case should be more than adequate.

Table 1. Effects of shaped pulse on target performance.

Pulse shape (see figure 5(*b*))	Laser (MJ)	Yield (MJ)	Gain	Maximum shell breakup (%)
A (standard)	2.4	430	180	83
B (small prepulse spike)	2.5	420	170	21
C (large prepulse spike)	3.1	360	110	2

3. KrF laser

KrF lasers are gas lasers that are pumped by electron beams, and lase at 248 nm. Development is being carried out with the Electra Programme at NRL. The key components under development are: an efficient and durable pulsed power system, a durable electron beam emitter (cathode), a long life, high transmission foil support structure (hibachi), a recirculator to cool and quiet the laser gas, and long-life optical windows [11]. Electra should produce 500–800 J in 100 ns when run as an amplifier. The technologies will be directly scalable to a fusion power plant sized laser beam line. The Electra laser facility is shown in figure 6. A first generation pulsed power system has been built to develop the laser components. The system produces two 500 keV, 100 kA, 100 ns electron beams, each with a cross-section 30 cm high by 100 cm wide. The pulsed power system can run at 5 Hz for 5 h (100 000 shots). Ten-thousand shot e-beam runs (10 kW) are commonplace. The system has run as a laser oscillator, and in early tests has produced 500 J of laser light per pulse in 10 shot bursts.

3.1. Advanced pulsed power

An all-new solid-state, laser-triggered switch has been developed that will become the basis for a pulsed power system that can meet the IFE requirements for rep-rate, efficiency, durability, and cost. The switch uses a four-junction silicon device that is optically triggered by two diode lasers. The lasers flood the entire switch volume with photons, whose energy is just above the band edge of the silicon. This gives switching times of the order of 100 ns, or more than 10 times faster than other solid-state switches. The lasers are kept on during the entire electrical pulse to increase the system efficiency. Using a four-junction device enables operation at voltages of 20 kV. We call this device a *Laser Gated and Pumped Thyristor*. For the first tests, an off-the-shelf Thyristor was modified to accommodate a single diode laser and the necessary optical coupling. The switch operated at 3.2 kV for 10^5 shots at 5 Hz. The current density was 2.7 kA cm^{-2} (121% of the IFE requirement) and the current rate of rise was 1.4×10^{10} A s^{-1} cm^{-2} (154% of the IFE requirement). A second generation switch has been built that uses advanced, purpose-built construction techniques, and accommodates the

two-sided pumping. This switch has operated at 15.2 kV, held 24 kV in a pulse charge, and is now undergoing durability tests.

3.2. Hibachi (foil support structure)

A hibachi concept has been developed that demonstrates an energy deposition transmission efficiency of up to 75% on Electra (500 keV), with the potential to go to greater than 80% at full system operating voltages (750 keV). The energy deposition efficiency is defined as the ratio of the energy deposited in the laser gas divided by the energy in the diode. The high transmission efficiency was achieved with two innovations: (1) eliminating the anode foil on the diode side of the hibachi structure, and (2) patterning the electron emitter into strips so that the beam 'misses' the hibachi ribs. While conceptually simple, these are difficult in practice: the beam strips spread due to the highly non-uniform electric fields caused by eliminating the anode, and the beam rotates and shears due to combined applied and self-magnetic fields. These effects are eliminated by narrowing and 'counter-rotating' the emitters so that the beam 'strips' propagate parallel to the ribs when they get to the hibachi. This concept is shown in figure 7. As a bonus, patterning the beam into strips also delays and reduces the 'transit time' instability that is characteristic of large area electron beams [12].

While the topology of the cathode strips can be determined empirically, this does not give the predictive capability needed to design larger systems. This is a rather complex phenomenon to model and requires a full three-dimensional PIC simulation of the exact experimental geometry, including the rib structure,

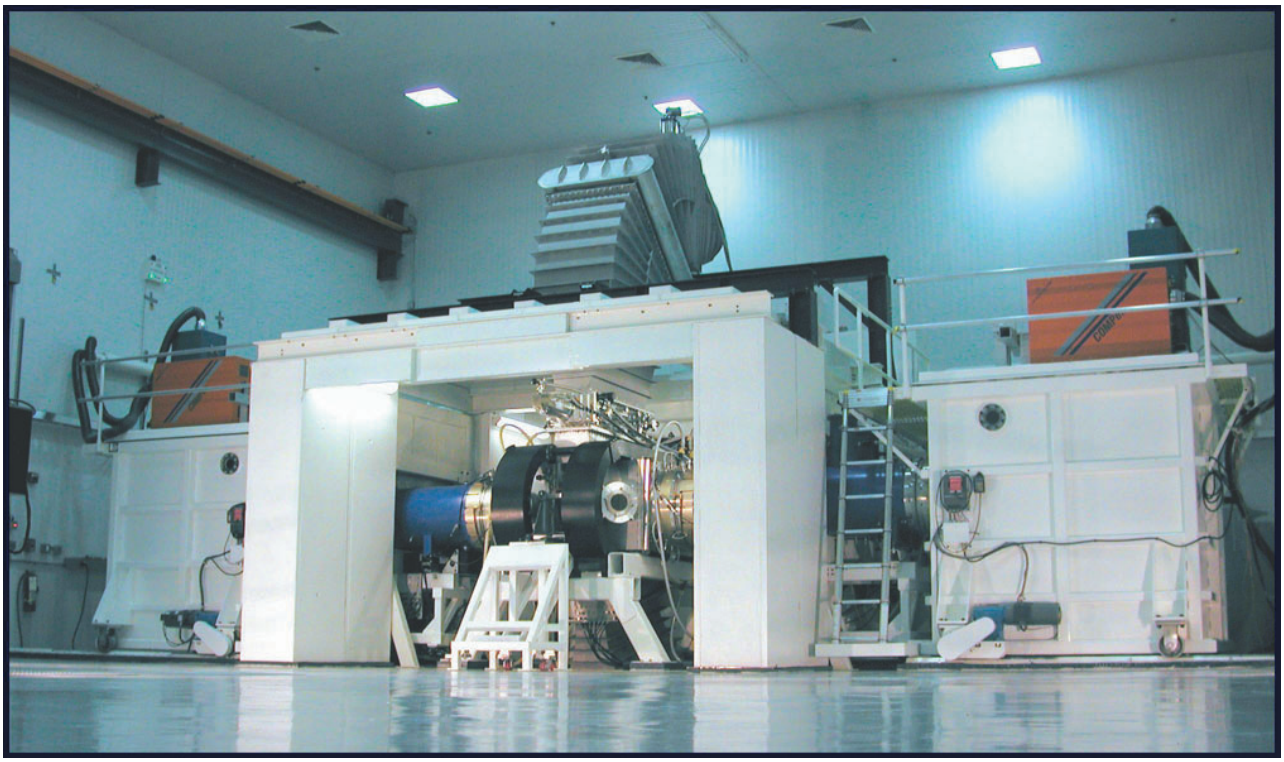

Figure 6. The Electra Laser Facility. Electra has repetitively produced 500 J per pulse of laser light.

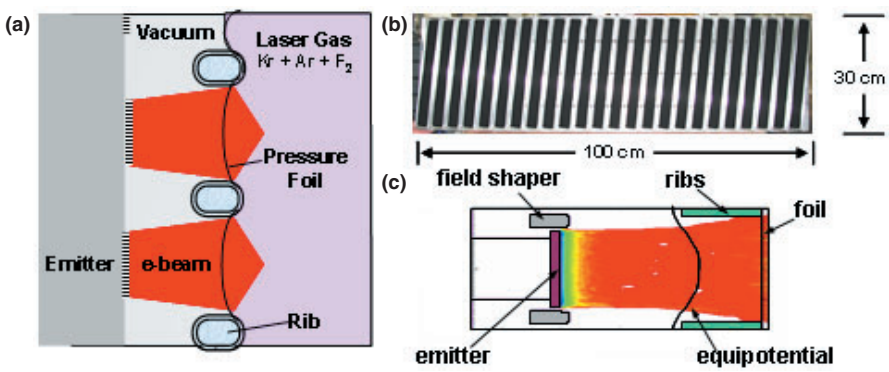

Figure 7. (*a*) Drawing of hibachi concept. (*b*) Photo of cathode showing the counter-rotated emitter strips. (*c*) LSP modelling of beam propagation past ribs.

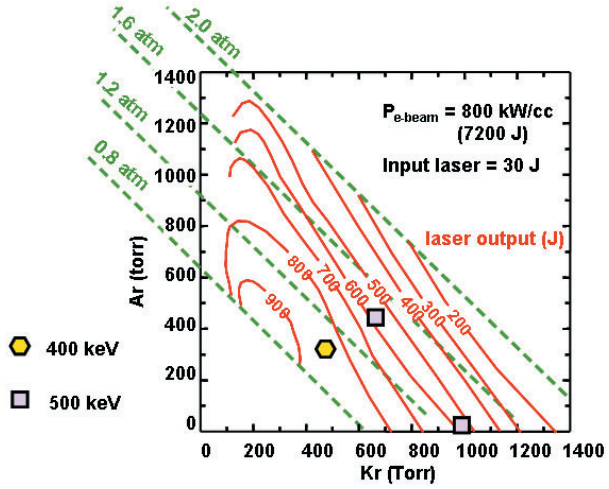

Figure 8. Orestes Code predictions for Electra main amplifier for two different e-beam energies.

laser gas, and magnetic field. This was achieved by running the Large Scale Plasma (LSP) code, developed by MRC, Albuquerque, on NRL's parallel processors. The simulations accurately predict both the cathode counter rotation angle and the energy deposition efficiency. A simulation of a beam 'strip' is also shown in figure 7.

3.3. KrF physics code development

The 'Orestes' KrF Physics code has been developed to both predict the behaviour of Electra and to serve as a tool to design full-scale (30–100 kJ) systems. Orestes follows 122 reactions with 24 species and has been benchmarked against a wide range of KrF experiments under different conditions. Using experimentally determined energy depositions, Orestes predicts the output for Electra to be between 550 and 850 J, depending on the experimental conditions. See figure 8.

3.4. KrF amplifier windows

The amplifier windows, which are typically UV grade fused silica, need to have an index matching dielectric coating to minimize transmission losses. The coatings operate in a hostile environment—intense laser light, fluorine, UV, x-rays, electrons, and, if there is even trace water present, HF. The development of the coatings is ongoing; however, good fluorine laser resistance with high transmission has been obtained with a MgF/Alumina/MgF dielectric stack.

4. Diode pumped solid state laser

Diode Pumped Solid State Laser (wavelength 351 nm) development is being carried out with the Mercury Program at LLNL. The ultimate goal is to produce a 100 J, 10 ns, 10 Hz, 10% efficient laser. Like the Electra KrF laser, the technologies developed on Mercury are scalable to a full-size power plant laser [13]. To achieve the goals of Mercury, three key technologies needed to be developed: high-peak-power diode arrays [14], $Yb^{3+}:Sr_5(PO_4)_3F$ (Yb : S-FAP) crystalline gain slabs [15], and helium gas cooling of the gain media [16]. A picture of the facility is shown in figure 9.

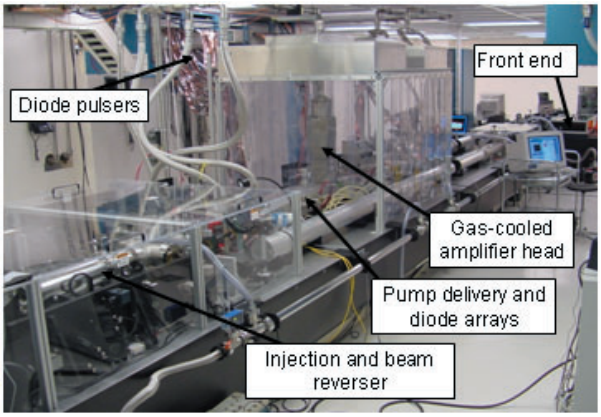

Figure 9. The mercury laser with a single amplifier head produces up to 34 J of energy per pulse.

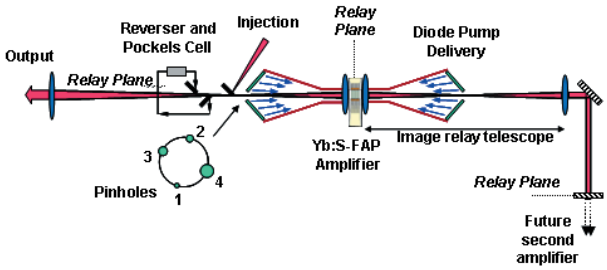

Figure 10. Schematic of the Mercury Laser.

The system is schematically illustrated in figure 10. Light from the diode array is guided to the amplifier slabs through multiple reflections within a hollow lens duct and homogenizer. The Yb : S-FAP amplifier slabs are potted into aerodynamic vanes, which are cooled by helium gas flowing at Mach 0.1. By means of angular multiplexing, the beam is injected into the main cavity and relay-imaged two times through the amplifier head. The beam is then re-injected via a U-turn loop (called a 'reverser'), which contains a birefringence-compensated Pockels cell [17] (used for ghost and parasitic beam suppression). This allows the beam to pass through the amplifier two more times. A device for 'spectral-sculpting' the input beam, so as to maximize the output bandwidth for beam smoothing, has been developed [18]. To date, one amplifier head has been activated and the system has generated 23 J at 5 Hz for 6×10^3 shots (20 min).

Improvements have been made in the growth of the ytterbium-doped strontium fluorapatite (Yb : S-FAP) crystals. These Czochralski-grown crystals were initially plagued by a number of growth-related defects [19]. However, the defects have been controlled with newly developed procedures including water cutting, acidic polishing, and diffusion bonding. The lifetime and durability of this material is expected to meet the IFE requirements, but will be evaluated experimentally on Mercury.

In the Mercury system, four diode arrays have been activated with each delivering 80 kW of peak power in a 750 μs pulse. An overall transfer efficiency of 83% through the pump delivery system was achieved, and the pump homogeneity matches the ray-trace models. A birefringence-compensated average power KD*P Pockels cell was fabricated and meets

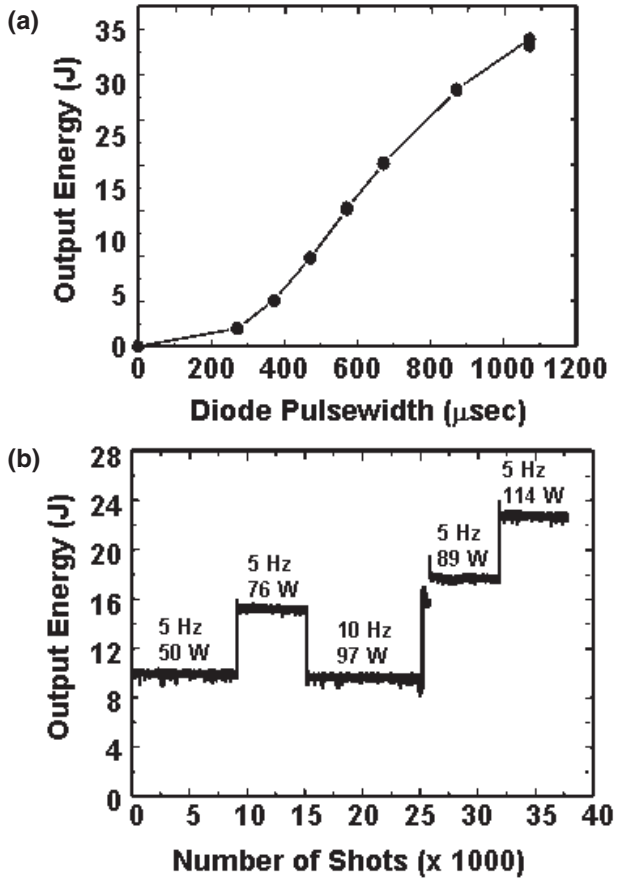

Figure 11. (*a*) Single shot laser energy. (*b*) Operations plot showing output energy and stability for various repetition rates.

the 200 : 1 extinction requirement at 100 W average power. All seven $4 \times 6\,\mathrm{cm}^2$ Yb : S-FAP slabs are currently installed in the amplifier. An example of performance results for one amplifier head appears in figure 11. Up to 34 J has been achieved and reliable operation at 23 J per pulse (20 ns) is plotted below.

5. Chamber development

The explosion of the target, which produces bursts of neutrons, gammas, x-rays and charged particles, is the central event in inertial fusion. Everything that happens before the explosion (laser operation, focusing optics, target fabrication and injection, laser–plasma interactions, and implosion) causes this event to occur. Everything that happens after the explosion (chamber protection, energy conversion, chamber recovery, activation, and balance of plant) is influenced by the target explosion. The development of a successful chamber depends on two issues:

1. Can an operating window be established in which a set of chamber parameters (radius, materials, wall temperature, and environment) simultaneously allows distortion-free propagation of the laser beams, successful injection of the target, survival of the first wall, and high thermal efficiency?
2. Can the chamber recover to this state to allow successful target injection and laser beam propagation on the next shot?

5.1. Operating windows

Establishing the operating window for an IFE chamber is a complex process that involves balancing several factors. The target produces a 'threat spectrum' of neutrons, x-rays, and charged particles. These propagate with different velocities and hence hit the chamber wall at different times. The first wall response depends on when these hit the wall, the energy they impart to the wall, and the wall material. In some designs the chamber is filled with Xe gas. The Xe absorbs energy from the ions (and to a lesser extent, the x-rays) and then re-radiates it on a longer timescale, as determined by the opacity and emission of the Xe. This stretches out the energy deposition on the wall and allows thermal conduction to keep the material below the temperature at which damage will occur. There are upper limits to the allowable gas density, however, as the background gas affects laser propagation, target tracking, and target survival.

5.1.1. Threat spectrum calculation. The threat spectra produced by the targets shown in figure 3 have been calculated using both LASNEX [20] and the one-dimensional Lagrangian radiative hydrodynamics code BUCKY [21]. Both codes predict the same gains as the NRL FAST Code. They predict similar threat spectra for both the low yield 154 MJ and high yield 400 MJ targets. About 1–2% of their output is in x-rays. Half of the photons have energy above 30 keV. Charged particles ('burn ions') comprise 13–14% of the target output, and 'debris ions' comprise 15–16%. The latter are moving considerably slower, allowing time of flight spreading to greatly mitigate the total threat to the wall. The balance of the energy release is, of course, in neutrons. An example of this energy partitioning (from BUCKY) is shown in figure 12.

5.1.2. First wall material choices. Development of the first wall for an IFE chamber faces many of the same challenges as for magnetic fusion energy (MFE). For both approaches thermodynamic efficiency is important. This tends to favour higher operating temperatures. For both systems a driving concern is the environmental acceptability of the power plant. Thus, both approaches call for low-activation materials. And for both approaches the time averaged energy flux to the wall are about the same. The loading on an IFE chamber wall has many of the same characteristics (frequency, particle flux, affected area, base temperature) as an ITER Type 1 ELM mode [22]. As a result of these considerations, the two current leading candidates for the chamber first wall material are similar to those for MFE: a carbon fibre composite, as in the SOMBRERO study [23, 24], and tungsten. The selection is based on both high thermal conductivity and high sublimation (C) or melting (W) temperatures.

(Although there are similarities between the IFE and MFE wall loading, the specific loading is substantially higher due to the pulsed nature of the IFE system. Specifically, the neutrons, photons, fast ions, and debris ions arrive at the wall within 2.5 μs. This yields an instantaneous heat loading of more

than 10 000 MW m^{-2} as compared to 10 MW m^{-2} for an MFE plant. Similarly, the instantaneous neutron displacement rate in IFE can be 10 displacements per atom per second compared to 10^{-6} for MFE.)

In order to develop the chamber operating windows, it is necessary to use models that predict the material response to the emissions from the target. To benchmark these code predictions, candidate chamber first wall materials have been exposed to ions and x-rays at fusion-relevant fluences and spectra. These were carried out with the Z (single shot x-rays) and RHEPP (repetitively pulsed ions) facilities at Sandia. Table 2 compares the experimental results, theoretical predictions, and anticipated threat for the two high gain targets shown in figure 3.

Note that the measured ablation and roughening thresholds are close to the code predictions. The predicted threat to the wall assumes a chamber radius of 6.5 m radius and no gas in the chamber. The number in parenthesis for the ion threat was obtained by applying a $t^{1/2}$ correction for the pulse width. The ions from RHEPP are produced in ~100 ns, whereas in an IFE chamber they are emitted in a double humped distribution over 2.1 μs. This scaling is only an approximation, as its validity depends on several factors (such as the ratio of the thermal diffusion length to the energy deposition length). The main reason is to demonstrate that both Z and RHEPP are producing relevant threats. From the table, it is clear that x-ray damage is not a problem with either target or wall material. The estimated ion fluence is slightly below the damage threshold for the lower yield target, and slightly above it for the higher yield one. This is why, as discussed below, the chamber needs to be filled with gas and the radius extended to 8.25 m for the higher yield target. Note that the addition of Re to tungsten increases its resistance. (However, the addition of Re brings up radiological issues that must be addressed.) All of these results are obtained with room temperature samples, and the behaviour at IFE relevant wall temperatures will be examined. In addition, the long-term effects of roughening will be investigated. It may turn out that roughening, which is due to repetitive thermo-mechanical stresses, rather than melting, may be the limit.

The data discussed above are taken for a few tens of shots. There is concern that damage may be cumulative and will become apparent only after many cycles. This will be studied with the new repetitive x-ray source XAPPER, which is being installed at LLNL. The source, produced by PLEX LLC, uses a radiofrequency-initiated Z-pinch [25], along with a grazing incidence ellipsoidal optic to deliver high fluences of low-energy (100–500 eV) x-rays to a sample. XAPPER will be used to access very high cycles (up to 10^6 pulses at 10 Hz) of x-rays to study surface effects for optics and wall materials for energy deposition levels lower than apparent threshold levels based upon low-cycle tests and single-shot calculations.

In addition to the above, a laser test facility has been set up at UCSD to investigate long-term material behaviour. The advantage of using a laser is that it can provide a clean, low-cost, repetitive, high-duty-cycle, energy source. At first glance it would appear that a laser, which deposits energy on the surface, would not faithfully duplicate the effects of x-rays and ions, which deposit their energy at different depths. This is true initially, but modelling has shown a 10 ns laser pulse can simulate the proper temperature evolution in the wall as it relaxes. The primary phenomena that lead to mass loss from the wall are sputtering, ion/neutron radiation damage, evolution of the wall temperature, and the chamber environment. The UCSD facility will look at the latter two. Comparison of these tests with those from the x-ray and ion tests will help elucidate the loss mechanism, as well as determine the fidelity of this laser-based approach.

5.1.3. Limitations on chamber gas density. As pointed out above, in some cases, particularly with the high yield target, the chamber will have to be filled with some density of Xe gas. There are three phenomena that determine the upper limits of the chamber gas density. In increasing order of allowable gas pressure, they are: survival during injection, tracking in the chamber, and high-fidelity propagation of the laser.

If there is any gas in the chamber at all, it will be at or above the wall temperature. Thus, this hot gas will warm up the injected cryogenic target through a energy exchange. This heat load is in addition to the radiation heating from the hot wall. As discussed in section 8, the temperature of the outer surface of the frozen DT in the target cannot rise above the triple point of solid DT (19.79 K). As shown in section 7, experiments have shown that smooth DT ice layers can be formed over foam layers at temperatures at least as low as 16 K. Thus, the target outer surface can warm up 3.79 K before the outer surface starts to melt. The allowable heat flux on the target depends on the injection velocity. For example, assuming the target is in the chamber for 16 ms (corresponding to a 6.5 m radius chamber and a 400 m s^{-1} injection velocity), the allowable heat flux on a target starting at 16 K is 1.4 W cm^{-2}. If the chamber wall is at 1000 K (727°C), the radiation heating from the wall alone is about 0.2 W cm^{-2}. Calculations show that, to stay below the 1.4 W cm^{-2} total limit, the gas pressure in the chamber should be below 15 mTorr. This assumes the gas temperature is at the wall temperature, and assumes the target shown in figure 1. If there were a 250 mg cc^{-1} foam coating outside the target to provide additional thermal insulation, these same calculations suggest the gas pressure could be 5–8 times higher. Further details of these temperature rise calculations are given in section 8.

In the case of tracking, the gas density has to be low enough such that aerodynamic forces do not appreciably perturb the target trajectory. The target motion becomes random, and the lateral excursions sufficiently large that it becomes difficult to maintain the $\pm 20\,\mu$m laser pointing accuracy required by target physics. Modelling shows that the upper limit to the gas pressure in this case is about 75 mTorr.

The limit on the gas pressure due to laser considerations was investigated in studies carried out at NRL [26]. The behaviour of an ablatively accelerated planar target was determined as a function of background gas pressures ranging from 10^{-6} Torr to 500 mTorr Xe. The experiments showed no evidence of laser beam breakup, nor changes in the central profiles of the shock breakout from the rear of the target. Also, the plasma profiles remained smooth and symmetric in all cases. Minor qualitative changes were seen in the edges of the shock break-outs at pressures above 200 mTorr, but these are thought to be irrelevant in a spherically illuminated target. Nevertheless, it is clear that laser propagation is not currently the factor that determines the allowable background gas.

5.1.4. Examples of chamber operating windows. Figure 13 gives an operating window for a 154 MJ target. The figure gives the temperature evolution at the wall surface and various depths. The example is for a 3 mm thick Tungsten armour, a chamber radius of 6.5 m, and a first wall starting temperature of 500°C. There is no gas in the chamber. Note the tungsten stays well below the melting temperature of 3410°C.

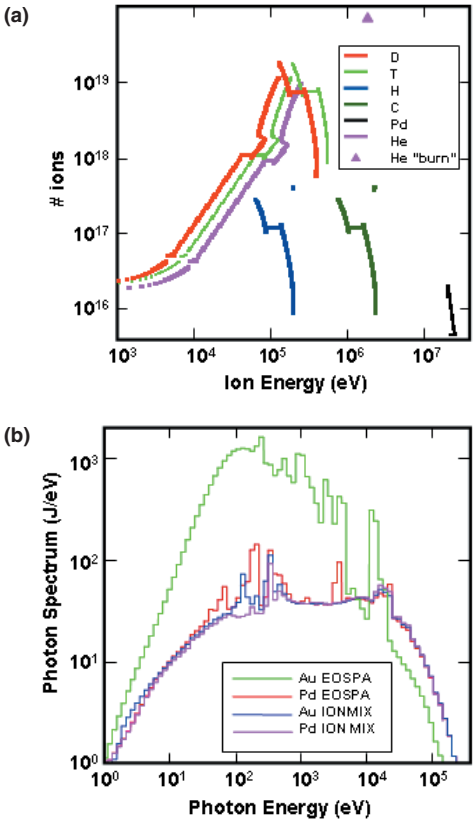

Figure 12. (*a*) Expected time-integrated x-ray spectra emitted by the NRL direct-drive target shown in figure 1. The coating was either 300 Å Au or 1200 Å Pd. Target yields were calculated to range from 300 to 400 MJ. The x-ray spectra were calculated based on two opacity models: EOSOPA (LTE) or IONMIX (Non-LTE). (*b*) Time integrated histogram showing the number of ions per eV. This is for a Pd-coated laser direct-drive target. IONMIX (non-LTE) opacities were used. Note, BUCKY does not presently have mix in the code, which is why some of the curves are similar.

Similar results were obtained for a wall with carbon armour. The initial photon-induced peak is much smaller since the photon energy deposition goes deeper inside the carbon. Also, the maximum temperature is <2000°C with an associated sublimation loss of less than 1 μm per year.

In these calculations the energy deposition in the W armour was first calculated for a one-dimensional slab geometry based on photon attenuation calculations (including photo-electric and Compton scattering effects), and on ion energy deposition (including both electronic and nuclear stopping powers). The photon calculations were performed using the methodology described in [27]. An interactive program based on these calculations can be found at http://aries.ucsd.edu/LIB/PROPS/PHOTON/. The ion stopping was calculated using an interactive programme called SRIM (Stopping and Range of Ions in Materials), which may be found at http://www.srim.org/. The underlying physics is discussed in [28]. The calculation procedure included the time of flight spreading of the photon and ion energy deposition [29]. The thermal analysis was then carried out using a one-dimensional model including melting and evaporation [29]. Temperature-dependent properties were utilized for both C and W.

The BUCKY code [21] was used to explore the options for the case of the 400 MJ target. In this case, the chamber must be filled with Xe gas. To establish the low-density, high-temperature conditions of the Xe at the time the ions transit the chamber, the opacity of the Xe was determined using IONMIX [30], a collisional radiative equilibrium screened

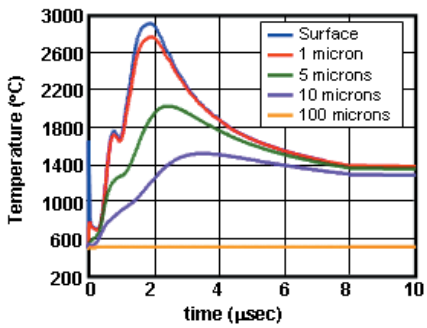

Figure 13. Temperature profiles of first wall in an IFE chamber, 154 target, tungsten wall.

Table 2. Summary of exposures of candidate first wall materials.

	Material	BUCKY predicted ablation threshold (J cm^{-3})	Analytic predicted ablation threshold (J cm^{-3})	Measured ablation threshold (J cm^{-3})	Measured roughening threshold (J cm^{-3})	Predicted threat to wall: 154 MJ target (J cm^{-3})	Predicted threat to wall: 400 MJ target (J cm^{-3})
X-rays (10 ns exposure)	Poco graphite	4.25	3.3	>8	<8 grain removal	0.40	1.20
	Tungsten (pure)	3.5–4.0	2.4	2.3–19	2.3		
	Tungsten + 25%Re			19	2.3		
	Tungsten + La			19	>2.3		
IONS (~100 ns exposure)	Poco graphite	3.2	1.8	2.5–3.0	<1	8.5	21.1
	Pyrolitic graphite	1.6–2.5	1.2–3.0	3.0–4.0	2.5		
	Tungsten (pure)	6	5.1	6	1.25		
	Tungsten + 25% Re			6	3.5	(1.82)	(4.54)

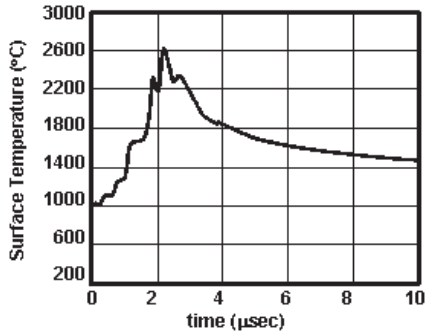

Figure 14. Wall surface temperature for a 8.25 m radius graphite chamber and the 400 MJ target.

hydrogenic model that interpolates between the low-density, high-temperature coronal equilibrium and the high-density, low-temperature Saha equilibrium. The wall is assumed to survive if the sublimation is less than one monolayer per shot. For a 6.5 m radius graphite chamber starting at 1000°C, the minimum Xe density required to avoid wall ablation is 80 mTorr, which is incompatible with target tracking as pointed out above. Increasing the chamber radius to 8.25 m reduces the threat to the wall sufficiently such that sublimation is avoided using 25 mTorr of Xe. Under these pressure and wall temperature conditions the target will require an outer layer of insulating foam to survive. Figure 14 displays the wall surface temperature evolution for a 8.25 m radius graphite chamber.

Both of these design window studies illuminate a few key points:

1. The photon energy deposition is very fast and creates an instantaneous temperature rise (for example, 1150°C in the case of the 154 MJ target with tungsten armour). The wall temperature starts to drop, and then peaks several microseconds later after the ions arrive.
2. With the 154 MJ target and tungsten wall chamber, the temperature stays under 3000°C for a 6.25 m chamber without any protective gas. This is below the W melting point limit (3410°C).
3. Similar arguments apply to the high-yield target and graphite wall. The temperature peaks under 2700°C for a 8.25 m chamber with 25 mTorr Xe, which is well below the temperature for significant sublimation.
4. In both cases the 'action' takes place in a very thin region ($<10\,\mu$m) from the surface. This gives the option to separate the functions of the first wall into two components: a thin armour, which is resistant to the target emissions, and an underlying substrate to provide the supporting structure and interface with the blanket. (Note that the blanket effectively sees steady-state conditions.)

5.1.5. Materials response: long-term behaviour. While the identification of chamber operating windows is a major step, long-term material behaviour is an issue, in particular tritium retention for carbon and helium retention for tungsten. It is anticipated that 0.1–2 MeV He, D, T, and H ions will penetrate several microns into the chamber wall. With carbon, the main concern is the build-up in tritium inventory due to co-deposition in colder regions. Additional concerns are dimensional stability, thermal conductivity following neutron irradiation, and physical and chemical sputtering. Good dimensional stability and thermal conductivity have recently been demonstrated for a high-quality three-dimensional composite irradiated at 800°C. Studies to higher, IFE relevant, temperatures (including tritium retention) are planned. In addition, safety studies carried out by two different groups suggest that oxidation due to a sudden ingress of air is not an issue with graphite-based first wall systems.

The main issue with tungsten is helium retention: the 3.45 MeV alpha particles embed themselves in the tungsten and, because of the extremely low mobility of helium, coalesce into bubbles that eventually cause the material to fracture. For example, for the anticipated fluence of 2×10^{18} He m^{-2} s^{-1}, it is estimated that this process will remove about 2 cm yr^{-1} from the wall. This is unacceptable, as the initial tungsten armour would be less than a few millimetres thick. We are addressing this issue with a multi-pronged approach:

1. The unacceptable removal rate is based on the assumption of limited helium mobility in tungsten. While this is documented at temperatures below 800°C [31], the behaviour at the elevated temperature of an IFE wall is unknown (note from figure 13 that the surface of the wall gets to almost 3000°C). Accordingly, experiments were performed to determine the diffusion of helium at IFE relevant temperatures. In these experiments, tungsten was irradiated at ∼1000°C and cyclically heated to 2000°C. Nuclear reaction analysis was used to determine the fate of the implanted helium. The results showed the amount of helium retained can be reduced by a factor of 2 or more. This work is preliminary and more experimental verification is needed—for example, the effects of neutron irradiation on helium mobility need to be evaluated.
2. In addition to these experimental results, preliminary modelling has shown the bubble formation may be not be a problem in an IFE system. This is because the ions produced by the target have a wide spectrum of energies, and thus the helium will be driven to a range of depths into the first wall, rather than into just one location. The predicted exfoliation, or loss, rate from the first wall would be an acceptable 0.078 cm per year. This result needs to be explored further and appropriate experiments conducted.
3. We are exploring the use of engineered materials such as tungsten fibres or nano-deposited tungsten. The idea is to provide a very short migration path for the helium to be transported back to the chamber. This can be accomplished by having the structure smaller than the helium mean free path, which is estimated to be of the order of a few tenths of microns. This material will also alleviate the roughening due to repetitive thermo-mechanical stresses, if that turns out to be an important factor.

5.2. Chamber dynamics

In a rep-rated laser-fusion facility, the pulse repetition rate is limited by the time it takes for the chamber environment to return to a sufficiently quiescent and clean low-pressure state to allow a second shot to be initiated. Laser propagation, beam quality on the target, and target injection and tracking will

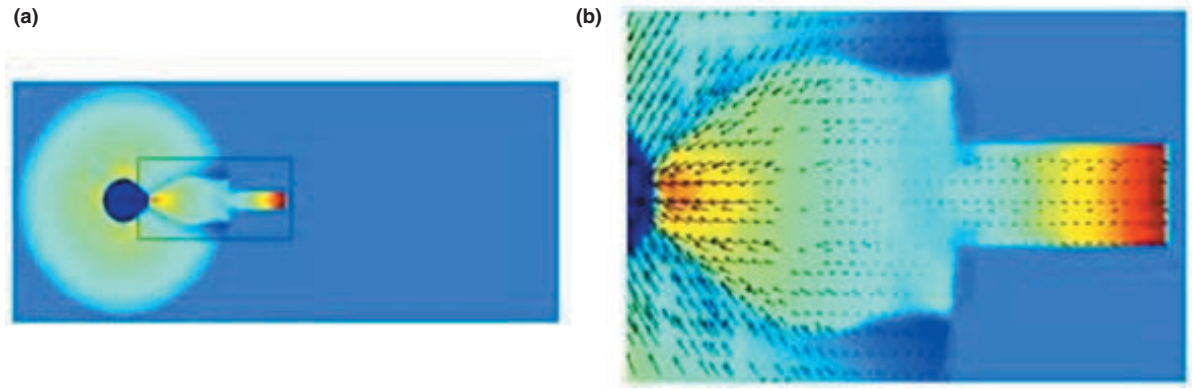

Figure 15. Conditions in the chamber 1.6 ms after the target blast. (*a*) Pressure and (*b*) velocity distribution. Pressure is the highest in the red zones (∼4 kPa) and lowest in the dark blue zones (∼300 Pa) and at intermediate values in the yellow zones (∼800 Pa). The blast has been reflected (once) from the chamber wall. A pressure wave is travelling in the laser beam channel toward the final optics.

all be affected by the chamber conditions (number density, temperature, mix of chamber constituents, and turbulence).

The physical phenomena occur on different timescales. In the first few microseconds, the x-ray burst and ions from the fireball traverse the chamber, and deposit their energy into the chamber constituents and onto the chamber wall. The chamber environment then evolves on a hydrodynamics timescale until a new equilibrium condition is achieved. This is expected to take 100–200 ms. To understand the chamber evolution and dynamic over this 'longer' timescale, a new simulation code, SPARTAN, has been developed.

SPARTAN solves the two-dimensional transient compressible Navier–Stokes equations. It uses split Godunov integrator in the CGF from [32, 33] that is second-order accurate in regions of smooth flow in order to capture the shocks with a minimum of numerical dissipation and overshoot. Several features have been included to make the code suitable for IFE applications:

1. In order to preserve the second-order accuracy of numerical algorithm, calculations are performed on a rectangular logical mesh. Arbitrary chamber geometry (e.g. inclusion of the laser beam ports) is handled by using an embedded boundary algorithm [34] that is also second-order accurate.
2. Viscous terms are added to the split Godunov integrator as viscosity plays an important role on this long timescale. The viscous interaction between the fluid and the embedded boundary was tested on the models of channel flow and lid driven flow in a square cavity. The channel direction was oriented at an arbitrary angle with respect to the mesh.
3. During the timescale of interest (100–200 ms or longer), the shock waves from the blast traverse the chamber many times. Large-scale pressure disturbances are set up that would require excessive computational time if a single homogeneous grid was used. As a result, an Adaptive Mesh Refinement Algorithm, AMR [35], has been employed. The integration of this algorithm into the code was done in collaboration with scientists at Lawrence Berkley National Laboratory [36]. The code can handle the strong shock waves in a computationally efficient manner, with fine grid surrounding the shock and coarse grid placed where the gradients of dependent variables are low.

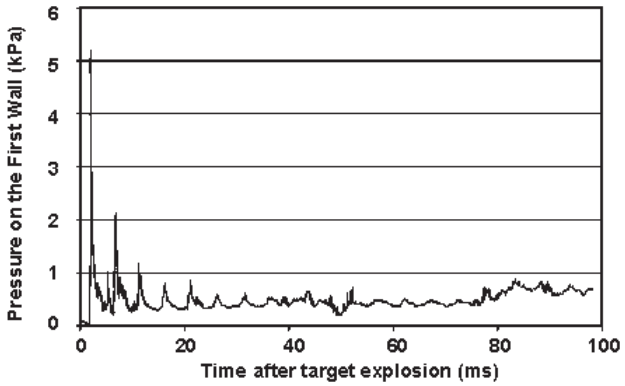

Figure 16. Pressure on the chamber wall as a function of time after target explosion. Initial peaks represent incidence of pressure waves on the chamber wall.

The code has been tested in simple geometries with both zero and small perturbation initial conditions. Some examples of the computational capabilities of the SPARTAN code are shown below. Figure 15 shows the pressure and velocity distribution in a cylindrical IFE chamber 1.6 ms after the blast. The chamber is 6.5 m in diameter and filled with Xe. One laser beam channel is included. The initial conditions for density, pressure, velocity, and energy of Xe gas are taken from the BUCKY [21] code after the temperature of the gas has fallen below 1 eV and radiation has become negligible. At the time shown in the figure, the blast wave has bounced from the chamber wall and is converging back towards the chamber centre. A pressure wave is travelling in the beam port towards final optics. Figure 16 shows the density distribution around the entrance of the laser beam channel at this time. The multi-dimensional nature of phenomena is clearly shown in these figures.

The code is currently investigating chamber conditions (pressure, velocity, density variations) 100–200 ms following the target blast. Non-uniformities have strong impact on target injection in the chamber and laser propagation. The code is also being used to study convection in the chamber, due to both off-centre target blasts and gravity, and to model the

impact of pressure waves on the final optics. Among planned improvements is the ability to handle multi-species transport. Of particular interest is the transport of dust in the beam tube channels.

6. Final optics

The final optics steer the laser beams to the target centre. They are the only optic to lie in the direct line of sight of the target. Their development represents the biggest challenge in the optical train, as they must not only have the high laser damage thresholds required of the other optics, they must also be resistant to the target emissions. The other optics will also require development, as their size, and hence to some extent the size of the system, will depend on their resistance to laser damage. But due to the greater challenges, resources have been concentrated on developing the final optic for now.

6.1. Grazing incidence metal mirror

The front-runner final optic concept is a grazing incidence metal mirror (GIMM). This was proposed over a decade ago in response to concerns over radiation damage to multi-layer dielectric mirrors [37]. The decision to develop the GIMM is based on its potential robustness, its ability to withstand some uniform erosion, and its applicability to both KrF and DPPSL wavelengths (241 nm and 351 nm, respectively). The final optic would consist of a pure aluminium surface bonded to a cooled, neutron transparent substrate [38]. Operation at a shallow angle ($\sim$85°) gives three advantages: reduced absorption for s-polarized light, lower average fluence on the surface due to the large footprint of the beam, and higher reflectivity. Experiments have established that, at least in small laser spot sizes, the aluminium mirror is both highly reflective (>98%) and can exceed the required laser damage threshold of 5 J cm^{-2}.

Laser damage is one of the most serious concerns for grazing-incidence mirrors. If the mirror operates at fluences beyond the normal incidence damage threshold, then minor defects may result in localized heating which causes further damage. The presence of contaminants, which could propagate from the chamber up the beamlines, might exacerbate this by creating a source term for localized defects. Therefore, initial testing has been focused on the basic stability of metal surfaces during long-term exposure. Aluminium is currently the preferred material due to its high reflectivity for UV wavelengths and the relatively large industrial database. Specifications for the damage threshold of commercially available Al-coated mirrors typically call for 20 mJ cm^{-2} of absorbed energy. With the reduced absorption and increased footprint of a grazing-incidence mirror, this should translate into a damage threshold of roughly 20 J cm^{-2} measured across the incident beam. We have set the goal laser fluence for the GIMM at 5 J cm^{-2} normal to the beam. This implies $\sim$400 m^2 of total mirror surface area for a 2 MJ laser.

The data were acquired using pure diamond-turned Al and a 2 J, 10 ns frequency-doubled Nd : YAG laser ($\lambda = 532$ nm). For these specimens, a natural density, 20–30 μm thick oxide coating is present. The results are shown in figure 17. The results confirm survival up to 10^4 shots for fluences well above

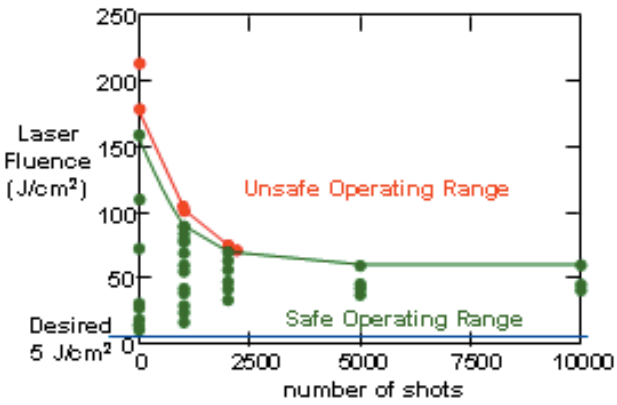

Figure 17. Laser-induced damage threshold (fluence is measured normal to the beam).

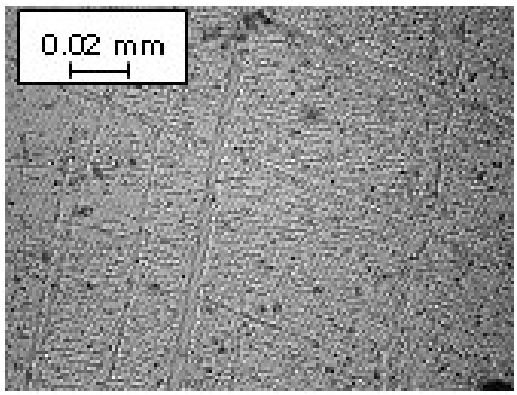

Figure 18. Morphology of thermo-mechanical damage to the surface.

20 J cm^{-2} [39]. Preliminary exposures at fusion-relevant UV wavelengths have shown that the damage threshold is lower, but still above the required 5 J cm^{-2}. The damage threshold, however, is highly dependent on the sample purity and the environment.

The morphology of damage in pure Al appears to be primarily thermo-mechanical in nature. Figure 18 shows a micrograph of the surface near a catastrophic damage site following 10^4 shots. Several types of roughness are evident. Large channels, thought to be the result of internal slip bands that propagate to the surface, appear in somewhat random fashion. Smaller elongated 'notches' appear in an orientation that corresponds with the direction of light propagation. These notches represent a rippling of the surface in a direction that does not affect the angle of incidence. Apparently, ripples aligned so as to produce a more normal angle of incidence to the beam are less likely to persist. The fine lines oriented at $\sim$45° are machining grooves resulting from diamond turning.

Since power plant optics are expected to be fabricated using thin coatings on a low-activation substrate, data on solid Al surfaces provide only a baseline for future testing of coated mirrors. Industrial collaborators recently have been engaged to fabricate coated optics. Their objectives are to demonstrate acceptable adhesion and damage threshold and to demonstrate the feasibility and optical characteristics of environmental protective surface coatings.

Table 3. Final optic threats.

Threat	Target emission (MJ shot)	Final optic
X-rays	5.6	0.11 J cm^{-2}
Neutrons	280	19.6 krad s^{-1}; 0.36 MW m^{-2}; 9.7×10^{12} n cm^{-2} s^{-1} (14 MeV)
γ-rays	$\ll$1	3.2 krad s^{-1}
Ionic debris	110	2.2 J cm^{-2} per shot; 0.15 MW m^{-2}

Multi-layer Fresnel, Kirchhoff scattering and ray-tracing analyses have been performed in order to better understand the optical characteristics of ideal and defected mirrors [40]. For example, a thin carbon coating on an oxidized Al mirror is harmful compared to a less absorptive water contaminant. Further studies are needed to fully characterize the effect of contaminants and their maximum allowable size and density, to demonstrate acceptable performance of prototypic coated substrates, to explore the effect of target emissions, and to scale up and integrate the final optic into integrated research facilities.

In addition to laser damage, the final optic is subjected to neutrons, x-rays, gamma rays and charged particles. Table 3 summarizes these threats at the final optic location, which is anticipated to be 20–30 m from the target chamber centre [23]. The threats assume no fill gas in the chamber. While the threats on the optic are reduced compared to that on the chamber walls at 6.5 m, these must still be addressed in view of the stringent beam quality requirements for target implosion. Our plan is to assess the effects of these threats on the optic. If they are found to be serious, we will then pursue mitigation techniques such as fast shutters, magnetic deflection, etc.

6.2. Transmissive optics

We have also investigated transmissive optics. The key issue is production of colour centres, which are induced by either neutrons or gammas, and which lead to optical absorption at the laser wavelength. The work has concentrated on SiO_2. Heating a SiO_2 optic allows the defect concentration to saturate at acceptable levels, at least at the DPSSL wavelength of 351 nm. For example, a 0.5 mm thick Fresnel lens operated at a temperature of 300°C is expected to have a laser absorption of $<$5% [41]. This is the equilibrium temperature the optic would reach (due to heating by laser and neutron absorption) if it was placed at a stand-off distance of 20 m. The defect population may be reduced further (with a corresponding reduction in optical absorption) by deliberately operating the optic at a higher temperature and taking advantage of thermal annealing. Figure 19 shows the laser absorption as a function of operating temperature of the final optic. For operation at 500°C, for example, the optical absorption falls to ∼0.6%. The power required to heat the optics to 500°C is of the order of 5 MW, which is more than compensated by the savings in required input power to the lasers.

The absorption is still too high at the KrF wavelength of 248 nm. This, plus the issues in fielding a thin, large area optic, has led us to give more attention to the GIMMs.

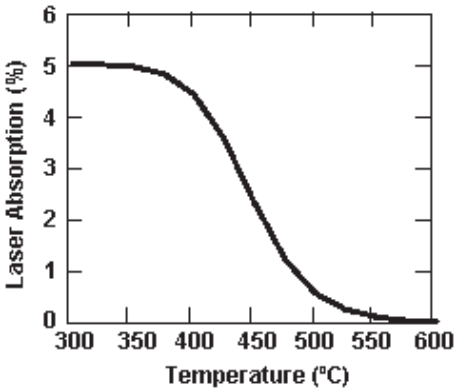

Figure 19. Heating the SiO_2 final optic to 500°C would reduce optical absorption at 351 nm to ∼0.6%.

7. Target fabrication

As discussed in section 2, the high gain target designs have a low density foam shell that has been overcoated with a thin layer of solid CH. An advanced divinyl benzene foam system was developed for this. This material was chosen because it has relatively high strength, it has no oxygen (which may be important for target physics), it can be made into IFE size shells by microencapsulation, and the overcoat can be chemically applied during the shell formation phase. Both of the latter are suited to mass production. Up to 300 shells, with proper diameter, density, and wall thickness, have been produced in a single batch (see figure 20). Methods to make target quality shells with the precise concentricity, reproducibility, and overcoating are being developed. In some target designs, the target is overcoated with a thin high-Z layer. A co-sputtering technique has been developed to apply an Au–Pd alloy coating to the outside of the target. Measurements show this Au–Pd alloy meets the requirements for DT permeation times (almost as good as pure Pd), and has high IR reflectivity (almost as good as pure gold) to help the target survive as it traverses the hot chamber. As discussed in section 2, target modelling shows this alloy does not compromise the gain.

A high gain target will require a smooth surface (less than 1.4 μm RMS) on the inner surface of the DT ice layer. Three advances have been made in this area:

1. Ultra smooth, DT ice layers have been made by growing the DT ice on a foam base. This arrangement replicates the current fusion energy target designs. A toroidal geometry was used in these experiments. The liquid DT was wicked into a low-density plastic foam, frozen at 19.7 K, and then slowly cooled to equilibrate at 19.25 K. The observed integrated (modes 4–256) variation in the DT ice surface finish was less than 0.6 μm, or more than two times better than what has been achieved without a foam underlay.
2. As the temperature is lowered, the smoothness of the DT ice layer grown over a foam layer suffered minimal degradation. For example, at temperatures just below 16 K (the limit of the equipment) the surface roughness increased by less than a factor of 2. This is comparable to the surface finish observed with a DT ice layer grown without foam *at the triple point*. This lack of layer

degradation is in contrast to DT layers grown without foam, in which the smoothness degrades catastrophically as the temperature is lowered.

3. A batch process layering technique is under development that is based on a fluidized bed technology. Experiments with a room temperature surrogate (oxalic acid) and an external infrared heat source (to mimic the natural heat from the tritium decay) have demonstrated the feasibility of this approach.

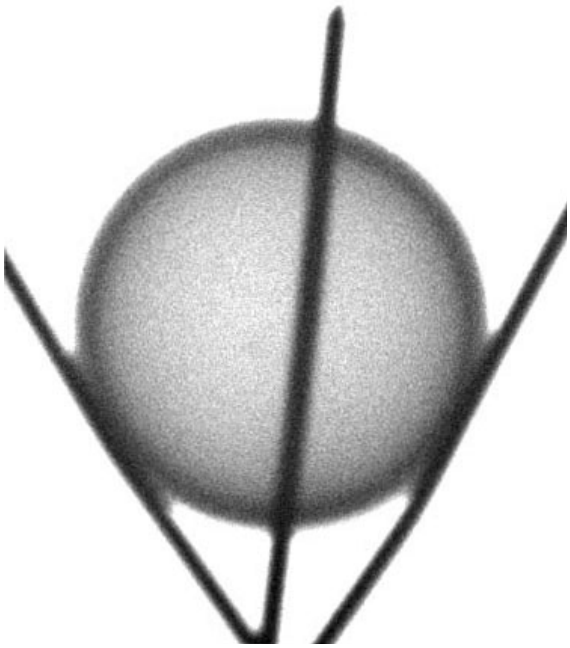

Figure 20. X-ray radiograph of a polymerized divinyl benzene foam shell. Shell is 4 mm diameter, has a wall of 300 μm thickness, and a density of 100 mg cc^{-1}.

Models have been developed to understand and guide the target production process. Using models of the material responses during the permeation filling step, the total tritium inventory in a laser fusion power plant could be under 300 g [42]. This is below the normally acceptable value of 1 kg. An analysis has been performed for estimating the cost for fabricating the direct drive targets discussed in section 2. This analysis was based on a chemical engineering analysis of all the process steps and assuming a commercial process plant environment. A conceptual plant is shown in figure 21. The analysis includes process flows, mass–energy balances, plant utilities, raw materials, quality control, waste handling and recycle, capital equipment cost amortization, and staffing requirements. The results give an estimated cost of producing a direct drive target of about 16.6 cents each. This is well under the 25 cents each called for by power plant studies [24], and resolves a major technical feasibility issue of Laser Fusion Energy.

8. Target injection

The two key issues with target injection are accuracy and target survival. In a power plant the target must be delivered to the chamber centre, to a precisely predicted target location at a repetition rate of 5 Hz. Target placement must be within $\pm$5 mm of a specified point at the target chamber centre. Target tracking must be accurate enough to enable precise alignment of the driver beams with the actual target position. Direct drive targets will require alignment of the centreline of the driver beams with the centreline of the target to less than about $\pm$0.02 mm. Target position prediction must be accomplished early enough to allow time for beam steering.

A system to study injection and tracking has been completed and is undergoing tests (see figure 22). This injector is designed to accelerate any target, be it of indirect

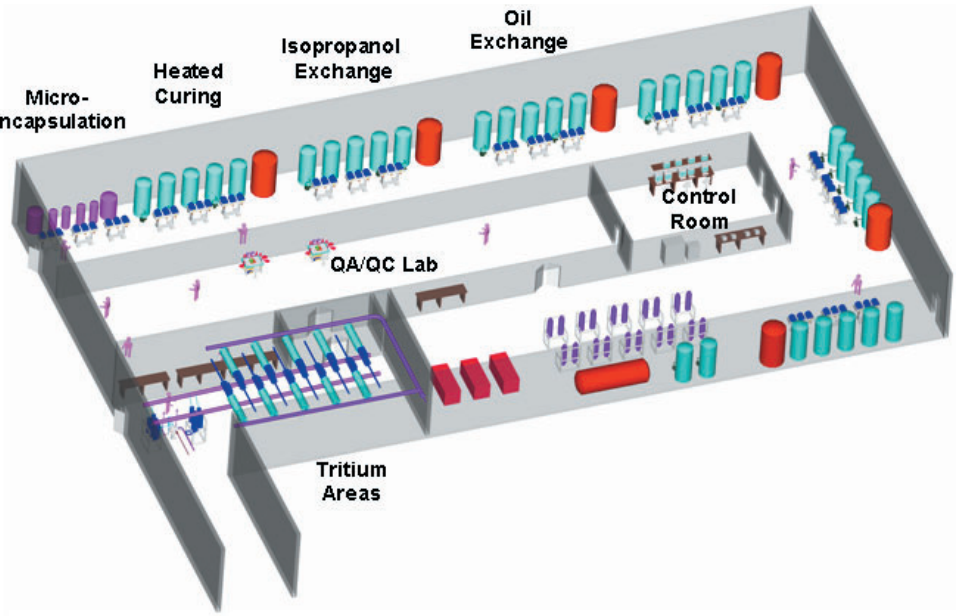

Figure 21. Preliminary plant layout for fabrication of high-gain, direct drive targets. Plant parameters are (*a*) 500 000 targets per day, (*b*) targets spend 2–3 weeks on the assembly line, (*c*) installed capital cost: \$97M, (*d*) annual operating cost: \$19M, and (*e*) estimated cost per target: 16.6 cents. Cost does not include tritium recovery, as per costing allocation in [24].

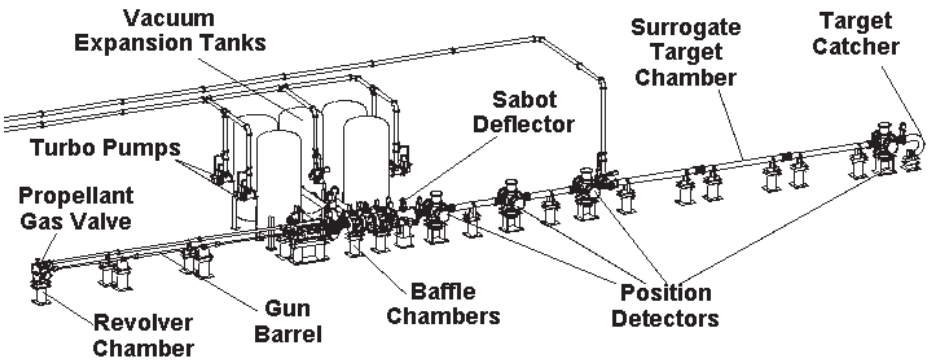

Figure 22. Drawing of target injection and tracking system.

or direct drive. For the direct drive targets, the concept of a separable sabot to protect the target during acceleration has been demonstrated. We are also performing experiments to measure the mechanical properties of frozen DT to predict the response of the target during the high g-loading of injection. Equipment is being constructed to develop and demonstrate accurate placement and precise tracking of targets during the injection [43].

Target survival, or how fast the target warms up on its way to the chamber centre, is one of the key factors that determine the chamber operating window described in section 5.1 (figures 13 and 14). The target heats up due to radiation from the wall and energy exchange with the gas [44]. The heat flux due to radiation ranges from 0.2 W cm^{-2} at 1000 K to 1.2 W cm^{-2} at 1500 K. The heat flux due to the gas is more complicated, as it depends on the target injection velocity, the gas condensation coefficient, and the gas temperature. Eventually the gas temperature will be determined by the chamber dynamics code, but for now we take a range of values. For example, for a gas pressure of 25 mTorr, a gas temperature of 2000 K, a target injected at 400 ms^{-1}, and a condensation coefficient of 1, the heat flux on the target due to the gas is 3 W cm^{-2}. In general, the total heat flux on the target is predicted to range from 1 to 10 W cm^{-2}. Starting at a lower target temperature helps in increasing the total allowable heat flux. Assuming the target velocity above, for every degree K that the target is cooled below the triple point temperature, an additional 0.34 W cm^{-2} can be absorbed. This is why the ability to produce smooth layers at the coldest possible temperatures is so important.

The maximum allowable temperature limit is open to question. One possible limit is when the internal stresses due to thermal expansion (non-uniform heating of the DT ice from the outside) are greater than the yield stress. Thus, this limit is reached when the inner ice surface smoothness is degraded by deformation. A more likely limit is when the outside layer of DT exceeds the triple point, 19.79 K, at which point the smooth outer surface of the solid cryogenic ice layer transitions to liquid or gas. If the outer surface of the DT goes to a pure uniform liquid that does not affect the areal mass distribution, the effect on the target implosion will be minimal. Hence, the allowable temperature limit could be much higher. However, if the DT goes to a liquid/gas state, bubbles may form at the seal coat/DT boundary which would affect the areal mass distribution and which could adversely impact the target stability. Whether the phase change is to liquid or to gas is governed by the local pressure at the interface of the outer DT surface and the hydrocarbon layer just above it. This is a very complex phenomenon. In the absence of any hard data or trustworthy models, the upper limit has been taken as the DT triple point as described above.

How fast the outside surface of the DT reaches the triple point depends on how fast the incident heat can be transported away from the DT surface. As the situation is dynamic, the calculations are carried out over the target time of flight. All the calculations are based on the available data on the properties of DT and plastic at cryogenic temperatures. Accurate and representative material property data are required for this modelling. Material property measurements, modelling of these effects, and experiments to measure the thermal response time of DT and DT + foam, are underway to provide a more accurate prediction of the target thermal response.

9. Development of laser fusion energy

We propose to develop a viable fusion energy source in three distinct phases. Specific critical issues must be resolved before advancing from one phase to the next. Each phase represents increasing confidence, decreasing technical risk, and increasing cost. In all phases the various components will be developed in concert with one another to ensure we are developing laser fusion energy as an integrated system. We are currently in Phase I, which will develop the critical science and technologies. Phase II would develop, test, and integrate full-size components. This will include a full-scale, power plant sized laser beam line and a separate facility to demonstrate repetitive injection of fusion quality targets into an IFE chamber environment. Phase III is the construction and utilization of a single flexible Engineering Test Facility (ETF). This ETF would serve several functions including: (1) optimization of the laser–target and target–chamber interactions; (2) development of materials and components; and (3) demonstration of substantial net electricity generation at a high duty factor from fusion. We believe that we could be prepared technically to start construction of the ETF facility within 10–12 years, with the basic issues resolved well before 2030. The knowledge base with ETF research should be sufficient that follow-on fusion facilities could be commercially attractive investments.

Table 4. Summary of progress and outstanding issues for laser fusion energy.

Target design	
Progress	1. Produced family of target designs, using benchmarked codes, that have one-dimensional gains ∼160 (fusion energy needs/gain >100)
	2. Newer two-dimensional calculations produced similar gains
	3. Produced a family of target designs that can meet the other needs for IFE: fabrication, injection, tritium inventory
Issues	1. Verify a robust family of target designs, using two-dimensional and three-dimensional modelling
	2. Benchmark designs with experiments
Lasers (KrF)	
Progress	1. Demonstrated repetitive first light
	2. Demonstrated pulsed power switch to meet efficiency and durability
	3. Demonstrated required efficiency in main components
Issues	1. Durability: hibachi foil and amplifier window
Lasers (DPPSL)	
Progress	1. Demonstrated repetitive first light in new type of laser architecture
	2. Demonstrated gas cooled amplifier head and high peak power diodes
Issues	1. Cost of diodes, development of large size crystals
Chambers	
Progress	1. Established chamber operating windows for wide range of targets
	2. Developed chamber clearing code, 'SPARTAN'
	3. Evaluated first wall materials response to x-rays and ions
Issues	1. Long-term materials: He bubble induced exfoliation for W, and T_2 retention for carbon
	2. Blanket and underlying, fusion neutron resistant-structures
Final optics	
Progress	1. Demonstrated GIMM meets reflectivity and laser damage requirements
Issues	1. Bonding of reflective layer to neutron transparent substrate
	2. Develop final optics structure that is resistant to degradation from neutrons, x-rays, ions, and debris
Target Fabrication	
Progress	1. Modelling shows target cost ∼$0.16 each
	2. Demonstrated ultra-smooth DT ice layer grown over foam
	3. Made foam shells with proper dimensions and density
	4. Developed Au–Pd coating for both DT permeation and IR reflectivity
Issues	1. Develop mass production cryogenic layering technique
	2. Make foam shells that meet all IFE specifications
Target Injection	
Progress	1. Target injector completed
	2. Separable Sabot concept demonstrated
	3. Demonstrated sufficiently smooth DT ice layers at $t < 16$ K
Issues	1. Demonstrate sufficient accuracy in target tracking ($< +/- 20\,\mu$m)
	2. Target designs with enhanced thermal heat load resistance (e.g. foam layer outside target) to open parameter space for injection

10. Summary: progress and challenges in the development of laser fusion energy

Table 4 gives a capsule summary of the technical progress and the critical issues that must be resolved before proceeding to Phase II in the development of laser fusion energy.

Acknowledgments

Others have made contributions to the development of Laser Fusion as part of this programme, although their specific work was not cited in the manuscript. These researchers are from the following institutions:

Government Labs: Naval Research Laboratory, Lawrence Livermore National Laboratory, Los Alamos National Laboratory, Oak Ridge National Laboratory, Sandia National Laboratory, Princeton Plasma Physics Laboratory.

Industry: General Atomics, Titan-Pulse Sciences Division, Schafer Corp., Science Applications International Corp., Northrop-Grumman Corp, Coherent, Inc, Commonwealth Technology, Inc.

Universities: University of California, San Diego; University of Wisconsin; University of California, Los Angeles; University of Rochester Laboratory for Laser Energetics; and the Georgia Institute of Technology.

This work is sponsored by the US Department of Energy, NNSA/DP.

References

[1] Bodner S.E., Colombant D.G., Schmitt A.J. and Klapisch M. 2000 High gain direct drive target design for laser fusion *Phys. Plasmas* **7** 2298

[2] Colombant D. *et al* 2000 Effects of radiation on direct drive laser fusion targets *Phys. Plasmas* **7** 2046

[3] Bodner S.E., Colombant D.G., Schmitt A.J., Lehmberg R.H., Obenschain S.P. and Gardner J.H. 2000 New high gain target design for a laser fusion power plant *IAEA Technical Committee Meeting on Physics and Technology of Inertial Fusion Energy Targets and Chambers (Madrid, Spain, 7–9 June 2000)*

[4] Skupsky S. *et al* 2002 High-gain direct-drive target designs for the national ignition facility *Inertial Fusion Sciences and Applications 2001* ed K.A. Tanaka, D.D. Meyerhofer and J. Meyer-ter-Vehn (Paris: Elsevier) pp 240–5

[5] Goncharov V.N. *et al* 2001 Modeling hydrodynamic instabilities in inertial confinement fusion targets *Phys. Plasmas* **7** 5118

[6] Betti R. *et al* 2001 Hot spot dynamics and deceleration-phase Rayleigh–Taylor instability of imploding inertial confinement fusion capsules *Phys. Plasmas* **8** 5257

[7] Obenschain S.P. *et al* 2002 Effects of thin high-Z layers on the hydrodynamics of laser-accelerated plastic targets *Phys. Plasmas* **9** 2234

[8] Collins T.J.B. and Skupsky S. 2002 Imprint reduction using an intensity spike in OMEGA cryogenic targets *Phys. Plasmas* **9** 275

[9] Betti R. *et al* 1998 Growth rates of the ablative Rayleigh–Taylor instability in inertial confinment fusion *Phys. Plasmas* **5** 1446

[10] Haan S.W. 1989 Onset of nonlinear saturation for Rayleigh–Taylor growth in the presence of a full spectrum of modes *Phys. Rev.* A **39** 5812

[11] Sethian J.D., Friedman M., Giuliani J., Lehmberg R., Myers M., Obenschain S., Hegeler F. and Swanekamp S. 2002 Electra: a krypton fluoride laser for fusion energy *Inertial Fusion Sciences and Applications* ed K.A. Tanaka, D.D. Meyerhoffer and J. Meyer-ter-Vehn (Amsterdam: Elsevier) p 495

[12] Friedman M., Myers M., Swanekamp S.B., Chan Y., Sethian J.D. and Obenschain S. 2002 Suppressing the transit-time instability in large-area electron-beam diodes *Appl. Phy. Lett.* **81** 1597

[13] Orth C.D., Payne S.A. and Krupke W.F. 1996 A diode pumped solid state laser driver for inertial fusion energy *Nucl. Fusion* **36** 75

[14] Skidmore J.A., Freitas B.L., Crawford J., Satariano J., Utterback E., DiMercurio L., Cutter K. and Sutton S. 2000 Silicon monolithic microchannel-cooled laser diode array *Appl. Phys. Lett.* **77** 10

[15] Marshall C.D., Payne S.A., Smith L.K., Powell H.T., Krupke W.F. and Chai B.H.T. 1995 1.0047 μm $Yb : Sr_5(PO_4)_3F$ energy storage optical amplifier *Selected Topics in Quantum Electron.* **1** 67

[16] Bayramian A.J., Bibeau C., Schaffers K.I., Lawson J.K., Marshall C.D. and Payne S.A. 1999 Development of ytterbium doped $Sr_5(PO_4)_3F$ for the mercury laser project *OSA Trends in Optics and Photonics Series* ed M.M. Fejer, H. Injeyan and U. Keller vol 26 of OSA Proceedings Series (Washington, DC: Optical Society of America) pp 635–41

[17] Ebbers C.A., Kanz K. and Nakano H. 2002 A thermally compensated, deuterated KDP Q-switch for high average power lasers *Conference for Lasers and Electro Optics (Long Beach, CA, 19–24 May)* Paper CTuI6

[18] Waxer I.J., Kelly J.H., Rothenberg J., Babushkin A., Bibeau C., Bayramian A. and Payne S. 2002 Precision spectral sculpting for narrow-band amplification of broadband frequency-modulated pulses *Opt. Lett.* **27** 1427

[19] Schaffers K.I., Tassano J.B., Bayramian A.B. and Morris R.C. 2003 Growth of Yb : S-FAP [Yb^{3+}: $Sr_5(PO_4)_3F$] crystals for the mercury laser *J. Cryst Growth* **253** 297–306

[20] Zimmerman G.B. and Kruer W.L. 1975 Numerical simulation of laser-initiated fusion *Comments Plasma Phys.* **2** 51

[21] Peterson R.R., MacFarlane J.J. and Moses G.A. 1996 BUCKY-1—a 1-D radiation hydrodynamics code for simulating inertial confinement fusion high energy density plasmas *Fusion Technol.* **30** 783

[22] Raffray R., Federici G., Hassanein A. and Haynes D. 2002 Dynamic chamber armor behavior in IFE and MFE *Proc. Sixth Int. Symp. on Fusion Nuclear Technology (San Diego, CA 7–12 April)* (Amsterdam: Elsevier Science Ltd, pp 63–4

[23] Sviatoslavsky I.N. *et al* 1992 A KrF laser driven inertial confinement fusion reactor 'SOMBRERO' *Fusion Technol.* **21** 1470

[24] Meier W.R. and von Rosenberg Jr C.W. 1992 Economic modeling and parametric studies for SOMBRERO—a laser-driven IFE power plant *Fusion Technol.* **21** 1552

[25] McGeoch M.W. 1998 Radio-frequency-preionized xenon Z-pinch source for extreme ultraviolet lithography *Appl. Opt.* **37** 1651

[26] Stamper J.A., Lehecka T., Lehmberg R.H., Deniz A.V. and McLean E.A. The use of inert gases in KrF laser-driven ICF reactors *Nuc. Fusion* submitted for publication

[27] Berger M.J. and Hubbell J.H. 1987 XCOM: photon cross sections on a personal computer National Bureau of Standards, NBSIR 87–3597

[28] Bohr N. 1948 *Mat. Fys. Medd. Dan. Vid. Selsk.* **18**

[29] Raffray A.R., Haynes D. and Najmabadi F. 2003 IFE chamber walls: requirements, design options, and synergy with MFE plasma facing components *J. Nucl. Mater.* **313** 23

[30] MacFarlane J.J. 1989 *Comput. Phys. Commun.* **56** 259

[31] Wang W., Roth J., Lindig S. and Wu C.H. 1999 Blister formation of tungsten due to ion bombardment *J. Nucl. Mater.* **299** 124

[32] Colella P., Glaz H.M. and Ferguson R.E. 1997 Multifluid algorithms for eulerian finite difference methods CGF 1/31/1997

[33] Colella P. and Glaz H.M. 1985 Efficient solution algorithms for the Riemann problem for real gases *J. Comput. Phys.* **59** 264

[34] Modiano D. and Colella P. 2001 A higher order embedded boundary method for time dependent simulation of hyperbolic conservation laws *Proc. ASME 2000 Fluids Engineering Division Summer Meeting (Boston, MA, June 2000)* New York: American Society of Mechanical Engineers p 267

[35] Almgren A.S., Bell J.B., Colella P., Howell L.H. and Michael L. Welcome 1998 An adaptive projection method for the variable density incompressible Navier–Stokes equations *J. Comput. Phys.* **142** 1

[36] Day M. 2002 Lawrence Berkeley National Laboratory, private communications

[37] Bieri R.L. and Guinan M.W. 1991 Grazing incidence metal mirrors as the final elements in a laser driver for inertial confinement fusion *Fusion Technol.* **19** 673

[38] Ghoniem N.M. and El-Azab A. 1995 Thermomechanical design of the grazing incidence metal mirror of the prometheus-LIFE reactor *Fusion Eng Des* **29** 89

[39] Zaghloul M.R., Tillack M.S. and Mau T.K. 2002 Laser-induced damage of metal mirrors under long-term exposure at shallow angle of incidence *Proc. 19th IEEE/IPSS Symp. on Fusion Engineering (Atlantic City, NJ, 21–25 Jan. 2002)* (New York: IEEE) p 272

[40] Mau T.K., Tillack M.S. and Zaghloul M.R. 2002 Modeling of mirror surface damage effects on beam propagation in a laser-driven IFE power plant *Proc. 19th IEEE/IPSS Symp. on Fusion Engineering (Atlantic City, NJ, 21–25 Jan. 2002)* (New York: IEEE) p 118

[41] Latkowski J.F., Kubota A., Caturla M.J., Dixit S.N., Speth J.A. and Payne S.A. 2003 Fused silica final optics for inertial fusion energy: radiation studies and system-level analysis *Fusion Sci. Technol.* **43** 1565

[42] Schwendt M., Nobile A., Gobby P.L., Steckle W.P., Colombant D.G., Sethian J.D., Goodin D.T. and Besenbruch G.E. 2003 Tritium inventory of inertial fusion energy target fabrication facilities: effect of foam density and consideration of target yield of direct drive targets *Fusion Sci. Technol.* **43** 217

[43] Petzoldt R.W., Goodin D.T., Nikroo A., Stephens E., Siegel N., Alexander N.B., Raffray A.R., Mau T.K., Tillack M., Najmabadi F., Krasheninnikov S.I. and Gallix R. 2002 Direct drive target survival during injection in an inertial fusion energy power plant *Nucl. Fusion* **42** 1351

[44] Goodin D.T., Alexander N.B., Gibson C.R., Nobile A., Petzoldt R.W., Siegel N.P. and Thompson L. 2001 Developing target injection and tracking for inertial fusion energy power plants *Nucl. Fusion* **41** 527

Appendix I
IFSA paper on A Power Plant Utilizing Z-Pinch Fusion Technology

ZP-3, A Power Plant Utilizing Z-Pinch Fusion Technology*

G.E. Rochau, G.L. Benavides, M.S. Derzon, C. L. Olson, R.E. Olson, A.R. Parker, G.A. Rochau, S.A. Slutz, K.W. Struve
P. Pankuch[1], C. Gibson[2], C. Morrow[3], P. Peterson[4], J. DeGroot[5], H. Tran[6]
E. Mogahed, I. Golovkin, G. Kulcinski, R. Peterson, I. Sviatoslavsky, M. Sawan[7]

Sandia National Laboratories,
P.O. Box 5800, Albuquerque, NM 87185-0748 USA
[1]EG&G Technical Services, Inc.
2450 Alamo Ave. SE, Albuquerque, NM 97106 USA
[2]General Atomics, ICF Group/Fusion Division,
P.O. Box 85608, San Diego, CA 95616 USA
[3]Morrow Consulting,
P.O. Box 51264, Albuquerque, NM 87181 USA
[4]University of California — Berkeley,
4155 Etcheverry Hall, Berkeley, CA 94720-1730 USA
[5]University of California — Davis, Plasma Research Group,
Davis, CA 95616 USA
[6]University of New Mexico, Dept. of Mechanical Engineering,
800 Bradbury Dr. SE, Albuquerque, NM 87106 USA
[7]University of Wisconsin, Fusion Technology Institute,
Madison, WI 73706 USA

The Z-Pinch Power Plant (ZP-3) is the first concept to use the results at Sandia National Laboratories' Z accelerator in a power plant application. Assuming high yield fusion pulses of 1 to 20 gigajoules per shot, a unique shock and energy absorbing system is being considered to contain the energy. The concept under investigation answers the need for system standoff from the fusion reaction by utilizing a replaceable mechanical cartridge that is manufactured in an on-site factory. System studies are in progress on integrated blanket design for absorbing the fusion energy, cartridge manufacture of all the recycled materials, and cartridge installation/replacement to maintain a reasonable duty cycle. An effective system design for ZP-3 requires an integrated blanket that can shield the permanent structures from the high-energy neutron flux and the strong shock wave, breed tritium, and in the process absorb the released fusion energy. The generation of this energy requires a fusion fuel cartridge to couple the repetitive pulsed power to a replaceable load using a Recyclable Transmission Line (RTL). This on-going project will combine viable economics with innovative blanket designs to produce a complete and consistent power plant concept that can be used to guide research leading to practical fusion energy.

1. Introduction

Z-Pinch technology has lead to efficient generation of x-rays [1]. Research on Sandia National Laboratories' Z accelerator has demonstrated enough progress to begin the examination of Z-pinch technology to fusion applications. Utilizing high current pulses from pulsed power technology, high-density plasmas are being compressed to produce x-rays of sufficient energy and intensity to indirectly heat a fusion capsule and cause it to burn. Sandia

* This work sponsored by Sandia National Laboratories, a multiprogram laboratory operated by Sandia Corporation, a Lockheed Martin Company, for the United States Department of Energy under contract DE-AC04-94AL85000.

National Laboratories has begun to explore how this technology can be utilized to produce electrical power.

2. Preliminary Plant Concept

The Z-Pinch Power Plant (ZP-3) utilizes inertial confinement fusion technology. The process begins with a small beryllium capsule filled with deuterium-tritium fuel in a solid form on the inside of the spherical capsule. These capsules are inserted into dynamic hohlraums and driven by a shaped 150 nanosecond rise time 60 - 100 million ampere pulse connected to a pulse power driver though a recyclable transmission line. Recyclable transmission lines, capsules, and hohlraums are assembled into a cartridge, which is repetitively inserted into a reaction chamber that is called the crucible. The objective of the first year of study has been to define one concept of a Z-Pinch Power Plant utilizing this approach. A process flow diagram for this approach is shown in Fig. 1.

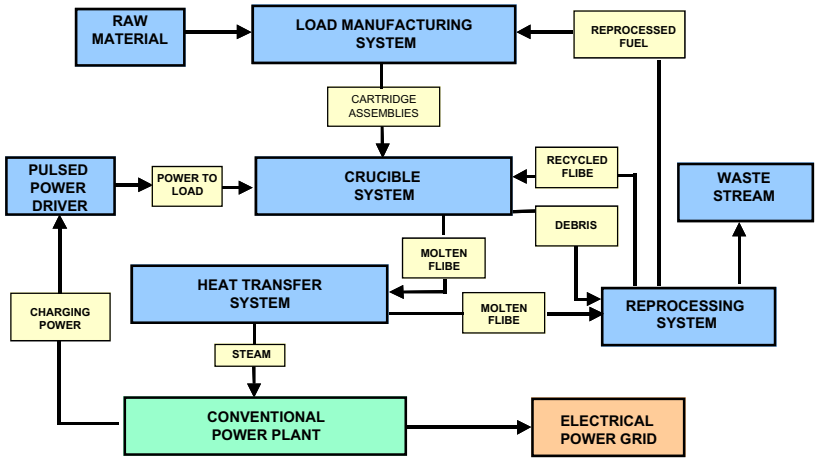

Fig. 1 - ZP-3 Process Flow Diagram

There are significant advantages to this approach as outlined in Table 1. The most important advantage is the elimination of spatial standoff requirements. We have chosen to directly connect the pulsed power driver to the cartridge for each pulse, destroying it and manufacturing a new cartridge for the subsequent pulse. To facilitate this, we have selected an operating philosophy for ZP-3, which uses well-tested intensive, but low technology, manufacturing techniques.

Table 1- Advantages and Disadvantages of a ZP-3

Advantages	Disadvantages
No vacuum requirements in fusion chamber	High yield challenges crucible strength
All components are mechanically aligned	Higher yields needed from IFE capsules
High fusion yield per pulse	
Low pulse repetition rate	
Magnetohydrodynamic direct conversion possible	
Low driver cost (~$20/Joule)	
Major components survive for plant operational life (30-40 years)	

To take advantage of an energy-rich system, we have selected to increase the energy yield per pulse and reduce the repetition rate of the pulses to allow time for moving equipment. We have assumed that the fusion yield for this approach is between 1 and 20

gigajoules (GJ). The actual yield has a significant impact on the plant design and is discussed in Section 2.6. A plant with 20 GJ yield is shown in Fig. 2. Details of this approach are summarized in the following sections.

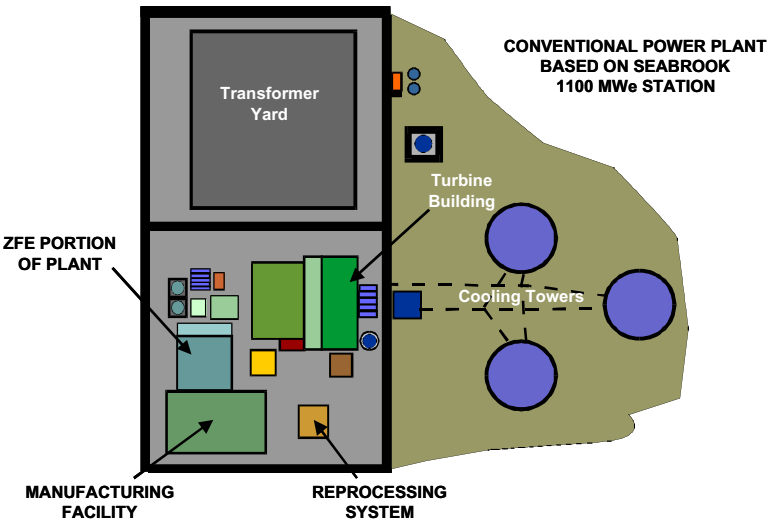

Fig. 2 - ZP-3 Site Layout

2.1. Cartridge

The cartridge is the central component of the ZP-3 system and is shown in Fig. 3. The cartridge consists of a two layer funnel-shaped Recyclable Transmission Line (RTL) [3] with a Dynamic Hohlraum (DH) on the end. The two layers of the RTL form a magnetically insulated transmission carrying a high current pulse to the DH. The DH contains a cryogenically layered fusion capsule surrounded by low-density foam coated with a thin ablative layer inside a wire array. This study only considers the components without specifying the details of the DH. The components are robotically assembled inside the vacuum of the RTL. Sufficient cryogen is contained in the assembly to maintain the layering requirements of the capsule before use. The flared end of the RTL contains a reused flange for connection to the Pulsed Power Driver.

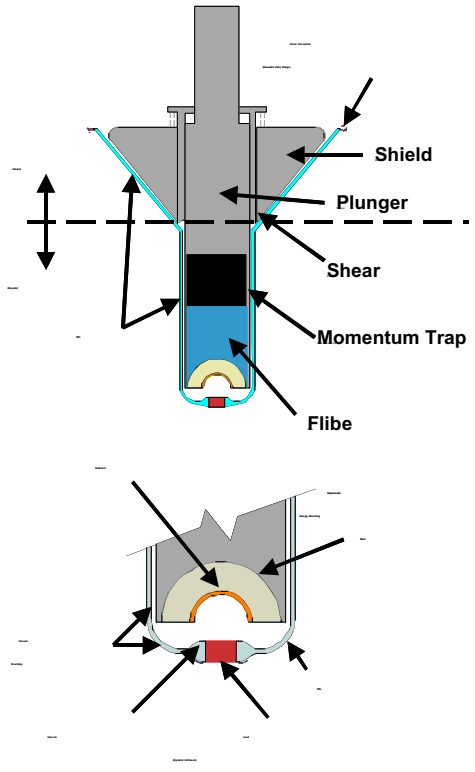

Fig. 3 - Cartridge Details

The RTL is attached to a shield-plunger assembly that places the cartridge into the crucible and connects it to the pulsed power driver. This robotic assembly manipulates the cartridge into position, dynamically connects the RTL to vacuum, allows the power pulse down the RTL and then begins to shear off the RTL to stop debris and preserving vacuum in the driver. The shield provides radiation shielding to the plant. The shield also contains an extension that enters the tube of the RTL and holds a recyclable hemispherical shell (Reflector), graded density material to absorb the momentum of the shell, and coolant to absorb the neutron energy. A momentum trap (containing crushable material) is included to mitigate the pressure impulse to the plunger.

2.2. Crucible and Containment

The Crucible contains and extracts energy from the high-yield fusion-energy pulse. The Crucible, shown in Fig. 4, is a steel vessel with coolant jets (run intermittently) and pools. These jets and pools are sized to minimize the pressure impulse to the crucible wall. The energy extraction materials have

been studied in the last year with the objective of selecting materials that permit simple mechanical separation of cartridge and coolant materials while collecting all the energy from the fusion reaction. Additionally, we desire to have lithium in the coolant to breed tritium to sustain the plant operation.

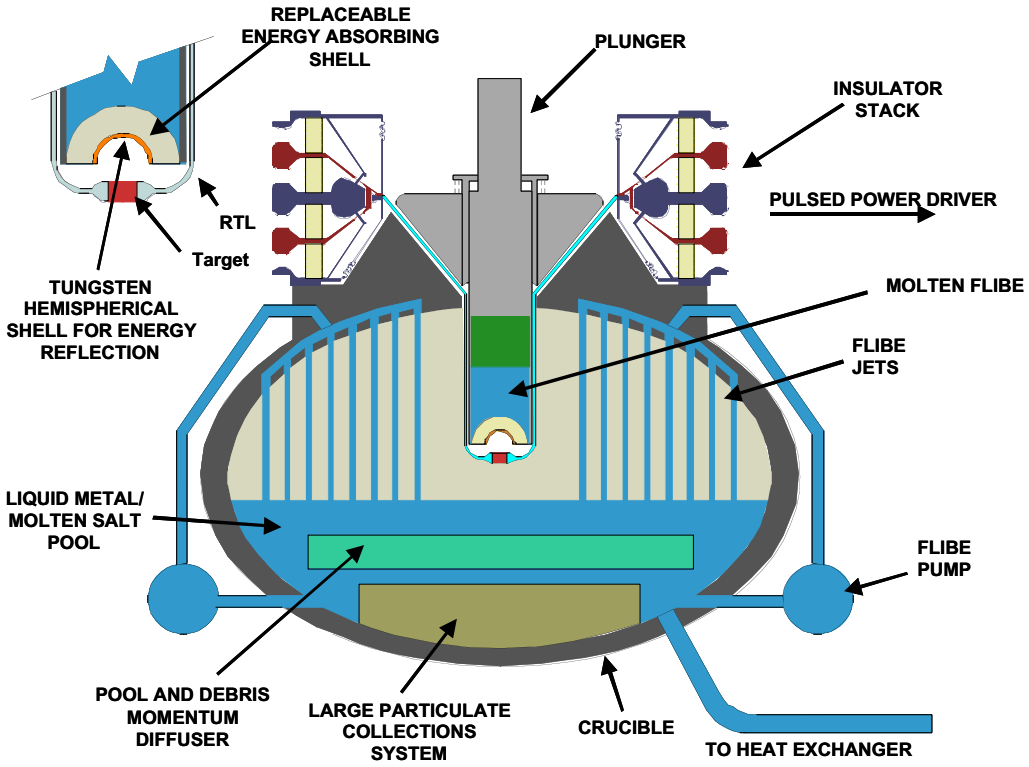

Fig. 4 -- ZP-3 Crucible and Containment

For this study, we have selected major materials for the coolant, RTL, Reflector, and Crucible. The coolant is a mixture of fluorine, lithium, and beryllium (FLIBE) that puts lithium in a chemically stable molten salt phase that can be pumped to facilitate energy absorption and tritium breeding. Carbon steel has been selected for the RTL since it has low long-lived activation and precipitates from the FLIBE as a solid that can be recovered through filtering. We are still considering using solid FLIBE as the RTL, but are using carbon steel to examine manufacturing issues. Tungsten has been selected as the high-Z material for the Reflector since it has low long-lived activation and can be recovered chemically from the steel phase. Ferritic steel has been selected for the Crucible wall because of the low long-lived activation and strength.

Our calculations conclude that FLIBE has good shielding characteristics with only 0.4 m of material required making the Crucible wall and pulsed power vacuum insulator lifetime components. Additional shielding is required to achieve 1 m of material required for a tritium-breeding ratio of 1.1. An energy multiplication of 1.1 will be achieved due to endoenergetic neutron reactions occurring in the coolant. With this shielding, only 10% of the fusion energy will be deposited in the crucible walls.

2.3. Pulsed Power Driver

For this study, the driver for the ZP-3 is modeled after a high-yield x-ray source concept, X-1 [4], developed by Sandia National Laboratories. This study does not attempt to expand the concept to higher energies or to address repetitive pulsing at this time. The X-1 driver is

expected to produce 16 to 20 megajoules of x-rays at a power of 1000 terawatts to produce 1 to 3 GJ of fusion energy per pulse. We assume that the pulsed power technology can be made repetitive at 0.1 Hz and can be maintained with minimum downtime of less than 20% for maintenance.

2.4. Energy Extraction

Several power production cycles are available for energy extraction at ZP-3. The goal of this study was to select a system to maximize plant efficiency consistent with the minimization of waste material generation. We have examined three possibilities: 1.) Super-critical Rankine Cycle with reheat for temperatures > 1200K; 2.) GT-MHR (Gas Turbine-Modular Helium Reactor) Helium Brayton Cycle for temperatures approximately 1100K; and 3.) Ultra-high temperature Brayton Cycle for temperatures on the order of 1600K. From a system efficiency perspective, the first and third possibilities are the most attractive. We have chosen the Super-Critical Rankine Cycle with reheat producing a net station efficiency of 45% as a proven technology approach. For a 1 GW plant and a temperature change of 33K, we expect a mass flow rate of FLIBE of 170,000 metric tonnes per hour.

2.5. Target Assemblies

The target assemblies for ZP-3 include cryogenically layered beryllium (Be) capsules as shown in Fig. 5. The capsule is formed by hot forging Be sheets into two hemispheres, one of which has a hole. The two hemispheres are bonded using copper braze at high temperature to form a sphere. The sphere is sealed in a high-pressure environment filled with Deuterium-Tritium (DT) gas using a laser weld. The capsule is then surrounded with tungsten covered low-density foam with liquid hydrogen reservoirs on each end of the cylinder. The low-density foam contains helium to maintain thermal contact with the capsule. Low-density foam at the bottom of the foam provides thermal isolation from the wire array and electrodes. The target assembly is then cryogenically cooled to solidify the DT gas and moved to a layering queue to allow the DT ice to smooth and become uniform.

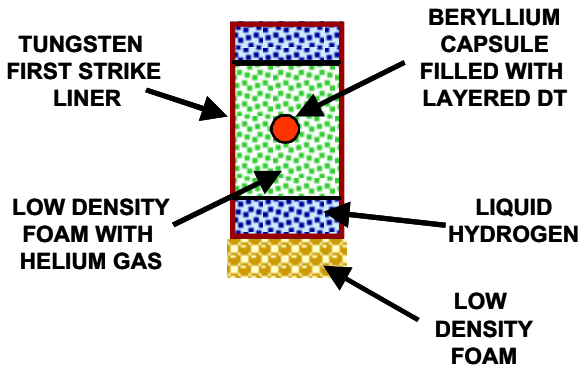

Fig. 5 - ZP-3 Target Assembly

2.6. Manufacturing

The approach chosen for ZP-3 is manufacturing intensive. The elements of the cartridge must be produced at 0.1 to 1.2 Hz. For example, the RTL can be manufactured by deep forming ferritic steels in 3 to 4 draws to 0.2 mm thickness depending on the quality of the steel. A plant containing 12 crucibles, operated at 6 pulses per minute each, requires 72 RTL per minute weighing 56 kg each (4 metric tones per minute total). The estimated cost of a drawn carbon steel RTL is $12-14 for raw material and can be reduced by a factor of 4 to 10 through material recycling. A previous estimate of cast FLIBE RTL's was approximately $.70 each.

This intensive approach can be compared to existing industrial practices. Steel beverage cans are produced at 2000 cans/minute. Automobiles can be manufactured at the rate of 2 autos/minute with formed automobile sheet metal panels at 22 panels/minute. The RTL rate falls between these examples, being more complex than cans and considerably less complex than automobiles. Thus, at 72 RTL's per minute, state of the art technology is required, however at 6 RTLs per minute, current technologies are adequate.

3. System Scaling

This study has taken a preliminary look at the scaling of ZP-3. The results are summarized in Table 2.

Table 2- System Scaling

DESCRIPTION	CURRENT STUDY VALUES	RATE CHALLENGE VALUES	YIELD CHALLENGE VALUES
Nuclear Energy Released per Pulse (GJ)	3	3	20
Energy Recovery Factor	80%	95%	95%
Thermal Energy Recovered per Pulse (GJ)	2.4	2.8	19
Pulse Frequency (Hz)	0.1	0.3	0.1
Thermal Power per Unit (GW)	0.24	0.9	1.9
Thermal Conversion Efficiency	45%	60%	60%
Electrical Output Power per Unit (GW)	0.11	0.5	1.1
Number of Units per Plant	12	2	1
Plant Availability	80%	95%	95%
Total Plant Power Output (GW)	1.04	1.0	1.1
Annual Power Sales (kWh)	9.1e9	8.5e9	9.5e9

Presented are three levels of performance to obtain a nominal 1,000 MW electrical plant output. There are two challenges to reduce the number of units; increased yield or increased pulse rate. The former requires significant increase in gain almost to mechanical limits of containment. The latter requires more from the driver and manufacturing system, but may be accomplished with less effort. Acceleration constraints during cartridge-insertion limit pulse rate to about 0.3 Hz. The significant variations are the fusion yield per pulse increased by a factor of 6.7 and the pulse rate by a factor of 7. Other variations include efficiency improvements ranging from typical to state-of-the-art for the challenge levels. Clearly, the maximum yield and the pulse rate are important factors in the reduction of the capital cost of the plant and to reduction of the manufacturing requirements. Intense study of the physics and engineering limitations of these bounding values will be important components of future studies.

4. Status and Conclusions

An initial study has been performed to define one concept of a z-pinch power plant. This study demonstrates that a power plant may be achieved through existing technologies using a z-pinch driven x-ray source. Yields of 3 GJ per shot require state-of-the-art-manufacturing facilities for RTL's, but yields of 20 GJ per shot utilize manufacturing technology currently available. Pulse rates of 0.7 Hz put considerable stress on the pulsed power driver and have the same result of reducing the manufacturing requirements. Both factors will require considerable development efforts to achieve the challenge level. This study is continuing and hopes to address questions such as the impulse loading of high yield shots on the crucible and the repetitive pulse power technology.

5. References

[1] Sanford, T.W.L., *et al*., Physical Review Letters, **83**, 5511 (1999)
[2] Slutz, S.A., *et al*., Physics of Plasmas, **8**, 1673 (2001)
[3] Slutz, S.A., *et al*., Proceedings of the 10th International Conference on Emerging Nuclear Energy Systems, van Dam and Kuijper, editors, September 24-28, 515 (2000)
[4] Rochau, G.E., *et al*., Fusion Technology, **34**, 825 (1998).

Appendix J
***Physics of Plasmas* Paper on Low Mass Recyclable Transmission Lines**

Low mass recyclable transmission lines for Z-pinch driven inertial fusion

S. A. Slutz and C. L. Olson
Sandia National Laboratories, Albuquerque, New Mexico 87185-1186

Per Peterson
University of California, Berkeley, California 94720-1730

(Received 31 May 2002; accepted 1 November 2002)

Recyclable transmission lines (RTLs) are being studied as a means to repetitively drive Z pinches. Minimizing the mass of the RTL should also minimize the reprocessing costs. Low mass RTLs could also help reduce the cost of a single shot facility such as the proposed X-1 accelerator and make Z-pinch driven nuclear space propulsion feasible. Calculations are presented to determine the minimum electrode mass to provide sufficient inertia against the magnetic pressure produced by the large currents needed to drive the Z pinches. The results indicate an electrode thickness which is much smaller than the initial resistive skin depth. This suggests that the minimum electrode thickness may be not be solely determined by inertial effects, but also by the ability of the electrode to efficiently carry the current. A series of experiments have been performed to determine the ability of the electrodes to carry current as a function of the electrode thickness. The results indicate that electrodes much thinner than the initial resistive skin depth can efficiently carry large currents presumably due to the formation of a highly conducting plasma. This result implies that a transmission line with only a few tens of kilograms of material can carry the large Z-pinch currents needed for inertial fusion. [DOI: 10.1063/1.1533789]

I. INTRODUCTION

Z-pinch physics has developed rapidly in the last few years. The use of wire arrays has resulted in the efficient conversion of pulsed power generated electrical current into thermal x rays. Nearly 2 MJ of thermal x rays have been generated by this approach[1] with an overall efficiency greater than 15%, and much higher efficiencies should be possible with pulse power machines optimized for efficiency. Z-pinch generated thermal x rays have been used to drive hohlraums[2] to temperatures greater than 145 eV, which is high enough to be of interest for driving inertial fusion capsules. One inertial fusion scenario[3] is to use two Z pinches to drive a central hohlraum containing a fusion capsule. Since Z-pinch implosions are subject to the Rayleigh–Taylor instability, this approach has the advantage of separating the nonuniformly emitting Z-pinch implosion from the inertial fusion capsule, but at the price of relatively low efficiency. Calculations[3] indicate that high yields ($\sim$0.4–1.2 GJ) could be obtained with 16 MJ of x-ray energy provided by two pinches driven with approximately 60 MA of current each. An alternate scheme[4] could provide much higher efficiency and thus lower the driver energy. In this ''dynamic hohlraum'' approach, a Z-pinch plasma is imploded onto a ''convertor,'' which surrounds the capsule. Numerical simulations[5] indicate that a single pinch with 12 MJ of kinetic energy (55 MA) could drive a 0.5 GJ yield capsule, using this approach. Recent experiments indicate that the radiation generated within this convertor is relatively unaffected by the Rayleigh–Taylor instability[6] indicating that this higher efficiency approach may indeed be feasible.

Pulse power machines are robust and inexpensive when compared to other approaches for generating high energy densities, such as lasers or heavy ion beams, and the capability to operate reliably at high repetition rates has been demonstrated at small scale.[7] Thus pulsed power driven Z pinch could be an attractive approach to inertial fusion energy. However, a Z-pinch driven fusion explosion will destroy a portion of the transmission line that delivers the electrical power to the Z pinch. On the present Z machine, these electrodes are constructed from five tons of stainless steel. The cost of repairing the transmission line would outweigh the value of the energy created by the fusion explosion. Thus, up until recently, it has been assumed that this technology is limited to single-shot experiments.

Various means of providing standoff for Z pinch have been suggested. One possible approach[8] is to use a high velocity projectile to compress a seed magnetic field. The compression of the field can generate the large current required to drive a Z pinch. This approach has difficulty generating short current pulses and will require either a large area projectile, an opening switch or a very large $B \gg 1$ T seed field. The seed field could possibly be generated by an electron beam, but this results in a fairly complicated and probably expensive system. Another approach is to use an ion beam to deliver power to an inverse diode[9] as proposed by one of the authors (S.A.S.). The inverse diode is a magnetically insulated gap, which also serves as a transmission line to deliver current to the Z pinch. The cathode side would be constructed from a thin foil that allows the ions to pass through, delivering their current to the anode. This current then flows through the Z-pinch wire assembly and back to the cathode foil. A potential problem in the inverse diode is that the large space-charge of the beam current is sufficient to generate a virtual anode that could reflect the ion beam, unless electrons

can effectively neutralize this space-charge. The effectiveness of the electron neutralization depends on electromagnetic fluctuations that allow them to cross magnetic field lines. Analytic theory[10] and numerical simulations[11] suggest this process is very effective. However, this process would have to be studied experimentally. Another potential problem is that the anode of the inverse diode will become a plasma and thus a source of ions. This will result in a loss of efficiency. The problem may be reduced by using a high-Z material for the anode, but surface contamination by hydrocarbons could still be a problem. This approach has complex physics issues that must be resolved. Also the inverse diode will be destroyed on each shot. Since it is a moderately complicated piece of equipment this approach may not be cost effective.

The most promising concept is the recyclable transmission line (RTL), which emerged at a workshop[9] at Sandia National Laboratories and was developed further at the Snowmass[12] workshop on fusion energy. This concept is much simpler than the two we have discussed previously. The idea is to construct the final portion of the transmission lines which delivers current to the Z pinch out of material that can be recycled inexpensively.

These RTLs could be formed inexpensively by casting of appropriate materials such as the reactor coolant flibe (fluorine, lithium, beryllium). Since flibe is an insulator, a conducting coating would be required. Preliminary experiments on the Saturn facility indicate that either lead or aluminum could be used.[13] Recent analysis suggest that an alloy of iron/carbon/tungsten would be a better choice for the conducting material. The components of this alloy are inert and immiscible in flibe, and will form a solid precipitate that can be recovered mechanically from the molten flibe by filtering and centrifugation processes. Activation products from these materials have relatively short half lives, so no long-lived radioactive waste would be generated. By maintaining carbon and tungsten concentrations around 1%–2% by weight, the iron maintains the properties of steel and can be formed using the same processes used for fabricating sheet-metal components of automobiles, although remote fabrication will be required due to the activity from short-lived activation products.

In this paper, we investigate the option of using low mass RTLs as a means of reducing the cost of reprocessing. Low mass RTLs could be used for inertial fusion energy, or to help reduce the cost of a single shot facility high yield facility such as the proposed X-1 accelerator. An additional application is pulsed nuclear space propulsion. Low mass RTLs are critical to this application because a portion of the RTL will become part of the rocket propellant. The portion of the RTL that impacts the craft could be captured and recycled. Since the portion of the RTL that is not captured is proportional to the total mass of the RTL, high specific impulses require low mass RTLs. Details of this application will be presented in a future publication. The present work will focus on the Z-pinch inertial fusion energy application.

Large currents are needed to drive Z-pinch inertial fusion. Numerical simulations[5] indicate that a current in excess of 55 MA will be required to drive a capsule with a fusion yield of 500 MJ. Numerical simulations, results of which will be published in a future article, indicate that substantially higher currents (~100 MA) will be required to drive capsules with a yield of several giga joules. Note that there are several high gain scenarios such as the fast ignitor concept[14] that could substantially reduce the required current. However, we shall assume that roughly 100 MA is required throughout the rest of this paper to maintain a conservative stance. High drive current generates very large magnetic pressure, which tends to push the electrodes apart. This motion is opposed by the inertial mass of the electrodes. The requirement that the gap between the electrodes does not change excessively during the current pulse places a minimum inertial mass for the electrodes. This is calculated in Sec. II.

It is found that the required areal density of the electrodes decreases strongly with radius and the outer portion of the RTL could be very thin. This calculated thickness is much smaller than the resistive skin depth of the cold electrode material. This suggests that there might be excessive resistive losses if very thin electrodes are used. It is difficult to calculate the magnitude of this effect, due to the complicated nature of surface breakdown phenomenon which can lead to highly conducting plasmas. Therefore experiments were performed to investigate the resistive effects of very thin electrodes. These experiments indicate that 20 μm of mylar is sufficient to carry the current with acceptable resistive losses. This result indicates that a transmission line with a mass as little as 2 kg could be used for energy applications. Note that we have assumed that the electrodes are thin sheets of material, possibly in the form of ribbons. An alternative idea,[9] suggested by Hammer, is to use an array of wires. This might allow even smaller transmission wire masses, but we were concerned that the explosion of the wires might cause unacceptable power flow losses so we pursued the more conservative scenario. The experiments on thin sheet electrodes are described in Sec. III. Some issues associated with the magnetic insulation of the transmission line are included in Sec. IV. A discussion of the results is provided in Sec. V.

II. CALCULATIONS OF MINIMUM RTL INERTIAL MASS

The RTL option for standoff is to construct a portion of the MITL (magnetically insulated transmission line) out of material that can be recycled. We wish to minimize the amount of material that is recycled each shot. The magnetic field generated by the current within the transmission line produces a pressure which pushes the electrodes apart. This pressure is typically much higher than the material strength of the electrode materials so the electrodes will accelerate away from each other during the current pulse. This outward motion of the electrodes increases the inductance of the transmission line making it more difficult to deliver the high currents required by the Z pinch. Assuming thin electrodes, the movement is determined by Newton's equation

$$F = \frac{B^2}{2\mu_0} A = M \frac{d^2x}{dt^2}, \tag{1}$$

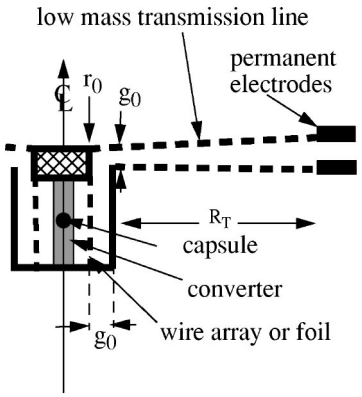

FIG. 1. A schematic of a low mass transmission line.

where x is the displacement of the electrodes and the magnetic field is determined by the relation $B=\mu_0 I/2\pi r$. The current profile produced by pulsed power accelerators such as Z can be approximated by

$$I=I_p\left(\frac{3\sqrt{3}}{2}\right)^{1/2}\tau\sqrt{1-\tau^4}, \tag{2}$$

where I_p is the peak current, $\tau=t/t_p$ and t_p is total current pulse length. This form admits an analytic solution to the Z-pinch implosion,[15] which we shall find useful. Equations (1) and (2) yield the result

$$x(t_p)=\frac{11\sqrt{3}}{224\pi\Gamma(r)}\left(\frac{\mu_0}{4\pi}\right)\left(\frac{I_p t_p}{r}\right)^2, \tag{3}$$

where $\Gamma(\mathbf{r})$ is the areal density (kg/m^2) of the electrodes. As can be seen from Eq. (3), the electrode motion is limited by the areal density (thickness) of the electrodes. Thus the acceptable amount of electrode motion determines the minimum areal density of the electrodes and hence the total mass of the transmission lines.

The electrode motion needs to be limited to a small fraction, Δg, of the transmission line gap, g. The outer portion of a low mass electrodes will have little shear strength. This limits this portion of the transmission line to sections of conics which can be supported by tensile strength alone. An example of this geometry is shown in Fig. 1. Note that the central portion of the RTL needs to be much thicker since the magnetic field pressure scales as r^{-2}. Therefore the central section can have a more complicated structure such as that depicted in Fig. 1. Power flow experiments indicate that the gap must remain finite near the pinch. Therefore we assume a gap given by

$$g=g_0+\Delta\theta(r-r_0). \tag{4}$$

Using Eqs. (3) and (4) we can solve for the areal density of the electrodes

$$\Gamma(r)=\frac{11\sqrt{3}}{112\pi}\left(\frac{\mu_0}{4\pi}\right)\frac{t_p^2 I_p^2}{\Delta g r^2[g_0+\Delta\theta(r-r_0)]}, \tag{5}$$

which scales roughly as r^{-3} for $r\gg r_0$. At some radius, r_x, the areal density of the electrode as calculated by Eq. (5) could be smaller than a minimum, Γ_n, required for structural strength or to conduct the current with acceptable resistive losses. We shall assume that $\Gamma=\Gamma_n$ for $r>r_x$. The total transmission line mass, assuming two electrodes, is then found from the integral

$$M_{\text{tot}}=2\int_{r_0}^{R_T}2\pi r\Gamma(r)dr \tag{6}$$

with the result

$$M_{\text{tot}}=\frac{11\sqrt{3}}{28\Delta g}\left(\frac{\mu_0}{4\pi}\right)\frac{t_p^2 I_p^2}{[g_0-\Delta\theta r_0]}\ln\left\{\frac{g_0 r_x}{r_0[g_0+\Delta\theta(r-r_0)]}\right\}+2\pi\Gamma_n(R_T^2-r_x^2). \tag{7}$$

Since this function decreases monotonically with $\Delta\theta$, it is instructive to consider the limit $\Delta\theta=\Gamma_n=0$, which yields

$$M_{\text{min}}=\frac{11\sqrt{3}}{28\Delta g}\left(\frac{\mu_0}{4\pi}\right)\frac{t_p^2 I_p^2}{g_0}\ln\left(\frac{R_T}{r_0}\right). \tag{8}$$

Using values appropriate for a fusion reactor, i.e., $I_p=100$ MA, $r_0=3$ cm, $R_T=4$ m, $t_p=150$ ns, and $\Delta g=0.1$, we obtain the surprisingly small result that $M_{\text{min}}=0.37$ kg. This should be compared to the mass of the transmission line in the Z accelerator, which weighs approximately 5 tons. Note that four transmission lines are used in the present Z accelerator with a current adding convolute just before the Z pinch. Using only two electrodes increases the voltage requirement, as calculated in Sec. IV. The higher voltage requirement should be attainable with a properly modified accelerator using present technology. Using these same parameters, Eq. (5) yields

$$\Gamma(r)=\frac{11\sqrt{3}}{112\pi}\left(\frac{\mu_0}{4\pi}\right)\frac{t_p^2 I_p^2}{\Delta g r^2 g_0}=\frac{6.1\times10^{-3}}{r^2}\ \text{kg/m}^2, \tag{9}$$

where r is in meters. At a 1 m radius, this corresponds to an electrode thickness of 0.75 μm for steel or 6 μm for plastic. If such extremely thin electrodes cannot be constructed which can carry the large currents needed to drive the Z pinch, the mass of the transmission line will be dominated by the second term in Eq. (7) and to a good approximation the transmission line mass needed to drive a fusion capsule is given by the simple expression

$$M_{\text{tot}}=2\pi\Gamma_n R_T^2. \tag{10}$$

In Sec. III we present the results of experiments on the Saturn facility to determine the appropriate value of Γ_n.

III. LOW MASS TRANSMISSION LINE EXPERIMENTS

In Sec. II it was found that, at the outer portion of the low mass RTL, very thin electrodes have sufficient inertia to resist the current generated magnetic pressure. This electrode thickness is much smaller than the resistive skin depth of typical cold electrode materials ($\sim$50 μm for aluminum). This suggests that there might be excessive resistive losses if very thin electrodes are used. However, it is difficult to calculate the magnitude of this effect, due to the complicated nature of surface breakdown phenomenon, which can lead to

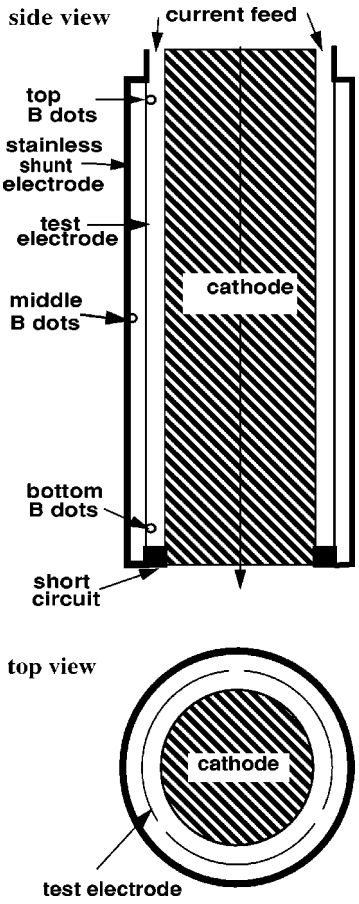

FIG. 2. A schematic of the experimental design.

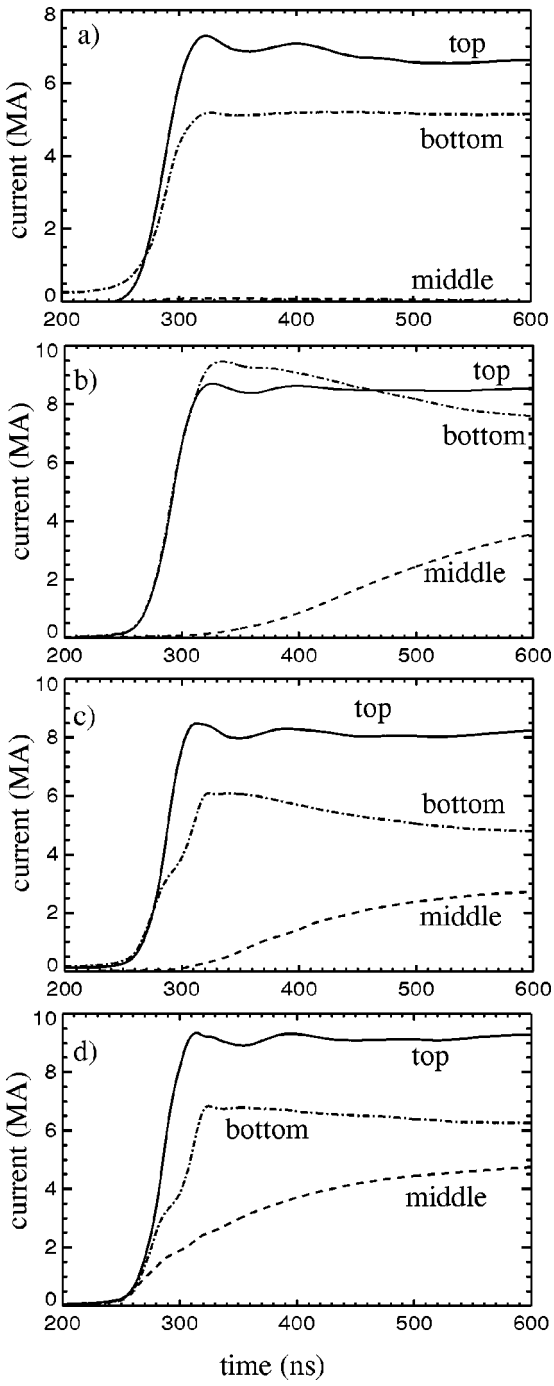

FIG. 3. The currents plotted as a function of time for (a) 250 μm carbon steel, (b) 100 μm carbon steel, (c) 50 μm carbon steel, and (d) 20 μm of mylar.

highly conducting plasmas. Therefore we designed an experiment to investigate the resistive effects of very thin electrodes. A schematic of the experimental setup is depicted in Fig. 2. Current is fed from the top by the Saturn accelerator with a nominal maximum short circuit current of about 10 MA. The test hardware is a coaxial transmission line with a short circuit at the end furthest from the accelerator (bottom). Since the transmission line is only 30 cm long it acts as a lumped inductance of approximately 4 nH. This brings the peak expected current down to about 9 MA. The hardware is divided into three azimuthal sections of 120° each, which are held together on the top and bottom by rings. Current monitors (Bdots) are placed in each of the azimuthal segments at the positions labeled in Fig. 2. The top and bottom Bdots determine the degree of magnetic insulation obtained within the transmission line. The top and bottom Bdots should have the same current profiles if the transmission line is 100% insulated. If the test electrode has a significant resistance, current will flow through the shunt electrode. This current is monitored by the middle Bdots.

Three carbon steel test electrodes of thicknesses 250, 100, and 50 μm were tried. Carbon steel has been identified as an excellent electrode material for Z-pinch driven fusion energy, due to its low activation and good separability from the reactor coolant material flibe. We also tried a 20 μm mylar test electrode as a possible candidate material for pulsed nuclear space propulsion.

The measured currents for these four shots are plotted in Fig. 3. A significant loss of current just below the top Bdot was indicated by post-shot inspection of the hardware for all of the shots except the 100 μm steel (case b). This is consistent with the measured currents at the top being larger than the bottom, except for case b, where the bottom current is slightly higher than at the top for a period of time. Since this is not actually possible, the difference gives some measure of the accuracy of the measurements. We speculate that the current loss was caused by the glue which was used to attach the test electrode just below the top Bdot monitor. We will use

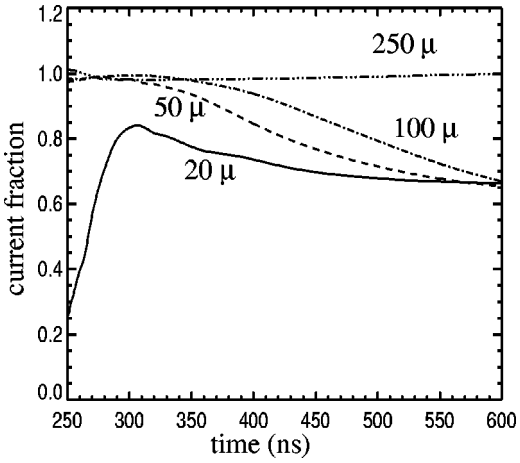

FIG. 4. The fraction of the current carried by the test electrode as a function of time.

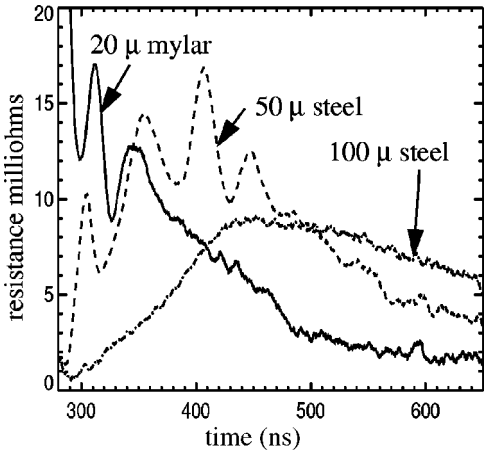

FIG. 5. The effective resistance of the test electrodes is plotted as a function of time.

the bottom Bdot current as a measure of the current that was carried by the test electrodes.

The current measured by the middle Bdots is considerably lower than either the top or the bottom for all of the shots. This is the current carried by the shunt electrode. As can be seen this current is negligible for the 250 μm case and increases as the test electrode thickness is decreased. Thus most of the current is being carried by the test electrode during the time of a typical Z-pinch implosion ($\sim$1.2–1.3 times the current rise time or about 100 ns for the Saturn accelerator). The top and bottom current monitors remain near the peak current for 400 ns after the initial rise. This behavior has often been seen with Bdot monitors. It is often assumed that the Bdots ''flash'' (short out possibly due to plasma formation in the loop) and do not register the negative voltage required to bring the integrated current back down. However, the rising current measured by the middle Bdots in this experiment implies that there is at least 4 MA of current carried by the cathode 400 ns after the initial current rise. This suggests that the top and bottom Bdots have not flashed and are actually measuring current which takes a long time to be resistively damped.

The fraction of the current carried by the test electrode is plotted for each shot in Fig. 4. The current carried by the test electrode is the difference between the bottom current and the middle current. This is then divided by total current, which is given by the bottom monitor. Note that the fraction of the current carried by the test electrode is high for all the carbon steel shots and that the fraction increases with thickness as we would expect. The 20 μm mylar electrode appears to start off as an insulator and then breaks down to carry most of the current. It should be noted that the fraction of the current carried by the test electrode would increase if the shunt electrode was moved further away due to increasing inductance. In a reactor scenario the first wall would play the role of the shunt electrode and due to the very large inductance would carry an insignificant current. Thus the fraction of the current carried by the test electrode is only a qualitative measure of performance.

The data can be used to obtain an effective resistance of the test electrode. The current carried by the test electrode is the difference between the bottom and the middle currents. The voltage across the test electrode is approximately $L dI/dt$, where $L \sim 4$ nH is the inductance between the test and shunt electrodes (gap$=3$ mm) and dI/dt is given by the unintegrated middle Bdots. Dividing the voltage across the test electrode by the current it carries yields a measure of the resistance of the test electrode. This effective resistance is plotted for each of the shots (except 250 μm steel) in Fig. 5. The 250 μm steel test electrode showed negligible effective resistance. This is presumably because the electrode was too thick for the magnetic field to diffuse through during the pulse. The rising portion of the resistance for the other steel test electrodes is probably due to the finite time it takes for magnetic diffusion. The falling portion of the curve should be more representative of the true resistance of the electrode. Note that the 20 μm mylar test electrode starts with a high effective resistance. This is because the mylar is initially an insulator and the magnetic field diffuses quickly through it. As the mylar breaks down the effective resistance drops below the thicker steel electrodes, probably because a relatively low atomic number plasma is formed at the surface.

We estimate the energy lost due to joule heating from the integral $E_{\text{joule}} = \int_0^t R_{\text{eff}}(t) I(t)^2 dt$, where $I(t)$ is the full current entering from the test electrodes. The maximum energy that Saturn could deliver to a Z-pinch load ($E_{\max} \sim 140$ kJ). We plot the ratio of $E_{\text{joule}}/E_{\max}$ as a function of time in Fig. 6. An optimal Z-pinch implosion occurs a little after peak current ($\sim$350 ns) in this experiment. At that time the resistive losses are approximately 7%, 32%, and 56% for 100 μm steel, 50 μm steel, and 20 μm mylar, respectively. The progression of increased losses with decreasing electrode thickness is clearly indicated. The Z-pinch energy and the resistive loss both scale as I^2, but the resistance also scales as L_T/r_T, where L_T is the length of the transmission line and r_T is the radius. If we scale our experimental data up to a transmission line carrying 100 MA of current we must increase the transmission line radius by roughly a factor of 10 ($r_T = 40$ cm) to maintain the same current density. Thus the fractional loss will be the same for a transmission line length

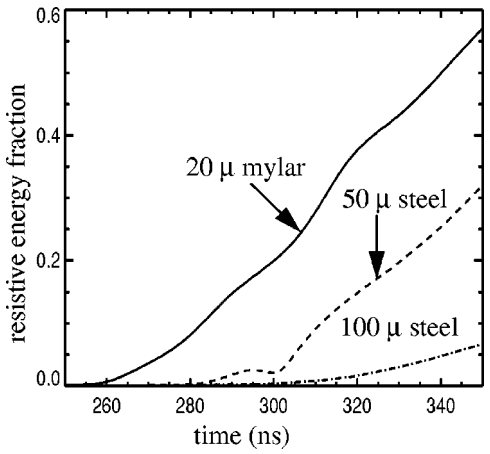

FIG. 6. The calculated resistive loss in the test electrode is plotted as a function of time.

of 3 m. The required standoff distance is not well known. Calculations indicate[16] that 4 m should be adequate even for yields of several giga joules. Assuming $R_T=4$ m, we have estimated the resistive losses for each test electrode material. We also use Eq. (10) to estimate the total mass of the low mass RTL assuming the minimum areal density is the same as each of the test electrodes. The results are summarized in Table I.

The resistive losses should be considered only a rough estimate, since that actual geometry will not be the same as the experiment (conics rather than coaxial). These results indicate that the low mass RTL mass can be quite modest (~80 kg) with a very small resistive loss (~7%). Substantially lower masses could be used with an acceptable increase in resistive losses. Pulsed power accelerators have been designed with efficiencies approaching 50%. In Sec. IV we show that roughly 1/2 of the forward going power delivered by the accelerator can be converted to kinetic energy of a Z pinch. Thus the overall efficiency of a system using 20 μm mylar electrodes would be approximately 10%. Since the conversion of Z-pinch kinetic energy into radiation is very efficient,[1] we can expect an overall efficiency of about 10%. This is competitive with the most efficient proposed laser drivers. Increasing the electrode mass to tens of kilograms would double the efficiency. Such low masses should reduce the cost of recycling transmission lines in an inertial fusion energy application. However, Eq. (10) is not an adequate approximation for applications such as microfission or magnetized target fusion that use long current pulses (>150 ns). We then need to determine the appropriate value of $\Delta\theta$, which is determined by requirements of power flow in the transmission line.

TABLE I. Summary of experimental results.

Electrode	Γ (kg/m^2)	M_{tot} (kg)	Resistive loss%
20 μm mylar	0.02	2.0	55
50 μm steel	0.4	40.0	32
100 μm steel	0.8	80.0	7
250 μm steel	2.0	200.0	<1

IV. POWER FLOW

A. Magnetic insulation

We shall now find the relationship between the value of $\Delta\theta$ and the degree of self-magnetic insulation of the low mass RTL. The condition for magnetic insulation is approximately

$$V<Bgc, \tag{11}$$

where V is the voltage applied to the transmission line. The time for the current pulse to propagate through the transmission line will be short ($\sim R_T/c\sim 10$ ns) relative to the rise time of the pulse (>100 ns) and so it will act approximately as a lumped inductance. The voltage along the transmission line will then be given by

$$V(r)=L_{\text{TL}}(r)\frac{dI}{dt}+\frac{d}{dt}(L_pI), \tag{12}$$

where L_p is the inductance of the Z pinch and $L_{\text{TL}}(r)$ is the inductance of the transmission line between the pinch and a radius, r. The inductance of the Z pinch increases as the pinch collapses. The radius of the pinch can be calculated analytically for the current profile of Eq. (2) with the result $r=r_0(1-\tau^4)$. The pinch inductance is thus

$$L_p\leqslant\frac{\mu_0}{2\pi}l_p\ln\left(\frac{r_0+g_0}{r_0(1-\tau^4)}\right), \tag{13}$$

where g_0 is the initial gap between the pinch and the return current electrode, r_0 is the initial radius of the pinch plasma, and l_p is the length of the pinch. We place an upper limit on the pinch inductance during the rising portion of the current pulse by using the pinch radius at peak current, i.e., $r=2r_0/3$. Using $g_0=2$ mm, $r_0=3$ cm, and $l_p=3$ cm we find that $L_p\sim 3$ nH.

The inductance of the transmission line is

$$L_{\text{LT}}(r)=\frac{\mu_0}{2\pi}\left\{(g_0-\Delta\theta r_0)\ln\frac{r}{r_0}+\Delta\theta(r-r_0)\right\}. \tag{14}$$

Substituting Eqs. (13) and (14) into Eqs. (12) and Eq. (11), then setting $dI/dt=I_p/t_r$, and using the maximum value of L_p, we find that $\Delta\theta\geqslant\theta_{\min}$, where

$$\theta_{\min}=\max\left(\frac{g_0\left(\ln\left(\frac{r}{r_0}\right)-\frac{F_Lct_r}{r}\right)+\frac{2\pi L_p}{\mu_0}}{(R_T-r_0)\left(\frac{F_Lct_r}{r}-1\right)+r_0\ln\left(\frac{r}{r_0}\right)}\right), \tag{15}$$

for $r_0\leqslant r\leqslant R_T$, where F_L is the fraction of the peak current needed before the transmission line is magnetically insulated, and t_r is the time to peak current. Defining

$$\alpha=\frac{F_Lct_r}{R_T}, \tag{16}$$

we find

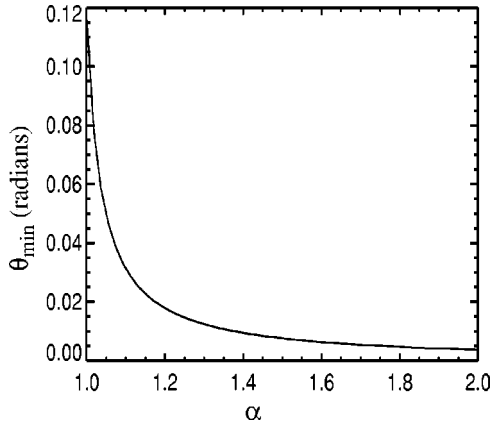

FIG. 7. The calculated minimum angle between the transmission line electrodes is plotted as a function of α.

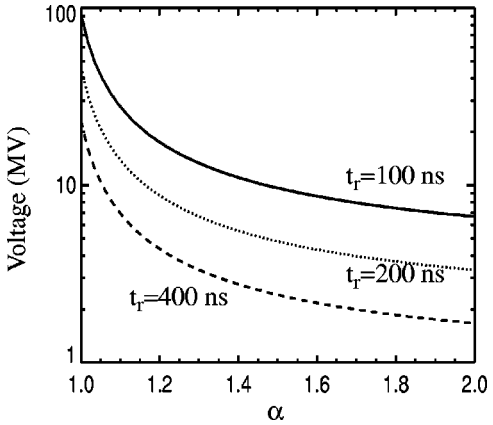

FIG. 9. The required driving voltage is plotted as a function of α for several values of the current rise time.

$$\theta_{\min}=\frac{g_0\left(\ln\left(\frac{R_T}{r_0}\right)-\alpha\right)+\frac{2\pi L_p}{\mu_0}}{(R_T-r_0)(\alpha-1)+r_0\ln\left(\frac{R_T}{r_0}\right)}. \tag{17}$$

Setting $R_T=4$ m, $r_0=3$ cm, and $L_p=3$ nH, the minimum angle is plotted as a function of α in Fig. 7. As can be seen, the minimum angle decreases strongly with increasing α. Substituting this result into Eq. (7), we calculate the transmission line mass which is plotted in Fig. 8 as a function of α. The parameters of the calculation were chosen to be consistent with a high yield capsule suitable for energy. The parameters are $\Delta g=0.1$, $I_p=100$ MA, $\Gamma_n=0.02$ kg/m^2. The mass increases for small angles (large α) because the gap between the electrodes is smaller and less electrode motion can be tolerated to maintain the same Δg. The smallest value of t_r corresponds to the present Z machine and the mass is nearly independent of α because the second term in Eq. (7) dominates. As can be seen the first term of Eq. (7) cannot be ignored as t_r is increased. Clearly the transmission line mass is minimized by decreasing α. Note that α must be greater than zero to maintain a finite value of $\theta_{\min}$. However, increasing $\Delta\theta$ increases the transmission line inductance and thus the voltage needed to drive the current. Using Eqs. (12) and (14), the driving voltage has been calculated. The results are shown in Fig. 9. As can be seen, the voltage is decreased by increasing the rise time of the current pulse and by increasing α.

Since the power is the product of current times voltage, it is clear that the total energy delivered to the transmission line will increase with driving voltage. However, the energy delivered to the pinch is only dependent on the current as given by[15]

$$E_p=\sqrt{3}l_p\left(\frac{\mu_0}{2\pi}\right)I_x^2. \tag{18}$$

Thus the efficiency of delivering energy to the pinch will increase with α. We calculate this efficiency using Eqs. (2) and (11)–(18). The result is plotted in Fig. 10 for two values of the transmission line radius. As can be seen, the efficiency is not a strong function of the transmission line radius. Note that it is independent of the current rise time at a fixed value of α.

Equation (16) indicates that increasing α corresponds to greater current lost before the transmission line becomes self-magnetically insulated. If the transmission line remains uninsulated for too long, surface plasmas may be formed. These plasmas could cause unacceptable leakage current

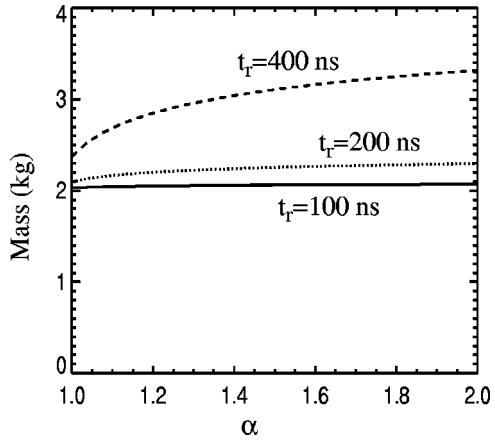

FIG. 8. The RTL mass plotted as a function of α for several values of the current rise time.

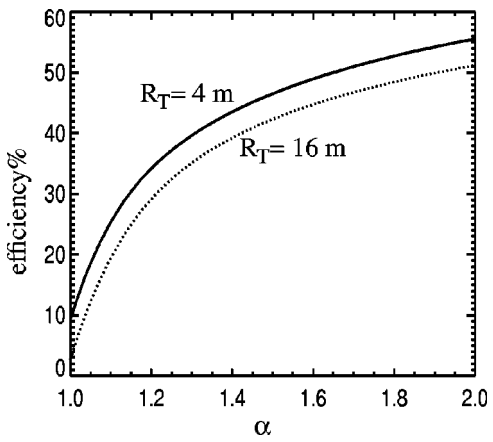

FIG. 10. The efficiency is plotted as a function of α for two values of the transmission line outer radius.

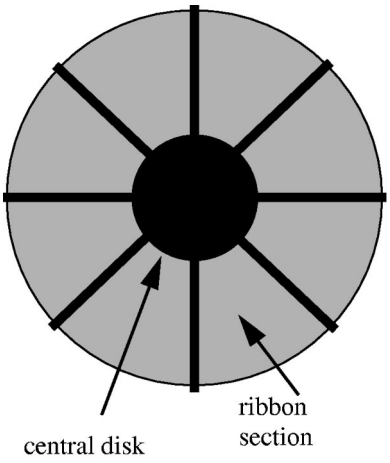

FIG. 11. A schematic of a disk electrode composed of triangular ribbon sections.

later in the pulse. Therefore there is a maximum practical value for α. The existing Z accelerator is self-insulated at about 0.15 of the peak current, i.e., $F_L=0.15$. This corresponds to $\alpha\sim 1.5$ for a 150 ns rise time. Experiments will be needed to determine if larger values of α can be used and if the value depends on the rise time of the current pulse. Using the value $\alpha=1.5$, the required driving voltage is approximately 8 MV and the efficiency is approximately 44% for a 150 ns rise time current pulse. The present Z accelerator is driven with about 3 MV, so this is not a very large extrapolation. The efficiency of 44% is quite acceptable. In principle this could be improved if a scheme to recapture the magnetic energy were devised.

B. Ion losses

The results of our experiments indicate that 20 μm mylar electrode may be about the minimum electrode thickness, thus $\Gamma_n\sim 0.02\ \mathrm{kg/m^2}$. A 20 μm foil is fairly strong, but would wrinkle easily. These wrinkles could be smoothed out by applying outward tension at the transition between the permanent electrodes and the low mass RTL. There may be some difficulty removing all of the wrinkles if the electrodes are a complete disk. A convenient alternative is to use trapazoidally shaped ribbons as shown in Fig. 11. This arrangement should make it much easier to remove wrinkles, but the edges could enhance a plasma breakdown process. This could be a concern if such a plasma forms on the anode side of the transmission line and allows ions to be accelerated across the gap. This ion current would not be delivered to the Z pinch and thus is a loss. The magnitude of this effect can be estimated as follows. Assume that some fraction, f_A, of the available anode area forms a plasma that acts as a space-charge-limit ion source. The ion current density is then given by the Child–Langmuir law

$$J=\frac{4}{9}\varepsilon_0\sqrt{\frac{2e}{m}}\frac{V^{3/2}}{d^2}. \tag{19}$$

If we assume $d=r\Delta\theta$, the voltage found from Eq. (12) is simplified to the following form:

$$V\approx\frac{\mu_0}{2\pi}\Delta\theta\frac{I_p}{t_r}r. \tag{20}$$

We then perform the integral

$$I_{\mathrm{loss}}=\int_0^{R_r}2\pi Jr\,dr \tag{21}$$

with the result

$$\frac{I_{\mathrm{loss}}}{I_p}=\frac{8}{27}\left(\frac{e\mu_0 I_p}{\pi m\Delta\theta}\right)^{1/2}\frac{f_A R_T^{3/2}}{c^2 t_r^{3/2}}\approx 0.26 f_A \tag{22}$$

assuming $I_p=100$ MA, $L_s=4$ m, and $\Delta\theta=0.01$, which corresponds to $\alpha=1.5$. Since plasma will only be formed at the boundaries, $f_A\ll 1$ and the ion loss current should be negligible. This analysis suggests that ribbons could be used. In fact the experiments reported in Sec. III used three sections.

Note that the existing Z accelerator delivers power efficiently through four transmission lines with an outside radius of about 2 m. This implies that most of the anode area of these transmission lines does not become a space-charge-limited source of ions. Experiments will be needed to determine if this benign behavior persists at the high current densities required to drive fusion capsules.

V. DISCUSSION

We have investigated the issue of minimizing the mass of a transmission line which delivers current to a Z pinch. We have shown that electrode thickness needed to provide sufficient inertia against the current induced magnetic field decreases strongly with radius and corresponds to very thin electrodes at the outer portion of the transmission line. We have performed experiments that indicate a minimum electrode thickness is required to avoid excessive resistive losses. These experiments indicate that 20 μm of mylar is sufficient to carry the current with acceptable resistive losses. This result indicates that a transmission line with a mass as little as 2 kg could be used for fusion energy applications. Increasing the RTL mass to a few tens of kilograms would result in negligible resistive losses. Reducing the mass of the transmission line will lower the cost of recycling the RTL, but an even more important effect is to lower the momentum delivered to the reactor vessel and the current feeds. Material close to the fusion explosion will be vaporized. The blast from this material should be effectively stopped by a screen of liquid, e.g., a flibe waterfall. At some distance from the explosion, the material will fragment, but remain solid. It may be more difficult to shield against this shrapnel. It is clear that minimizing the mass of the transmission line at large radii will be an advantage. In fact a significant portion of the outer transmission line will be vaporized by the current driving the Z pinch. Detailed calculations of these processes will be needed to determine if the RTL is a viable concept for obtaining fusion energy with Z pinches.

ACKNOWLEDGMENTS

We gratefully acknowledge the experimental support of Dustin Romero and all of the Saturn-crew. The interest and

support of Jeff Quintenz, Keith Matzen, Tom Mehlhorn, and Dillon McDaniel is gratefully acknowledged.

This work was performed under an LDRD at Sandia National Laboratories for the United States Department of Energy under Contract No. DE-AC04-94AL85000.

[1]R. B. Spielman, C. Deeney, and G. A. Chandler, Phys. Plasmas **5**, 2105 (1998).
[2]J. L. Porter, Bull. Am. Phys. Soc. **42**, 1948 (1998); R. J. Leeper *et al.*, Nucl. Fusion **39**, 1283 (1999).
[3]J. H. Hammer, M. Tabak, S. C. Wilks, J. D. Lindl, D. S. Bailey, P. W. Rambo, A. Toor, and G. B. Zimmerman, Phys. Plasmas **6**, 2129 (1999).
[4]J. H. Brownell and R. L. Bowers, Bull. Am. Phys. Soc. **40**, 1848 (1995).
[5]J. Lash, G. A. Chandler, G. Cooper, M. S. Derzon, M. R. Douglas, D. Hebron, R. J. Leeper, M. K. Matzen, T. A. Mehlhorn, T. J. Nash, R. E. Olson, C. L. Ruiz, T. W. L. Sanford, S. A. Slutz, D. L. Peterson, and R. E. Chrien, *Proceedings of Inertial Fusion Science and Applications 99, Bordeaux*, France, September, 1999, edited by C. Labaune, W. J. Hogan, and K. A. Tanaka (Elsevier, Paris, 2000), Vol. I, p. 583.
[6]J. E. Bailey, G. A. Chandler, S. A. Slutz *et al.*, Phys. Rev. Lett. **89**, 095004 (2002).
[7]D. L. Johnson, K. W. Reed, H. C. Harjes *et al.*, *Proceedings of the Ninth IEEE International Pulsed Power Conference*, Albuquerque, NM, 1993, edited by K. Prestwich and W. Baker (IEEE, Albuquerque, 1993), p. 437.
[8]See National Technical Information Service Document No. DE-00013848 (LLNL Report UCRL-ID-135082 by D. Ryutov and A. Toor, 1999). Copies may be ordered from the National Technical Information Service, Springfield, VA 22161.
[9]See National Technical Information Service Document No. DE-2002750245 (SNLA Report SAND99-3155 by R. B. Spielman, 1999). Copies may be ordered from the National Technical Information Service, Springfield, VA 22161.
[10]S. A. Slutz and M. P. Desjarlais, J. Appl. Phys. **67**, 6705 (1990).
[11]S. A. Slutz, J. W. Poukey, and T. D. Pointon, Phys. Plasmas **1**, 2072 (1994).
[12]*Proceedings of the 1999 Fusion Summer Study, Snowmass, CO*, edited by R. Hawryluk, G. Logan, and M. Mauel; C. L. Olson, Comments Plasma Phys. Control. Fusion, Comments Mod. Phys. **2**, 113 (2000).
[13]See National Technical Information Service Document No. DE00787789 (SNLA Report SAND2001-1736 by C. L. Olsen, S. A. Slutz, G. E. Rochau, M. S. Derzon, P. F. Peterson, J. S. DeGroot, G. A. Rochau, and R. R. Peterson, 2001). Copies may be ordered from the National Technical Information Service, Springfield, VA 22161.
[14]M. Tabak, J. Hammer, M. E. Glinsky, W. L. Kruer, S. C. Wilks, J. Woodworth, E. M. Campbell, M. D. Perry, and R. J. Mason, Phys. Plasmas **1**, 1626 (1994).
[15]S. A. Slutz, M. R. Douglas, J. S. Lash, R. A. Vesey, G. A. Chandler, T. J. Nash, and M. S. Derzon, Phys. Plasmas **8**, 1673 (2001).
[16]P. F. Peterson, C. Cole, A. Donelli, and D. R. Olander, *Proceedings of the First International Conference on Inertial Fusion Sciences and Applications, Bordeaux, France, 1999*, edited by C. Labaune, W. J. Hogan, and K. A. Tanaka (Elsevier, Paris, 2000), p. 629.

Appendix K
***Nature* Papers on Fast Ignition**

- **Fast heating of ultrahigh-density plasma as a step towards laser fusion ignition**

- **Fast heating scalable to laser fusion ignition**

terrestrial atmosphere (Fig. 1), suggesting that opaque grains and matrix portions are poor in subsolar gas. On the other hand, one matrix portion (4Mx in Table 1) shows a high ^{132}Xe concentration along with elemental ratios essentially identical to those of 'Q-gas'—this indicates that residual 'phase-Q' is located in the matrix portion, as in other chondrite classes[2].

How were large amounts of noble gases trapped in chondrules and retained within the chondrule-forming minerals? Implantation of high-energy particles from the young Sun would explain the high ^{36}Ar concentration in silicate materials, as in the case of lunar soils abundant in solar gases[7]. For example, the 'X-wind' model[15] proposed particle irradiation in the early Solar System. Our estimate predicts that diffusive loss[16] of solar-type noble gases from silicate melt can explain ^{20}Ne/^{36}Ar/^{132}Xe ratios and abundances of subsolar gas. In the calculation, we assumed that Ne, Ar and Xe of initial concentrations equal to lunar soil[7] migrated through chondrule-sized materials heated at 1,600 K for 1,000 s. Even the energetic solar flare particles (up to 100 MeV per nucleon) can penetrate at most 1 mm into silicate matter[17], and hence noble-gas implantation would have occurred on fine grains of chondrule-precursor materials. If this is the case for the subsolar gases in chondrules, it is reasonable to expect that chondrules in other chondrite classes might also contain solar-type noble gas—in contrast to the limited reports that most chondrules in other chondrites are free of primordial noble gases[2–4]. Alternatively, chondrules in each chondrite class might have been produced from different precursor materials, and/or through different heating events during which solar gases trapped in the chondrule precursors would be lost due to high peak temperatures and a slow cooling rate.

On the other hand, astronomical observations have established that young solar-mass stars go through a phase of increased activity (the T Tauri phase), during which particle fluxes are considerably greater[18] than present solar fluxes. If abnormally high-energy particles were available during this active phase, they could have penetrated into the interior of chondrules; thus noble-gas implantation onto the surface of the EC parent body at the inner region of protosolar nebula could be responsible for the subsolar gas in chondrules. The elemental ratios of subsolar gas in chondrules can be explained by diffusive loss of solar-type noble gases, as mentioned above, while the subsolar-gas depletion in matrix portions could be the result of diffusion loss through small silicate grains (5 μm across). However, explaining the absence of noble gases in large opaque grains remains difficult.

Other mechanisms for trapping noble gases are adsorption on chondrule precursor materials, and solution into enstatite melt. The high concentrations of noble gases found in chondrules means that a high adsorption efficiency would have been required—this, in turn, requires very low temperatures. And such low-temperature adsorption would have brought a large amount of water into chondrule precursor materials: but there are no hydrous minerals in ECs[19], so we consider this mechanism unlikely. The solution of solar-nebula Ar in an enstatite melt[20] is also unlikely, because it would have required very high gas pressures during chondrule formation to compensate for the low solubility. □

Methods

Extraction efficiencies of the laser system were determined by comparing noble-gas concentrations obtained by the laser-ablation method with those obtained by a conventional total-melting method. Laser pits (~200 shots) were made at even intervals over the whole surface of thin slices (S6 and S8) as a check pattern, and gave a modal abundance of ablated minerals similar to that of each whole rock. The same samples as used for the laser-ablation method were heated at 1,800 °C for 20 min in a Mo crucible. The total-melting method guarantees complete degassing and thus no elemental fractionation. Based on the experiment, we estimated extraction efficiencies of 1.39, 1.09 and 1.08 for ^{36}Ar, ^{84}Kr and ^{132}Xe, respectively. Though a slight increase in the extraction efficiency for the lighter noble gas ^{36}Ar was observed, the mass releasing ^{36}Ar is only 40% larger than the melted material in each laser pit. Hence the spatial resolution of the laser system for ^{36}Ar is only 1.2 times as large as the apparent diameter of the laser pit—typically 50–80 μm.

Received 9 March; accepted 9 July 2001.

1. Rubin, A. E. Petrologic, geochemical and experimental constraints on models of chondrule formation. *Earth Sci. Rev.* **50,** 3–27 (2000).
2. Nakamura, T., Nagao, K. & Takaoka, N. Microdistribution of primordial noble gases in CM chondrites determined by in situ laser microprobe analysis: Decipherment of nebular processes. *Geochim. Cosmochim. Acta* **63,** 241–255 (1999).
3. Kim, J. S. & Marti, K. Distribution of some highly volatile elements in chondrules. *Meteoritics* **29,** 482 (1994).
4. Miura, Y. N. & Nagao, K. *Antarctic Meteorites* Vol. 22, 118–120 (National Inst. Polar Res., Tokyo, 1997).
5. Crabb, J. & Anders, E. Noble gases in E-chondrites. *Geochim. Cosmochim. Acta* **45,** 2443–2464 (1981).
6. Wacker, J. F. & Marti, K. Noble gas components in clasts and separates of the Abee meteorite. *Earth Planet. Sci. Lett.* **62,** 147–158 (1983).
7. Eberhardt, P. *et al.* Trapped solar wind noble gases in Apollo 12 lunar fines 12001 and Apollo 11 breccia 10046. *Proc. Lunar Planet. Sci. Conf.* **III,** 1821–1856 (1972).
8. Okazaki, R. *Origin of Noble Gases in Enstatite Chondrites and Ureilites: Evolutional Processes of Meteoritic Materials in the Early Solar System.* Thesis, Kyushu Univ. (2000).
9. Lewis, R. S., Srinivasan, B. & Anders, E. Host phases of a strange xenon component in Allende. *Science* **190,** 1251–1262 (1975).
10. Wieler, R., Anders, E., Baur, H., Lewis, R. S. & Signer, P. Characterisation of Q-gases and other noble gas components in the Murchison meteorite. *Geochim. Cosmochim. Acta* **56,** 2907–2921 (1992).
11. Crabb, J. & Anders, E. On the siting of noble gases in E-chondrites. *Geochim. Cosmochim. Acta* **46,** 2351–2361 (1982).
12. Kimura, M. & Lin, Y. Petrological and mineralogical study of enstatite chondrites with reference to their thermal histories. *Antarct. Meteorit. Res.* **12,** 1–18 (1999).
13. Okazaki, R., Takaoka, N., Nakamura, T. & Nagao, K. Cosmic-ray exposure ages of enstatite chondrites. *Antarct. Meteorit. Res.* **13,** 153–169 (2000).
14. Hewins, R. H. in *Chondrules and the Protoplanetary Disk* (eds Hewins, R. H., Jones, R. H. & Scott, E. R. D.) 257–264 (Cambridge Univ. Press, 1996).
15. Shu, F. H., Shang, H., Gounelle, M., Glassgold, A. E. & Lee, T. The origin of chondrules and refractory inclusions in chondritic meteorites. *Astrophys. J.* **548,** 1029–1050 (2001).
16. Hiyagon, H. *Preliminary Studies on Partition of Rare Gases between Crystals and Melts.* Thesis, Univ. Tokyo (1981).
17. Goswami, J. N., Lal, D. & Wilkening, L. L. Gas-rich meteorites: Probes for particle environment and dynamical processes in the inner solar system. *Space Sci. Rev.* **37,** 111–159 (1984).
18. Edwards, S., Ray, T. & Mundt, R. in *Protostars and Planets III* (eds Levy, E. H. & Lunine, J. I.) 567–602 (Univ. Arizona Press, Tucson, 1993).
19. Dodd, R. T. *Meteorites: a Petrologic-chemical Synthesis* (Cambridge Univ. Press, 1981).
20. Kirsten, T. Incorporation of rare gases in solidifying enstatite melts. *J. Geophys. Res.* **73,** 2807–2810 (1968).
21. Anders, E. & Grevesse, N. Abundances of the elements: Meteoritic and solar. *Geochim. Cosmochim. Acta* **53,** 197–214 (1989).
22. Ozima, M. & Podosek, F. A. *Noble Gas Geochemistry* (Cambridge Univ. Press, 1983).
23. Pepin, R. O. On the origin and early evolution of terrestrial planet atmospheres and meteoritic volatiles. *Icarus* **92,** 2–79 (1991).

Correspondence and requests for materials should be addressed to R.O. (e-mail: okazaki@eqchem.s.u-tokyo.ac.jp).

Fast heating of ultrahigh-density plasma as a step towards laser fusion ignition

R. Kodama*, P. A. Norreys†, K. Mima*, A. E. Dangor‡, R. G. Evans§, H. Fujita*, Y. Kitagawa*, K. Krushelnick‡, T. Miyakoshi*, N. Miyanaga*, T. Norimatsu*, S. J. Rose†, T. Shozaki*, K. Shigemori*, A. Sunahara*, M. Tampo*, K. A. Tanaka*‖, Y. Toyama*, T. Yamanaka* & M. Zepf‡

* *Institute of Laser Engineering, Osaka University, 2-6 Yamada-oka, Suita Osaka 565-0871, Japan*
† *Rutherford Appleton Laboratory, Chilton, Didcot OX11 0QX, UK*
‡ *Blackett Laboratory, Imperial College, London SW7 2BZ, UK*
§ *Department of Physics, University of York, Heslington, York YO1 5DD, UK*
‖ *Faculty of Engineering, Osaka University, 2-6 Yamada-oka, Suita Osaka 565-0871, Japan*

Modern high-power lasers can generate extreme states of matter that are relevant to astrophysics[1], equation-of-state studies[2] and fusion energy research[3,4]. Laser-driven implosions of spherical polymer shells have, for example, achieved an increase in density of 1,000 times relative to the solid state[5]. These densities are large

enough to enable controlled fusion, but to achieve energy gain a small volume of compressed fuel (known as the 'spark') must be heated to temperatures of about 10^8 K (corresponding to thermal energies in excess of 10 keV). In the conventional approach to controlled fusion, the spark is both produced and heated by accurately timed shock waves[4], but this process requires both precise implosion symmetry and a very large drive energy. In principle, these requirements can be significantly relaxed by performing the compression and fast heating separately[6–10]; however, this 'fast ignitor' approach[7] also suffers drawbacks, such as propagation losses and deflection of the ultra-intense laser pulse by the plasma surrounding the compressed fuel. Here we employ a new compression geometry that eliminates these problems; we combine production of compressed matter in a laser-driven implosion with picosecond-fast heating by a laser pulse timed to coincide with the peak compression. Our approach therefore permits efficient compression and heating to be carried out simultaneously, providing a route to efficient fusion energy production.

In order to heat the compressed matter separately, the heating energy needs to be deposited on a timescale of less than 10^{-11} s, as the compression disassembles on this timescale. This is the fast ignitor[7] approach. Present-day short-pulse laser technology is, in principle, capable of delivering sufficient energy in the required timescale, the largest laser to date having a peak power of 10^{15} W and pulse durations of 10^{-12} s (ref. 11). The laser energy is coupled to the highly compressed plasma via relativistic electrons that are efficiently generated when such an ultra-intense laser interacts with a high-density plasma[11–21]. The extremely large electromagnetic fields of the laser accelerate the electrons into the high-density matter. (For a laser with a wavelength of 1 μm, the typical conversion efficiency to the relativistic electrons has been measured to be about 30–40% at intensities above 10^{19} W cm^{-2} (refs 10, 21).) The electrons then propagate to the high-density region where they deposit their energy.

We have measured the propagation of such relativistic electrons in a solid, and the associated heating effects, by examining the interactions of a 40-TW/0.5-ps laser pulse with a solid aluminium target. Images (obtained using ultraviolet light; Fig. 1) showing heated regions were temporally separated from any other hydrodynamic heating such as shock-wave and/or heat-wave propagation processes by the use of a two-dimensional (2D) spatially resolved high-speed sampling camera[22]. The heating images indicate the propagation of the high-density electrons and collimation with a divergence (full-width at half-maximum) of 20–30°. The propagation of the large relativistic electron current is made possible by a return current of colder electrons that compensates the relativistic current almost perfectly. Magnetic fields associated with the current flow also serve to keep the electrons flowing initially in a narrow filament of the order of the laser spot diameter[23–25].

The experiments on heating of ultrahigh-density plasmas were performed on the Gekko XIII laser at the University of Osaka. This laser has 12 beams for nanosecond pulses, with a maximum energy of 15 kJ at 0.53 μm wavelength, and a synchronized subpicosecond-pulse beam with a power of 100 TW and a pulse energy of 60 J (ref. 26). Conventional laser fusion experiments are conducted with spherically symmetrical targets to achieve high densities and the formation of the spark. This geometry was also envisaged in the original fast ignitor proposal[7]. Potential problems with this approach are propagation losses and deflection[27] of the ultra-intense laser pulse in the plasma surrounding the highly compressed plasma, and the transport of the relativistic electron beam through a substantial length of a plasma[28]. Here we describe an experiment that departs from the original arrangement by inserting a gold cone (with an opening angle of 60°) into the shell (Fig. 2a; and S. Hatchett, unpublished work). The cone is designed to keep the propagation path of the short-pulse laser free from the plasma that forms around the imploding shell, thereby completely avoiding laser propagation issues. The cone tip was set at 50 μm from the centre of the shell, and ensures that the compressed dense plasma forms at the tip of the cone while leaving the cone intact. The proximity between the cone tip and the core plasma also reduces the sensitivity to electron-beam propagation instabilities and losses. The cone walls are on a radius from the centre of the shell, minimizing disruptions to the spherical symmetry of the implosion so that high densities can be achieved. The laser energy used for compression here was restricted to 1.2 kJ in 1-ns-long pulses to ensure that the internal energy of the core after compression (which is about 5% efficient) was of similar magnitude to the short-pulse laser energy available (~60 J). This facilitates the measurement of the core plasma heating.

Figure 2b is a typical X-ray image of the implosion of the

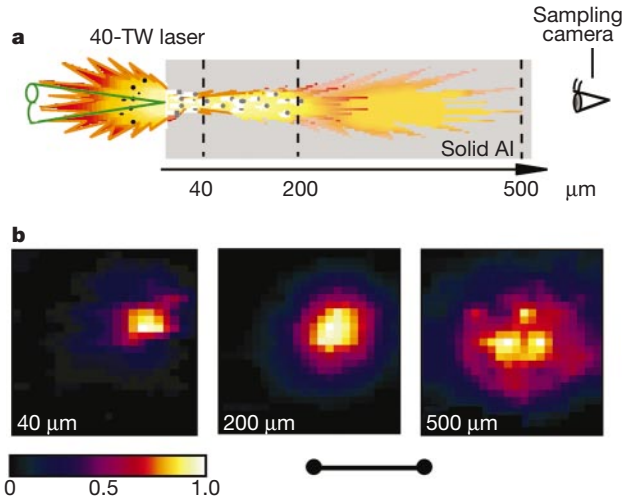

Figure 1 Ultraviolet images showing the heating of solid targets by relativistic electrons, and a sketch of the set-up used to obtain the images. **a**, 40-TW/20-J laser light was interacted with the Al solid target to create the electrons. The electrons heated the rear of the target, and this side of the target was imaged with the high-speed sampling camera. **b**, The heating images were obtained with the sampling camera for targets of different thickness (from 10 μm to 500 μm). The scale bar below the images corresponds to 200 μm on the target. The colour bar presents a linear intensity scale of the emission normalized by the peak intensity for each of the targets, to show clearly the difference in pattern. The relative peak intensities are about 5, 1 and 0.8 for the 40-μm, 200-μm and 500-μm targets, respectively.

deuterated-polystyrene (CD) shell without injection of the short-pulse laser. The imploded core plasma was created at the centre of the unimploded shell, close to the tip of the cone. The compressed density was estimated by time-resolved radiographic measurements—the compressed plasma was illuminated with X-rays from a secondary target, and the images were recorded on a multi-frame high-speed camera (100 ps per frame). The core plasma size was measured in this way to be 40–45 μm in diameter. In addition, the area corresponding to a density of 0.1–0.5 g cm^{-3} was obtained from the reduced brightness of the backlighting radiation surrounding the core using the calculated opacity (Fig. 2c). We know the initial mass of the shell target is 4×10^{-6} g, the mass of the absorbing area is 2.8×10^{-7} g from the opacity measurement, and the remaining mass after long-pulse laser ablation is 2.2×10^{-6} g (the ablated mass is 1.5×10^{-6} g) from both simulations and the experimental database on the mass ablation rate. From these, we estimate the average core density as 50–70 g cm^{-3} for the 40–45 μm core diameter. Given the non-uniformity of the laser illumination, the inferred density is consistent with that calculated using two-dimensional hydrodynamic simulations (an average density of 80–100 g cm^{-3}; Fig. 2c). The simulation also suggests that the insertion of the cone only marginally reduces the achieved compressed density (by about 20–30%) compared with full spherical implosion. This shows that implosions with a cone insert are compatible with achieving the high densities required for achieving fusion gain, while at the same time allowing for reliable and efficient coupling of the laser to the highly compressed plasma.

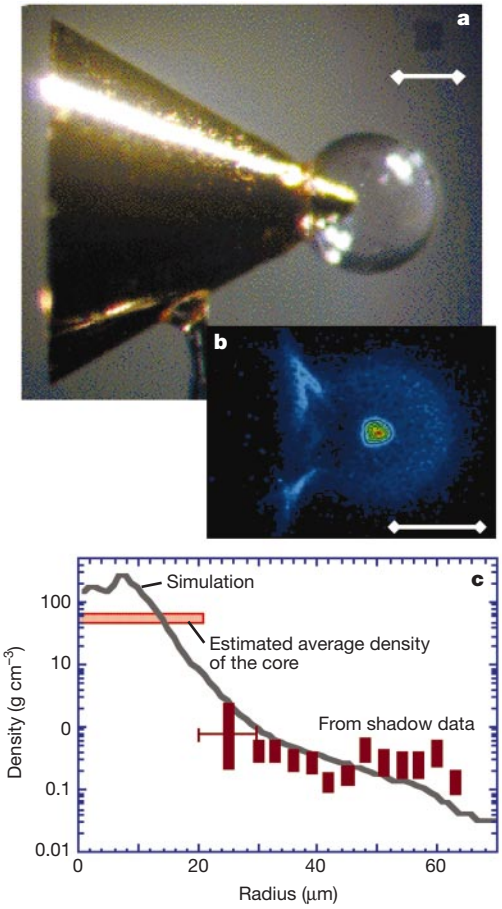

Figure 2 The implosion target for efficient heating of the highly compressed plasma, an X-ray image of the implosion, and the density profile of the plasma. The scale bars correspond to 250 μm on the target. **a**, A gold cone is attached to a deuterated-polystyrene (CD) shell (500 μm diameter, 7 μm wall thickness). 9 laser beams with a 1-ns duration are used to implode the shell at the tip of the cone. The 100-TW short-pulse laser is injected from the open side of the cone. **b**, Typical X-ray image showing the well imploded core plasma on the tip of the cone. The dimmer features correspond to the outline of the cone (left). The halo concentric with the bright core feature is emitted during the acceleration phase of the shell. **c**, Density profiles of the compressed plasma from the X-ray shadow, and a two-dimensional (2D) hydrodynamic simulation. The densities from the shadow are obtained by taking into account the opacity calculation. The errors shown are due to the spatial resolution. The 2D simulation code[29] is coupled with a one-dimensional (1D) simulation code including all the important physics. The initial conditions of the density and temperature given at the laser plasma interaction phase from the 1D code are introduced to the 2D code. In the code, incomplete spherical shock convergence and the interaction of the shell with the cone are treated, including long-wavelength hydrodynamic instability processes. However, no account is taken of shorter-wavelength perturbations of the shell caused at the acceleration phase.

We investigated the heating efficiency by injecting the 100-TW heating laser into the cone at the moment of maximum compression. The electron beam created by the 100-TW laser was measured with electron spectrometers during interactions with the cone target; we found that kT for the beam was 2–3 MeV. The conversion efficiency was obtained using the same laser with a plane target at a similar intensity (10^{19} W cm^{-2}); the energy of the electron beam was 18–24 J, representing 30–40% of the laser energy. To check the shape and divergence of the heated region associated with the electron beam in this new geometry, the 100-TW laser was injected into an identical cone target, but the tip of the cone touched an Al block (with a thickness of 200 μm at the point of contact), rather than being embedded in the CD shell. The heating area was elliptical in shape (40×25 μm^2; Fig. 3a), and the beam divergence was less than 20° from the size (130×80 μm^2) of the heated region on the back of the 200-μm Al. Figure 3b shows an image sequence of the core emission with the heating pulse injected at the time of maximum compression in the cone insert geometry. Figure 3c shows a similar sequence, but this time the heating pulse arrives 150 ps after the peak compression. The heating due to the short-pulse beam is clearly visible in the sequence in Fig. 3c: the first peak of the core emission coincides with the peak compression, and then decreases before peaking again after the injection of the heating pulse. The size of the emission region due to the peak in compression is about 30 μm, and increases to 50 μm after the injection of the heating pulse—in good agreement with the independent measurement of the heating region using the Al block.

Heating of the highly compressed plasma was quantified by

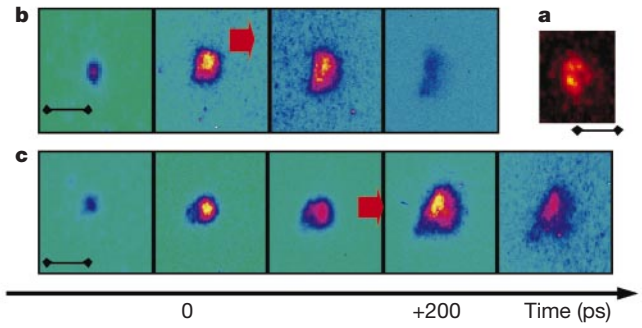

Figure 3 Time-integrated X-ray image of the short-pulse laser heating, and time-resolved X-ray images of the highly compressed plasma heated by the short-pulse laser. Time separation between each of the time-resolved images is 100 ps. The red arrows in the figure correspond to the timing of the short-pulse laser injection. The scale bar of the images shows 50 μm on the target. **a**, The image is observed from the beam-injection side of the cone attached to an Al block instead of the shell. **b**, The short-pulse laser was injected at a time close to the maximum compression of the shell. **c**, The injection timing is about 150 ps after the maximum compression. The heating by the short-pulse laser is temporally separated from the maximum compression heating of the shell.

Table 1 Neutron yield from the dense plasmas at different conditions

Target	E_i, no. of beams	E_s	N_y
Cone+shell	1.2 kJ, 9 beams	60 J	$(1–3)\times10^5$
Cone+shell	1.2 kJ, 9 beams	0	$(0.8–1)\times10^4$
Spherical shell only	2.6 kJ, 12 beams	0	$(2–3)\times10^5$

Thermal neutron yields N_y from the highly compressed plasmas are listed for different targets, implosion laser energy E_i and heating energy from the short-pulse laser E_s. The E_i is nominal energy measured after the focusing lens and through a random phase plate. These neutron yields indicates temperatures of several hundred eV.

measuring the increase in production of thermonuclear neutrons. Neutrons are generated by the fusion of two deuterium nuclei to a ^{3}He nucleus (d(d,n)^{3}He) in the imploded plasma, and provide a precise measurement of the plasma temperature. The neutron energy spectra were obtained using time-of-flight scintillator/photomultiplier detectors from two different angles. Peaks at an energy of 2.45 MeV are observed, corresponding to neutrons from a thermonuclear d(d,n)^{3}He reaction. The neutron time-of-flight spectrum in Fig. 4 shows a signal corresponding to a thermonuclear neutron yield of $(2\pm1)\times10^5$ neutrons, and was taken when the heating pulse was injected at maximum compression. This neutron yield was more than 10 times the numbers ($(9\pm1)\times10^3$) observed when no heating pulse was present or when the heating pulse was not timed to coincide with maximum compression. In order to replicate the neutron yield achieved at optimal timing in the conventional fashion (no heating pulse and a spherically symmetric implosion), a laser energy of 2.6 kJ was required to drive the implosion. Therefore the total energy required to achieve the observed neutron yield has been reduced by half, which is a clear demonstration of the increased efficiency that can be achieved by separating the compression and the heating phase in laser fusion experiments. These results, summarized in Table 1, provide (to our knowledge) the first clear evidence of effective heating of compressed plasma using an ultrahigh-intensity, short-pulse laser.

The efficiency of the energy coupling of the energetic electrons to the highly compressed plasma can be estimated from the neutron yield and the heated volume inferred from the X-ray images. In order to increase the neutron yield by a factor of 10–30, a temperature increase of about 120 eV (± 20%) is required for initial temperature regions of several hundred eV. The heated mass is estimated from the density (50–70 g cm^{-3}), and the volume is estimated from the size of the electron beam ($25\times40\,\mu m^2$) and the length of the high-density plasma (40 μm). Taking account of the beam divergence, the volume might be 1.2–1.3 times larger than this assumption. The heated distance might also be 30 μm from the core emission instead of 40 μm. Then the volume assumption will include an error of about ±30%. To heat uniformly the volume of density 50–70 g cm^{-3} ($25\times40\times40\,\mu m^3$) requires 12–16 J of the energetic electrons produced by the short-pulse laser. The total coupling efficiency of this laser to the compressed dense plasma could therefore be 20–27%, having estimation errors of ± 8% (12–35%) from the temperature and from the heated volume. This is an encouraging result.

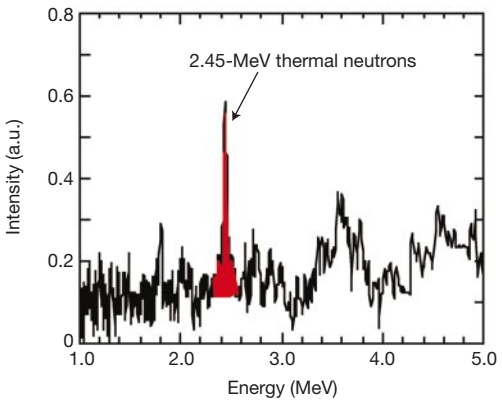

Figure 4 Neutron spectrum from the highly dense plasma heated by the short-pulse laser at the time of maximum compression. The peak at 2.45 MeV corresponds to neutrons from the thermonuclear deuterium–deuterium fusion reaction. The signal to noise ratio is ≥5.

Using the minimum 20% coupling efficiency observed in this experiment, we estimate the short-pulse laser energy needed to create a sufficiently large spark to ignite a deuterium–tritium (DT) fusion pellet ($T = 12$ keV, $\rho = 600$ g cm^{-3} and $\rho r = 0.4–0.6$ g cm^{-2}) to be 10–20 kJ (ref. 6), which seems feasible. Of course, we are still uncertain how the increase in the electron beam current will affect the propagation and energy deposition in the highly compressed DT plasma for a full-scale fusion experiment. For example, a fourfold increase in energy concentration is required as compared with this first demonstration experiment (as a smaller, 16-μm-diameter core needs to be heated due to the higher compression needed for ignition). Another issue to be resolved for the future ignition experiments is the fabrication of a uniform cryogenic fuel layer, such as a foam shell filled with liquid DT fuel. Nevertheless, we emphasized that the temperature of the energetic electrons used in our experiment is closely matched to the requirements of a full-scale fusion experiment. □

Received 4 May; accepted 6 July 2001.

1. Remington, B. A., Arnet, D., Drake, R. P. & Takabe, H. Modeling astrophysical phenomena in the laboratory with intense lasers. *Science* **284,** 1488–1493 (1999).
2. Ichimaru, S. & Kitamura, H. Pycnonuclear reactions in dense astrophysical and fusion plasmas. *Phys. Plasmas* **6,** 2649–2671 (1999).
3. Nuckolls, J., Wood, L., Thiessen, A. & Zimmerman, G. Laser compression of matter to super-high densities. *Nature* **239,** 139–142 (1972).
4. Lindl, J., McCrory, R. L. & Campbell, E. M. Progress toward ignition and burn propagation in inertial confinement fusion. *Phys. Today* **45,** 32–40 (1992).
5. Azechi, H. *et al.* High density compression experiments at ILE, Osaka. *Laser Part. Beams* **9,** 193–207 (1991).
6. Piriz, A. R. & Sanchez, M. M. Analytical model for the dynamics of fast ignition. *Phys. Plasmas* **5,** 2721–2726 (1998).
7. Tabak, M. *et al.* Ignition and high gain with ultrapowerful lasers. *Phys. Plasmas* **1,** 1626–1634 (1994).
8. Atzeni, S. Inertial fusion fast ignitor: Igniting pulse parameter window vs the penetration depth of the heating particles and the density of the precompressed fuel. *Phys. Plasmas* **6,** 3316–3326 (1999).
9. Norreys, P. *et al.* Experimental studies of the advanced fast ignitor scheme. *Phys. Plasmas* **7,** 3721–3726 (2000).
10. Kodama, R. *et al.* Fast ignition research at the institute of laser engineering Osaka University. *Phys. Plasmas* (in the press).
11. Perry, M. D. & Mourrou, G. Terawatt to petawatt subpicosecond lasers. *Science* **264,** 917–924 (1994).
12. Kruer, W. E. and Estabrook, K. JxB heating by very intense laser light. *Phys. Fluids* **28,** 430–432 (1985).
13. Brunel, F. Not-so-resonant, resonant absorption. *Phys. Rev. Lett.* **59,** 52–55 (1987).
14. Lefebvre, E. & Bonnaud, G. Transparency/opacity of a solid target illuminated by an ultrahigh-intensity laser pulse. *Phys. Rev. Lett.* **74,** 2002–2005 (1995).
15. Malka, G. & Miquel, J. L. Experimental validation of the linear theory of stimulated Raman scattering driven by a 500-fs laser pulse in a preformed underdense plasma. *Phys. Rev. Lett.* **74,** 4655–4658 (1996).
16. Pukhov, A. & Meyer-ter-Vehn, J. Laser hole boring into overdense plasma and relativistic electron currents for fast ignition of ICF targets. *Phys. Rev. Lett.* **79,** 2686–2689 (1997).
17. Key, M. H. *et al.* Hot electron production and heating by hot electrons in fast ignitor research. *Phys. Plasmas* **5,** 1966–1972 (1998).
18. Kodama, R. *et al.* Long-scale jet formation with specularly reflected light in ultraintense laser-plasma interactions. *Phys. Rev. Lett.* **84,** 674–677 (2000).
19. Santala, M. I. K. *et al.* Effect of the plasma density scale length on the direction of fast electrons in relativistic laser-solid interactions. *Phys. Rev. Lett.* **84,** 1459–1463 (2000).
20. Tanaka, K. A. *et al.* Studies of ultra-intense laser plasma interactions for fast ignition. *Phys. Plasmas* **7,** 2014–2022 (2000).
21. Wharton, K. B. *et al.* Experimental measurements of hot electrons generated by ultraintense ($>10^{19}$W/cm^2) laser plasma interactions on solid-density targets. *Phys. Rev. Lett.* **81,** 822–825 (1998).
22. Kodama, R. *et al.* Development of a two-dimensional space-resolved high speed sampling camera. *Rev. Sci. Instrum.* **70,** 625–628 (1999).
23. Davies, J. R., Bell, A. R. & Tatarakis, M. Magnetic focusing and trapping of high-intensity laser generated fast electrons at the rear of solid targets. *Phys. Rev. E* **59,** 6032–6036 (1999).
24. Tatarakis, M. *et al.* Plasma formation on the front and rear of plastic targets due to high-intensity laser-generated fast electrons. *Phy. Rev. Lett.* **81,** 999–1002 (1998).
25. Honda, M., Meyer-ter-Vehn, J. & Pukhov, A. Collective stopping and ion heating in relativistic-electron-beam transport for fast ignition. *Phys. Rev. Lett.* **85,** 2128–2131 (2000).
26. Kato, Y *et al.* Fast ignition and related plasma physics issues with high-intensity lasers. *Plasma Phys. Control. Fusion* **39,** 145–151 (1997).

27. Duda, B. J., Hemker, R. G., Tzeng, K. C. & Mori, W. B. A long-wavelength hosing instability in laser-plasma interactions. *Phys. Rev. Lett.* **83,** 1978–1981 (1999).
28. Hain, S., Cornolti, F. & Opower, H. Hydrodynamic models and schemes for fast ignition. *Laser Part. Beams* **17,** 245–263 (1999).
29. Sunahara, A., Takabe, H & Mima, K. 2D simulation of hydrodynamic instability in ICF stagnation phase. *Fusion Eng. Design* **44,** 163–169 (1999).

Acknowledgements

We thank the mm-Wave Technology Centre at the Rutherford Appleton Laboratory, and the target fabrication, laser operation and data acquisition groups at ILE Osaka University. This work was supported by the Japan Society for the Promotion of Science, and the UK Royal Society.

Correspondence and requests for materials should be addressed to R.K. (e-mail: ryo@ile.osaka-u.ac.jp).

Formation of ordered ice nanotubes inside carbon nanotubes

Kenichiro Koga*, G. T. Gao†‡, Hideki Tanaka§ & X. C. Zeng†

* *Department of Chemistry, Fukuoka University of Education, Fukuoka 811-4192, Japan*
† *Department of Chemistry and Center for Materials and Analysis, University of Nebraska, Lincoln, Nebraska 68588, USA*
§ *Department of Chemistry, Okayama University, 3-1-1, Tsushima, Okayama 700-8530 Japan*

Following their discovery[1], carbon nanotubes have attracted interest not only for their unusual electrical and mechanical properties, but also because their hollow interior can serve as a nanometre-sized capillary[2–7], mould[8–11] or template[12–14] in material fabrication. The ability to encapsulate a material in a nanotube also offers new possibilities for investigating dimensionally confined phase transitions[15]. Particularly intriguing is the conjecture[16] that matter within the narrow confines of a carbon nanotube might exhibit a solid–liquid critical point[17] beyond which the distinction between solid and liquid phases disappears. This unusual feature, which cannot occur in bulk material, would allow for the direct and continuous transformation of liquid matter into a solid. Here we report simulations of the behaviour of water encapsulated in carbon nanotubes that suggest the existence of a variety of new ice phases not seen in bulk ice, and of a solid–liquid critical point. Using carbon nanotubes with diameters ranging from 1.1 nm to 1.4 nm and applied axial pressures of 50 MPa to 500 MPa, we find that water can exhibit a first-order freezing transition to hexagonal and heptagonal ice nanotubes, and a continuous phase transformation into solid-like square or pentagonal ice nanotubes.

Carbon nanotubes can be wetted by liquids[4] whose surface tension does not exceed about 200 mN m^{-1}. Thus, in principle, pure water can be drawn into open-ended nanotubes by capillary suction[5]. Once inside, water molecules are expected to form quasi-one-dimensional (Q1D) structures that might form new phases of ice, different from the 13 polymorphic phases of bulk ice identified experimentally thus far[18]. We carried out molecular dynamics (MD) simulations at constant temperature (T) and axial-pressure (P_{zz}) of water confined within 'armchair'[19] (R,R) single-walled carbon nanotubes (SWCNs). We used nanotubes with indices R = 14–18, corresponding to tubes with diameters of 11.1, 11.9, 12.6, 13.4 and 14.2 Å, respectively. The phase behaviour of the confined water was examined in several series of the MD simulations, each series corresponding to an isobaric path or an isothermal path in the P_{zz}–T phase diagram at a given R (see Methods for details).

The first series of simulations follows an isobaric path of 50 MPa. The temperature was lowered stepwise starting from 320 K or higher, where the system is in a liquid state, to 240 K or lower. The potential energy of water in each type of SWCN is plotted in Fig. 1. In the wide SWCNs (16,16) and (17,17), the potential energy drops abruptly (Fig. 1c and d) on cooling and jumps sharply on heating. This marked hysteresis-loop behaviour signifies a first-order phase transition. Structural analysis reveals that the low-T phase is a Q1D n-gonal 'ice nanotube' composed of orderly stacked n-membered water rings[20], where n = 6 (hexagonal) in (16,16) and n = 7 (heptagonal) in (17,17) SWCNs. In both types of nanotube, the molar volume of water decreases during the liquid-to-ice nanotube transition; that is, the confined water shrinks on freezing. In the widest SWCN (18,18), however, crystallization was not observed within the timescale of simulation. In the narrower SWCNs (14,14) and (15,15), the potential energy also drops markedly on cooling below 300 K, but the change is not as sharp as in the wider nanotubes. Structural analysis shows that confined water has liquid-like disordered structure at high T but turns into solid-like ordered structure at low T—a square nanotube in (14,14) and a pentagonal nanotube in (15,15) SWCN. At 240 K, the calculated diffusion constants (along the axial direction) are $D = 3 \times 10^{-10}$ cm^2 s^{-1} in the (14,14) SWCN, and $D < 1 \times 10^{-10}$ cm^2 s^{-1} in the (15,15) SWCN, which are comparable to D of bulk ice[21]. At 300 K, $D = 1 \times 10^{-5}$ cm^2 s^{-1} and $D = 2 \times 10^{-5}$ cm^2 s^{-1} respectively. More interestingly, besides the less sharp charge in the potential energy, the hysteresis loop was not observed in the cooling and heating process, a signature of continuous transformation from liquid-like to solid-like state of water.

In real-world experiments, the atomic structures of Q1D crystals can be determined by using transmission electron microscopy[11]. Simulations provide this information directly. Figure 2 displays snapshots of the Q1D n-gonal (n = 4–6) ice nanotubes and the corresponding Q1D liquid phases inside the (14,14), (15,15) and

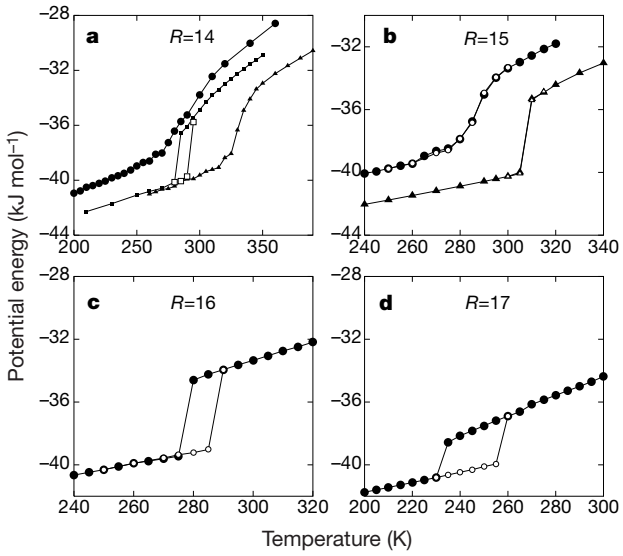

Figure 1 Potential energy against temperature for water confined in four types of single-walled carbon nanotube. The nanotubes are armchair (R,R) SWCNs, where R = 14–17 (**a**–**d**, respectively). The potential energy is due to the water–water intermolecular interactions, and the water–SWCN interaction energy is excluded. The applied axial pressure is 50 MPa (circles), 200 MPa (squares), and 500 MPa (triangles). Filled and unfilled symbols indicate the cooling and heating process, respectively.

‡ Present address: Department of Chemistry, U.S. Naval Academy, Annapolis, Maryland 21402, USA

Nuclear fusion

Fast heating scalable to laser fusion ignition

Rapid heating of a compressed fusion fuel by a short-duration laser pulse is a promising route to generating energy by nuclear fusion[1], and has been demonstrated on an experimental scale using a novel fast-ignitor geometry[2]. Here we describe a refinement of this system in which a much more powerful, pulsed petawatt (10^{15} watts) laser creates a fast-heated core plasma that is scalable to full-scale ignition, significantly increasing the number of fusion events while still maintaining high heating efficiency at these substantially higher laser energies. Our findings bring us a step closer to realizing the production of relatively inexpensive, full-scale fast-ignition laser facilities.

In advanced laser ignition of fusion[3,4], high-density energetic electrons generated by petawatt lasers instantaneously heat a compressed fusion fuel to its ignition temperature with high coupling efficiency[5]. We tested fast heating by a petawatt laser[6] and the GEKKO XII laser systems on targets in which a hollow gold cone (30° or 60° angle) was inserted into a deuterated polystyrene ('CD') shell (500 μm diameter, 7 μm thick)[2].

The shell was imploded using nine beams of the laser system operated at a wavelength of 0.53 μm and with an energy of 2.5 kJ for 1.2-ns flat-top pulses. The fast-heating laser was injected into the cone's interior and generated energetic electrons at the end of the cone, at the stagnation of the shell compression with a power of 0.5 petawatts (PW). The imploded core plasma was created near to the centre of the shell, close to the tip of the cone; the compressed density was estimated by using an X-ray backlight method[2] as 50–100 g ml^{-1} for cores of diameter 30–50 μm. A single laser oscillator[7] was used for both laser systems to provide perfect synchronization between shell compression and fast electron heating.

To quantify the heating of these highly compressed plasmas, we measured the increase in thermonuclear neutron production as a function of the injection timing of the heating pulse, with respect to the time of peak compression. Neutrons are generated by fusion of two deuterium nuclei to form a helium nucleus (atomic configuration, $d(d,n)\,^3$He) in the compressed CD plasma.

Neutron energy spectra were obtained using time-of-flight scintillator/photomultiplier detectors. The coincidence of signals from detectors at different distances and angles confirmed that the neutrons were thermonuclear in origin. Neutron enhancement was about three orders of magnitude at 0.5 PW, compared with neutrons obtained with no heating pulse ($2–5 \times 10^4$ for a 1.2 flat-pulse implosion).

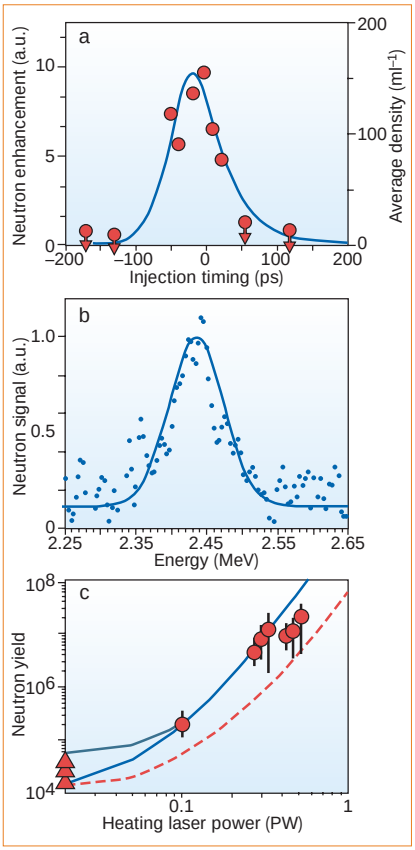

Figure 1 Fast heating of highly compressed plasmas with a petawatt (PW)-class laser pulse. **a,** Neutron enhancement (a.u., arbitrary units) as a function of injection timing (in picoseconds) of the heating pulse. Line represents the temporal profile of the average density of the compressed plasma from a hydrodynamic simulation. Arrows denote data points that fall below the background noise level ($S/N < 1$) or that correspond to the noise level. **b,** Neutron spectrum observed from an angle of 42° for a 0.5-PW laser heating at maximum compression. Line is a gaussian fit to the data points, indicating an ion temperature of 0.8 keV. **c,** Yield of thermonuclear neutrons from the compressed plasma as a function of heating laser power for the pulse duration of 0.6 ps. Solid and dashed lines, neutron yields for an energy coupling from laser to core of 30% and 15%, respectively; neutron yields obtained without a heating pulse are shown in the 0.02-PW position.

Figure 1a shows this enhancement as a function of injection timing of the heating pulse. The timing of heating was checked with X-ray streak images, as well as the injection timing of the pulse to maximum compression, from hydrodynamic simulations of the shell implosion. Enhancement was evident during ±40 ps, which corresponds to the stagnation time of the imploded plasma; the heating pulse is 0.6 ps, which is two orders of magnitude shorter than the stagnation time. These results indicate that heating for ignition might be achieved by using pulses that are close to the duration of stagnation.

If a gaussian profile is fitted to the neutron spectrum (Fig. 1b), the spectral width of the 0.5-PW heating shot is 90 ± 5 keV, which is greater than that (60 keV) for 0.1-PW heating. The width of the 0.1-PW-heating spectrum was similar to that for no heating pulse, which was less than, or close to, the spectral resolution corresponding to the ion temperature of 0.4 keV. Taking into account the spectral resolution, the width (90 ± keV) for 0.5-PW heating corresponds to an ion temperature of 0.8 ± 0.1 keV, indicating that the temperature of core plasmas could be doubled by this heating.

This finding is consistent with the enhancement, by three orders of magnitude, of neutron yield through heating; this indicates that the temperature increases from 0.3–0.4 to 0.8 keV. Our results are also consistent with the change in intensity and spectra of X-rays from heated core plasmas. The intensity increases by a factor of 1.5–2.0 compared with the absence of a heating pulse, and a continuum slope of the X-ray spectra (3–4 keV), temporally resolved with an X-ray streak camera, shows that the increase in temperature (1 ± 0.1 keV compared with 0.4 keV) is more than doubled.

Neutron yields are summarized in Fig. 1c for 0.6-ps laser pulses. Simple predictions of the neutron yield normalized to the yield without heating from energy conservation are also shown as a function of the heated laser energy, for the coupling from laser to the core plasma of 15% and 30%. The yield increases with the energy of the heating laser, implying almost constant coupling from the laser to the core plasma. However, there may be a small decrease in the coupling, from about 30% to 20%, as the laser power is increased from 0.1 PW to 0.5 PW. This could be due to an increase in the energetic electron temperature, resulting in a reduction in the stopping power of electrons for a fixed spot diameter.

Efficient fast heating of imploded plasmas has been accomplished with a petawatt laser at powers that are almost equivalent to those required in fast-ignition conditions. The period for sufficient heating is similar to the stagnation time (± 40 ps), suggesting that the heating laser's energy could be increased to ignite the fuel with a heating pulse of up to 10–20 ps or more at similar irradiance. It may eventually be possible to ignite a compressed deuterium–tritium fusion plasma with a relatively inexpensive fast-ignition facility comprising a petawatt-class laser.

R. Kodama & the Fast-Ignitor Consortium*
Institute of Laser Engineering, Osaka University, 2-6 Yamada-oka, Suita Osaka 565-0871, Japan
e-mail: ryo@ile.osaka-u.ac.jp
*H. Shiraga, K. Shigemori, Y. Toyama, S. Fujioka, H. Azechi, H. Fujita, H. Habara†, T. Hall‡, Y. Izawa, T. Jitsuno, Y. Kitagawa, K. M. Krushelnick§, K. L. Lancaster†§, K. Mima, K. Nagai, M. Nakai, H. Nishimura, T. Norimatsu,

P. A. Norreys†, S. Sakabe ||, K. A. Tanaka||, A. Youssef, M.Zepf¶, T. Yamanaka
†Rutherford Appleton Laboratory, Oxfordshire OX11 0QX, UK; ‡University of Essex, Colchester CO4 3SQ, UK; §Blacket Laboratory, Imperial College, London SW7 2BZ, UK; ||Institute of Laser Engineering and Faculty of Engineering, Osaka University, Suita Osaka 565-0871, Japan; ¶Queen's University of Belfast, Belfast BT7 1NN, UK

1. Tabak, M. *et al. Phys. Plasmas* **1,** 1626–1634 (1994).
2. Kodama, R. *et al. Nature* **412,** 798–802 (2001).
3. Norreys, P. *et al. Phys. Plasmas* **7,** 3721–3726 (2000).
4. Kodama, R. *et al. Phys. Plasmas* **8,** 2268–2274 (2001).
5. Key, M. H. *Nature* **412,** 775–776 (2001).
6. Kitagawa, Y. *et al. Phys. Plasmas* **9,** 2202–2207 (2002).
7. Yoshida, H. *et al. Conf. Laser Elec. Opt. 2002* **4,** 402–403 (2002).
Competing financial interests: declared none.

Tumorigenesis

RAF1 RAS oncogenes and mismatch-repair status

Genes of the *RAF* family encode kinases that are regulated by Ras and mediate cellular responses to growth signals. Activating mutations in one *RAF* gene, *BRAF*, have been found in a high proportion of melanomas and in a small fraction of other cancers[1]. Here we show that *BRAF* mutations in colorectal cancers occur only in tumours that do not carry mutations in a *RAS* gene known as *KRAS*, and that *BRAF* mutation is linked to the proficiency of these tumours in repairing mismatched bases in DNA. Our results not only provide genetic support for the idea that mutations in *BRAF* and *KRAS* exert equivalent effects in tumorigenesis[2], but also emphasize the role of repair processes in establishing the mutation spectra that underpin human cancer.

To determine how alterations in *BRAF* and *KRAS* might affect one another, we systematically evaluated mutations in these genes in 330 colorectal tumours (Table 1). We identified 32 mutations in *BRAF*: 28 cases with thymine-to-adenine (T–A) transversions at nucleotide position 1,796 (corresponding to an amino-acid swap of glutamate for valine at residue 599; V599E), and one case each of a guanine-to-thymine (G–T) transversion at nucleotide 1,382 (R461I), a T–G transversion at nucleotide 1,385 (I462S), a G–A transition at nucleotide 1,388 (G463E), and an A–G transition at nucleotide 1,798 (K600E). All but two of these mutations seemed to be heterozygous, and in all 20 cases for which normal tissue was available, the mutations were shown to be somatic. In the same set of tumours, there were 169 mutations in *KRAS*, including alterations to codons 12, 13, 59 and 61. No tumour exhibited mutations in both *BRAF* and *KRAS*.

Mutations in either *BRAF* or *KRAS* occurred in all Duke's stages of cancer (results not shown) and also in premalignant lesions. Mutations in both genes seemed to be more common in adenomas larger than 1 cm across than they were in smaller adenomas.

There was also a striking difference in the frequency of *BRAF* mutations between cancers with and without mismatch-repair (MMR) deficiency ($P < 10^{-6}$, χ^2 test; Table 1). All but one of the 15 *BRAF* mutations identified in MMR-deficient cases resulted in a V599E substitution.

These results provide strong support for the hypothesis that *BRAF* and *KRAS* mutations are equivalent in their tumorigenic effects[2]. Both genes seem to be mutated at a similar phase of tumorigenesis, after initiation but before malignant conversion. Moreover, we found no tumour that concurrently contained both *BRAF* and *KRAS* mutations. In view of the large number of mutations of both genes found in colorectal cancers, this observation is highly statistically significant ($P < 10^{-6}$, χ^2-test) and cannot be easily explained in other ways. This conclusion could not have been reached through the study of melanomas or of most other tumour types in which only one of the two genes is commonly mutated. It is consistent with biochemical observations[3] and was suggested by Davies *et al.*[1].

Our results also show that MMR-deficient tumours have a very high incidence of *BRAF* mutations and a lower incidence of *KRAS* mutations compared with MMR-proficient colorectal cancers. This is consistent with the idea that both tumour types progress through the same biochemical pathways, but that the mutation spectrum depends on the nature of the underlying genetic instability[4]. The V599E mutation is the most frequent nucleotide substitution ever identified in a repair-deficient tumour.

The only other tumour type with a *BRAF*-mutation frequency as high as that seen in MMR-deficient colorectal cancers is melanoma[1]. Melanomas and MMR-deficient colorectal cancers also share a high incidence of mutations in the oncogene that encodes β-catenin[5,6]. It will be interesting to see whether melanomas have a repair defect that makes them susceptible to the types of mutation found in MMR-deficient colorectal cancers, and to determine what structural or sequence elements surrounding *BRAF* codon 599 make it prone to mutagenesis in a repair-deficient background.

Table 1 *BRAF* and *KRAS* mutations in colorectal tumours

Tumours	*No. of cases*	BRAF *mutation*	KRAS *mutation*
All types	330	32 (10%)	169 (51%)
BRAF mutants	1	R461I	WT
	1	I462S	WT
	1	G463E	WT
	28	V599E	WT
	1	K600E	WT
KRAS mutants	169	WT	MUT
Other	129	WT	WT
Clinical cancers	276	30 (11%)	154 (56%)
Adenomas > 1 cm	20	2 (10%)	12 (60%)
Adenomas ≤ 1 cm	34	0 (0%)	3 (9%)
MMR-deficient cancers	49	15 (31%)	21 (43%)
MMR-proficient cancers	227	15 (7%)	133 (59%)

DNA was purified from microdissected primary tumours ($n = 54$), first-passage xenografts ($n = 189$) or cell lines ($n = 87$) as described[7]. The complete coding sequences of exons 11 and 15 of *BRAF* and exons 2 and 3 of *KRAS* were amplified by polymerase chain reaction using intronic primers and the products were sequenced as described[8]. Mutations were identified using the Mutation Explorer package (SoftGenetics). This strategy allowed us to identify all mutations previously known to occur in these two genes. Mismatch-repair (MMR) deficiency was assessed by analysis of microsatellite instability, using the *BAT26* marker and at least 12 microsatellite repeat markers[9]. WT, wild-type sequence; MUT, mutations in codons 12, 13, 59 or 61 in *KRAS*.

Harith Rajagopalan, Alberto Bardelli*, Christoph Lengauer, Kenneth W. Kinzler, Bert Vogelstein, Victor E. Velculescu
Sidney Kimmel Comprehensive Cancer Center, Howard Hughes Medical Institute, and Program in Cellular and Molecular Medicine, Johns Hopkins University School of Medicine, Baltimore, Maryland 21231, USA
e-mail: velculescu@jhmi.edu
**On leave from the Institute for Cancer Research, University of Torino, Torino, Italy*

1. Davies, H. *et al. Nature* **417,** 949–954 (2002).
2. Storm, S. M. & Rapp, U. R. *Toxicol. Lett.* **67,** 201–210 (1993).
3. Marais, R., Light, Y., Paterson, H. F., Mason, C. S. & Marshall, C. J. *J. Biol. Chem.* **272,** 4378–4383 (1997).
4. Kinzler, K. W. & Vogelstein, B. *Cell* **87,** 159–170 (1996).
5. Sparks, A. B., Morin, P. J., Vogelstein, B. & Kinzler, K. W. *Cancer Res.* **58,** 1130–1134 (1998).
6. Rubinfeld, B. *et al. Science* **275,** 1790–1792 (1997).
7. Thiagalingam, S. *et al. Proc. Natl Acad. Sci. USA* **98,** 2698–2702 (2001).
8. Wang, T. L. *et al. Proc. Natl Acad. Sci. USA* **99,** 3076–3080 (2002).
9. Markowitz, S. *J. Clin. Oncol.* **18** (suppl.), 75–80 (2000).
Competing financial interests: declared none.